Infrared subtraction at next-to-next-to-leading order for gluonic initial states

JOAO NUNO R G PIRES

Infrared subtraction at next-to-next-to-leading order for gluonic initial states

João Pires

A Thesis presented for the degree of
Doctor of Philosophy

Institute for Particle Physics Phenomenology
Physics Department
Durham University
England

January 2010

Infrared subtraction at next-to-next-to-leading order for gluonic initial states

João Pires

Submitted for the degree of Doctor of Philosophy
January 2010

Abstract

In this thesis we describe a procedure for isolating the infrared singularities present in gluonic scattering amplitudes at next-to-leading and next-to-next-to-leading order. We adopted the antenna subtraction framework which has been successfully applied to the calculation of NNLO corrections to the 3-jet cross section and related event shape distributions in electron-positron annihilation. We consider processes with coloured particles in the initial state, and in particular two-jet production in hadron-hadron collisions at accelerators such as the Large Hadron Collider (LHC). We derive explicit formulae for subtracting the single and double unresolved contributions from the double radiation gluonic processes using antenna functions with initial state partons. We show numerically that the subtraction term effectively approximates the matrix element in the various single and double unresolved configurations.

Declaration

The work in this thesis is based on research carried out at the Institute for Particle Physics Phenomenology, Department of Physics, Durham University. No part of this thesis has been submitted elsewhere for any other degree or qualification and it is all my own work unless referenced to the contrary in the text.

Acknowledgements

In first place I would like to thank my supervisor Nigel Glover for his guidance throughout my studies in Durham. Working with him has been a very rewarding experience on a professional and personal level that I will always be grateful for.

I would also like to thank everyone everyone at the IPPP for making this PhD a good experience. My office mates Sophy Palmer, Callum Durnford, Christopher Orme, John Tully, Ciaran Williams and Nehir Ikzilerli in particular for making our workplace an entertaining place and also for all the out of the office activities that we managed to organise.

The same applies for all the good *"international"* friends that I made in Ustinov College who are too many to mention. Spending time with you in the GCR bar and in most Durham pubs and bars was very amusing. On a more personal note I wish to thank also Francisco, Sergio, Joao, Vasco, Paula and Rui for their friendship. Our lives met when we all came to Durham as PhD students and it has been extremely enjoyable spending time together. I will take many memories with me from our time here in Durham and I also learned a lot from your own individual personalities and points of view towards life. I wish you the best for your future career paths and look forward to seeing you always.

I finally want to thank my parents, brother and sister and Dalila for their continuous support and love. This thesis is dedicated to them.

The work presented here was supported by the award of a Fundação para a Ciência e Tecnologia (FCT - Portugal) PhD studentship.

Contents

List of Figures

List of Tables

Preface

With the start up of the new Large Hadron Collider (LHC) imminent attention is firmly focused on the high energy frontier. The main goal is to probe the mechanism of electroweak symmetry breaking and, if the Standard Model is correct, to discover the Higgs boson in the first years of LHC operation. Because of its prominent role in electroweak symmetry breaking, the Higgs boson is especially sensitive to any new physics that could explain in a satisfactory way the stability of the electroweak scale against higher energy corrections. Therefore the LHC provides an extraordinary opportunity for addressing the great questions surrounding the structure of matter, the unification of fundamental forces, and the nature of the universe. It is expected that high luminosity pp collisions at the LHC at the TeV scale could result in new phenomena such as the production of supersymmetric particles, new families in the quark sector, new gauge interactions and/or extra dimensions and many detailed analyses of these scenarios are available in the literature.

On the other hand, to firmly establish the discovery or any other new physics, precision studies of QCD processes have to be made. This involves understanding the standard model backgrounds to both the Higgs production and to the new physics signals which are governed by the dynamics of QCD. This can be achieved by making theoretical predictions including next-to-leading order (NLO) or when needed, next-to-next-to-leading order (NNLO) effects to reduce the theoretical uncertainty.

In parallel with this, there is an opportunity for the precision study of the free parameters of the theory using the LHC data. The single jet inclusive cross section $\sigma(pp \rightarrow j + X)$ constrains α_s and the density of gluons in the proton at large values of x. Their determination proceeds by fits of the best experimental data with the best theoretical predictions. It is expected that the uncertainty from the

experimental data will be smaller that the current NLO predictions which means that a next-to-next-to-leading order (NNLO) estimate is mandatory.

This thesis focuses on the perturbative calculation of next-to-next-to-leading order (NNLO) corrections to two-jet production at the LHC. The bottleneck in this calculation is a procedure to handle the infrared divergences present in intermediate steps of the calculation. The antenna subtraction method is a potential solution to this problem. We look at the extension of this method to tackle processes with coloured particles in the initial state which is relevant for both hadron-hadron or hadron-lepton colliders.

The thesis is structured as follows. In chapter 1, we review some of the basic concepts of QCD. Chapter 2 describes the phenomena of jet production at colliders. In chapter 3, we describe the antenna subtraction method to compute observables at NLO. Chapter 4 discusses the NNLO extension of the antenna subtraction method. In chapter 5 we look at the sector decompisition method as another approach to perform NNLO calculations. For the remainder of the thesis we develop the antenna subtraction method. In chapter 6 we deal with the regularisation of the double real contribution relevant to the NNLO cross section for two-jet production at hadron colliders. Subsequently, in chapter 7 we test our implementation of the matrix element and the NNLO subtraction term. We summarise our findings in chapter 8.

Chapter 1

Higher order corrections in perturbative QCD

Since the main work of this thesis is the higher order calculation of a QCD observable, in this chapter we will briefly collect all the ingredients that make such an observable well defined.

First we explain the concept of asymptotic freedom and why the methods of perturbation theory are useful at high energy. Then we look at the procedures used to regulate the different types of singularities that appear in intermediate steps in the perturbative calculation. It is important to have a formal method to describe the singularities of the problem so that we can assemble all the divergent pieces to obtain a finite physical result. The methods of choice are Dimensional Regularisation, Renormalisation and Factorisation and the way they are implemented is explained below.

Then we introduce the ideas of the helicity basis and colour decomposition used in the derivation of the matrix elements for gluon scattering and finally we recall the universal behaviour of colour ordered QCD gluonic amplitudes for up to two unresolved particles. This is essential for the derivation of NLO and NNLO subtraction terms within the antenna subtraction method we introduce in the following chapters.

1.1 Running α_s and perturbative expansions in QCD

Consider now a dimensionless physical observable R which depends on a single energy scale Q. By assumption the scale Q is much bigger than all other dimensionful parameters such as quark masses ($m^2/Q^2 \ll 1$) and we shall therefore set the masses to zero. Setting the quark masses to zero introduces infinities when computing higher order corrections to R, however, a sensible zero mass limit exists within dimensional regularisation and we will discuss it in more detail in section 1.3.

When we calculate R as a perturbation series in the coupling constant $\alpha_s = g^2/4\pi$ the perturbation series requires renormalisation to remove ultraviolet divergences. This procedure will be explained in section 1.4 but what is important is that it will introduce a second mass scale μ - the point at which the subtractions that remove the ultraviolet divergences are performed. Since this renormalisation scale μ is arbitrary, physical observables should be independent of the choice made for μ. The μ-independence of R may be expressed by:

$$\mu^2 \frac{d}{d\mu^2} R(Q^2/\mu^2, \alpha_s) = \left[\mu^2 \frac{\partial}{\partial \mu^2} + \mu^2 \frac{\partial \alpha_s}{\partial \mu^2} \frac{\partial}{\partial \alpha_s} \right] R = 0 \tag{1.1}$$

where R can only depend on the ratio Q^2/μ^2 and the renormalised coupling constant α_s. The second term in the previous equation defines the renormalisation coefficient β. Its form is:

$$\beta(\alpha_s) = \mu^2 \frac{\partial \alpha_s}{\partial \mu^2} \tag{1.2}$$

This equation represents the Renormalisation Group Equation which provides the μ dependence of the strong coupling constant. Rewriting this equation in its integral form we obtain:

$$\log\left(\frac{Q^2}{\mu^2}\right) = \int_{\alpha_s(\mu^2)}^{\alpha_s(Q^2)} \frac{d\alpha_s}{\beta(\alpha_s)} \tag{1.3}$$

This equation governs the evolution of the coupling constant from one scale μ to another scale Q. The solution to this equation can be approximately found when the QCD β function is expanded as a perturbative series in α_s:

$$\frac{\beta(\alpha_s)}{2\pi} = -\beta_0 \left(\frac{\alpha_s}{2\pi}\right)^2 - \beta_1 \left(\frac{\alpha_s}{2\pi}\right)^3 - \mathcal{O}(\alpha_s^4) \tag{1.4}$$

where the coefficients are extracted from the higher-order (loop) corrections to the bare vertices of the theory. The coefficients β_0 and β_1 for N_F (massless) quark flavours are:

$$\beta_0 = \frac{11C_A - 4T_R N_F}{6}\,, \qquad \beta_1 = \frac{17C_A^2 - 10C_A T_R N_F - 6C_F T_R N_F}{6} \tag{1.5}$$

where N is the number of colours, and

$$C_F = \frac{N^2-1}{2N}, \qquad C_A = N, \qquad T_R = \frac{1}{2} \tag{1.6}$$

for $SU(N)$ gauge theory.

If we solve equation (1.3) to first order (keeping only the first term in (1.4) proportional to β_0 we get:

$$\alpha_s(Q^2) = \frac{\alpha_s(\mu^2)}{1 + \alpha_s(\mu^2)(\beta_0/2\pi)\log(Q^2/\mu^2)} \tag{1.7}$$

This gives the relation between $\alpha_s(Q^2)$ and $\alpha_s(\mu^2)$ when both are small enough to lie in the perturbative region. As the scale Q^2 becomes large the running coupling $\alpha_s(Q^2)$ decreases. This is the property of *asymptotic freedom*. The positive sign β_0 is crucial for this effect and we can see that this is the case for a number of active flavours $N_F \leq 16$ which is realised in nature.

We can now rewrite equation (1.1) by defining $t = \log(Q^2/\mu^2)$ and obtain:

$$\left[-\frac{\partial}{\partial t} + \beta(\alpha_s)\frac{\partial}{\partial \alpha_s}\right] R(e^t, \alpha_s) = 0 \tag{1.8}$$

It is easy to prove that $R(1, \alpha_s(Q^2))$ is a solution of the last equation. Indeed,

$$\begin{aligned} \frac{\partial R(1,\alpha_s(Q^2))}{\partial t} &= \frac{\partial \alpha_s}{\partial t}\frac{\partial R(1,\alpha_s(Q^2))}{\partial \alpha_s} \\ &= \beta(\alpha_s)\frac{\partial R(1,\alpha_s(Q^2))}{\partial \alpha_s} \end{aligned} \tag{1.9}$$

which completes the proof. This analysis shows that all the scale dependence in R enters through the running of the coupling constant $\alpha_s(Q^2)$. From equation (1.7) we found that for big energy scales α_s becomes small and this is the property which allows a perturbative expansion of a QCD observable in terms of α_s for large energies:

$$R = R(1, \alpha_s(Q^2)) = r_1\alpha_s(Q^2) + r_2\alpha_s(Q^2)^2 + r_3\alpha_s(Q^2)^3 + \cdots \tag{1.10}$$

1.1.1 Scale choice and uncertainty

Keeping the leading order term (LO) in equation (1.10) we can express R in terms of $\alpha_s(\mu^2)$ using equation (1.7):

$$R(1, \alpha_s(Q^2)) = r_1 \alpha_s(\mu^2) \times \left[1 - \alpha_s(\mu^2) \left(\frac{\beta_0}{2\pi} \right) \log \left(\frac{Q^2}{\mu^2} \right) + \alpha_s(\mu^2)^2 \left(\frac{\beta_0}{2\pi} \right)^2 \log \left(\frac{Q^2}{\mu^2} \right)^2 - \cdots \right] \tag{1.11}$$

using the known series:

$$\frac{1}{1+x} = 1 - x + x^2 - ...$$

Thus order by order in perturbation theory there are logarithms of Q^2/μ^2 which are automatically resummed by using the running coupling. The leading log behaviour of (1.11) is $\alpha_s(\mu^2)^N \log(Q^2/\mu^2)^{N-1}$. Higher order terms in R such as r_2 (NLO) or r_3 (NNLO) when expanded give terms with fewer logarithms per power of α_s. For example an NLO term $r_2\alpha_s^2$ would give:

$$r_2 \alpha_s(Q^2)^2 \to r_2 \alpha_s(\mu^2)^2 \left[1 - 2\alpha_s(\mu^2) \left(\frac{\beta_0}{2\pi} \right) \log \left(\frac{Q^2}{\mu^2} \right) \right] \tag{1.12}$$

with one less logarithm in each term, ie $\alpha_s(\mu^2)^N \log(Q^2/\mu^2)^{N-2}$.

It is important to keep all terms with the correct power of α_s when computing higher order NLO or NNLO corrections to a given observable R. For example at NNLO we have to include the solution of the renormalisation group equation keeping more terms. Including the NLO β_1 coefficient in the beta function (1.4) we find the following solution to the renormalisation group equation (1.3):

$$\frac{1}{\alpha_s(Q^2)} - \frac{1}{\alpha_s(\mu^2)} + \frac{\beta_1}{\beta_0} \log \left(\frac{\alpha_s(Q^2)}{\alpha_s(\mu^2)} \right) - \beta_0 \log \left(\frac{Q^2}{\mu^2} \right) = 0 \tag{1.13}$$

Because there is no rule on how to pick the value for the renormalisation scale μ - the point at which the subtractions that remove the ultraviolet divergences are performed, it becomes natural to chose a scale μ not far from the physical scale Q. This way we avoid large logarithms of the form $\log(Q^2/\mu^2)$.

So far we have indicated that the theoretical calculations in QCD can be carried out perturbatively for small coupling corresponding to the high energy regime. In

principle the full prediction from the theory is an infinite number of terms in the perturbative expansion but in practice we can only calculate a finite number of them. It is important to have this in mind when it comes to comes to comparing the theoretical predictions with the experimental observations. An equivalent expansion of a general observable without the resummation of the logarithms to all orders is:

$$R(\alpha_s(Q^2), Q^2/\mu^2) = \sum_{n=1}^{\infty} r_n(Q^2/\mu^2)\alpha_s(\mu^2)^n \tag{1.14}$$

We can consider the effect of truncation of the perturbative series to N terms by calculating its μ dependence:

$$\frac{d}{d\log\mu^2}\sum_{n=1}^{N} r_n(Q^2/\mu^2)\alpha_s(\mu^2)^n = -\frac{d}{d\log\mu^2}\sum_{n=N+1}^{\infty} r_n(Q^2/\mu^2)\alpha_s(\mu^2)^n \sim \mathcal{O}(\alpha_s^{N+1}) \tag{1.15}$$

where we have used the renormalisation group equation (1.1). The truncated series on the l.h.s of equation (1.15) is dependent on the scale μ as determined by the absent higher order terms on the r.h.s. of equation (1.15). This means that when we truncate the series we introduce a residual dependence in the QCD prediction on the value of the renormalisation scale. We can see however that the remainder of the truncated series is of order α_s^{N+1}. This means that when higher order terms are included the dependence on the renormalisation scale is reduced as the cancellation of the scale dependence occurs between different orders. This is shown in figure 1.1 for the cross-section for single inclusive jet production with transverse energy $E_T = 100$ GeV at leading order (LO), next-to-leading order (NLO) and next-to-next-to-leading order (NNLO) for proton-antiproton collisions at $\sqrt{s} = 1800$ GeV. The NNLO curve is based solely on the renormalisation scale dependence prediction of the lower order terms because the NNLO coefficient is presently unknown.

This is the main motivation for the huge effort to compute higher order corrections to a multitude of QCD observables and processes. The predictions become more accurate at higher order as the theoretical uncertainty is reduced. We can make high precision tests of the theory and also extract its free parameters with more accuracy.

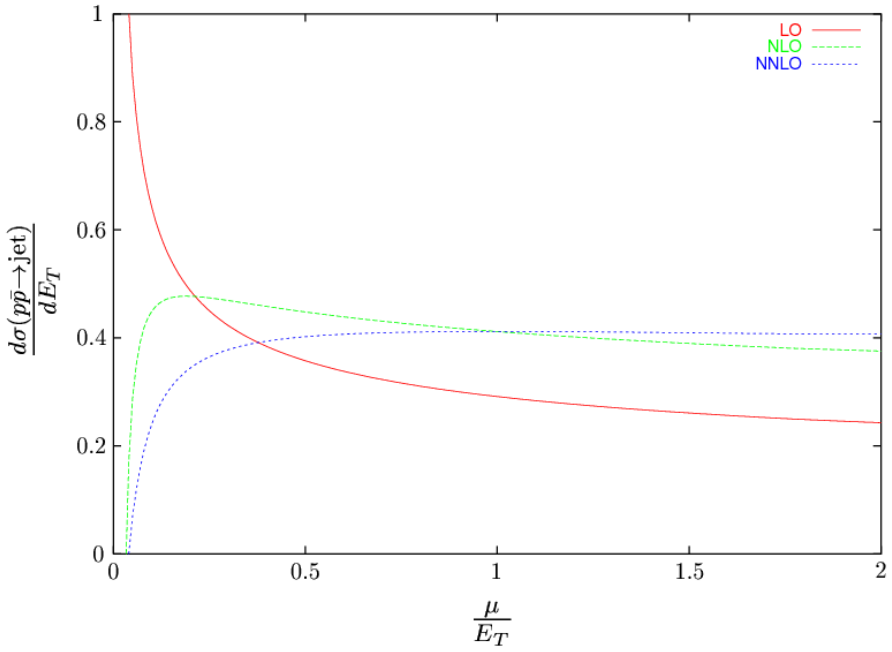

Figure 1.1: Renormalisation scale dependence for the production of single jet with transverse jet energy $E_T = 100$ GeV in proton-antiproton collisions at $\sqrt{s} = 1800$ GeV at different orders in the perturbative series [1].

1.1.2 Determination of α_s from experiment

At this point it is important to remember that QCD makes no prediction for the value of the coupling constant α_s. As a free parameter in the theory it must be extracted from experimental measurements. In theory it should be possible to make a number of experimental observations at different energy scales Q and thus extract measurements of $\alpha_s(Q)$ over a broad range of Q and test that the coupling runs as we expect. This is shown in figure 1.2 where the decrease in $\alpha_s(Q)$ with increasing Q is demonstrated.

Its more convenient to convert all measurements of $\alpha_s(Q)$ into a value at $Q = M_Z$, the mass of the Z boson, and use the following running coupling to one loop approximation:

$$\alpha_s(Q) = \frac{\alpha_s(M_Z)}{1 + \left(\frac{\beta_0}{2\pi}\right) \log\left(\frac{Q}{M_Z}\right) \alpha_s(M_Z)} \tag{1.16}$$

This is because at the scale $Q = M_Z$ we are sufficiently far away from quark thresholds (and hence non-zero mass effects) and also close to the asymptotic region where

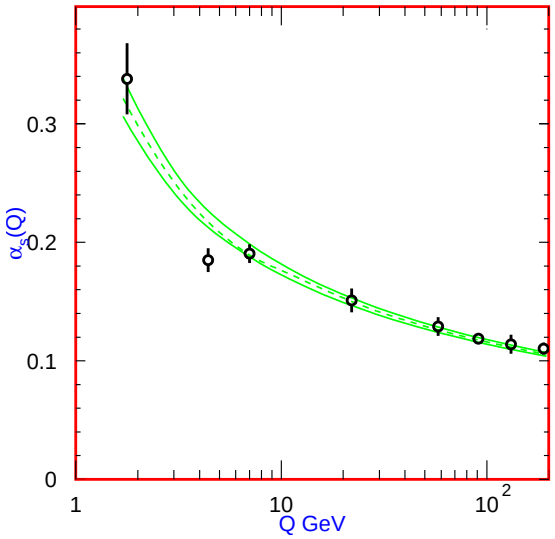

Figure 1.2: Summary of the values of $\alpha_s(Q)$ at the values of Q where they are measured taken from the PDG review 2008 [2]. The running coupling is determined by solving the renormalisation group equation to two loop order, shown by the dashed line.

perturbation theory should apply ($\alpha_s \sim 0.1$). In addition the experimental measurements on the Z pole are of high precision due to high statistics of the LEP data.

One recent analysis is the first determination of the strong coupling constant using an NNLO prediction for hadronic event shapes in e^+e^- annihilations. In this study a fit was made with the QCD predictions calculated at next-to-next-to-leading order (NNLO) and matched to resummation in the next-to-logarithmic approximation (NLLA) to the data collected by the ALEPH detector in e^+e^- annihilations at LEP. By combining the results for six event-shape variables and eight centre-of-mass energies ranging between 91 and 206 GeV the following result was obtained [3]:

$$\alpha_s(M_Z) = 0.1224 \pm 0.0009(stat) \pm 0.0009(sys) \pm 0.012(had) \pm 0.0035(theo) \tag{1.17}$$

1.2 IR and UV singularities

In the previous sections we have shown the validity of the use of perturbative methods to compute the predictions from the theory and the importance of higher order

corrections. The leading order estimate contains large errors due to the renormalisation scale dependence and clearly is a good tool to estimate relative magnitudes of processes, but not enough to do precision studies or to identify a discovery with a particular model.

However when we try to compute higher order corrections using perturbation theory we encounter a new difficulty. Obviously we would expect the first order (NLO) corrections to be a small contribution to the (LO) estimate and the second order (NNLO) corrections even smaller. This we expect by the convergence of the perturbative series. However we encounter a new difficulty which is the appearance of infinities from ultraviolet (UV) and infrared (IR) divergences in the higher order diagrams. We will now look at their origin and find a way to obtain finite corrections that can be tested against the experimental observations.

For example we can consider the following one-loop integral, associated with the fermion-antifermion gauge boson vertex for massless fermions such that $p_1^2 = p_2^2 = 0$ and $(p_1 + p_2)^2 \neq 0$,

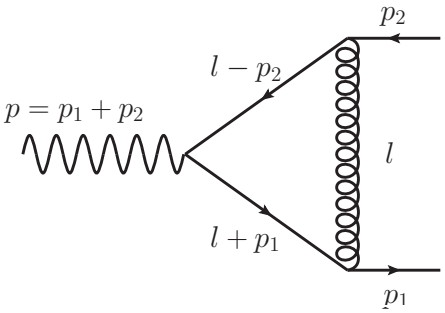

Figure 1.3: Virtual one-loop correction to the fermion-antifermion gauge boson vertex.

$$I = \int \mathrm{d}^4 l \frac{f(l^2)}{(l^2 + i\epsilon)((l + p_1)^2 + i\epsilon)((l - p_2)^2 + i\epsilon)} \tag{1.18}$$

Within perturbation theory the integral I must be carried out over all possible values of the virtual momenta l^μ. We find divergences associated with high virtual momenta,

$$|l| \to \infty \quad \Longrightarrow \quad I \to \infty \qquad \textit{(logarithmically)}$$

called *ultraviolet (UV) divergences*. There are also divergences appearing when one of the propagators in the loop becomes zero for a specific value of the momenta,

$$|l| \to 0, -p_1, p_2 \quad \Longrightarrow I \to \infty$$

called *infrared (IR) divergences*[1]. We considered $p_1^2 = p_2^2 = 0$ but if the propagators are massive, e.g. $(l+p)^2 - m^2$, the mass plays the role of regulator. In QCD, the presence of massless gluons and the assumption of light quarks, gives rise to this divergent behaviour.

The UV divergences are then associated with high energy modes of the theory and will be dealt with a procedure called renormalisation that we will explain in detail in section 1.4.

The IR divergences are associated with low energy modes of the theory and will cancel order by order when we consider also the diagrams from real radiative corrections[2]:

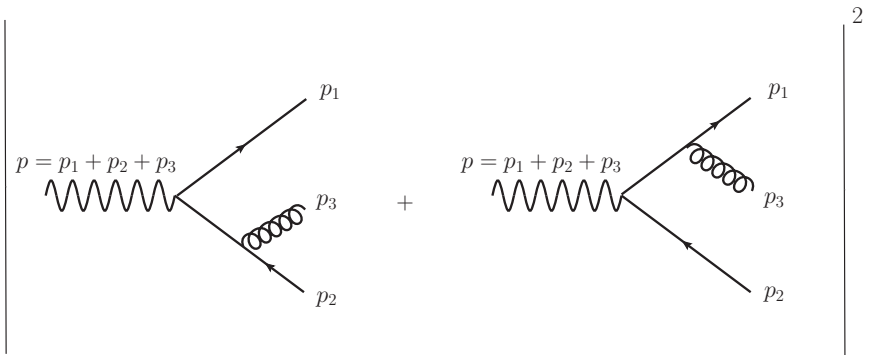

Figure 1.4: Real correction single emission diagrams.

Computing these two diagrams gives the following matrix element:

$$|\mathcal{M}|^2_{qg\bar{q}} \sim \left(\frac{s_{qg}}{s_{\bar{q}g}} + \frac{s_{\bar{q}g}}{s_{qg}} + \frac{2 s_{q\bar{q}} s_{q\bar{q}g}}{s_{qg} s_{\bar{q}g}} \right) \tag{1.19}$$

Parametrising p_q and p_g gives:

$$p_q = E_q(1, \overrightarrow{p_q}), \quad p_g = E_g(1, \overrightarrow{p_g}) \quad \Rightarrow \quad s_{qg} = 2E_g E_q(1 - \cos\theta_{qg}) \tag{1.20}$$

[1] We will use *infrared* to denote both soft and collinear divergences.

[2] The cancellation happens when we add the interference of the virtual amplitude of figure 1.3 with the tree diagram $\gamma \to q\bar{q}$ to the real emission diagrams of figure 1.4. Both quantities are of the same order in α_s.

Therefore, in the regions where the radiated gluon becomes soft ($E_g \to 0$) or collinear with the hard partons ($\theta_{qg} \to 0$) this correction becomes divergent and the final state is indistinguishable from the diagram related to the virtual correction. In this limit the radiated parton cannot be observed by any physical detector so it makes sense to add the cross section for producing these low-energy modes to the cross section without radiation. After regulating both diagrams we see that the IR divergences cancel in the combined result for a particular kind of observables and a finite result is obtained. An example of this will be given in chapter 3.

This example will just be a particular case of the theorems due to Bloch and Nordsieck [4] and Kinoshita [5], Lee and Nauenberg [6] that prove that the IR divergences present in both real and virtual corrections cancel to all orders in perturbation theory.

This means that we have identified the ingredients that build up the higher order corrections for an observed cross section. We must include unresolved contributions up to the order in perturbation theory we wish to calculate. For instance at NLO one must include all real emission diagrams which are single unresolved. This includes single soft and collinear emission which is at equivalent order in α_s to the loop (virtual) corrections. The real emission must be integrated over the unresolved phase space:

$$\sigma_n^{NLO} = \sigma^{(1)}_{n,\text{virtual}} + \int dLIPS(1)\sigma^{(0)}_{n+1,\text{real}} \tag{1.21}$$

At two loops (NNLO) the situation is more complicated as we must include single unresolved contributions at 1-loop and double unresolved contributions at tree level:

$$\sigma_n^{NNLO} = \sigma^{(2)}_{n,\text{virtual}} + \int dLIPS(1)\sigma^{(1)}_{n+1,\text{real}} + \int dLIPS(2)\sigma^{(0)}_{n+2,\text{real}} \tag{1.22}$$

The behaviour at the amplitude level in various soft/collinear limits is universal and we will study it in detail for colour ordered gluonic amplitudes in section 1.8. This will be important to derive counterterms that make the real correction contribution finite in four dimensions. However to perform the analytic cancellation of the IR singularities between real and virtual corrections, as anticipated by the mentioned KLN theorem, and the removal of the UV singularities with renormali-

sation, we still need a regularisation method that will separate the infinities present in these contributions from the finite parts.

The dimensional regularisation scheme works equally for UV and IR divergences and will be described in the next section.

1.3 Dimensional Regularisation

Dimensional regularisation due to 't Hooft and Veltman [7], assumes that the space-time dimension is not 4 but rather D which need not be an integer. Therefore the Lagragian is changed from 4 to D, but the action is still dimensionless. The Feynman integrals become analytic functions of the number of dimensions $D = 4 - 2\epsilon$. Divergent quantities in the usual 4 dimensional space appear now as poles in ϵ, i.e, $1/\epsilon^n$ with $n = 1, 2, ...$ since the $\epsilon \to 0$ limit is equivalent to the $D \to 4$ limit. By doing this, divergent quantities are properly controlled and mathematical manipulations are made legitimately.

At the end of the day for experimentally observable quantities such as cross sections or decay-rates the limit $D \to 4$ ($\epsilon \to 0$) should be well-defined, as all the singularities in the calculation will have dropped out according to the considerations of the previous section.

When going from 4 to D dimensions one must apply the following modifications:

- In the Feynman rules the measure we use to integrate over each loop-momentum k_i changes:

$$\int \frac{d^4 k_i}{(2\pi)^4} \to \int \frac{d^D k_i}{(2\pi)^D}$$

  The poles in ϵ will appear explicitly after the D dimensional integration that we must learn how to perform.

- In D dimensions the metric $g^{\mu\nu}$ obeys $g^{\mu\nu} g_{\mu\nu} = D$. The Clifford algebra will also be affected with Dirac matrices being manipulated as a set of D 4×4 matrices whose contraction identities are modified to:

$$\gamma^{\mu\nu}\gamma_\mu = -2(1-\epsilon)\gamma^\nu, \qquad \gamma^{\mu\nu\rho}\gamma_\mu = 4g^{\nu\rho} - \epsilon\gamma^\nu\gamma^\rho, \ ...$$

- The measure of the phase-space integration over the final state external momenta will also have to be converted:

$$\int \frac{d^3p}{2E(2\pi)^3} \cdots (2\pi)^4\delta^4(p_i - p_f) \to \int \frac{d^{D-1}p}{2E(2\pi)^{D-1}} \cdots (2\pi)^D\delta^D(p_i - p_f)$$

  The soft and collinear singularities are regulated appearing as poles in ϵ.

- the action

$$\mathcal{S} = \int d^D x\, \mathcal{L}$$

  is a dimensionless quantity, so the QCD Lagrangian has to be modified to have a consistent number of dimensions. From the kinetic energy terms of the quarks and gluons of this Lagrangian, we can see that the mass dimension of their fields are

$$\begin{aligned} \text{from} \quad m\bar{\Psi}_f\Psi_f \quad &\Longrightarrow \quad [\Psi_f] = \frac{D-1}{2} \\ \text{from} \quad \partial_\mu A^a_\nu \partial_\nu A^a_\mu \quad &\Longrightarrow \quad [A^a_\mu] = \frac{D}{2} - 1 \end{aligned}$$

  Then the interaction term $g\bar{\Psi}_f \not{A}\Psi_f$ is actually telling us that $[\bar{\Psi}_f \not{A}\Psi_f] = 3D/2 - 2$. Imposing that the interaction term in the Lagrangian should have dimension D we fix the dimension of the coupling constant g to be:

$$[g] = 2 - \frac{D}{2} = \epsilon$$

  In $D = 4$ the coupling constant has no dimension. Since we decided to use the number of dimensions as a regulator our theory acquires one more scale. We introduce an arbitrary mass μ and replace the coupling strength with

$$g \to g\mu^\epsilon \tag{1.23}$$

  where $\epsilon = \frac{4-D}{2}$.

This regularisation method has the advantages that it preserves the gauge invariance of the theory and this guarantees as we will see in the next section the renormalisability of the theory. Also Lorentz invariance is preserved. Other regularisation schemes such as the Cut-off regularisation or the Pauli-Villars regularisation do not enjoy these properties.

Let us now look at the way the D dimensional integrals are done. We can consider as an example the following scalar D-dimensional integral:

$$I_1 = \int \frac{d^D k}{(2\pi)^D} \frac{1}{(k^2 - m^2 + iO^+)^n} \tag{1.24}$$

Starting from the definition of the Gamma function

$$\Gamma(n) = \int_0^\infty dt\ t^{n-1} e^{-t} = \int_0^\infty d(at)(at)^{n-1} e^{-at} = a^n \int_0^\infty dt\ t^{n-1} e^{-at} \tag{1.25}$$

we derive the following identity:

$$\frac{1}{a^n} = \frac{1}{\Gamma(n)} \int_0^\infty dt\ t^{n-1} e^{-at} \tag{1.26}$$

The result for the D dimensional gaussian integral is also useful:

$$\int d^D k e^{-k^2} = \int dk_1 e^{-k_1^2} \int dk_2 e^{-k_2^2} \int ... \int dk_0 e^{-k_0^2} = \pi^{D/2} \tag{1.27}$$

Applying (1.26) to the integral (1.24) we obtain:

$$\begin{aligned} I_1 &= \frac{1}{\Gamma(n)} \frac{(-1)^n}{(2\pi)^D} \int dt\ t^{n-1} \int d^D k e^{-t(-k^2 + m^2 - iO^+)} \\ &= \frac{1}{\Gamma(n)} \frac{(-1)^n}{(2\pi)^D} \int dt\ t^{n-1} e^{-tm^2} \int d^D \left(\frac{k}{\sqrt{t}}\right) e^{k_0^2 - \vec{k}\cdot\vec{k}} \\ &= i \frac{1}{\Gamma(n)} \frac{(-1)^n}{(2\pi)^D} \int_0^\infty dt\ t^{n-1} e^{-tm^2} t^{-D/2} \pi^{D/2} \end{aligned} \tag{1.28}$$

where in the last step we took the $iO \to 0$ limit and did a Wick rotation $k_0 \to ik_0$. The remaining integration is done with (1.25) and we finally obtain:

$$I_1 = \int \frac{d^D k}{(2\pi)^D} \frac{1}{(k^2 - m^2 + iO^+)^n} = \frac{i(-1)^n}{(4\pi)^{D/2}} \frac{\Gamma(n - D/2)}{\Gamma(n)} (m^2)^{D/2 - n} \tag{1.29}$$

Setting $n = 2$ and $D = 4 - 2\epsilon$ in (1.29) we find that:

$$I_1 = \frac{1}{(4\pi)^2} \left(\frac{1}{\epsilon} + \ln(4\pi) - \gamma_e - \ln(m^2) + \mathcal{O}(\epsilon) \right) \tag{1.30}$$

We can see that the singularity reveals itself as a pole of $1/\epsilon$ as anticipated. Other scalar/tensor integrals with more than one propagator can also be calculated along the lines described.

After continuation of the loop momenta into D dimensions one is still left with some freedom concerning the dimensionality of the momenta of the external particles

as well as the number of polarisations for internal and external particles. Within the Conventional Dimensional Regularisation scheme (CDR) no distinction is made between real or virtual particles and massless quarks are considered to have 2 helicity states while gluons have $D-2$ helicities.

In the 't Hooft-Veltman scheme external particles are 4 dimensional and external gluons have 2 helicity states whereas virtual particles are D dimensional and virtual gluons have $D-2$ helicity states. Finally in the four dimensional helicity scheme (FDH) the number of helicity states is 2 for internal and external gluons. Only the momenta of the virtual particles is kept D dimensional. We will mention in more detail the helicity basis for the computation of the amplitudes in section 1.6.

1.4 Renormalisation

The idea behind renormalisation is to reinterpret the parameters of the Lagragian. We proceed by redefining all the fields and parameters in the QCD Lagrangian by a multiplicative factor:

$$A^a_\mu = Z_3^{1/2} A^a_{r,\mu} \tag{1.31}$$

$$\Psi_{f,i} = Z_2^{1/2} \Psi_{r\,f,i} \tag{1.32}$$

$$g_s = Z_g g_{r,s} \tag{1.33}$$

$$\dots$$

Each field/parameter on the left-hand side represents a bare field/parameter whilst those on the right represent renormalised fields/parameters. The renormalisation constants Z absorb the UV divergences and hence represent infinite quantities.

With these modifications the Green's function of the renormalised fields become UV-divergent free as all the UV divergences are now in the multiplicative factors.

In this way the renormalised fields are interpreted as the ones that have a physical meaning and the renormalised couplings as the ones we measure. We can then determine the values of these parameters with a few experiments and compute any other observable in terms of them and the predictive power of theory is not lost.

The renormalisability of the theory is guaranteed by the fact that we don't have

an infinite number of different types of divergent diagrams. The diagrams we need to consider are the quark self-energy, vacuum polarisation or gluon self-energy and the quark-gluon vertex functions, and the divergent terms always appear in the final answer combined with the bare parameters. There is a proof that the divergences in these diagrams can be eliminated to all orders by redefining the free parameters of the theory [7].

It is important to remember now that to regularise the mentioned diagrams we use dimensional regularisation and a new scale μ is introduced in the theory to keep the action dimensionless. The relation between the renormalised strong coupling constant and the "bare" coupling constant is given by:

$$\alpha_b = Z_g^2(\mu^2)^\epsilon \alpha_r \tag{1.34}$$

where the value of Z_g can be calculated perturbatively to give

$$\alpha_b S_\epsilon = (\mu^2)^\epsilon \alpha_r \left[1 - \frac{\beta_0}{\epsilon}\left(\frac{\alpha_r}{2\pi}\right) + \left(\frac{\beta_0^2}{\epsilon^2} - \frac{\beta_1}{2\epsilon}\right)\left(\frac{\alpha_r}{2\pi}\right)^2 + \mathcal{O}(\alpha_r^3)\right] \tag{1.35}$$

where

$$S_\epsilon = e^{-\epsilon\gamma}(4\pi)^\epsilon \tag{1.36}$$

The finite part of the $Z's$ is not fixed at all and to define it we need a renormalisation scheme. In the MS (minimal subtraction *scheme*) the finite part is set to 0 whereas in the $\overline{MS}$ (modified minimal subtraction *scheme*) we remove the UV pole defined as:

$$\frac{1}{\bar{\epsilon}} = (4\pi)^\epsilon e^{-\epsilon\gamma}\frac{1}{\epsilon} \quad \text{with } \gamma \text{ being the Euler's constant.} \tag{1.37}$$

This choice simplifies our calculation because in practice the finite part of the poles always appear in the combination:

$$\frac{\Gamma(1+\epsilon)}{\epsilon}(4\pi)^\epsilon = \frac{1}{\epsilon} + \ln(4\pi) - \gamma + \mathcal{O}(\epsilon) = \frac{1}{\bar{\epsilon}} + \mathcal{O}(\epsilon) \tag{1.38}$$

We have now described the procedure of renormalisation and its final importance in the description of the theory comes from the renormalisation group equations. As we have seen in section 1.1 the invariance of the renormalised quantities under a change of the renormalisation scale μ gives an indication of the asymptotic behaviour of the theory at high energy.

1.5 Factorisation

In this section we will derive the formalism that allows us to tackle computations for processes with hadrons in the initial state. Reviews of this topic can be found in [8–10].

The cross section for a hard scattering process initiated by two hadrons with four-momenta P_1 and P_2 can be written as:

$$\sigma(P_1, P_2) = \sum_{i,j} \int dx_1 dx_2 f_i(x_1) f_j(x_2) \hat{\sigma}_{ij}(x_1 P_1, x_2 P_2, \alpha_s(\mu^2), Q^2/\mu^2) \qquad (1.39)$$

The formula (1.39) is called the parton-model formula and we must discuss its validity when computing hadronic cross sections.

When applying (1.39) we must always require a very large momentum transfer in the reaction. This is because if the scale of the event Q^2 is much bigger than the hadronic scale Λ, characteristic of the binding of the quarks and gluons, the partons behave as free particles in the collision. This means that we can see the hadronic reaction as a scattering of the partons, that is, the point-like constituents of the hadrons. Soft processes will follow that create gluons and quark-antiquark pairs that neutralise colour and respect confinement so that the scattered partons appear as a jet of hadrons travelling in the direction of the momentum transfer. This hadronisation process occurs at an energy scale much lower than the scale Q^2 of the event and therefore has no influence on the hard scattering itself.

We have just stated that the initial state interactions happen too early to affect short-time scale of the hard interaction while the final state interactions between fragments happen too late. The hard scattering depends on the density of partons and the hadronic cross section may be written as the probability of finding a parton with given momentum fraction, in each of the colliding hadrons, times the cross section for the scattering of the two partons as in (1.39).

These effects were first observed experimentally in deep inelastic scattering collisions at SLAC in the 70's. Analogously to the Rutherford experiment with α particles that probed the structure of the atom and led to the discovery of the atomic nucleus, large angle scattering of high-energy electrons probing the proton suggested that the proton is made of smaller, point-like particles that can deflect

the electron by a large amount.

In equation (1.39) the parton distribution functions are universal, that is, independent of the particular hard scattering process that we treat. Their non-perturbative nature implies that they are not computable with the methods of perturbative QCD but instead are obtained by means of a global fit to experimental data for one or more physical processes which can be calculated using perturbative QCD. This is a legitimate procedure as the coupling is small at high energy and the short-distance cross section can be calculated as a perturbation series in the running coupling α_s.

We will now look at the inclusion of higher-order corrections to the parton-model. We will focus on initial-state radiative corrections because they will introduce an important modification of the parton-model formula (1.39). The initial state correction is described by the following diagram:

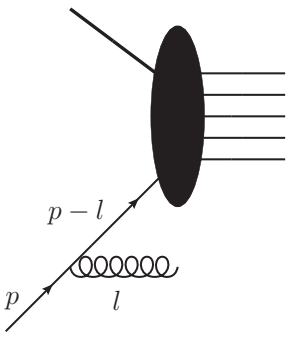

$$A = g_s \mathcal{M}(p-l)\, \frac{\not{p}-\not{l}}{(p-l)^2}\, \gamma^\mu\, u(p) \epsilon_\mu(l)$$

Figure 1.5: NLO corrections to the parton model.

where $\epsilon_\mu(l)$ is the polarisation vector of the emitted gluon and $\mathcal{M}(p-l)$ is the amplitude for a partonic cross section initiated by a quark with momentum $p-l$. We are neglecting at this order a process in which an initial state gluon splits into a quark-antiquark pair. As l becomes parallel to p we expect a collinear singularity and thus it is convenient to write l in the following way:

$$l^\mu = (1-z)p^\mu + l_\perp^\mu + \xi n^\mu \tag{1.40}$$

with $p^2 = 0$ and n is an arbitrary vector such that $n^2 = 0$ and $n \cdot l_\perp = 0$ but $n \cdot p \neq 0$. In terms of these variables the phase space for the emission of the gluon is:

$$\frac{d^3 l}{2l^0 (2\pi)^3} = \frac{d^2 l_\perp}{2(2\pi)^3} \frac{dz}{1-z} \tag{1.41}$$

which yields, from the on-shell conditions for the gluon:

$$\xi = \frac{|l_\perp^2|}{2p \cdot n(1-z)} \quad \text{and} \quad (p-l)^2 = -\frac{|l_\perp^2|}{1-z} \tag{1.42}$$

The amplitude for the radiative correction can now be written as:

$$A = g_s \mathcal{M}(p-l) \frac{\not{p} - \not{l}}{-|l_\perp^2|/(1-z)} \gamma^\mu u(p) \epsilon_\mu(l) \tag{1.43}$$

Using Dirac algebra and keeping only singular terms we can square (1.43) and obtain:

$$|A|^2 = g_s^2 \frac{2}{|l_\perp^2|}(1+z^2)\mathcal{M}(p-l)\frac{\not{p}}{2}\mathcal{M}^\dagger(p-l) \tag{1.44}$$

To get the cross section, we should multiply the above expression by N/p^0 and integrate over the phase space. We obtain:

$$\sigma_q^{(1)} = \frac{\alpha_s C_F}{2\pi} \int \sigma_q^{(0)}(zp) \frac{1+z^2}{1-z} \frac{dl_\perp^2}{l_\perp^2} dz \tag{1.45}$$

where

$$\sigma_q^{(0)}(zp) = N\mathcal{M}(p-l)\frac{\not{p}}{2p^0}\mathcal{M}^\dagger(p-l) \tag{1.46}$$

and we have made use of the relation $g_s^2 = 4\pi\alpha_s$ and the factor $C_F = 4/3$ arises from the colour algebra. This is the contribution due to the real emission of a gluon. Virtual corrections, where the gluon is emitted and reabsorbed by the same line, are also present and when included the final result is:

$$\sigma_q^{(1)} = \frac{\alpha_s C_F}{2\pi} \int \left[\sigma_q^{(0)}(zp) - \sigma_q^{(0)}(p)\right] \frac{1+z^2}{1-z} \frac{dl_\perp^2}{l_\perp^2} dz \tag{1.47}$$

We see that there is an apparent singularity at $z = 1$ corresponding to soft gluon emission which cancels between real and virtual corrections. However the $l_\perp^2$ integral is still divergent in the lower limit. Its upper limit is the scale Q of the typical momenta involved in the hard process.

This is different from the case of final state collinear singularities where we obtain a similar formula to equation (1.47) but with a very important difference: in the born cross section for real emission we would have $\sigma^{(0)}(p)$ instead of $\sigma^{(0)}(zp)$. This property is characteristic of splitting processes taking place in the final state rather than in the initial state. The figure below illustrates this fact:

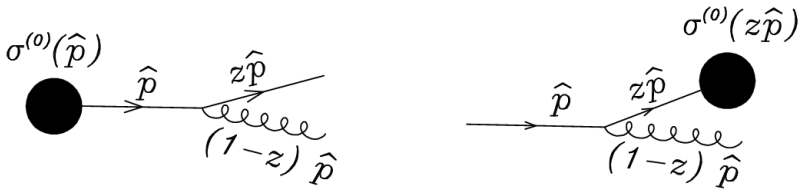

Figure 1.6: Collinear processes in the final and in the initial state.

This means that collinear singularities cancel in the final state, between real and virtual corrections, but the "naive" parton model has uncancelling collinear divergences in the initial state.

In order to proceed we need to introduce some modifications to the parton model to allow the computation of higher order corrections. First of all we define:

$$P_{qq}^{(0)}(z) = C_F \left(\frac{1+z^2}{1-z} \right)_+ \tag{1.48}$$

where the notation with the + suffix is called the *plus prescription*. This prescription introduces a '+'-distribution:

$$\mathcal{D}_n(z) = \left(\frac{\ln^n(1-z)}{(1-z)} \right)_+ \tag{1.49}$$

defined by its action on a generic test function:

$$\int_0^1 dz g(z) \left[\mathcal{D}_n(z)\right]_+ = \int_0^1 dz [g(z) - g(1)] \mathcal{D}_n(z) \tag{1.50}$$

According to this, the expression in (1.48) is to be interpreted as a distribution and its integral against a smooth function $f(z)$ is given by:

$$\int_0^1 \left(\frac{1+z^2}{1-z} \right) f(z) dz = \int_0^1 \frac{1+z^2}{1-z} (f(z) - f(1)) dz \tag{1.51}$$

The quark cross section including one-loop corrections can now be written as:

$$\sigma_q(p) = \sigma_q^{(0)}(p) + \sigma_q^{(1)}(p) = \int \left(\delta(1-z) + \frac{\alpha_s}{2\pi} \log \frac{Q^2}{\lambda^2} P_{qq}^{(0)}(z) \right) \sigma_q^{(0)}(zp) dz \tag{1.52}$$

where we have performed the $l_\perp$ integral in (1.47) with an infrared cutoff λ. We can see that the previous equation has the form of the parton model cross section (1.39) except for the Q^2 dependence. It is telling us that we should consider a parton as

having structure that depends upon the scale at which we are probing it. If we multiply the previous formula by the parton density $f_q(y)$ and integrate in y we get:

$$\sigma(P) = \int dydz f_q(y)\Gamma_{qq}(z, Q^2)\sigma^{(0)}(yzP) \tag{1.53}$$

where

$$\Gamma_{qq}(z, Q^2) = \left(\delta(1-z) + \frac{\alpha_s}{2\pi}\log\frac{Q^2}{\lambda^2}P_{qq}^{(0)}(z)\right) \tag{1.54}$$

The formula (1.53) is the probability to find a parton q in the hadron with a fraction y of its momentum, times the probability to find a parton q in parton q with a fraction z of its momentum, times the cross section for the final parton with momentum yzP. It is more convenient to introduce the identity $\int dx\delta(x-yz)$ so that we can finally obtain:

$$\sigma(P) = \int dx f_q(x, \mu^2)\hat{\sigma}(xP, \mu^2) \tag{1.55}$$

where:

$$\hat{\sigma}(xP, \mu^2) = \sigma^{(0)}(xP) + \frac{\alpha_s}{2\pi}\log\left(\frac{Q^2}{\mu^2}\right)\int dz P_{qq}(z)^{(0)}\sigma^{(0)}(zxP) \tag{1.56}$$

and:

$$\begin{aligned} f_q(x, \mu^2) &= \int dydz f_q(y)\Gamma_{qq}(z, \mu^2)\delta(x-zy) \\ &= f_q(x) + \frac{\alpha_s}{2\pi}\int_x^1 \frac{dy}{y} f_q(y)\log\left(\frac{\mu^2}{\lambda^2}\right) P_{qq}\left(\frac{x}{y}\right) \end{aligned} \tag{1.57}$$

The formula (1.55) is called the *improved parton model* formula and it is the generalisation of the "naive" parton model formula (1.39). To achieve it we introduced a new scale μ called *factorisation scale* that separates long and short distance physics. A parton emitted with transverse momentum less than μ is considered to be part of the hadron structure and is absorbed into the PDF by the redefinition given by equation (1.57). Exactly as for the renormalisation of the coupling constant, we can regard $f_q(x)$ as an unmeasurable *bare* distribution. The collinear singularities are absorbed into this bare distribution at a factorisation scale μ which plays a similar role to the renormalisation scale. The finite contribution which is absorbed into the distribution defines the factorisation scheme. In the $\overline{MS}$ scheme in addition to

the divergent piece a contribution of the form $\ln(4\pi) - \gamma_e$ is also absorbed. Once a scheme has been fixed it must be used in all cross section calculations so that the same results are obtained independent of the scheme used. For example the higher-order corrections to a cross section in hadron-hadron collisions use the same factorisation scheme used to define the parton distributions.

After this procedure is completed we can safely use equation (1.55) because the partonic cross section $\hat{\sigma}(xP, \mu^2)$ is now free from collinear singularities and the redefined parton distribution function $f_q(x, \mu^2)$ which receives contributions from the long-distance (non-perturbative) part of the strong interaction, can be determined from experimental data at any particular scale. A schematic representation of the improved parton model formula is given in figure 1.7.

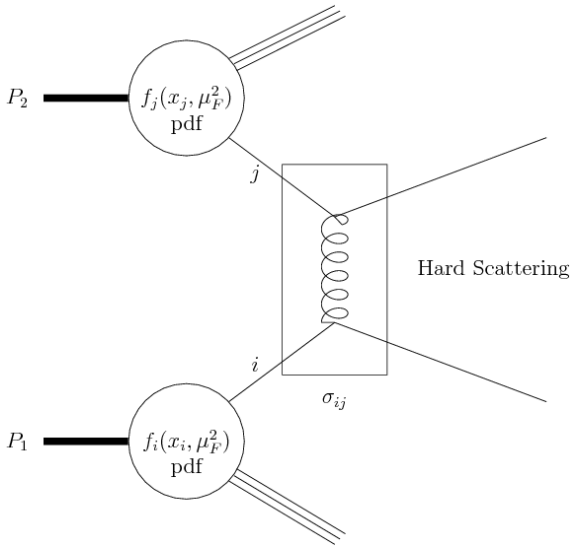

Figure 1.7: Schematic representation of factorisation of hadron/hadron collisions with the improved parton model formula.

In this case the improved parton model formula is:

$$\sigma(P_1, P_2) = \sum_{i,j} \int dx_1 dx_2 f_i(x_1, \mu_F^2) f_j(x_2, \mu_F^2) \hat{\sigma}_{ij}(p_1, p_2, \alpha_s(\mu^2), s/\mu^2, s/\mu_F^2)$$

Also in analogy to the renormalisation group equations already mentioned before we can too calculate the dependence of the parton distribution function on the factorisation scale μ. This is done by demanding μ independence of the hadronic

cross section:

$$\mu^2 \frac{\partial}{\partial \mu^2} \sigma(P) = 0 \tag{1.58}$$

which gives in the general case the Dokshitzer-Gribov-Lipatov-Altarelli-Parisi equation [11–13]:

$$\frac{\partial}{\partial \log \mu^2} f_i(x,\mu) = \int_x^1 \frac{dz}{z} \sum_j P_{ij}(\alpha_s(\mu), z) f_j(x/z, \mu) \tag{1.59}$$

With the equation above, given the parton distribution function at a specified value of μ, we can compute it at any other value. The functions P_{ij} are called splitting functions and have a perturbative expansion in powers of $\alpha_s(\mu)$:

$$P_{ij}(\alpha_s(\mu), z) = \frac{\alpha_s(\mu)}{2\pi} P_{ij}^{(0)} + \left(\frac{\alpha_s(\mu)}{2\pi}\right)^2 P_{ij}^{(1)} + \left(\frac{\alpha_s(\mu)}{2\pi}\right)^3 P_{ij}^{(2)} + \mathcal{O}(\alpha_s^4) \tag{1.60}$$

They can be found in [11] and in [14–17]. Their complete NNLO corrections have been computed and are documented in [18, 19].

The *Factorisation Theorem* [8] generalises our argument to the case of an initial state gluon splitting and proves that the factorisation holds to all orders in perturbation theory.

1.6 Helicity method

In this section we review the helicity method for the computation of tree and loop amplitudes. In this approach the amplitudes are calculated for fixed helicities of all external particles with each possible configuration treated separately.

In the traditional Feynman diagram approach as the number of external particles increases the number of diagrams increases factorially. This leads, in intermediate stages of the calculation, to expressions which become much more complicated than the full result. This is because of large cancellations between different diagrams that are related by gauge invariance. By decomposing the calculation in colour and helicity gauge-invariant pieces, called *partial amplitudes*, we not only reduce the number of diagrams that need to be evaluated but also identify the ones that vanish using the colour/helicity information. This formalism was first developed in references [20–25].

The number of fixed helicity amplitudes that need to be computed can be reduced thanks to symmetries such as parity, that allows one to simultaneously reverse all helicities in an amplitude, and, charge conjugation which allows one to exchange a quark and an anti-quark. Further to this we will see in the next section that the gluonic amplitudes used throughout this thesis decomposed in colour obey cyclic invariance on the gluon indices, line reversal and Ward identities and this reduces the number of independent objects to calculate. The use of supersymmetric identities can also simplify the calculation of loop amplitudes by managing the spins of the particles propagating around the loop.

Once the independent helicity configurations, according to the scattering process that we are interested in, are known, we can evaluate them as complex numbers and then square to obtain the amplitude summed over helicities numerically.

We will now review how to write the amplitude in the most compact form, by using spinor products, and how to evaluate the spinor products numerically to compute the amplitude. We follow closely the notation in [26].

The solutions of the massless Dirac equation contain positive and negative energy solutions interpreted as particles and antiparticles $u(k)$ and $v(k)$. These solutions are identical up to normalisation conventions. Applying the projection operator $P = \frac{1}{2}(1 \pm \gamma_5)$ on $u(k)$ and $v(k)$ yields two helicity states for particles and antiparticles:

$$\begin{aligned} u_\pm(k) &= \frac{1}{2}(1 \pm \gamma_5)u(k) \\ v_\mp(k) &= \frac{1}{2}(1 \pm \gamma_5)v(k) \end{aligned} \tag{1.61}$$

The opposing signs in the equation above reflect that for the negative energy solution $v(k)$ the *helicity* of the antiparticle is the opposite of its *chirality*. The conjugate spinors are:

$$\begin{aligned} \overline{u_\pm(k)} &= \overline{u(k)}\frac{1}{2}(1 \mp \gamma_5) \\ \overline{v_\mp(k)} &= \overline{v(k)}\frac{1}{2}(1 \mp \gamma_5) \end{aligned} \tag{1.62}$$

For amplitudes with a large number of lightlike momenta we use the shorthand notation:

$$|i^\pm\rangle \equiv |k_i^\pm\rangle \equiv u_\pm(k_i) = v_\mp(k_i) \qquad \langle i^\pm| \equiv \langle k_i^\pm| \equiv \overline{u_\pm(k_i)} = \overline{v_\mp(k_i)} \tag{1.63}$$

Amplitudes are expressed in terms of spinor inner products, combinations of the spinor brackets above. They are defined by:

$$\langle ij\rangle \equiv \langle i^-|j^+\rangle = \overline{u_-(k_i)}u_+(k_j) \qquad [ij] \equiv \langle i^+|j^-\rangle = \overline{u_+(k_i)}u_-(k_j) \tag{1.64}$$

For numerical evaluation of the spinor products it is useful to have explicit formulae for them, for some representation of the Dirac γ matrices. In the Dirac representation,

$$\gamma_0 = \begin{pmatrix} \mathbf{1} & \mathbf{0} \\ \mathbf{0} & \mathbf{-1} \end{pmatrix} \qquad \gamma_i = \begin{pmatrix} \mathbf{0} & \sigma^i \\ -\sigma^i & \mathbf{0} \end{pmatrix} \qquad \gamma_5 = \begin{pmatrix} \mathbf{0} & \mathbf{1} \\ \mathbf{1} & \mathbf{0} \end{pmatrix}$$

the massless spinors can be chosen as follows,

$$u_+(k) = v_-(k) = \frac{1}{\sqrt{2}} = \begin{bmatrix} \sqrt{k^+} \\ \sqrt{k^-}e^{i\varphi_k} \\ \sqrt{k^+} \\ \sqrt{k^-}e^{i\varphi_k} \end{bmatrix}, \qquad u_-(k) = v_+(k) = \frac{1}{\sqrt{2}} = \begin{bmatrix} \sqrt{k^-}e^{-i\varphi_k} \\ -\sqrt{k^+} \\ -\sqrt{k^-}e^{-i\varphi_k} \\ \sqrt{k^+} \end{bmatrix}$$

where,

$$e^{\pm i\varphi_k} \equiv \frac{k^1 \pm ik^2}{\sqrt{(k^1)^2+(k^2)^2}} = \frac{k^1 \pm ik^2}{\sqrt{k^+k^-}}, \qquad k^\pm = k^0 \pm k^3 \tag{1.65}$$

We can obtain explicit formulae for spinor products for the case when both energies are positive,

$$\begin{aligned} \langle ij\rangle &= \sqrt{k_i^-k_j^+}e^{i\varphi_{k_i}} - \sqrt{k_i^+k_j^-}e^{i\varphi_{k_j}} = \sqrt{|s_{ij}|}e^{i\phi_{ij}} \\ [ij] &= -\sqrt{k_i^-k_j^+}e^{-i\varphi_{k_i}} + \sqrt{k_i^+k_j^-}e^{-i\varphi_{k_j}} = \sqrt{|s_{ij}|}e^{-i(\phi_{ij}+\pi)} \end{aligned} \tag{1.66}$$

where $s_{ij} = (k_i + k_j)^2 = 2k_i \cdot k_j$ and

$$\cos(\phi_{ij}) = \frac{k_i^1k_j^+ - k_j^1k_i^+}{\sqrt{|s_{ij}|k_i^+k_j^+}}, \qquad \sin(\phi_{ij}) = \frac{k_i^2k_j^+ - k_j^2k_i^+}{\sqrt{|s_{ij}|k_i^+k_j^+}} \tag{1.67}$$

The spinor products are, up to a phase, square roots of Lorentz products. If both or one of the energies are negative we use the same formula (1.66) but with k_i replaced by $-k_i$ if $k_i^0 < 0$ and similarly for k_j, and, with an extra multiplicative factor of i for each negative energy particle. We define $[ij]$ through the identity:

$$\langle ij\rangle[ji] = \langle i^-|j^+\rangle\langle j^+|i^-\rangle = \mathrm{tr}\left(\frac{1}{2}(1-\gamma_5)\not{k}_i\not{k}_j\right) = 2k_i \cdot k_j = s_{ij} \tag{1.68}$$

We have showed that external fermions can be treated as helicity spinors $|i^{\pm}\rangle$ and $\langle i^{\pm}|$. For gluonic amplitudes we also can to construct polarisation vectors from spinor products. Each outgoing gluon or photon is written as a polarisation vector $\epsilon^{\pm}(p,k)$ where p is the momentum of the gluon and k is a reference momentum:

$$\epsilon_{\mu}^{\pm}(p,k) = \pm\frac{\langle p^{\pm}|\gamma_{\mu}|k^{\pm}\rangle}{\sqrt{2}\langle k^{\mp}|p^{\pm}\rangle} \tag{1.69}$$

This form has the desired properties such that states with helicity ± 1 are produced by $\epsilon^{\pm}$. We can make different choices of reference momenta k for each gluon in an amplitude because when all the different terms that contribute are added we always obtain a gauge invariant expression. This can be used to simplify the calculation by making many terms and diagrams vanish.

The convention adopted to label the amplitudes is to assign the helicities to bosons as well as fermions when they are considered outgoing. If they are incoming the helicity is reversed. This means that in the amplitudes derived all the momenta are outgoing. We can then apply crossing symmetry, by exchanging momenta to the initial state, to obtain different scattering amplitudes from the same expression.

1.7 Colour decomposition

Further simplification in the computation of matrix elements comes from treating the colour degree of freedom in a similar manner to the spin degree of freedom described in the previous section. By keeping track of the colour information of external particles it will be possible to factorise the matrix elements as a colour structure times *partial amplitudes* [27–29] . The partial amplitudes are functions of the kinematic invariants only and are easier to calculate than the full amplitude.

To achieve this we begin by identifying all possible colour structures that can appear. The colour, in a general $SU(N)$ theory, comes from quarks carrying a fundamental colour index $i = 1, ..., N$, antiquarks carrying antifundamental "anti-colour" index $\bar{\jmath} = 1, ..., N$ and gluons carrying an adjoint colour index $a = 1, ..., N^2 - 1$.

The generators of the group $T^a_{i\bar{\jmath}}$ connect the fundamental, antifundamental and adjoint representations of the $SU(N)$. This means that for each $q\bar{q}g$ vertex we

introduce a term proportional to $T^a_{i\bar{j}}$ whereas gluons couple through f^{abc} with f being the structure constants of $SU(N)$ defined by:

$$[T^a, T^b]_{i\bar{j}} = i\sqrt{2} f^{abc} T^c_{i\bar{j}} \tag{1.70}$$

We proceed by eliminating any structure constants f^{abc} appearing in Feynman diagrams in favour of the T^a's using:

$$\mathrm{Tr}\left(T^a T^b\right) = \delta^{ab} \tag{1.71}$$

$$f^{abc} = -\frac{i}{\sqrt{2}}\Big(\mathrm{Tr}\left(T^a T^b T^c\right) - \mathrm{Tr}\left(T^c T^b T^a\right)\Big) \tag{1.72}$$

The first property represents the normalisation of the colour algebra that is used in the remainder of this thesis. The advantage of the choice of normalisation in (1.71) is to avoid a proliferation of $\sqrt{2}$'s in the partial amplitudes. If we now apply the previous equation to eliminate the structure constants f_{abc} in favour of the T^a's, we can reduce any tree diagram for n-gluon scattering into a sum of single trace terms. This leads to the following decomposition of the n-gluon tree amplitude:

$$\mathcal{A}_n^{\text{tree}}(\{k_i, \lambda_i, a_i\}) = g^{n-2} \sum_{\sigma \in S_n/Z_n} \mathrm{Tr}(T^{a_{\sigma(1)}} \cdots T^{a_{\sigma(n)}}) A_n^{tree}(\sigma(1^{\lambda_1}), \cdots, \sigma(n^{\lambda_n})) \tag{1.73}$$

Here g is the gauge coupling ($\frac{g^2}{4\pi} = \alpha_s$), k_i, λ_i are the gluon momenta and helicities, and $A_n^{\text{tree}}(1^{\lambda_1}, \cdots, n^{\lambda_n})$ are the colour ordered *partial amplitudes*.

The colour ordered amplitudes are far simpler to calculate than the full amplitude $\mathcal{A}$ because they only receive contributions from diagrams with a particular cyclic ordering of the gluons. Most importantly they are all separately gauge invariant and this allows us to choose a gauge which simplifies the calculation for each colour ordered amplitude independently. They satisfy the following properties:

- $A_n(1, 2, ..., n)$ is gauge invariant
- cyclic symmetry: $A_n(1, 2, ..., n) = A_n(2, 3, ..., 1)$
- reflection symmetry: $A_n(1, 2, ..., n) = (-1)^n A_n(n, n-1, ..., 1)$
- dual Ward identity:
  $A_n(1, 2, 3, ..., n) + A_n(2, 1, 3, ..., n) + ... + A_n(2, 3, ..., 1, n) = 0$

- factorisation of $A_n(1,2,...,n)$ on multi-gluon poles

- incoherence to leading order in the number of colours:

$$\sum_{colours} |\mathcal{A}_n|^2 = (g^2)^{n-2} N^{n-2}(N^2-1) \sum_{\sigma \in S_n/Z_n} \left\{ |A_n(\sigma(1^{\lambda_1}), \cdots, \sigma(n^{\lambda_n}))|^2 + \mathcal{O}(N^{-2}) \right\}$$

To determine the singularities of the colour ordered amplitudes we must remember that fixing the ordering of the gluons means that the poles can only occur in the invariants made out of cyclically adjacent momenta. But for now we leave the discussion of the factorisation on multi-gluon poles mentioned to be done in more detail in the next section.

For amplitudes involving external quarks there are in addition to traces some strings of T^a's terminated by fundamental indices in the colour structure. In this case the Fierz identity between the T matrices:

$$T^a_{i_1\bar{j}_1} T^a_{i_2\bar{j}_2} = \delta_{i_1\bar{j}_2}\delta_{i_2\bar{j}_1} - \frac{1}{N}\delta_{i_1\bar{j}_1}\delta_{i_2\bar{j}_2} \tag{1.74}$$

allows us to find the following colour decomposition for a $\bar{q}qgg\cdots g$ amplitude at tree level:

$$\mathcal{A}_n^{tree}(\{k_i,\lambda_i,a_i\}) = g^{n-2} \sum_{\sigma \in S_{n-2}} (T^{a_{\sigma(3)}} \cdots T^{a_{\sigma(n)}}) A_n^{tree}(1_{\bar{q}}^{\lambda_1}, 2_q^{\lambda_2}, \sigma(3^{\lambda_3}), \cdots, \sigma(n^{\lambda_n})) \tag{1.75}$$

where numbers without subscripts refer to gluons.

This procedure can be continued at the loop level where new structures are generated. This is again an important simplification as it makes possible to break the calculation of even more complex loop matrix elements into many gauge invariant components that can be worked out separately.

1.8 Universal behaviour of QCD gluonic amplitudes

In this section we will recall the divergent behaviour of the colour ordered amplitudes. Unlike QED [30], it is the colour ordered partial amplitudes mentioned in the previous section that have nice factorisation properties in the unresolved limits.

Following from the factorisation of the primitive amplitudes on multi-gluon poles we want to look at the factorisation properties at the amplitude squared level which is valid for the leading colour diagonal piece. These were first derived in [31]. We will consider first one unresolved parton, which is appropriate for isolation of infrared singularities of $(n+1)$ parton scattering processes contributing at next-to-leading order and then, two unresolved partons relevant to isolate singularities of the $(n+2)$ scattering processes contributing at next-to-next-to-leading order.

In both cases we find that the factorisation is:

- *universal*, in the sense that we only need to specify the type of singular limit and the singular behaviour (at leading order in colour) will have a characteristic structure
- is *process independent*, in the sense that it does not depend on the detailed structure of $|A_{n+1}(1,2,\ldots,n+1)|^2$
- is always in the form of *singular term*$\times$*finite subamplitude squared*

This study provides many insights into the infrared structure of QCD amplitudes. In addition to this, subtraction methods to handle the occurrence of infrared divergences at higher order, like the one used in this thesis, rely on constructing counterterms with the same pointwise singular behaviour of the divergent amplitudes. The precise formulation of the antenna subtraction method employed in this work and how the counterterms are derived will be established in chapters 3,4. However, the following results will be fundamental to guarantee that both matrix elements and subtraction terms have the same infrared structure for one unresolved parton (NLO) up to two unresolved partons (NNLO).

1.8.1 One unresolved particle

For an n tree gluon amplitude we have, in the limit where gluon b is soft, the QED-like factorisation into an eikonal-type singular factor and a colour ordered tree-level squared amplitude where gluon b has been removed:

$$|A_{n+1}(1,\ldots,a,b,c,\ldots,n+1)|^2 \overset{b_g\to 0}{\longrightarrow} S_{abc}\,|A_n(1,\ldots,a,c,\ldots,n+1)|^2 \quad (1.76)$$

with the eikonal factor given by:

$$S_{abc} = \frac{2s_{ac}}{s_{ab}s_{bc}} \tag{1.77}$$

Similarly in the limit where two gluons become collinear, the sub-amplitudes factorise. If gluons a and b become collinear and form gluon c, then adjacent gluons give a singular contribution:

$$|A_{n+1}(1,\ldots,a,b,\ldots,n+1)|^2 \quad \xrightarrow{a//b} \quad \frac{1}{s_{ab}} P_{gg\to g}(z)|A_n(1,\ldots,c,\ldots,n+1)|^2 \tag{1.78}$$

while separated gluons do not,

$$|A_{n+1}(1,\ldots,a,\ldots,b,\ldots,n+1)|^2 \quad \xrightarrow{a//b} \quad \text{finite} \tag{1.79}$$

In equation (1.78), z is the fraction of momentum carried by one of the gluons and, after integrating over the azimuthal angle of the plane containing the collinear particles with respect to the hard process, the Altarelli-Parisi [11] collinear splitting function $P_{gg\to g}$ is given by:

$$P_{gg\to g}(z) = 2\left(\frac{z}{1-z} + \frac{1-z}{z} + z(1-z)\right) \tag{1.80}$$

As we mentioned before the singular limits (1.76) and (1.78) are of the form of a singular term times a finite subamplitude squared with one less gluon.

1.8.2 Two unresolved particles

In the case of two real unresolved particles there are a variety of different configurations extensively studied in [32–34]. The expressions for these universal limits are organised according to whether the two unresolved particles are colour connected or not. In the unconnected case, the singular limits are merely obtained by multiplying single unresolved factors. However, when the particles are colour connected, the structure is more involved.

To define colour connection we return to the equation (1.73) where the n gluon subamplitude is associated with the colour structure $\mathrm{Tr}(T^{a_{\sigma(1)}}\cdots T^{a_{\sigma(n)}})$ depicted in figure 1.8.

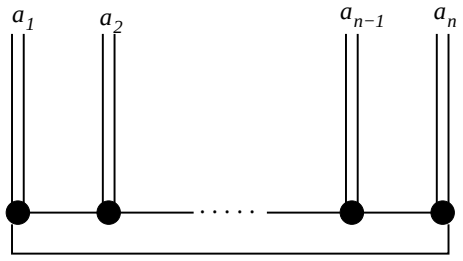

Figure 1.8: Colour flow contained in the colour ordered amplitude $A_n^{tree}(1^{\lambda_1}, \cdots, n^{\lambda_n})$.

This is a colour antenna with ordered emission of gluons with colour $a_1, a_2, \ldots, a_{n-1}, a_n$. Within this colour antenna, gluon 1 is colour connected to gluon 2 which is colour connected to next gluon in the chain until gluon n which is colour connected to gluon 1.

Two collinear pairs - colour unconnected

Two pairs of particles may become collinear separately, but the particle in one or both the pairs themselves not "colour connected". In these cases there are no singular contributions containing both of the vanishing invariants. For instance if partons $\{a, d\}$ and $\{b, c\}$ are collinear then,

$$|\mathcal{A}(\ldots, a, \ldots, b, \ldots, c, \ldots, d, \ldots)|^2 \rightarrow \text{less singular} \tag{1.81}$$

By this we mean there is no contribution proportional to $1/s_{ad}s_{bc}$ and, when integrated over the small region of phase space relevant for this approximation yields a negligible contribution.

The situation where two pairs of colour "connected" gluons are collinear is rather trivial. If gluons a and b form P while c and d cluster to form Q so that P and Q are themselves colour unconnected then,

$$|\mathcal{A}(\ldots, a, b, \ldots, c, d, \ldots)|^2 \rightarrow \frac{1}{s_{ab}} P_{gg\rightarrow G}(z_1) \frac{1}{s_{cd}} P_{gg\rightarrow G}(z_2) |\mathcal{A}(\ldots, P, \ldots, Q, \ldots)|^2 \tag{1.82}$$

Here z_1 and z_2 are the momentum fractions carried by a and c respectively. As before, azimuthal averaging of the collinear particle plane is understood.

Triple collinear factorisation - colour unconnected

If three collinear particles are colour "unconnected" then there is no singularity. So if a,b and c all become collinear,

$$|\mathcal{A}(\ldots,a,\ldots,b,\ldots,c,\ldots)|^2 \to \text{finite} \tag{1.83}$$

and there is no singular contribution involving the invariants s_{ab},s_{bc} or s_{abc}. As before, because the region of phase space where the triple collinear limit is valid is extremely small, this gives a negligible contribution to the cross section. When two of the three collinear particles are colour "unconnected" we find a singular result,

$$|\mathcal{A}(\ldots,a,\ldots,b,c,\ldots)|^2 \to 1/s_{bc}$$

However, when integrated over the triple collinear region of phase space that requires s_{ab},s_{bc} or s_{abc} all to be small, we again obtain a negligible contribution that is proportional to the small parameter defining the extent of the triple collinear phase space. We therefore ignore contributions of this type.

Soft/collinear factorisation - colour unconnected

Two particles may be unresolved if one of them is a soft gluon and another gluon pair is collinear. When the soft gluon g is not colour connected to either of the colour "connected" collinear particles c and d, factorisation is straightforward,

$$|\mathcal{A}(\ldots,a,g,b,\ldots,c,d,\ldots)|^2 \to S_{agb}(s_{ab},s_{ag},s_{bg})\frac{1}{s_{cd}}P_{gg\to G}(z)|\mathcal{A}(\ldots,a,b,\ldots,P,\ldots)|^2$$

Two soft gluons - colour unconnected

When two unconnected gluons are soft, factorisation is again simple. For gluons g_1 and g_2 soft we find,

$$\begin{aligned}|\mathcal{A}(\ldots,a,g_1,b,\ldots,c,g_2,d,\ldots)|^2 \;&\to S_{ag_1b}(s_{ab},s_{ag_1},s_{bg_1})S_{cg_2d}(s_{cd},s_{cg_2},s_{dg2})\\ &\times|A(\ldots,a,b,\ldots,c,d,\ldots)|^2\end{aligned} \tag{1.84}$$

so that the singular factor is merely the product of two single soft gluon emission factors given by (1.77). Note that $b=c$ is allowed.

Triple collinear factorisation - colour connected

In this configuration three colour connected gluons cluster to form a single parent gluon. The colour ordered sub-amplitude squared then factorises:

$$|\mathcal{A}(\ldots,a,b,c,\ldots)|^2 \to P_{ggg\to G}(w,x,y,s_{ab},s_{ac},s_{bc},s_{abc})|\mathcal{A}(\ldots,P\ldots)|^2 \qquad (1.85)$$

where w, x and y are the momentum fractions of the clustered partons,

$$p_a = wp_P, \qquad p_b = xp_P, \qquad p_c = yp_P, \qquad \text{with} \quad w+x+y=1 \qquad (1.86)$$

The colour ordered function $P_{ggg} \to G$ is given by,

$$\begin{aligned} P_{abc\to G}(w,x,y,s_{ab},s_{bc},s_{abc}) = 2\times \Bigg\{ & \\ + \quad & \frac{(1-\epsilon)}{s_{ab}^2 s_{abc}^2}\frac{(xs_{abc}-(1-y)s_{bc})^2}{(1-y)^2} + \frac{2(1-\epsilon)s_{bc}}{s_{ab}s_{abc}^2} + \frac{3(1-\epsilon)}{2s_{abc}^2} \\ + \quad & \frac{1}{s_{ab}s_{abc}}\left(\frac{(1-y(1-y))^2}{yw(1-w)} - 2\frac{x^2+xy+y^2}{1-y} + \frac{xw-x^2y-2}{y(1-y)} + 2\epsilon\frac{x}{(1-y)}\right) \\ + \quad & \frac{1}{2s_{ab}s_{bc}}\left(3x^2 - \frac{2(2-w+w^2)(x^2+w(1-w))}{y(1-y)} + \frac{1}{yw} + \frac{1}{(1-y)(1-w)}\right)\Bigg\} \\ + \quad & (s_{ab}\leftrightarrow s_{bc}, w\leftrightarrow y)\ , \end{aligned} \qquad (1.87)$$

This splitting function is symmetric under the exchange of the outer gluons (a and c), and contains poles only in s_{ab} and s_{bc}.

Soft/collinear factorisation - colour connected

In the situation when gluon a is soft, gluons b and c are collinear and colour connected the gluonic subamplitude factorises as:

$$|\mathcal{A}|(\ldots,d,a,b,c,\ldots)|^2 \to P_{d;abc}|\mathcal{A}(\ldots,d,P,\ldots)|^2 \qquad (1.88)$$

In this limit the collinear gluons form parton P and carry momentum fractions,

$$p_b = zp_P, \qquad p_c = (1-z)p_P \qquad (1.89)$$

and we write the soft/collinear factor as,

$$P_{d;abc}(z,s_{ab},s_{bc},s_{abc},s_{ad},s_{bd},s_{cd}) \qquad (1.90)$$

This limit can be obtained directly from the triple collinear limit of the previous section by keeping only terms proportional to $1/w$ and subsequently replacing $1/w$ by $(s_{bd}+s_{cd})/s_{ad}$, $1/(1-w)$ by 1 and y by $(1-z)$.

In fact in this limit we find a universal soft factor multiplied by a collinear splitting function,

$$P_{d;abc}(z, s_{ab}, s_{bc}, s_{abc}, s_{ad}, s_{bd}, s_{cd}) = S_{d;abc}(z, s_{ab}, s_{bc}, s_{abc}, s_{ad}, s_{bd}, s_{cd})\frac{1}{s_{bc}}P_{gg\to G}(z) \tag{1.91}$$

where,

$$S_{d;abc}(z, s_{ab}, s_{bc}, s_{abc}, s_{ad}, s_{bd}, s_{cd}) = \frac{(s_{bd}+s_{cd})}{s_{ab}s_{ad}}\left(z + \frac{s_{ab}+zs_{bc}}{s_{abc}}\right) \tag{1.92}$$

A similar result holds for gluon c becoming soft,

$$|\mathcal{A}(\ldots, a, b, c, e, \ldots)|^2 \to P_{abc;e}|\mathcal{A}(\ldots, P, e, \ldots)|^2 \tag{1.93}$$

where,

$$P_{abc;e} = P_{d;abc}(a \leftrightarrow c, d \leftrightarrow e) \tag{1.94}$$

In the case that b is soft the matrix element do not possess sufficient singularities since the collinear gluons a and c are not directly colour-connected,

$$|\mathcal{A}(\ldots, a, b, c, \ldots)|^2 \to \text{less singular} \tag{1.95}$$

Here, there may be two powers of small invariants in the denominator, but, when integrated over the appropriate (small) region of phase space this yields a vanishing contribution.

Two soft gluons factorisation - colour connected

For gluons b and c soft the colour ordered subamplitude factorises,

$$|\mathcal{A}(\ldots, a, b, c, d, \ldots)|^2 \to S_{abcd}(s_{ad}, s_{ab}, s_{cd}, s_{bc}, s_{abc}, s_{bcd})|\mathcal{A}(\ldots, a, d, \ldots)|^2 \tag{1.96}$$

where the connected double soft gluon function is given by,

$$S_{abcd}(s_{ad}, s_{ab}, s_{cd}, s_{bc}, s_{abc}, s_{bcd}) = \frac{2s_{ad}^2}{s_{ab}s_{bcd}s_{abc}s_{cd}}$$

$$+\frac{2s_{ad}}{s_{bc}}\left(\frac{1}{s_{ab}s_{cd}}+\frac{1}{s_{ab}s_{bcd}}+\frac{1}{s_{cd}s_{abc}}-\frac{4}{s_{abc}s_{bcd}}\right)+\frac{2(1-\epsilon)}{s_{bc}^2}\left(\frac{s_{ab}}{s_{abc}}+\frac{s_{cd}}{s_{bcd}}-1\right)^2. \tag{1.97}$$

Here a and d are the hard gluons surrounding the soft pair.

1.9 Summary

In this chapter we have collected all the ingredients required to calculate a perturbative solution to QCD in powers of the strong coupling α_s. By doing this we reviewed some of the most important aspects of the theory and a practical application should now be addressed. This will be the topic of the next chapter.

Chapter 2

Dijet production

In the previous chapter we described in a general way the technicalities that are inherent in the theoretical description of a physical observable. Now we want to apply those concepts to the study of dijet production at the LHC.

We proceed by making the definition of a jet from both the theoretical and experimental point of view in section 2.1. Subsequently, the first theoretical estimates for jet production are given by the leading order cross section that we review in section 2.2.

We already know that beyond leading order a method is required to handle the infrared divergences present in the intermediate steps of the calculation. We will address this problem in the next chapter.

2.1 Jet definition

Since the first propostion for the quark model was announced independently by Gell-Mann [35] and Zweig [36, 37] in 1964, several searches to disprove it or confirm it were attempted. The quark model was able to classify the baryons and mesons that were discovered throughout the 50's and 60's in a simple picture, where every baryon is composed of three elementary quarks and every meson is composed of a quark and an antiquark. New combinations of these states led to the prediction and subsequent discovery of additional hadrons. So far combinations which are excluded from the quark model have not been found.

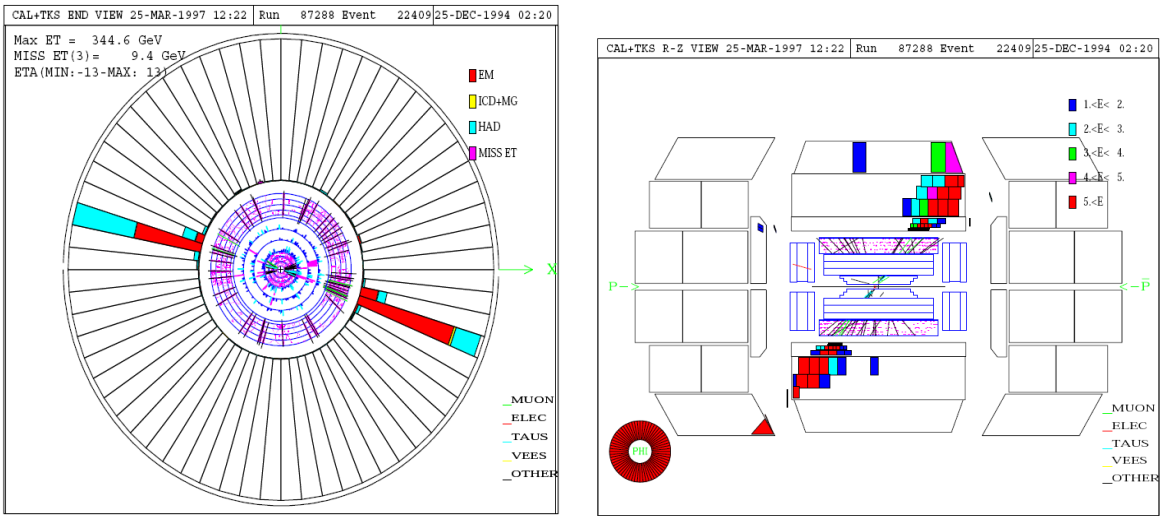

Figure 2.1: (a) End view and (b) side view of a high E_T event recorded at D0.

The structure of the proton in terms of quarks is one of the predictions of the model and experiments carried out in the late 60's at the Stanford Linear Accelerator Center (SLAC), indicated that indeed the proton has substructure. By increasing the energy in the collisions involving protons we would expect to be able to break this substructure apart and observe the quarks in the detector. Signals of this should be straightforward because quarks carry fractional electric charge and at least one of them should be absolutely stable. However in successive generations of experiments with more and more powerful colliders, isolated quarks have never been observed.

This problem with the quark model has been reformulated by introducing the idea of *quark confinement*. In this notion quarks are *absolutely confined* within baryons and mesons and cannot be studied or observed in any more direct way than at a hadron level. This property of QCD is intuitively related to the fact that the force-carrying gluons of the strong interaction are charged and as a consequence the force between quarks increases as they are separated. In this picture free quarks fly apart but when they reach a separation distance of around 10^{-15} m (the diameter of a hadron) their strong interaction is so great that new quark-antiquark pairs are produced mainly from gluons. Thus many quark and antiquark pairs are produced in a typical modern experiment that subsequently join together in combinations of mesons and baryons that are actually recorded by the detector. This results in a

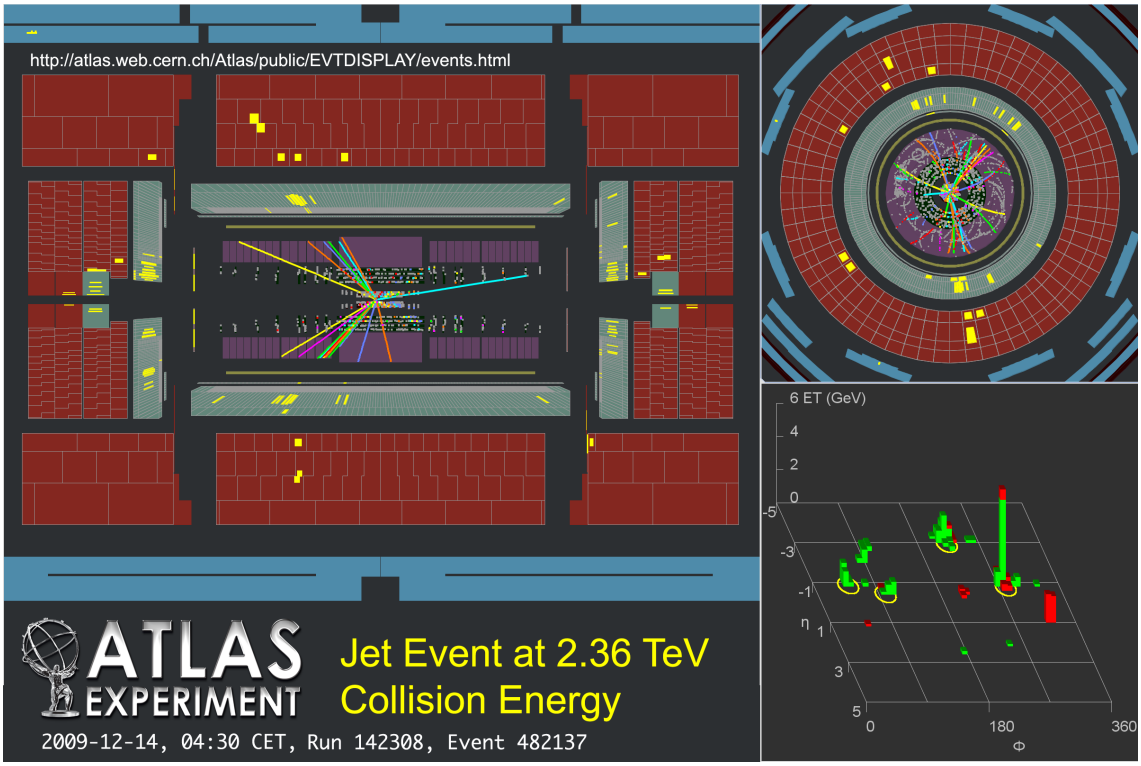

Figure 2.2: Display of an event recorded by ATLAS with jets from the first pp collisions at center of mass energy of 2.36 TeV. (Taken on December 14th 2009).

"spray" of roughly collinear colourless hadrons that are called jets.

In figure 2.1 we show an example of a two-jet event recorded at the Tevatron resulting from a $p\bar{p}$ collision. We identify two clusters of energy appearing back to back with high transverse energy which are composed of individual hadron tracks highly collimated. We also see additional tracks and energy deposits between the two outgoing hard scattered jets. These contain hadrons that do not fit in the jets and constitutes the underlying event. This underlying event consists of particles that arise from the beam-beam remnants and from multiple parton interactions. It is an unavoidable background to most collider observables and it is the reason why hadron-hadron collisions are more "messy" than electron-positron annihilations.

In figure 2.2 we show the first events with jets recorded by the ATLAS detector with the LHC running at the highest center of mass energy achieved to date of 2.36 TeV.

To understand these reactions we have to proceed then by classifying the hadronic

events according to the number of such clusters of energetic particles, referred to as jets. The rate of these events can then be measured by introducing a procedure to quantify the number of jets in the event at the detector level that we will discuss below. On the theoretical side we use the concept of local parton-hadron duality which postulates that the quantum numbers and momentum flow of the produced hadrons closely follow those of the partons that initiated the jet. If we suppose that the effects of hadronisation - the process whereby quarks and gluons cluster to form hadrons - are small, we should obtain a reasonable agreement between theory and experiment associating one jet with each parton.

This means that the measured cross section for high-E_T jet production in hadron colliders should follow closely the prediction obtained by computing the same cross section in the parton model, considering the scattering of free partons given by the matrix elements at fixed order in perturbative QCD.

To make this description more accurate and hence closer to the real world we can compute the hard scattering cross section to higher order in the strong coupling α_s. This introduces additional partons in the final state that can cluster to form a spray of partons, much like the spray of hadrons observed in the experiments.

However since it is impossible to calculate and integrate the matrix elements for the typical large number of partons produced in a collision (of the order of 30) another refinement is the inclusion of a parton shower, matched to the fixed-order perturbative calculation, that simulates soft and collinear QCD radiation from the hard scattering scale down to the hadronisation scale where hadronisation models can be incorporated to describe the formation of hadrons from quarks and gluons.

Jet algorithms

As we mentioned in the previous section, we need to formulate a procedure to quantify the meaning of a jet. The goal is to apply an algorithm both to data and to the theoretical calculation without ambiguities such that a reliable comparison can be made between the two. The jet algorithms must satisfy certain criteria. For example, on the experimental side they should be:

- detector independent, as they should not depend on the details of the detector

geometry.

- minimising energy smearing or angular biases.
- stable with luminosity, that is the jet size behaves well under multiple scatterings and high detector occupancy.
- computationally efficient in the reconstruction of jets from N particles.
- easy to calibrate.

On the theoretical side the requirements are:

- infrared and collinear safety, as the cross sections must be finite at any order of perturbation theory and emission of soft particles should not change the number of jets in the event.
- low sensitivity to hadronisation.
- invariant under longitudinal boosts.
- produce the same number of jets at parton, particle and detector level.

According to this, two broad classes of jet algorithms are in widespread use at modern colliders. These are the sequential recombination type algorithms and cone type algorithms that we describe in the next subsections. A recent extensive review on the topic of jet algorithms can be found in [38].

Sequential recombination type algorithms

Sequential recombination type algorithms such as k_t [39,40] and Cambridge/Aachen [41,42] define jets by repeatedly combining particles that are close in some distance measure d_{ij}. For e^+e^- experiments the following steps are implemented:

1. For each pair of particles i, j compute the distance measure d_{ij}.
2. Find the minimum d_{min} of all the d_{ij}.
3. If d_{min} is below some jet resolution threshold d_{cut} then recombine i and j into a single new particle and repeat step 1.

4. Otherwise, declare all remaining particles to be jets and terminate the iteration.

For these algorithms a single parameter d_{cut} controls the number of jets. As d_{cut} approaches zero we allow very narrow jets until eventually all hadrons are identified as separate jets. Conversely, increasing the value of d_{cut} produces broader jets with far fewer multi-jet events.

When it comes to derive a corresponding hadron collider algorithm there is an introduction of an additional particle-beam distance d_{iB}. In that case if d_{iB} is the smallest distance we declare i to be a final state jet and remove it from the list of particles before returning to step 1.

These type of algorithms are infrared and collinear safe because any soft or collinear particle will get recombined right at the start of the clustering.

The choice of the distance measure d_{ij} is what defines the sequential recombination algorithm. This choice has to be adapted to e^+e^- experiments or experiments with incoming hadrons. For example in pp collisions it is important that the choice of distance is invariant under longitudinal boosts.

Problems with this type of algorithms are the irregular shape of the jets (which makes them harder to calibrate at the detector level) and how to incorporate non-perturbative corrections. They are also often quoted as computationally slow as the procedures needed to cluster N particles scale like N^3. We will look at new developments that address these issues in the next section.

anti-k_t jet clustering algorithm

The anti-k_t [43] jet algorithm for hadron colliders generalises the distance measure of the k_t [39, 40] and Cambridge/Aachen [41, 42]:

$$\begin{aligned} d_{ij} &= \min(k_{t_i}^{2p}, k_{t_j}^{2p})\frac{\Delta R_{ij}^2}{R^2}, \qquad \Delta R_{ij}^2 = (y_i - y_j)^2 + (\phi_i - \phi_j)^2, \\ d_{iB} &= p_{t_i}^{2p} \end{aligned} \tag{2.1}$$

where k_{t_i}, y_i and ϕ_i are respectively the transverse momentum, rapidity and azimuth of particle i. The d_{ij} are the distances between entities i and j and d_{iB} is the distance

between entity i and the beam (B). From their definitions we can easily see that the distances are invariant under longitudinal boosts.

The clustering process proceeds by identifying the smallest of the distances and, if it is a d_{ij}, recombining entities i and j, while if it is d_{iB} identifying i as a jet and removing it from the list of entities. The distances are recalculated and the procedure repeated until no entities are left. We have introduced a new parameter R that acts as a size and defines what gets called a jet. The remaining parameter p takes the values $p = 1$ for the k_t algorithm and $p = 0$ for the Cambridge/Aachen.

The value $p = -1$ defines the anti-k_t algorithm and the distance measure $d_{ij} = \min(1/k_{t_i}^2, 1/k_{t_j}^2)\Delta_{ij}^2/R^2$ defines its general behaviour. According to the definition of d_{ij}, the distance between similarly separated hard and soft particle or two soft particles will be larger in the latter case due to the transverse momentum of the hard particle. This causes soft particles to cluster with hard ones before they cluster among themselves [43]. If a hard particle has no hard neighbours within a distance $2R$ then it will simply accumulate all the soft particles within a circle of radius R, resulting in a perfectly conical jet.

The case of two hard particles within $R < \Delta_{12} < 2R$ creates two hard jets. If $k_{t_1} \gg k_{t_2}$ then jet 1 will be conical and jet 2 will be partly conical missing the part overlapping with jet 1. Instead if $k_{t_1} = k_{t_2}$ neither jet will be conical and the overlapping part will simply be divided by a straight line equally between the two. For the general case $k_{t_1} \sim k_{t_2}$, both cones will be clipped, with the boundary b between them defined by $\Delta R_{1b}/k_{t_1} = \Delta R_{2b}/k_{t_2}$.

Finally when we have $\Delta_{12} < R$ hard particles 1 and 2 will cluster to form a single jet. If $k_{t_1} \gg k_{t_2}$ then it will be a conical jet centered on k_{t_1}. For $k_{t_1} \sim k_{t_2}$ the shape will be the union of the cones (with radius $< R$) around each hard particle plus a cone (of radius R) centred on the final jet.

The previous paragraphs tell us that soft particles do not modify the shape of the jet, while hard particles do. The jet boundary in the anti-k_t algorithm is then resilient with respect to soft radiation, but flexible with respect to hard radiation.

To address the speed issue of the sequential-recombination clustering algorithms, reference [44] proposed a solution that reduces the computational time for the re-

construction of N particles from N^3 to $N \ln N$. This solution comes from rewriting the problem of jet-finding into a two dimensional (rapidity and azimuth coordinates) computational geometry nearest neighbour finding problem.

Technically, the problem is that of establishing and maintaining a nearest-neighbour graph on the 2-dimensional surface of a cylinder. In computational geometry this is addressed with Voronoi diagrams as a main structure. This has an approach implemented in a public code CGAL that handles dynamic point sets in the construction of Voronoi diagrams for N points with $\mathcal{O}(N \ln N)$ operations.

Combining these ideas and other strategies an implementation of the anti-k_t jet clustering algorithm is publicly available in the FastJet [45] implementation.

Cone type algorithms

The cone type algorithms follow a different approach to the jet definition. In such algorithms, a seed particle i sets some initial direction, and one sums the momenta of all particles j within a circle ("cone") of radius R around i in azimuthal angle ϕ and rapidity y:

$$\Delta R_{ij}^2 = (y_i - y_j)^2 + (\phi_i - \phi_j)^2 < R^2 \tag{2.2}$$

where y_i and ϕ_i are respectively the rapidity and azimuth of particle i. The direction of the resulting sum is then used as a new seed direction and one iterates the procedure until the direction of the resulting cone is stable.

Therefore seeded algorithms have to define how to pick the seeds and then two main procedures, one to find a "stable cone" (a cone pointing in the same direction as the momentum of its contents) and a "split-merge" procedure to convert those cones into jets, somehow resolving the problem of cones that have particles in common.

One solution is to take as the first seed the particle with the largest transverse momentum. Once a stable cone has been found with this seed, one calls it a jet and removes all the particles contained in that jet. After that, the next seed is the hardest particle among those that remain and use that to find the next jet, repeating the procedure until no particles are left. This procedure guarantees that there are no overlapping cones but it is collinear unsafe, as the splitting of the hardest particle

(say p_1) into a nearly collinear pair (p_{1a}, p_{1b}) can alter the ordering of the hardest particles in the event and thus leading to a different final set of jets.

The split-merge approach merges a pair of cones if more than a fraction f of the softer cone's transverse momentum is in particles shared with the harder cone; otherwise the shared particles are assigned to the cone to which they are closer. Generally the overlap threshold f is chosen to be 0.5 or 0.75. One of the main issues with this approach is again not being collinear safe since the addition of a new soft seed particle can lead to new stable cones being found involving hard particles and thus, altering the final set of jets.

Infrared and collinear unsafety problems have to be corrected since they can violate the finiteness of perturbative QCD calculations, by altering the cancellation between real and virtual corrections, but also invalidate the correspondence between the complex hadron level and a simple few-parton picture of an event. This happens when a random 1 GeV non-perturbative particle changes the multi-hundred GeV events.

A solution to these problems is to carry out a seedless search for all stable cones. We will see an example of that in the next section.

SISCone - Seedless infrared safe cone algorithm

In a seedless cone algorithm, the addition of a soft particle may lead to the presence of new stable cones, however none of those new cones will involve hard particles and therefore the multi-hundred GeV events are not altered and therefore the set of hard stable cones is infrared safe.

To find the stable cones one takes all subsets of particles and draws a circle around the jet axis of each particle, made from the momentum of all the particles within a radius of it, and checks if the points contained in the circle are exactly as those in the initial subset.

However, this procedure takes $\mathcal{O}(N2^N)$ time to compute all the subsets and check the stable cone property, making it impossible to use at hadron or detector level. The SISCone implementation [46] reduces this to $\mathcal{O}(N^2 \ln N)$, following the observations in [44] that considering the geometrical aspects of the problem can be

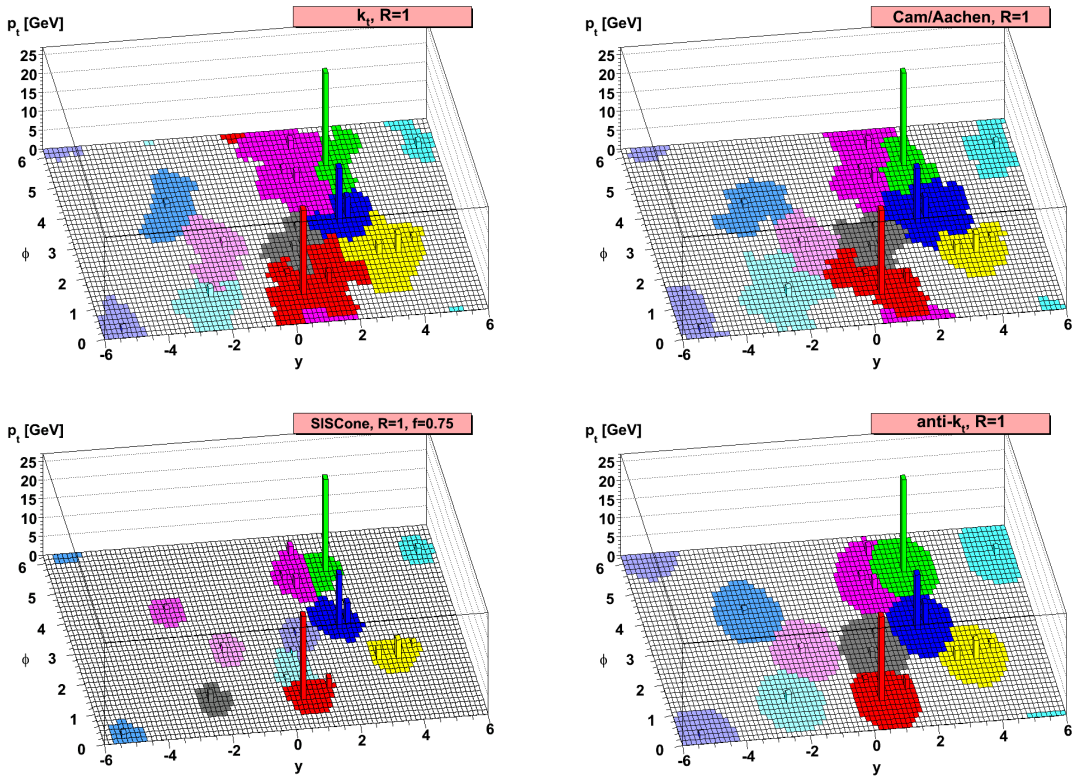

Figure 2.3: A sample parton-level event together with many random soft "ghosts", clustered with four different jet algorithms, illustrating the "active" catchment areas of the resulting hard jets [38].

advantageous.

In the SISCone approach, the stable cone search reduces to a 2D "all distinct circular enclosures" problem solved by considering all circles having a pair of particles on their circumference, resulting in an seedless infrared safe cone algorithm that takes $\mathcal{O}(N^2 \ln N)$ time to reconstruct the jets. The code for the algorithm is available publicly [47] both in standalone form and as a FastJet [45] plugin.

Jet algorithms - final remarks

We presented two types of strategies for jet definition: the use of sequential recombination jet algorithms and cone algorithms. Both methods will be used in future experiments, as it has been noted in [48], that for some observables they provide complementary sensitivities to different classes of non-perturbative corrections.

It is crucial that jets are defined in an infrared safe way to make measurements meaningful when compared to fixed order (LO,NLO,NNLO) predictions. In addition, they should be computationally efficient in the jet reconstruction and we have reviewed two examples that address both issues.

Figure 2.3 illustrates the jets that are produced with four different IRC-safe algorithms, showing among other things the degree of regularity of the boundaries of the resulting jets. Also in figure 2.4 the timings in terms of scaling with N are shown for a subset of commonly used algorithms.

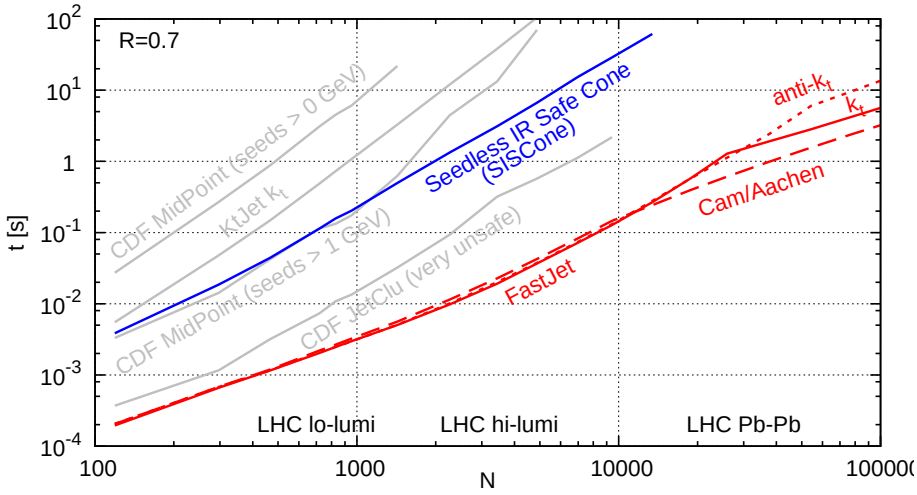

Figure 2.4: Timings for the clustering of a simulated 50 GeV dijet event, to which increasing numbers of simulated minimum-bias events have been added (both simulated with Pythia) [38].

At the time of writing both ATLAS and CMS will incorporate FastJet [45] within their software frameworks. CMS will use the k_t algorithm and SISCone as their default jet collections whereas ATLAS has adopted the anti-k_t jet clustering as the standard choice.

2.2 LO cross section

In this section we review the leading order (LO) cross section for dijet production:

$$p + p \rightarrow j + j \tag{2.3}$$

This reaction will be investigated at the LHC, *i.e.* pp collisions at $\sqrt{s} = 14$ TeV where the jets arises from the large angle scattering of the elementary constituents of the hadrons, the quarks and gluons. The use of a jet algorithm in the prediction allows to determine also the single inclusive jet cross section $pp \to j + X$ according to the experimental cuts. This offers an important precision test of QCD since this reaction can be measured to a very high experimental accuracy and therefore be used for measurements of the strong coupling constant and of parton distribution functions. It is also important if we want to look for a breakdown of the standard model due, for example, to the composite structure of quarks or production of new particles. For this we would analyse the scattering of quarks and gluons at the largest p_T scale possible and look for deviations in the form of resonances or in the shape of the QCD prediction.

The hadronic cross section for the process initiated by two hadrons with four-momenta P_1 and P_2 can be written in factorised form as:

$$d\sigma(P_1, P_2) = \sum_{i,j} \int dx_1 dx_2 f_i^{(h_1)}(x_1, \mu_F^2) f_j^{(h2)}(x_2, \mu_F^2) \mathrm{d}\hat{\sigma}_{ij}(p_1, p_2, \alpha_s(\mu_R^2), Q^2/\mu_R^2) \tag{2.4}$$

The sum is over the parton flavors i, j in the hadrons h_1, h_2 and $f_i^{(h_1)}$, $f_j^{(h_2)}$ are the corresponding parton densities. The initial state partons i,j for the hard scattering partonic process carry momenta $p_1 = x_1 P_1$ and $p_2 = x_2 P_2$. The characteristic scale of the hard scattering denoted by Q could be the transverse momentum of a jet. The μ_F and μ_R are respectively the factorisation and renormalisation scales introduced in chapter 1. The partonic cross section can be calculated perturbatively and it gives at leading order:

$$\mathrm{d}\hat{\sigma}_{ij}^{LO} = \mathrm{d}\Phi_2(p_k, p_l; p_1, p_2) \frac{1}{S_2} \overline{\sum_{\substack{colour \\ spin}}} |M^0_{ij\to kl}|^2 J_2^{(2)}(p_k, p_l) \tag{2.5}$$

where the matrix elements that we need to consider are:

$$\begin{aligned} q + q' &\to q + q' \\ q + q &\to q + q \\ q + \bar{q} &\to g + g \end{aligned}$$

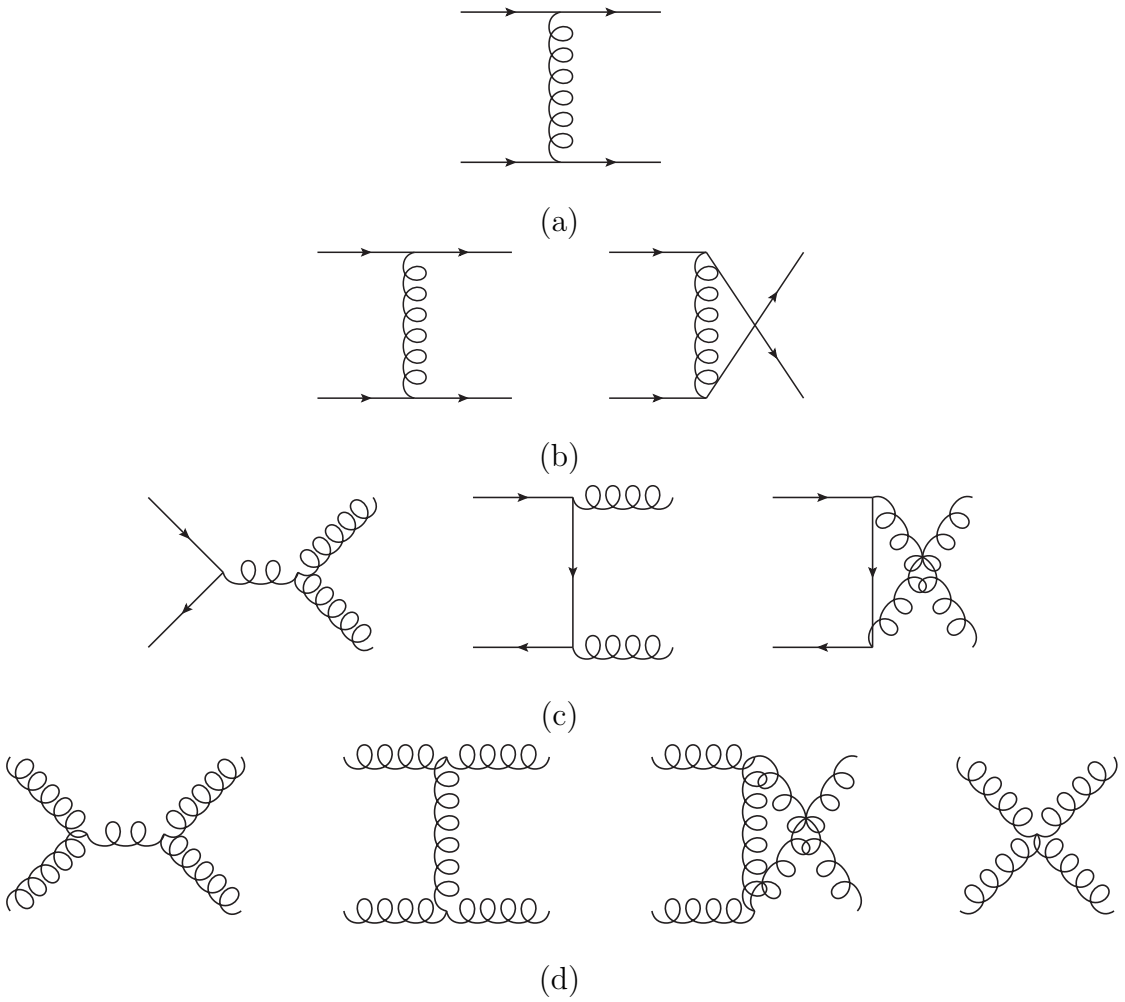

Figure 2.5: Diagrams for jet production at leading order.

$$g + g \;\rightarrow\; g + g \tag{2.6}$$

which are shown in figure 2.5. These are the independent matrix elements squared for $2 \to 2$ parton subprocesses with massless partons [49]. All other channels can be obtained from the above by time reversal and crossing. S_2 is the symmetry factor for identical partons in the final state and $\overline{\sum}$ denotes an appropriate sum and average over spin and colour degrees of freedom for incoming and outgoing particles. Each quark in the initial state is ascribed a colour average of $1/N$ while gluons receive a factor $1/(N^2-1)$. Since a fermion has two spin degrees of freedom, an additional factor of $1/2$ has to be included for unpolarised quarks. For gluons $2(1-\epsilon)$ polarisation states are possible in d dimensions. $\mathrm{d}\Phi_2(p_k, p_l; p_1, p_2)$ is the

$2 \to 2$ phase space for a final state with total momentum $p_1^\mu + p_2^\mu$:

$$\mathrm{d}\Phi_2(p_k, p_l; p_1, p_2) = \frac{\mathrm{d}^{d-1}p_k}{2E_k(2\pi)^{d-1}} \frac{\mathrm{d}^{d-1}p_l}{2E_l(2\pi)^{d-1}} (2\pi)^d \delta^d(p_1 + p_2 - p_k - p_l) \tag{2.7}$$

Finally the function $J_n^{(m)}$ defines an n-jet final state through cuts on the m-parton final state momenta. In this case, there are two partons, each of which must produce a jet.

Because the center of mass of the parton-parton scattering is normally boosted with respect to that of the two incoming hadrons, it is useful to classify the final state in terms of variables which transform simply under longitudinal boosts. We proceed by parameterising the four-momentum of a particle with mass m using the rapidity y, the transverse momentum p_T and the azimuthal angle ϕ:

$$\begin{aligned} p^\mu &= (E, p_x, p_y, p_z) \\ &= (m_T \cosh\, y, p_T \sin\phi, p_T \cos\phi, m_T \sinh\, y) \end{aligned} \tag{2.8}$$

where the transverse mass is defined as $m_T = \sqrt{p_T^2 + m^2}$. The rapidity y is defined by:

$$y = \frac{1}{2} \ln\left(\frac{E + p_z}{E - p_z}\right) = \frac{1}{2} \ln\left(\frac{1 + \beta\cos\theta}{1 - \beta\cos\theta}\right) \tag{2.9}$$

and is additive under the restricted class of Lorentz transformations corresponding to a boost along the z direction. Rapidity differences are boost invariant.

In the high energy limit ($\beta \to 1$) or in the massless case ($m \to 0$) the rapidity is often replaced by the pseudorapidity variable η:

$$\eta = -\ln\tan(\theta/2) \tag{2.10}$$

It is a more convenient variable experimentally, since the angle θ from the beam direction is measured directly in the detector. It is also standard to use the transverse energy:

$$E_T = E\sin\theta \tag{2.11}$$

rather than the transverse momentum p_T, because it is the former quantity which is measured in the hadron calorimeter. For massless particles the rapidity y and

pseudorapidity η may be used interchangeably, as may the transverse momentum p_T and transverse energy E_T.

The cross section for a $2 \rightarrow 2$ scattering process is given by:

$$\frac{E_3 E_4 \mathrm{d}\sigma^{LO}}{d^3p_3 d^3p_4} = \frac{1}{16\pi^2} \overline{\sum_{\substack{colour \\ spin}}} |\mathcal{M}|^2 \delta^4(p_1 + p_2 - p_3 - p_4) \tag{2.12}$$

We can obtain the inclusive jet cross section at the parton level, in terms of the new variables, by integrating (2.12) over the momentum of one of the jets:

$$\frac{E\mathrm{d}\sigma^{LO}}{d^3p} \equiv \frac{\mathrm{d}\sigma^{LO}}{dyd^2p_T} = \frac{1}{8\pi^2} \overline{\sum_{\substack{colour \\ spin}}} |\mathcal{M}|^2 \delta(s + t + u) \tag{2.13}$$

where t and u are fixed by s and the center of mass scattering angle,

$$t = -\frac{1}{2}s(1 - \cos\theta) \qquad u = -\frac{1}{2}s(1 + \cos\theta) \tag{2.14}$$

There are several limitations when we truncate the prediction at leading order. The calculation becomes strongly dependent on the choice of renormalisation scale, that enters using the running coupling constant, due to the absence of higher order terms. Also, the absence of diagrams including initial sate radiation means that at this order the jets always appear back to back. Furthermore, a single parton is identified with a jet and there are no extra radiation to give the jet a shape. Thus the cross section is independent of the parameter R that defines the jet size contrary to what is measured in a detector and this also makes it impossible to study the energy profile of a jet.

2.3 Summary

In this chapter we defined from the experimental and theoretical point of view the jet production phenomena as observed in hadron colliders.

On the experimental side we discussed the need for good algorithms that can classify the recorded events at the detector level according to the number of produced jets. For hard scattering events we expect an agreement between the measured data and QCD predictions. These also implement the same jet algorithms to define jet

observables and are given by the partonic cross section which can be calculated perturbatively as a power series in the coupling constant folded with the parton distribution functions.

We analysed the LO term of the series for jet production in pp collisions and will turn to the more interesting case of NLO contributions in the next chapter.

Chapter 3

NLO antenna subtraction

When we consider now the NLO corrections to an observable we expect to find the divergences mentioned in chapter 1. As we have seen theorems guarantee that these singularties cancel when all the divergent pieces are assembled together. That is usually achieved within a subtraction formalism.

Therefore we introduce the antenna subtraction method as a solution to this problem. We leave the next-to-next-to-leading order (NNLO) extension of this method to the next chapter and concentrate for the moment on the next-to-leading order (NLO) antenna subtraction. The building blocks are, as we will see, antenna functions that we introduce in section 3.1. The numerical implementation for final-final, initial-final and initial-initial kinematic configurations is also treated in section 3.2.

After that we illustrate the application of the method for the next-to-leading order (NLO) real and virtual corrections to dijet production in sections 3.3, 3.4. As we expect for an infrared safe observable, we will obtain the cancellation of infrared divergences between the two contributions.

We finally end the chapter with the motivation to extend this calculation to next-to-next-to-leading order (NNLO) accuracy.

3.1 Antenna subtraction at NLO

Suppose we want to compute the m-jet cross section to NLO. According to the considerations of chapter 1, we have to consider the exclusive cross section $\mathrm{d}\sigma^R$ with $(m+1)$-partons in the final state, the one-loop correction $\mathrm{d}\sigma^V$ with m-partons in the final state, and a mass factorisation counterterm $\mathrm{d}\sigma^{MF}$ to absorb the divergences arising from initial state collinear radiation into the parton densities:

$$\mathrm{d}\sigma_{NLO} = \int_{\mathrm{d}\Phi_{m+1}} \mathrm{d}\sigma^R_{NLO} + \int_{\mathrm{d}\Phi_m} \mathrm{d}\sigma^V_{NLO} + \int_{\mathrm{d}\Phi_m} \mathrm{d}\sigma^{MF}_{NLO} \tag{3.1}$$

The terms on the right hand side of (3.1) are separately divergent although their sum is finite. To write a Monte Carlo program to compute those integrals we must first isolate and cancel the singularities of the different pieces and then numerically evaluate the finite remainders of the $(m+1)$ and m-parton channels to obtain the NLO contribution to the cross section.

Subtraction schemes are a well established solution to this problem. They work by finding a suitable counterterm $\mathrm{d}\sigma^S_{NLO}$ for $\mathrm{d}\sigma^R_{NLO}$. It has to satisfy two properties, namely it must have the same singular behaviour in all appropriate limits as $\mathrm{d}\sigma^R_{NLO}$ and yet be simple enough to be integrated analytically over all singular regions of the $(m+1)$-parton phase space in d dimensions. We proceed by rewriting (3.1) in the following form:

$$\mathrm{d}\sigma_{NLO} = \int_{\mathrm{d}\Phi_{m+1}} \left(\mathrm{d}\sigma^R_{NLO} - \mathrm{d}\sigma^S_{NLO}\right) + \int_{\mathrm{d}\Phi_m} \left(\int_1 \mathrm{d}\sigma^S_{NLO} + \mathrm{d}\sigma^V_{NLO} + \mathrm{d}\sigma^{MF}_{NLO}\right) \tag{3.2}$$

In its unintegrated form $\mathrm{d}\sigma^S_{NLO}$ has the same singular behaviour as $\mathrm{d}\sigma^R_{NLO}$ such that the first integral is finite by definition and can be integrated numerically in four dimensions over the $(m+1)$-parton phase space. The integrated form of the counterterm $\mathrm{d}\sigma^S_{NLO}$ then analytically cancels the explicit singularities of the virtual contribution $\mathrm{d}\sigma^V_{NLO}$ and the mass factorisation counterterm $\mathrm{d}\sigma^{MF}_{NLO}$ as required by the KLN and *Factorisation theorems* mentioned in chapter 1. After checking the cancellation of the pole pieces, we can take the finite remainders of these contributions and perform the last integral on the right hand side of (3.2) numerically over the m-parton phase space.

The actual form of the counterterm $\mathrm{d}\sigma^S_{NLO}$ depends on the subtraction formalism employed because there are many ways of approximating the $(m+1)$-parton matrix elements in the neighbourhood of its soft and collinear singularities.

Using the general properties of soft and collinear emission Catani and Seymour [50] proposed a subtraction method that is completely *process independent*. They derived an improved factorisation formulae, called dipole formulae:

$$\mathrm{d}\sigma^S_{NLO} = \sum_{\text{dipoles}} \mathrm{d}\sigma_{LO} \otimes \mathrm{d}V_{\text{dipole}} \tag{3.3}$$

The dipole factors are universal, i.e., completely independent on the details of the process and built from the physical knowledge of how the $(m+1)$-parton matrix elements behave in soft and collinear limits. They can be computed once and for all and applied to any process to mimic any of the $(m+1)$-parton singularities that are kinematically degenerate with a given m-parton state.

Alternative approaches include the FKS subtraction [51–53] and more recently [54]. It is also important to mention that both the Catani-Seymour [50] and FKS [51] subtraction terms have been implemented in an automated way in [55–60] and [61] respectively. These packages aim to automatically generate the subtraction terms and real emission amplitudes for any given process. Used in conjunction with recent automated packages that compute the virtual contribution [62–65], there is the exciting possibility of having an automated NLO QCD parton level event generator available in the near future.

For the rest of this thesis we are going to employ the antenna subtraction method [66–69]. This method has been extended to NNLO but we leave that discussion to the next chapter. Here we focus only on the antenna subtraction at NLO. In this method, antenna functions describe the colour-ordered radiation of unresolved partons between a pair of hard (radiator) partons. We must distinguish three possible configurations of radiators: final-final when both radiators are final state partons, initial-final when one radiator is an initial state parton and the other radiator is a final state parton and, finally, initial-initial where both radiators are initial state partons.

This means that we will derive subtraction formulae decomposed in these three

	final-final	initial-final	initial-initial
e^+e^-	✓	✗	✗
ep	✓	✓	✗
pp	✓	✓	✓

Table 3.1: Antennae configurations needed according to the scattering process

configurations and label them with a superscript $(ff), (if), (ii)$. In table 3.1 we distinguish the configurations that are needed according to the scattering process that we are interested in. Even though we will write down all formulae specifically for pp collisions these formulae can be easily adapted to ep or e^+e^- for the configurations they have in common. To achieve that we should only modify the number of partons that enter the matrix elements in these formulae. This is because we obtain an m-jet production at leading order from an m-parton matrix element in e^+e^-, an $(m+1)$-parton matrix element in ep and an $(m+2)$-parton matrix element in pp.

To proceed we write down the m-jet real radiation cross section at NLO in pp collisions:

$$\begin{aligned} \mathrm{d}\sigma^R_{NLO} &= \mathcal{N} \sum_{\text{perms}} \mathrm{d}\Phi_{m+1}(k_1, \ldots, k_{m+1}; p_1, p_2) \frac{1}{S_{m+1}} \\ &\quad \times |\mathcal{M}_{m+3}(k_1, \ldots, k_{m+1}; p_1, p_2)|^2 J^{(m+1)}_m(k_1, \ldots, k_{m+1}) \end{aligned} \tag{3.4}$$

The normalisation factor $\mathcal{N}$ includes all QCD-independent factors as well as the dependence on the renormalised QCD coupling constant α_s. $|\mathcal{M}_{m+3}(k_1, \ldots, k_{m+1}; p_1, p_2)|^2$ is a colour ordered amplitude squared and the sum in (3.4) is over all colour orderings including a symmetry factor S_{m+1} for identical partons in the final state. The initial state momenta are labeled as usual as p_1 and p_2 whereas the $(m+1)$-momenta in the final state are labeled $k_1, \ldots, k_{m+1}$. $\mathrm{d}\Phi_{m+1}$ is then the $2 \to m+1$ particle phase space:

$$\begin{aligned} &\mathrm{d}\Phi_{m+1}(k_1, \ldots, k_{m+1}; p_1, p_2) = \\ &\frac{\mathrm{d}^{d-1}k_1}{2E_1(2\pi)^{d-1}} \cdots \frac{\mathrm{d}^{d-1}k_{m+1}}{2E_{m+1}(2\pi)^{d-1}} (2\pi)^d \delta^d(p_1 + p_2 - k_1 - \ldots - k_{m+1}) \end{aligned} \tag{3.5}$$

The jet function $J^{(m+1)}_m(k_1, \ldots, k_{m+1})$ defines the procedure for building m-jets from

$(m+1)$-partons. The main property of $J_m^{(m+1)}$ is that the jet observable defined above is collinear and infrared safe.

Antenna subtraction - final-final configuration

When summing over all colour orderings in equation (3.4) we find terms of this type:

$$|M_{m+3}(\ldots,i,j,k,\ldots)|^2 \tag{3.6}$$

where i,j,k are colour connected final state partons. This configuration contains a singularity when j is unresolved between i and k which can be approximated by:

$$X_{ijk}|M_{m+2}(\ldots,\widetilde{IJ},\widetilde{JK},\ldots)|^2 \tag{3.7}$$

where X_{ijk} is a final-final antenna function that describes all configurations (for this colour-ordered amplitude) where parton j is unresolved. The momenta for the new partons $\widetilde{IJ}$ and $\widetilde{JK}$ are linear combinations of k_i,k_j,k_k obtained with a final-final mapping that we describe in section 3.2.1. Both radiator partons i and k are in the final state and we call this situation a final-final antenna, depicted in figure 3.1. We still have to sum over all possible unresolved partons in this colour ordered amplitude. After that we can then sum over all colour orderings to obtain the full subtraction term, for the final-final configuration, to use with (3.4). The subtraction term for this configuration reads:

$$\begin{aligned}\mathrm{d}\sigma^{S,(ff)} &= \mathcal{N}\sum_{\text{perms}}\mathrm{d}\Phi_{m+1}(k_1,\ldots,k_{m+1};p_1,p_2)\frac{1}{S_{m+1}}\\ &\times\sum_j X^0_{ijk}|\mathcal{M}_{m+2}(k_1,\ldots,\tilde{K}_{IJ},\tilde{K}_{JK},\ldots;p_1,p_2)|^2 J_m^{(m)}(k_1,\ldots,\tilde{K}_{IJ},\tilde{K}_{JK},\ldots,k_{m+1})\end{aligned} \tag{3.8}$$

The subtraction term involves the $(m+2)$-parton amplitude depending only on the redefined on-shell momenta $k_1,\ldots,\tilde{K}_{IJ},\tilde{K}_{JK},\ldots,k_{m+1}$, where $\tilde{K}_{IJ},\tilde{K}_{JK}$ are linear combinations of k_i,k_j,k_k, while the tree antenna function X^0_{ijk} depends only on k_i,k_j,k_k. The momenta redefinition that generates on-shell momenta $\tilde{K}_{IJ},\tilde{K}_{JK}$ and implements momentum conservation will be discussed in section 3.2.1.

The jet function $J_m^{(m)}$ in (3.8) does not depend on the individual momenta k_i, k_j and k_k, but only on $\tilde{K}_{IJ},\tilde{K}_{JK}$. One can therefore carry out the integration over the

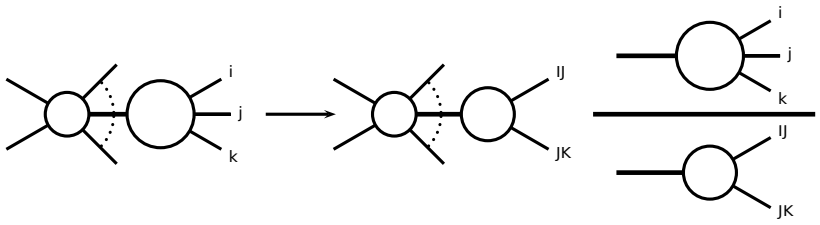

Figure 3.1: Antenna factorisation for the final-final situation.

unresolved dipole phase space appropriate to k_i, k_j and k_k analytically, exploiting the factorisation of the phase space,

$$\begin{aligned}&\mathrm{d}\Phi_{m+1}(k_1,\ldots,k_{m+1};p_1,p_2) = \\ &\quad \mathrm{d}\Phi_m(k_1,\ldots,\tilde{K}_{IJ},\tilde{K}_{JK},\ldots,k_{m+1};p_1,p_2)\cdot \mathrm{d}\Phi_{X_{ijk}}(k_i,k_j,k_k;\tilde{K}_{IJ}+\tilde{K}_{JK}) \quad (3.9)\end{aligned}$$

The NLO antenna phase space $\mathrm{d}\Phi_{X_{ijk}}$ is proportional to the three-particle phase space relevant to a $1 \to 3$ decay.

For the analytic integration, we can use (3.9) to rewrite each of the subtraction terms in the form:

$$|\mathcal{M}_{m+2}|^2 \, J_m^{(m)} \, \mathrm{d}\Phi_m \int \mathrm{d}\Phi_{X_{ijk}} \, X_{ijk}^0,$$

The analytic integral of the subtraction term is therefore defined as the antenna function integrated over the fully inclusive antenna phase space, normalised appropriately,

$$\mathcal{X}_{ijk}^0(s_{ijk}) = \frac{1}{C(\epsilon)} \int \mathrm{d}\Phi_{X_{ijk}} \, X_{ijk}^0. \quad (3.10)$$

where

$$C(\epsilon) = (4\pi)^\epsilon \frac{e^{-\epsilon\gamma}}{8\pi^2} \quad (3.11)$$

This integration is performed analytically in d dimensions to make the infrared singularities explicit and added directly to the one-loop m-particle contributions. The factor $(8\pi^2\,(4\pi)^{-\epsilon}\,e^{\epsilon\gamma})$ in the above equation is related to the normalisation of the renormalised coupling constant (1.35).

Factors of g^2 that appear in real radiation and virtual contributions can be combined with $C(\epsilon)$ to give:

$$g^2 C(\epsilon) = \left(\frac{\alpha_s}{2\pi}\right) \bar{C}(\epsilon) \quad (3.12)$$

where:

$$\bar{C}(\epsilon) = (4\pi)^{\epsilon} e^{-\epsilon\gamma} \tag{3.13}$$

Antenna subtraction - initial-final configuration

In the presence of hadrons in the initial state, matrix elements exhibit singularities that are not accounted by the subtraction terms discussed in the previous section. These singularities are due to soft or collinear radiation within an antenna where one or the two hard partons are in the initial state [68]. This occurs in equation (3.4) when in the ordered amplitude parton j is unresolved between an initial state parton and a final state parton:

$$|\mathcal{M}_{m+3}(\hat{1}, \hat{2}, j, k, \ldots)|^2 \tag{3.14}$$

The hat denotes the initial state partons. The singularities of j between initial state parton $\hat{2}$ and final state parton k can be approximated by:

$$X_{2,jk}|\mathcal{M}_{m+2}(\hat{1}, x\hat{2}, \widetilde{JK}, \ldots)|^2 \tag{3.15}$$

where $X_{2,jk}$ is an initial-final antenna function that describes configurations (for this colour-ordered amplitude) where parton j is unresolved. The mapping that generates the new momenta $\widetilde{JK}$ and the fraction x will be discussed in 3.2.2. This configuration is depicted in figure 3.2. The full subtraction term for the the initial-final configuration reads:

$$\begin{aligned} \mathrm{d}\sigma^{S,(if)} &= \mathcal{N} \sum_{\text{perns}} \mathrm{d}\Phi_{m+1}(k_1, \ldots, k_{m+1}; p_1, p_2) \, \frac{1}{S_{m+1}} \\ &\times \sum_j X^0_{2,jk} \left| \mathcal{M}_{m+2}(k_1, \ldots, \tilde{K}_{JK}, \ldots, k_{m+1}; p_1, xp_2) \right|^2 \, J^{(m)}_m(k_1, \ldots, \tilde{K}_{JK}, \ldots, k_{m+1}) \end{aligned} \tag{3.16}$$

Replacing $1 \to 2$ generates the subtraction term associated with singularities with the other incoming parton.

The terms necessary to subtract singularities associated with coloured particles in the initial state can then be simply obtained by crossing the corresponding antennae for final state singularities. Due to the different kinematics involved, the factorisation of the phase space is slightly more involved and the corresponding phase space

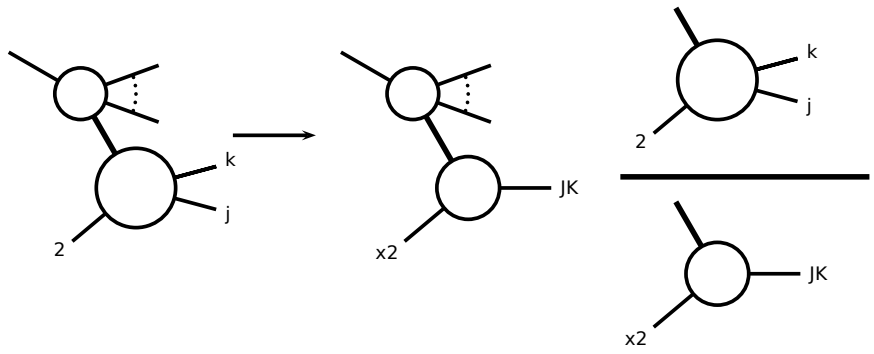

Figure 3.2: Antenna factorisation for the initial-final situation.

mappings are different. To cancel explicit infrared poles in virtual contributions and in terms arising from parton distribution mass factorisation, the crossed antennae must be integrated, analytically, over the corresponding phase space.

The tree antenna $X^0_{i,jk}$, depending only on the original momenta p_i, k_j and k_k, contains all the configurations in which parton j becomes unresolved. The $(m+2)$-parton amplitude depends only on redefined on-shell momenta $k_1, \ldots, \tilde{K}_{JK}, \ldots$, and on the momentum fraction x.

The jet function, $J^{(m)}_m$, in (3.16) depends on the momenta k_j and k_k only through $\tilde{K}_{JK}$. Thus, provided a suitable factorisation of the phase space, one can perform the integration of the antennae analytically. Due to the hard particle in the initial state, the factorisation of phase space is not as straightforward as for final-final antennae.

The phase space can be factorised as an m-parton phase space convoluted with a two particle phase space [68]:

$$\begin{aligned} \mathrm{d}\Phi_{m+1}(k_1, \ldots, k_{m+1}; p_1, p_2) &= \mathrm{d}\Phi_m(k_1, \ldots, \tilde{K}_{JK}, \ldots, k_{m+1}; p_1, xp_2) \\ &\times \frac{Q^2}{2\pi}\mathrm{d}\Phi_2(k_j, k_k; p_2, q)\frac{\mathrm{d}x}{x} \end{aligned} \tag{3.17}$$

with $Q^2 = -q^2$ and $q = k_j + k_k - p_2$. Replacing the phase space in (3.16), we can explicitly carry out the integration of the antenna factors over the two particle phase space. When combining the integrated subtraction terms with virtual contributions and mass factorisation terms, it turns out to be convenient to normalise the

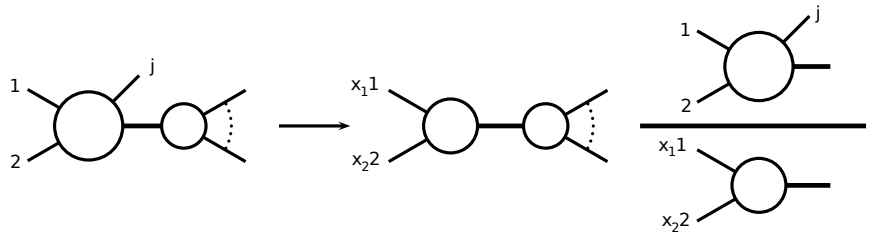

Figure 3.3: Antenna factorisation for the initial-initial situation.

integrated antennae as follows

$$\mathcal{X}_{i,jk} = \frac{1}{C(\epsilon)} \int \mathrm{d}\Phi_2 \frac{Q^2}{2\pi} X_{i,jk} \,, \tag{3.18}$$

where $C(\epsilon)$ is given in (3.11).

Antenna subtraction - initial-initial configuration

The last situation to be considered is when the two hard radiators are in the initial state. The following colour ordered amplitude:

$$|\mathcal{M}(\hat{1}, j, \hat{2}, k, l, \ldots)|^2 \tag{3.19}$$

has the singularities of j between initial state partons $\hat{1}$ and $\hat{2}$. These singularities can be approximated by:

$$X_{12,j} |\mathcal{M}(x_1 p_1, x_2 p_2, \tilde{k}, \tilde{l}, \ldots)|^2 \tag{3.20}$$

where $X_{12,j}$ is an initial-initial antenna function that describes configurations (for this colour-ordered amplitude) where parton j is unresolved. The momentum fractions x_1 and x_2 as well as the tilde momenta will be discussed in section 3.2.3. This configuration is displayed in figure 3.3. The full subtraction term for the initial-initial configuration can be written as:

$$\begin{aligned} \mathrm{d}\sigma^{S,(ii)} \;=\; & \mathcal{N} \sum_{\text{perms}} \mathrm{d}\Phi_{m+1}(k_1, \ldots, k_{j-1}, k_j, k_{j+1}, \ldots, k_{m+1}; p_1, p_2) \, \frac{1}{S_{m+1}} \\ & \sum_j X^0_{12,j} \left| \mathcal{M}_{m+2}(\tilde{k}_1, \ldots, \tilde{k}_{j-1}, \tilde{k}_{j+1}, \ldots, \tilde{k}_{m+1}; x_1 p_1, x_2 p_2) \right|^2 \\ & \times J^{(m)}_m(\tilde{k}_1, \ldots, \tilde{k}_{j-1}, \tilde{k}_{j+1}, \ldots, \tilde{k}_{m+1}) \,. \end{aligned} \tag{3.21}$$

In order to fulfill overall momentum conservation all the momenta in the arguments of the reduced matrix elements and the jet functions have been redefined. The two hard radiators are simply rescaled by factors x_1 and x_2 respectively that we will discuss in section 3.2.3. The spectator momenta are boosted by a Lorentz transformation onto the new set of momenta $\{\tilde{k}_l,\, l \neq j\}$.

The phase space factorises into the convolution of an m particle phase space, involving only the redefined momenta, with the phase space of parton j [68]:

$$\begin{aligned} \mathrm{d}\Phi_{m+1}(k_1,\ldots,k_{m+1};p_1,p_2) &= \mathrm{d}\Phi_m(\tilde{k}_1,\ldots,\tilde{k}_{j-1},\tilde{k}_{j+1},\ldots,\tilde{k}_{m+1};x_1p_1,x_2p_2) \\ &\quad\times\delta(x_1-\hat{x}_1)\,\delta(x_2-\hat{x}_2)\,[\mathrm{d}k_j]\,\mathrm{d}x_1\,\mathrm{d}x_2\,. \end{aligned} \tag{3.22}$$

Inserting the factorised expression for the phase space measure in eq. (3.21), the subtraction terms can be integrated over the antenna phase space. The integrated form of the subtraction terms must be, then, combined with the virtual and mass factorisation terms to cancel the explicit poles in ϵ. In the case of initial-initial subtraction terms, the antenna phase space is trivial: the two remaining Dirac delta functions can be combined with the one particle phase space, such that there are no integrals left. We define the initial-initial integrated antenna functions as follows:

$$\mathcal{X}_{ik,j}(x_1,x_2) = \frac{1}{C(\epsilon)}\int [\mathrm{d}k_j]\,x_1\,x_2\,\delta(x_1-\hat{x}_1)\,\delta(x_2-\hat{x}_2)\,X_{ik,j} \tag{3.23}$$

where $C(\epsilon)$ is given in (3.11).

Antenna functions

In the previous subsections we have seen that the subtraction term is constructed from products of antenna functions with reduced matrix elements (with fewer final state partons than the original matrix element), and integrated over a phase space which is factorised into an antenna phase space (involving all unresolved partons and the two radiators) multiplied with a reduced phase space (where the momenta of radiators and unresolved radiation are replaced by two redefined momenta). The full subtraction term is obtained by summing over all antennae required for the problem under consideration. In the most general case (two partons in the initial state, and two or more hard partons in the final state), this sum includes final-final,

initial-final and initial-initial antennae. We will see an example of this in section 3.3 when we compute the NLO corrections to the dijet cross section.

To conclude this section we will briefly review how to derive the antenna functions.

Each antenna is determined by both the external state and the pair of hard partons it collapses to. In general we denote the antenna function as X. For antennae that collapse onto a hard quark-antiquark pair, $X = A$ for $qg\bar{q}$. Similarly, for quark-gluon antenna, we have $X = D$ for qgg and $X = E$ for $qq'\bar{q}'$ final states. Finally, we characterise the gluon-gluon antennae as $X = F$ for ggg, $X = G$ for $gq\bar{q}$ final states.

We are considering only tree level three-particle antennae involving only one unresolved parton which suffices at NLO. At NNLO we will need four-particle antennae involving two unresolved partons and one-loop three-particle antennae.

In all cases antenna functions are derived from physical matrix elements: the quark-antiquark antenna functions from $\gamma^* \to q\bar{q}$ + (partons) [70], the quark-gluon antenna functions from $\tilde{\chi} \to \tilde{g}$ + (partons) [71] and the gluon-gluon antenna functions from $H \to$ (partons) [72]. The tree-level antenna functions are obtained by normalising the colour-ordered three- and four-parton tree-level squared matrix elements to the squared matrix element for the basic two-parton process,

$$X^0_{ijk} = S_{ijk,IK} \frac{|\mathcal{M}^0_{ijk}|^2}{|\mathcal{M}^0_{IK}|^2} ,$$
$$X^0_{ijkl} = S_{ijkl,IL} \frac{|\mathcal{M}^0_{ijkl}|^2}{|\mathcal{M}^0_{IL}|^2} , \tag{3.24}$$

where S denotes the symmetry factor associated with the antenna, which accounts both for potential identical particle symmetries and for the presence of more than one antenna in the basic two-parton process.

3.2 Numerical implementation of NLO antenna functions

In the colour-ordered quark-gluon and gluon-gluon antenna functions derived from physical matrix elements for neutralino decay [71] and Higgs boson decay [72], it is

in general not possible to identify the hard radiators and the unresolved partons in a unique manner. The reason for this ambiguity is in the cyclic nature of the colour orderings, which is already evident in the three-parton antenna functions: each pair of two partons can in principle act as hard radiators, resulting in more than one antenna configuration present in a single antenna function. This means that we have to disentangle the multiple singularities of these antennae into sub-antennae where an appropriate mapping can be used.

We will concentrate on the pure gluon channel and describe the numerical implementation of the gluon-gluon antenna function with a pure gluonic final state F_3^0.

3.2.1 Final-Final emitters

The tree level three-parton antenna corresponding to the gluon-gluon-gluon final state is [67]:

$$\begin{aligned} F_3^0(1_g,2_g,3_g) &= \frac{2}{s_{123}^2}\left(\frac{s_{123}^2 s_{12}}{s_{13}s_{23}}+\frac{s_{123}^2 s_{13}}{s_{12}s_{23}}+\frac{s_{123}^2 s_{23}}{s_{12}s_{13}}+\frac{s_{12}s_{13}}{s_{23}}+\frac{s_{12}s_{23}}{s_{13}}+\frac{s_{13}s_{23}}{s_{12}}\right. \\ &\left. +4s_{123}+\mathcal{O}(\epsilon)\right) \end{aligned} \tag{3.25}$$

where the invariant masses between final-state momenta are always defined with a plus sign:

$$s_{ij} = (k_i + k_j)^2$$

The simple unresolved limits of $F_3^0(1,2,3)$ are:

1. Soft limits:

$$\begin{aligned} F_3^0(1,2,3) &\xrightarrow{1_g\to 0} S_{213}\,, \\ F_3^0(1,2,3) &\xrightarrow{2_g\to 0} S_{123}\,, \\ F_3^0(1,2,3) &\xrightarrow{3_g\to 0} S_{132}\,, \end{aligned} \tag{3.26}$$

2. Collinear limits:

$$F_3^0(1,2,3) \xrightarrow{1_g\| 2_g} \frac{1}{s_{12}} P_{gg\to G}(z)\,,$$

$$
\begin{aligned}
F_3^0(1,2,3) &\xrightarrow{1_g \| 3_g} \frac{1}{s_{13}} P_{gg\to G}(z) \,, \\
F_3^0(1,2,3) &\xrightarrow{2_g \| 3_g} \frac{1}{s_{23}} P_{gg\to G}(z)
\end{aligned}
\tag{3.27}
$$

where the single eikonal factor S_{ijk} and the splitting function $P_{gg\to G}(z)$ were defined in (1.77) and (1.80) respectively. As can be seen from the pole structure, this tree level antenna function contains three antenna configurations, corresponding to the three possible configurations of emitting a gluon in between a gluon pair. We decompose [67]:

$$
F_3^0(1,2,3) = f_3^0(1,3,2) + f_3^0(3,2,1) + f_3^0(2,1,3) \tag{3.28}
$$

where:

$$
f_3^0(1,3,2) = \frac{1}{s_{123}^2}\left(2\frac{s_{123}^2 s_{12}}{s_{13}s_{23}} + \frac{s_{12}s_{13}}{s_{23}} + \frac{s_{12}s_{23}}{s_{13}} + \frac{8}{3}s_{123} + \mathcal{O}(\epsilon) \right) \tag{3.29}
$$

This sub-antenna $f_3^0(i,j,k)$ has the full j soft limit and some of the $i \parallel j$ and $j \parallel k$ limits of the full antenna (3.25), such that i and k can be identified as hard radiators. Therefore this is the antenna we use in the numerical implementation with a unique $\{3\to 2\}$ momenta mapping: $(i,j,k) \to ((\widetilde{ij}),(\widetilde{jk}))$:

$$
\begin{aligned}
\tilde{K}^\mu_{(IJ)} &= x\, k_i^\mu + r\, k_j^\mu + z\, k_k^\mu \\
\tilde{K}^\mu_{(JK)} &= (1-x)\, k_i^\mu + (1-r)\, k_j^\mu + (1-z)\, k_k^\mu
\end{aligned}
\tag{3.30}
$$

where:

$$
\begin{aligned}
x &= \frac{1}{2(s_{ij}+s_{ik})}\Big[(1+\rho)\, s_{ijk} - 2\, r\, s_{jk}\Big] \\
z &= \frac{1}{2(s_{jk}+s_{ik})}\Big[(1-\rho)\, s_{ijk} - 2\, r\, s_{ij}\Big]
\end{aligned}
$$

$$
\rho^2 = 1 + \frac{4\, r(1-r)\, s_{ij}s_{jk}}{s_{ijk}s_{ik}} \tag{3.31}
$$

The parameter r can be chosen conveniently, we use [73, 74]:

$$
r = \frac{s_{jk}}{s_{ij}+s_{jk}} \,.
$$

This mapping implements momentum conservation $\tilde{K}_{(IJ)} + \tilde{K}_{(JK)} = k_i + k_j + k_k$ and satisfies the following properties:

$$\begin{aligned}
\tilde{K}^2_{(IJ)} &= 0 & \tilde{K}^2_{(JK)} &= 0 & \\
\tilde{K}_{(IJ)} &\to k_i & \tilde{K}_{(JK)} &\to k_k & \text{when } j \text{ is soft} \\
\tilde{K}_{(IJ)} &\to k_i + k_j & \tilde{K}_{(JK)} &\to k_k & \text{when } i \text{ becomes collinear with } j \\
\tilde{K}_{(IJ)} &\to k_i & \tilde{K}_{(JK)} &\to k_j + k_k & \text{when } j \text{ becomes collinear with } k
\end{aligned}$$

This guarantees proper subtraction of infrared singularities.

As it was mentioned in the description of the antenna formulation we also need the analytic integral of the subtraction term to combine it with the virtual corrections and obtain the cancellation of the singularities analytically. That necessarily implies that we need the integrated form of the antenna over the antenna phase space (final state kinematics) which has been calculated and documented in [67].

3.2.2 Initial-Final emitters

In this section we use invariant masses between a final state momentum and an initial state momentum that we define with a minus sign:

$$s_{if} = (p_i - k_f)^2$$

The initial-final gluon-gluon-gluon antenna function like all NLO initial-final antenna functions can be obtained by appropriate crossing of particles from the final to the initial state [68]. Its unintegrated form can then be obtained from (3.25) by making the replacements:

$$\begin{aligned}
s_{23} &\to (k_2 + k_3)^2 \\
s_{12} &\to (p_1 - k_2)^2 \\
s_{13} &\to (p_1 - k_3)^2 \\
Q^2 &= s_{12} + s_{13} + s_{23}
\end{aligned}$$

and it reads [68]:

$$F_3^0(\hat{1}_g, 2_g, 3_g) = \frac{1}{2(Q^2)^2}\left(\frac{8s_{12}^2}{s_{13}} + \frac{8s_{12}^2}{s_{23}} + \frac{8s_{13}^2}{s_{12}} + \frac{8s_{13}^2}{s_{23}} + \frac{8s_{23}^2}{s_{12}} + \frac{8s_{23}^2}{s_{13}}\right.$$

$$+\frac{12s_{12}s_{13}}{s_{23}}+\frac{12s_{23}s_{13}}{s_{12}}+\frac{12s_{12}s_{23}}{s_{13}}+\frac{4s_{12}^3}{s_{23}s_{13}}+\frac{4s_{13}^3}{s_{23}s_{12}}+\frac{4s_{23}^3}{s_{12}s_{13}}$$
$$+24s_{23}+24s_{12}+24s_{13}+\mathcal{O}(\epsilon)\Big) \tag{3.32}$$

where the hat identifies the gluon crossed to the initial state. It is convenient to decompose this antenna in the following way:

$$F_3^0(\hat{1},2,3)=f_3^0(\hat{1},2,3)+f_3^0(\hat{1},3,2) \tag{3.33}$$

where:

$$\begin{aligned} f_3^0(\hat{1},2,3) &= \frac{1}{2(Q^2)^2}\Big(\frac{8s_{13}^2}{s_{12}}+\frac{8s_{23}^2}{s_{12}}+\frac{12s_{23}s_{13}}{s_{12}}+\frac{4s_{13}^3}{s_{23}s_{12}}+\frac{4s_{23}^3}{s_{12}(s_{12}+s_{13})} \\ &\quad +\frac{8s_{13}^2}{s_{23}}+\frac{6s_{12}s_{13}}{s_{23}}+12s_{23}+12s_{12}+12s_{13}+\mathcal{O}(\epsilon)\Big) \end{aligned}$$

This sub-antenna $f_3^0(\hat{1},j,k)$ has the full j soft limit, the full $1\parallel j$ limit and some of the $j\parallel k$ limit of the full antenna (3.32), such that we can identify $\hat{1}$ as the initial state radiator and k the final state radiator. To numerically implement this antenna we use the following $\{3\to2\}$ mapping: $(\hat{1},j,k)\to(\hat{\tilde{1}},\widetilde{(jk)})$ [68]:

$$\begin{aligned} \bar{p}_1^\mu &= x\,p_1^\mu \\ \tilde{K}_{(JK)}^\mu &= k_j^\mu+k_k^\mu-(1-x)\,p_1^\mu \end{aligned} \tag{3.34}$$

where the bar denotes a rescalling of the initial state parton and x is given by:

$$x = \frac{s_{1j}+s_{1k}+s_{jk}}{s_{1j}+s_{1k}} \tag{3.35}$$

Proper subtraction of infrared singularities requires that the momenta mapping satisfies:

$$\begin{aligned} &xp_1\to p_1\,, \qquad \tilde{K}_{(JK)}\to k_k \qquad \text{when } j \text{ becomes soft}\,,\\ &xp_1\to p_1\,, \qquad \tilde{K}_{(JK)}\to k_j+k_k \qquad \text{when } j \text{ becomes collinear with } k\,,\\ &xp_1\to p_1-k_j\,, \qquad \tilde{K}_{(JK)}\to k_k \qquad \text{when } j \text{ becomes collinear with } \hat{1}\,. \end{aligned}$$

In this way, infrared singularities are subtracted locally, except for angular correlations, *before convoluting with the parton distributions*. That is, matrix elements

and subtraction terms are convoluted together with PDFs. In addition, the re-defined momentum $\tilde{K}_{(JK)}$ must be on shell and momentum must be conserved, $p_1 - k_j - k_k = xp_1 - \tilde{K}_{(JK)}$, for the phase space to factorise in (3.17).

The integrated form of the antenna (3.32) over the antenna phase space (initial state kinematics) has been calculated and documented in [68].

3.2.3 Initial-Initial emitters

In this section the invariant mass between two initial state momenta is defined with a plus sign:

$$s_{12} = (p_1 + p_2)^2$$

The initial-initial gluon-gluon-gluon antenna function is obtained immediately from the corresponding initial-final (3.32), but the Mandelstam invariants have to be replaced by:

$$\begin{aligned} s_{12} &\to (p_1 + p_2)^2 \\ s_{13} &\to (p_1 - k_3)^2 \\ s_{23} &\to (p_2 - k_3)^2 \\ Q^2 &= s_{12} + s_{13} + s_{23} \end{aligned}$$

and it reads [68]:

$$\begin{aligned} F_3^0(\hat{1},\hat{2},3) = \frac{1}{2(Q^2)^2}\Bigg(& \frac{8s_{13}^2}{s_{23}} + \frac{8s_{13}^2}{s_{12}} + \frac{8s_{23}^2}{s_{13}} + \frac{8s_{23}^2}{s_{12}} + \frac{8s_{12}^2}{s_{13}} + \frac{8s_{12}^2}{s_{23}} \\ & + \frac{12s_{13}s_{23}}{s_{12}} + \frac{12s_{12}s_{23}}{s_{13}} + \frac{12s_{13}s_{12}}{s_{23}} + \frac{4s_{13}^3}{s_{12}s_{23}} + \frac{4s_{23}^3}{s_{12}s_{13}} + \frac{4s_{12}^3}{s_{13}s_{23}} \\ & + 24s_{12} + 24s_{13} + 24s_{23} + \mathcal{O}(\epsilon) \Bigg) \end{aligned} \tag{3.36}$$

where the hat identifies the gluons crossed to the initial state.

In the antenna $F_3^0(\hat{1},\hat{2},j)$ the only gluon that can be soft is j, because the initial state gluons are not allowed to be soft by kinematics, and it can also be collinear with the initial state gluons $\hat{1}$ or $\hat{2}$. This antenna can then be used with a single initial-initial mapping where j is unresolved and 1 and 2 act as the initial state radiators and

therefore does not need to be further decomposed in sub-antennae. The mapping used in this configuration is the following $\{\hat{1},\hat{2},j,...,l,m,...\} \rightarrow \{\hat{\tilde{1}},\hat{\tilde{2}},...,\tilde{l},\tilde{m},...\}$ [68]:

$$\begin{aligned}
\bar{p}_1^\mu &= x_1\, p_1^\mu \\
\bar{p}_2^\mu &= x_2\, p_2^\mu \\
&... \\
\tilde{k}_l^\mu &= k_l^\mu - \frac{2k_l\cdot(q+\tilde{q})}{(q+\tilde{q})^2}\,(q^\mu+\tilde{q}^\mu) + \frac{2k_l\cdot q}{q^2}\,\tilde{q}^\mu \\
&... \\
q^\mu &= p_1^\mu + p_2^\mu - k_j^\mu \\
\tilde{q}^\mu &= \bar{p}_1^\mu + \bar{p}_2^\mu
\end{aligned} \tag{3.37}$$

where the bar denotes rescaling of both the initial state partons and the tilde momenta are all the momenta in the final that are not actually part of the antenna but require boosting in order to restore momentum conservation. This is because $\tilde{q} \equiv \bar{p}_1 + \bar{p}_2$ lies along the beam axis but the vector component of $q \equiv p_1 + p_2 - p_j$ is in general not along the beam axis. The x_1 and x_2 are given by [68]:

$$\begin{aligned}
x_1 &= \sqrt{\frac{s_{12}+s_{2j}}{s_{12}+s_{1j}}}\sqrt{\frac{s_{12}+s_{1j}+s_{2j}}{s_{12}}} \\
x_2 &= \sqrt{\frac{s_{12}+s_{1j}}{s_{12}+s_{2j}}}\sqrt{\frac{s_{12}+s_{2j}+s_{1j}}{s_{12}}}
\end{aligned} \tag{3.38}$$

It yields the correct soft and collinear limits:

1. j soft: $x_1 \rightarrow 1$, $x_2 \rightarrow 1$.

2. $k_j = z_1 p_1 \parallel p_1$: $x_1 = (1-z_1)$, $x_2 = 1$.

3. $k_j = z_2 p_2 \parallel p_2$: $x_1 = 1$, $x_2 = (1-z_2)$.

It should be pointed out the transformation is not unique. Possible transformations are however strongly constrained. If one requires a symmetrical treatment of x_1 and x_2, rotations are not allowed as transformation. To show that, we take p_j to be transverse to the beam axis. Bringing q to the beam axis with a rotation will force us to choose to rotate $\vec{q}$ either towards the p_1 or the p_2 side. This would favor

either x_1 or x_2. The only way to bring q to the beam axis, without having to choose between x_1 and x_2 is in this case a boost transverse to the beam axis.

The integrated form of the antenna (3.36) over the antenna phase space (initial state kinematics) has been calculated and documented in [68].

3.3 NLO real corrections to dijet production

We are now ready to implement the antennae functions as building blocks for subtraction at NLO. We consider the real radiative corrections to dijet production from the pure gluon channel where the antennae decompositions of the previous sections can be immediately applied. In this case the LO cross section is:

$$\mathrm{d}\sigma^B_{LO} = \mathrm{d}\Phi_2(p_3,p_4;p_1,p_2)\frac{1}{2!}\overline{\sum_{\substack{colour\\spin}}}|M^0_{gg\to gg}|^2 J^{(2)}_2(p_3,p_4) \tag{3.39}$$

Using the colour ordered decomposition of section 1.7 we can rewrite it in the following form:

$$\begin{aligned}\mathrm{d}\sigma^B_{LO} &= N_{Born}\mathrm{d}\Phi_2(p_3,p_4;p_1,p_2)\frac{1}{2!}\sum_{\{2,\ldots,4\}'} A^0_4(\hat{1}_g,\sigma(\hat{2})_g,\sigma(i)_g,\sigma(j)_g)\; J^{(2)}_2(p_i,p_j)\\ &= N_{Born}\mathrm{d}\Phi_2(p_3,p_4;p_1,p_2)\frac{1}{2!}\sum_{P(i,j)\in(3,4)}\Big(2A^0_4(\hat{1}_g,\hat{2}_g,i_g,j_g)J^{(2)}_2(p_i,p_j)\\ &+A^0_4(\hat{1}_g,i_g,\hat{2}_g,j_g)J^{(2)}_2(p_i,p_j)\Big)\end{aligned} \tag{3.40}$$

where the $\{2,...,4\}'$ are the 3! permutations in the four gluon amplitude where index $\hat{1}$ is kept fixed. In the second equality we reduced these to 2! using the cyclic symmetry of the amplitudes A^0_4. Finally the factor N_{Born} contains the sum and average over spin and colour degrees of freedom for incoming and outgoing particles, as well as the coupling constant, that appears at leading order:

$$N_{Born} = \frac{N^2(N^2-1)}{4(N^2-1)^2}g^4 \tag{3.41}$$

Using the same colour ordered decomposition of section 1.7 we can write the five gluon real radiation cross section in the following form:

$$\mathrm{d}\sigma^R_{NLO} = N\,N_{born}\left(\frac{\alpha_s}{2\pi}\right)\frac{\bar{C}(\epsilon)}{C(\epsilon)}\mathrm{d}\Phi_3(p_3,p_4,p_5;p_1,p_2)\,\frac{2}{3!}$$

$$\sum_{P(i,j,k)\in(3,4,5)} \Bigg(A_5^0(\hat{1}_g, \hat{2}_g, i_g, j_g, k_g)\, J_2^{(3)}(p_i, p_j, p_k) + A_5^0(\hat{1}_g, i_g, \hat{2}_g, j_g, k_g)\, J_2^{(3)}(p_i, p_j, p_k) \Bigg) \tag{3.42}$$

With the help of the antennae functions defined in the previous sections we will now write the subtraction term for the single unresolved configurations of the $gg \to ggg$ matrix element of (3.42). The real radiation subtraction term reads:

$$\begin{aligned}
\mathrm{d}\sigma^S_{NLO} = \; & N\, N_{born} \left(\frac{\alpha_s}{2\pi}\right) \frac{\bar{C}(\epsilon)}{C(\epsilon)} \mathrm{d}\Phi_3(p_3, p_4, p_5; p_1, p_2)\, \frac{2}{3!} \sum_{P(i,j,k)\in(3,4,5)} \Bigg\{ \\
& f_3^0(\hat{2}_g, i_g, j_g) A_4^0(\hat{1}_g, \hat{\tilde{2}}_g, (\widetilde{ij})_g, k_g)\, J_2^{(2)}(\widetilde{p_{ij}}, p_k) \\
& + f_3^0(i_g, j_g, k_g) A_4^0(\hat{1}_g, \hat{2}_g, (\widetilde{ij})_g, (\widetilde{jk})_g)\, J_2^{(2)}(\widetilde{p_{ij}}, \widetilde{p_{jk}}) \\
& + f_3^0(j_g, k_g, \hat{1}_g) A_4^0(\hat{\tilde{1}}_g, \hat{2}_g, i_g, (\widetilde{kj})_g)\, J_2^{(2)}(p_i, \widetilde{p_{kj}}) \\
& \\
& + F_3^0(\hat{1}_g, i_g, \hat{2}_g) A_4^0(\hat{\tilde{1}}_g, \hat{\tilde{2}}_g, \tilde{j}_g, \tilde{k}_g)\, J_2^{(2)}(\tilde{p_j}, \tilde{p_k}) \\
& + f_3^0(\hat{2}_g, j_g, k_g) A_4^0(\hat{1}_g, i_g, \hat{\tilde{2}}_g, (\widetilde{jk})_g)\, J_2^{(2)}(p_i, \widetilde{p_{jk}}) \\
& + f_3^0(j_g, k_g, \hat{1}_g) A_4^0(\hat{\tilde{1}}_g, i_g, \hat{2}_g, (\widetilde{kj})_g)\, J_2^{(2)}(p_i, \widetilde{p_{kj}}) \\
& \Bigg\}
\end{aligned} \tag{3.43}$$

where we have used a combination of gluon-gluon-gluon antenna functions with two emitters in the final state, initial state and one emitter in the final state and one in the initial state. Each of these antennae has a reduced matrix element evaluated with hard momenta given by the momentum mappings of the previous sections. The total number of antenna functions used is equal to the total number of unresolved particles in the final state per colour ordered amplitude.

This subtraction term has been checked with phase space trajectories generated with `RAMBO` [75]. In each singular region the ratio of the matrix element with the subtraction approaches unity.

3.4 NLO virtual corrections to dijet production

The virtual contribution has the following form:

$$\begin{aligned}
\mathrm{d}\sigma^{V}_{NLO} &= \mathrm{d}\Phi_2(p_3,p_4;p_1,p_2)\frac{1}{2!}\overline{\sum_{\substack{colour\\spin}}} 2\,\mathrm{Re}(\mathcal{M}^{*}_{LO}\mathcal{M}_{\text{1-loop}})J^{(2)}_2(p_i,p_j)\\
&= N\,N_{born}\left(\frac{\alpha_s}{2\pi}\right)\mathrm{d}\Phi_2(p_3,p_4;p_1,p_2)\,\frac{1}{2!}\,2\,\mathrm{Re}\sum_{\{2,\ldots,4\}'}\\
&\mathcal{M}^{*}_{4,0}(\hat{1}_g,\sigma(\hat{2})_g,\sigma(i)_g,\sigma(j)_g)\mathcal{M}_{4,1}(\hat{1}_g,\sigma\hat{(2)}_g,\sigma(i)_g,\sigma(j)_g)J^{(2)}_2(p_i,p_j)
\end{aligned} \tag{3.44}$$

where $\mathcal{M}^{*}_{4,0}$ and $\mathcal{M}_{4,1}$ are the four gluon tree and one-loop primitive amplitudes. The singular part of the loop amplitude is given by [76]:

$$\begin{aligned}
&\mathcal{M}_{4,1}(\hat{1}_g,\hat{2}_g,i_g,j_g) = \frac{\Gamma(1-\epsilon)^2\Gamma(1+\epsilon)(4\pi)^{\epsilon}}{\Gamma(1-2\epsilon)}\\
&\left[-\frac{2}{\epsilon^2}-\frac{11}{3\epsilon}+\frac{1}{\epsilon}\left(\ln\left(-\frac{s_{12}}{\mu^2}\right)+\ln\left(-\frac{s_{2i}}{\mu^2}\right)\right)\right]\mathcal{M}_{4,0}(\hat{1}_g,\hat{2}_g,i_g,j_g)\\
&+\mathcal{O}(\epsilon^0)
\end{aligned} \tag{3.45}$$

Keeping only the divergent poles in $1/\epsilon^2$ and $1/\epsilon$ we can rewrite the virtual correction in a more appropriate form to perform the analytic cancellation of the infrared singularities:

$$\begin{aligned}
&\mathrm{d}\sigma^{V}_{NLO} =\\
&= N\,N_{Born}\left(\frac{\alpha_s}{2\pi}\right)\mathrm{d}\Phi_2(p_3,p_4;p_1,p_2)\frac{1}{2!}\frac{\Gamma(1-\epsilon)^2\Gamma(1+\epsilon)(4\pi)^{\epsilon}}{\Gamma(1-2\epsilon)}\sum_{P(i,j)\in(3,4)}2\,\mathrm{Re}\Bigg\{\\
&\quad\left[-\frac{2}{\epsilon^2}-\frac{11}{3\epsilon}+\frac{1}{\epsilon}\left(\ln\left(-\frac{s_{12}}{\mu^2}\right)+\ln\left(-\frac{s_{2i}}{\mu^2}\right)\right)\right]2A^0_4(\hat{1}_g,\hat{2}_g,i_g,j_g)J^{(2)}_2(p_i,p_j)\\
&+\left[-\frac{2}{\epsilon^2}-\frac{11}{3\epsilon}+\frac{1}{\epsilon}\left(\ln\left(-\frac{s_{1i}}{\mu^2}\right)+\ln\left(-\frac{s_{2i}}{\mu^2}\right)\right)\right]A^0_4(\hat{1}_g,i_g,\hat{2}_g,j_g)J^{(2)}_2(p_i,p_j)\Bigg\}\\
&+\mathcal{O}(\epsilon^0)
\end{aligned} \tag{3.46}$$

Using the symmetry of the gluon phase space the 2! permutations precisely cancel the identical particle factor of 1/2! and it is more convenient to keep one particular ordering. The virtual contribution becomes:

$$\mathrm{d}\sigma^{V}_{NLO} \;=\; N\,N_{Born}\left(\frac{\alpha_s}{2\pi}\right)\mathrm{d}\Phi_2(p_3,p_4;p_1,p_2)\frac{(4\pi)^{\epsilon}}{\Gamma(1-\epsilon)}2\,\mathrm{Re}\Bigg\{$$

$$\left[-\frac{2}{\epsilon^2}-\frac{11}{3\epsilon}+\frac{1}{\epsilon}\left(\ln\left(-\frac{s_{12}}{\mu^2}\right)+\ln\left(-\frac{s_{23}}{\mu^2}\right)\right)\right]2A_4^0(\hat{1}_g,\hat{2}_g,3_g,4_g)J_2^{(2)}(p_3,p_4)$$
$$+\left[-\frac{2}{\epsilon^2}-\frac{11}{3\epsilon}+\frac{1}{\epsilon}\left(\ln\left(-\frac{s_{13}}{\mu^2}\right)+\ln\left(-\frac{s_{23}}{\mu^2}\right)\right)\right]A_4^0(\hat{1}_g,3_g,\hat{2}_g,4_g)J_2^{(2)}(p_3,p_4)\Bigg\}$$
$$+\mathcal{O}(\epsilon^0) \tag{3.47}$$

where we have used the identity:

$$\frac{\Gamma(1-\epsilon)^2\Gamma(1+\epsilon)}{\Gamma(1-2\epsilon)}=\frac{1}{\Gamma(1-\epsilon)}+\mathcal{O}(\epsilon^3) \tag{3.48}$$

Introducing now the colour ordered infrared singularity operator:

$$\boldsymbol{I}_{gg}^{(1)}(s_{gg})=-\frac{e^{\epsilon\gamma}}{2\Gamma(1-\epsilon)}\left[\frac{1}{\epsilon^2}+\frac{11}{6\epsilon}\right]\mathrm{Re}\left(-\frac{s_{gg}}{\mu^2}\right)^{-\epsilon} \tag{3.49}$$

we can rewrite the virtual contribution as:

$$\begin{aligned}\mathrm{d}\sigma_{NLO}^{V} &= N\,N_{Born}\left(\frac{\alpha_s}{2\pi}\right)\mathrm{d}\Phi_2(p_3,p_4;p_1,p_2)\bar{C}(\epsilon)2\Bigg\{\\ &\left[\boldsymbol{I}_{gg}^{(1)}(s_{12})+\boldsymbol{I}_{gg}^{(1)}(s_{23})+\boldsymbol{I}_{gg}^{(1)}(s_{34})+\boldsymbol{I}_{gg}^{(1)}(s_{14})\right]2A_4^0(\hat{1}_g,\hat{2}_g,3_g,4_g)J_2^{(2)}(p_3,p_4)\\ &+\left[\boldsymbol{I}_{gg}^{(1)}(s_{13})+\boldsymbol{I}_{gg}^{(1)}(s_{23})+\boldsymbol{I}_{gg}^{(1)}(s_{24})+\boldsymbol{I}_{gg}^{(1)}(s_{14})\right]A_4^0(\hat{1}_g,3_g,\hat{2}_g,4_g)J_2^{(2)}(p_3,p_4)\Bigg\}\\ &+\mathcal{O}(\epsilon^0)\end{aligned} \tag{3.50}$$

3.5 Cancellation of infrared divergences

We will now collect the leading poles of the integrated antenna functions used to write down the subtraction term $d\sigma^S$ [67, 68]:

$$\frac{1}{C(\epsilon)}\int\mathrm{d}\Phi_{123}\,f_3^0(1,2,3)=-2\boldsymbol{I}_{gg}^{(1)}(s_{123})+\mathcal{O}(\epsilon^0)$$
$$\frac{1}{C(\epsilon)}\int\mathrm{d}\Phi_{1,23}\,f_3^0(\hat{1},2,3)=-2\boldsymbol{I}_{gg}^{(1)}(Q^2)\delta(1-x)-\left(\frac{Q^2}{\mu^2}\right)^{-\epsilon}\frac{1}{2\epsilon}p_{gg}^{(0)}(x)+\mathcal{O}(\epsilon^0)$$
$$\frac{1}{C(\epsilon)}\int\mathrm{d}\Phi_{12,3}\,F_3^0(\hat{1},\hat{2},3)=-\boldsymbol{I}_{gg}^{(1)}(Q^2)\delta(1-x_1)\delta(1-x_2)-\boldsymbol{I}_{gg}^{(1)}(Q^2)\delta(1-x_2)\delta(1-x_1)$$
$$-\left(\frac{Q^2}{\mu^2}\right)^{-\epsilon}\frac{1}{2\epsilon}p_{gg}^{(0)}(x_1)\delta(1-x_2)-\left(\frac{Q^2}{\mu^2}\right)^{-\epsilon}\frac{1}{2\epsilon}p_{gg}^{(0)}(x_2)\delta(1-x_1)+\mathcal{O}(\epsilon^0)$$

where the colour ordered splitting kernel is:

$$p_{gg}^{(0)}(x)=\frac{11}{6}\delta(1-x)+2\mathcal{D}_0(x)+\frac{2}{x}-4+2x-2x^2 \tag{3.51}$$

and the distributions $\mathcal{D}_0(x)$ were defined in (1.49). The analytic integration of the subtraction term over the factorised phase space can be carried out using the previous results. Using the symmetry of the gluon phase space the 3! permutations in (3.43) precisely cancels the identical particle factor of 1/3! and it is more convenient to keep one particular ordering in (3.43). After relabeling the final state particles we obtain the following for the poles of the integrated counterterm:

$$\begin{aligned}
\int \mathrm{d}\sigma^S_{NLO} = N\ N_{\mathrm{Born}} \left(\frac{\alpha_s}{2\pi}\right) \bar{C}(\epsilon) 2 \Bigg\{ & \\
& \mathrm{d}\Phi_2(p_3,p_4;p_1,p_2) 2A_4^{(0)}(\hat{1}_g,\hat{2}_g,3_g,4_g) J_2^{(2)}(p_3,p_4) \\
& \Big[-\boldsymbol{I}^{(1)}_{gg}(s_{23}) - \boldsymbol{I}^{(1)}_{gg}(s_{34}) - \boldsymbol{I}^{(1)}_{gg}(s_{14}) - \boldsymbol{I}^{(1)}_{gg}(s_{12}) \Big] \\
& -\mathrm{d}\Phi_2(p_3,p_4;\bar{p}_1,p_2) 2A_4^{(0)}(\hat{\bar{1}}_g,\hat{2}_g,3_g,4_g) J_2^{(2)}(p_3,p_4) \left(\frac{Q^2}{\mu^2}\right)^{-\epsilon} \int \frac{dx}{x} \frac{1}{2\epsilon} p^{(0)}_{gg}(x) \\
& -\mathrm{d}\Phi_2(p_3,p_4;p_1,\bar{p}_2) 2A_4^{(0)}(\hat{1}_g,\hat{\bar{2}}_g,3_g,4_g) J_2^{(2)}(p_3,p_4) \left(\frac{Q^2}{\mu^2}\right)^{-\epsilon} \int \frac{dx}{x} \frac{1}{2\epsilon} p^{(0)}_{gg}(x) \\
& +\mathrm{d}\Phi_2(p_3,p_4;p_1,p_2) A_4^{(0)}(\hat{1}_g,3_g,\hat{2}_g,4_g) J_2^{(2)}(p_3,p_4) \\
& \Big[-\boldsymbol{I}^{(1)}_{gg}(s_{24}) - \boldsymbol{I}^{(1)}_{gg}(s_{14}) - \boldsymbol{I}^{(1)}_{gg}(s_{13}) - \boldsymbol{I}^{(1)}_{gg}(s_{23}) \Big] \\
& -\mathrm{d}\Phi_2(p_3,p_4;\bar{p}_1,p_2) A_4^{(0)}(\hat{\bar{1}}_g,3_g,\hat{2}_g,4_g) J_2^{(2)}(p_3,p_4) \left(\frac{Q^2}{\mu^2}\right)^{-\epsilon} \int \frac{dx}{x} \frac{1}{2\epsilon} p^{(0)}_{gg}(x) \\
& -\mathrm{d}\Phi_2(p_3,p_4;p_1,\bar{p}_2) A_4^{(0)}(\hat{1}_g,3_g,\hat{\bar{2}}_g,4_g) J_2^{(2)}(p_3,p_4) \left(\frac{Q^2}{\mu^2}\right)^{-\epsilon} \int \frac{dx}{x} \frac{1}{2\epsilon} p^{(0)}_{gg}(x)
\end{aligned} \tag{3.52}$$

The poles contained in the operator $\boldsymbol{I}^{(1)}_{gg}$ match exactly the ones appearing with opposite sign in the virtual contribution. The remaining poles correspond to the mass factorisation contribution. The mass factorisation counterterm is given by [50]:

$$\begin{aligned}
\mathrm{d}\sigma^{MF}_{NLO} \;=\; & -\left(\frac{\alpha_s}{2\pi}\right) \frac{1}{\Gamma(1-\epsilon)} \int \mathrm{d}x_1 \mathrm{d}x_2\, \mathrm{d}\sigma^B_{LO}(i,j;\bar{p}_1,\bar{p}_2) \Bigg\{ \\
& \delta(1-x_2) \left[-\frac{1}{\epsilon} \left(\frac{4\pi\mu^2}{\mu_F^2}\right)^{\epsilon} N p^{(0)}_{gg}(x_1) + K^{gg}_{F.S.}(x_1) \right] \\
& +\delta(1-x_1) \left[-\frac{1}{\epsilon} \left(\frac{4\pi\mu^2}{\mu_F^2}\right)^{\epsilon} N p^{(0)}_{gg}(x_2) + K^{gg}_{F.S.}(x_2) \right] \Bigg\}
\end{aligned} \tag{3.53}$$

where the actual form of the kernel $K^{gg}_{F.S.}(x)$ specifies the factorisation scheme. Setting $K^{gg}_{F.S.}(x) = 0$ defines the $\overline{\mathrm{MS}}$ factorisation scheme. Introducing the expression

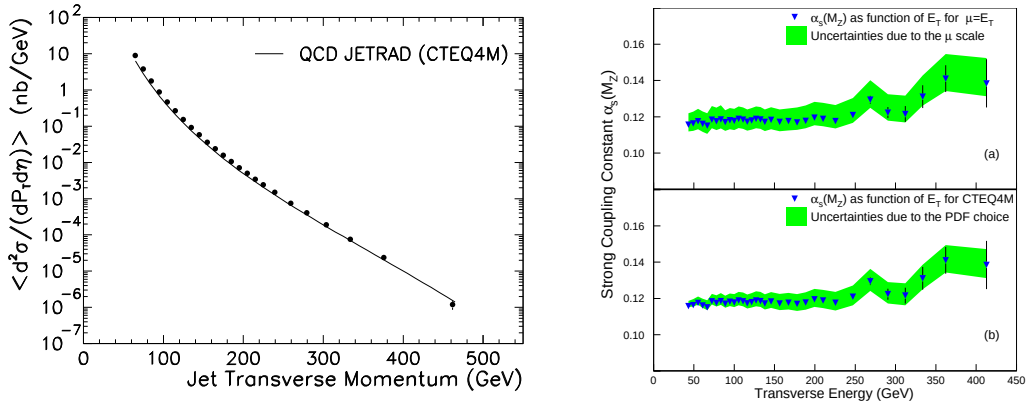

(a) (b)

Figure 3.4: (a) Single jet inclusive cross section at NLO compared to D0 data [77] and (b) errors on extraction of α_s at CDF [78].

for the born cross section (3.40) in the previous equation we achieve the cancellation of the remaining collinear singularities in (3.52).

3.6 Beyond NLO

As we have argued in chapter 1 the inclusion of the NLO correction makes the QCD prediction more accurate. This can be seen in figure 3.4(a) where a good agreement (over 6 orders of magnitude) between NLO QCD and experimental data on the single jet inclusive cross section is observed.

However, when using this data to determine the strong coupling constant α_s, it turns out that the dominant source of error in this extraction comes from the unknown higher order corrections. Figure 3.4(b) shows the theoretical uncertainty in the prediction in excess of the experimental errors. As a result, CDF find from their Run I data

$$\alpha_s(M_Z) = 0.1178 \pm 0.0001(\text{stat})^{+0.0081}_{-0.0095}(\text{sys})\ ^{+0.0071}_{-0.0047}(\text{scale}) \pm 0.0059(\text{pdf}).$$

To lower the theoretical error, it is mandatory to compute next-to-next-to-leading order (NNLO) corrections to the single jet inclusive cross section.

Furthermore the high-E_T jet data helps to constrain the gluon parton distribution function at large values of x. However, as the truncated cross section depends on the

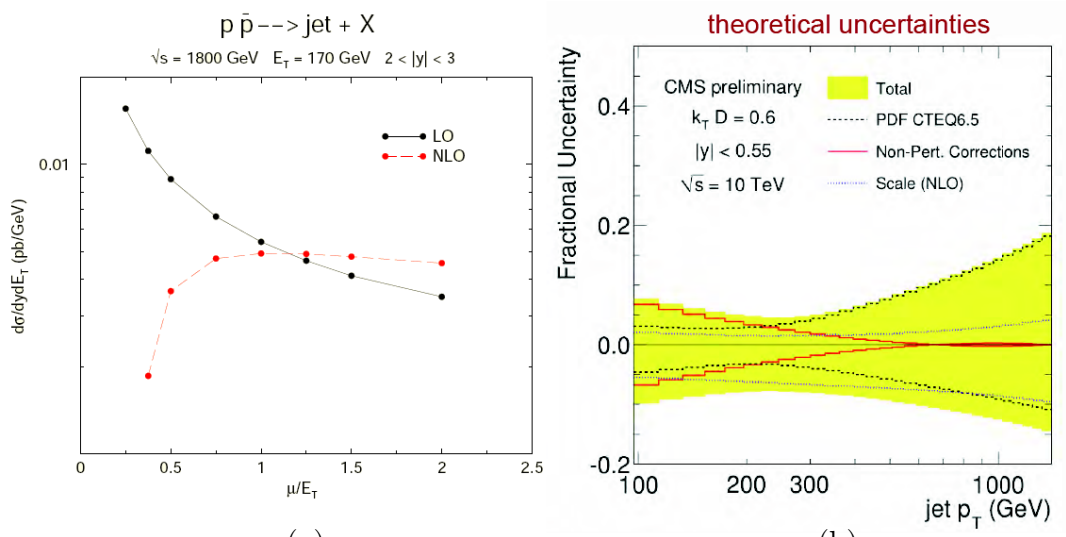

(a) (b)

Figure 3.5: (a) Scale dependence of the jet cross section at $E_T = 70$ GeV at the Tevatron [79] and (b) total theoretical uncertainties at the LHC as a function of the jet transverse momentum [80].

choice of scale, then, as the scale is varied, the parton distribution function will have to change in order to be able to fit the data. Figure 3.5(a) shows that doing a fit with a larger renormalisation scale causes the high-x gluon pdf to be larger since the high-E_T partonic cross section has decreased. Therefore the scale dependence of the cross section makes a contribution to the pdf uncertainty. A better determination of the gluon pdf, which requires all observables computed consistently at NNLO, can then be used as a new input to improve the theoretical accuracy of any hadronic scattering prediction such as the Higgs boson production.

Figure 3.5(b), taken from the CMS physics analysis summary [80], shows the different contributions to the total theoretical uncertainty at the LHC for the inclusive jet cross section as a function of the jet transverse momentum.

It is hoped that the inclusion of the hitherto unknown NNLO contribution will reduce the theoretical uncertainties. An example of this is given in Figure 3.6 that shows, for the electroweak boson rapidity distribution, the excellent convergence of the perturbative expansion when going from LO to NNLO and an increased stability against scale variations.

At this order, the inclusion of initial state radiation (in figure 3.7) gives the final

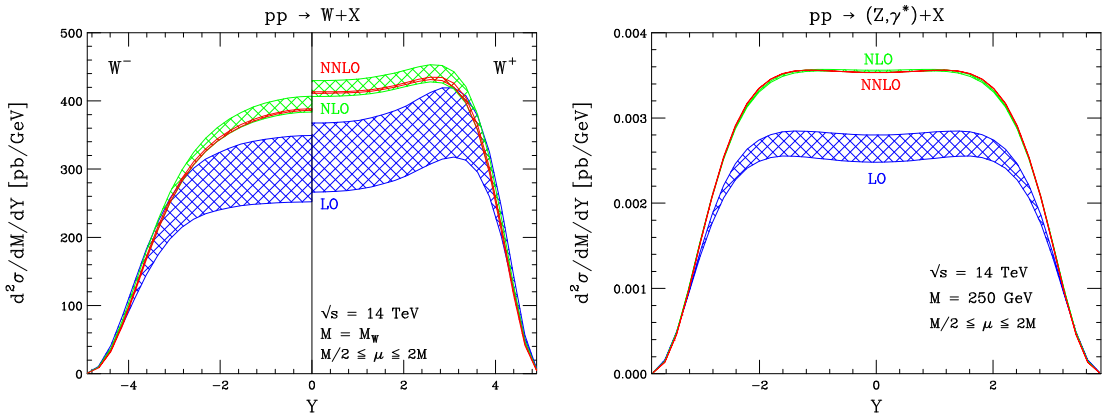

Figure 3.6: Electroweak rapidity gauge boson distributions at NNLO for the LHC. The bands indicate the residual scale dependence [81].

state a transverse momentum kick. At LO the incoming particles have no transverse momentum with respect to the beam such that the jets always appear back to back. The effects of initial state radiation give a more complex final state and a more theoretical accurate description of transverse momentum distributions.

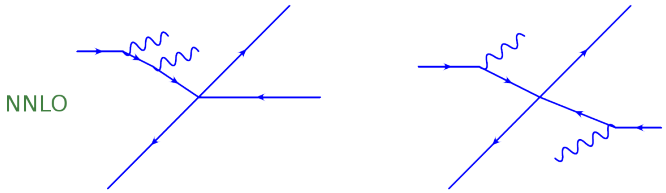

Figure 3.7: Radiative corrections coming from the initial lines

Also at NNLO the reconstruction of the jets where up to two partons can cluster to form a jet becomes more precise (figure 3.8). The additional radiation gives a much more rich structure to the jet.

3.7 Summary

In this chapter we looked at the antenna subtraction method to perform calculations at NLO. This formalism is completely general at this order in perturbation theory for e^+e^-, ep and pp collisions for massless fermions [68]. In all cases it allows the cancellation between real and virtual diverging pieces to be done analytically. An

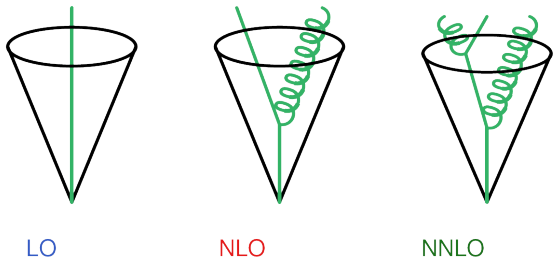

Figure 3.8: Jets modeled by extra partons at NNLO

extension to include massive fermions already appeared [69].

Also in this chapter we derived, as an example, an implementation of the method for the NLO corrections to the dijet cross section. However we have seen that there are strong arguments to extend this calculation to NNLO accuracy. This necessarily implies the extension of the method to NNLO which is going to be the topic of the next chapter.

Chapter 4

NNLO antenna subtraction

In this chapter we discuss the NNLO extension of the antenna subtraction method. We begin by identifying the ingredients for the computation of a NNLO observable and review the general subtraction formula at this order in section 4.1.

In section 4.2 we concentrate on the tree level double real subtraction term that subtracts singularities corresponding to two partons becoming simultaneously soft and/or collinear. In this derivation there are several configurations to consider depending on the colour connection of the unresolved partons. It is very important to understand this general formula as we will apply it in chapter 6 to build the NNLO real corrections to gluon scattering, the dominant contribution for the two-jet cross section at NNLO.

As we will see, subtraction terms for all these configurations can be constructed using either single four-parton antenna functions or products of three-parton antenna functions. The four-parton antenna functions are a new ingredient at NNLO. We end the chapter discussing the numerical implementation of the gluon-gluon-gluon-gluon antenna function F_4^0 for the three possible assignments of radiators: final-final, initial-final and initial-initial.

4.1 NNLO general infrared subtraction term

There have been several approaches to build a general subtraction scheme at NNLO [82–90]. We will follow the antenna subtraction method which was derived in [67].

This formalism has been applied in the computation of NNLO corrections to three-jet production in electron-positron annihilation [91–94] and related event shapes [95–99], which were subsequently used in precision determinations of the strong coupling constant [3, 100–103].

The aim of this thesis is to show that this method can also tackle computations of NNLO processes with coloured particles in the initial-state, which is relevant for both hadron-hadron or hadron-lepton colliders. We will concentrate on the double real corrections within the pure gluon channel for the two-jet production at NNLO. To achieve this we need a new ingredient - the 4-parton (or NNLO) F_4^0 antenna function for the three possible assignments of radiators: final-final, initial-final and initial-initial.

The unintegrated form of all NNLO antennae, derived from physical matrix elements, for the final-final configuration is documented in [67]. However, as we have seen in the NLO example of the previous chapter, it is the inclusive integrated antennae over the antenna phase space that explicitly cancels the singularities arising from virtual contributions. Obtaining the analytic integration of all the NNLO antennae functions is then crucial to establish the generality of the method at this order. For the final-final configuration of radiators, reference [104] used a reduction procedure based on methods developed for multi-loop integrals, to relate all antennae integrals into four four-particle phase space master integrals. Their analytical evaluation followed by direct analytic integration in closed form and by unitarity relations between known multi-loop integrals and phase space integrals.

The results for these master integrals were also checked numerically with the sector decomposition approach to the $1 \to 4$ particle phase space. We will look at the sector decomposition method in the next chapter.

For the initial-final radiator configuration, we can obtain the unintegrated form of all initial-final antennae by crossing particles to initial state in the corresponding final-final antennae. These have to be analytically integrated over the appropriate antenna phase-space (initial-state kinematics) and this was achieved recently in [105]. These results can now be implemented in a parton-level event generator programme and allow the full calculation of NNLO corrections to jet production

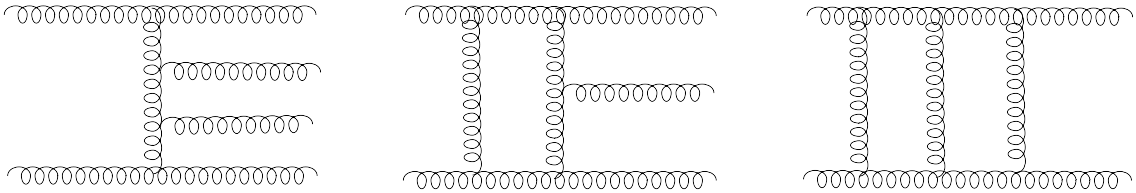

$A_6^{(0)}(gg \to gggg)$ $A_5^{(1)}(gg \to ggg)$ $A_4^{(2)}(gg \to gg)$

Figure 4.1: Sample diagrams for matrix elements contributing to the dijet inclusive rate at NNLO

observables in deeply inelastic electron-proton scattering.

For hadron-hadron scattering processes we still need initial-initial antennae functions, which can again be obtained from the corresponding initial-final ones by crossing. However the integrated initial-initial antenna functions are at the present known only to NLO, and work on their integration at NNLO is ongoing. To proceed we will now look now at the contributions that enter the NNLO corrections.

NNLO calculations for $pp \to m$-jets require several ingredients: the two-loop $(m+2)$-parton matrix elements, the one-loop $(m+3)$-parton matrix elements and the tree level $(m+4)$-parton matrix elements:

$$\begin{aligned}\hat{\sigma}_{NNLO} \sim & \int \left[\langle \mathcal{M}^{(0)}|\mathcal{M}^{(0)}\rangle\right]_{m+4} \mathrm{d}\Phi_{m+2} J_m^{(m+2)} \\ + & \int \left[\langle \mathcal{M}^{(0)}|\mathcal{M}^{(1)}\rangle + \langle \mathcal{M}^{(1)}|\mathcal{M}^{(0)}\rangle\right]_{m+3} \mathrm{d}\Phi_{m+1} J_m^{(m+1)} \\ + & \int \left[\langle \mathcal{M}^{(1)}|\mathcal{M}^{(1)}\rangle + \langle \mathcal{M}^{(0)}|\mathcal{M}^{(2)}\rangle + \langle \mathcal{M}^{(2)}|\mathcal{M}^{(0)}\rangle\right]_{m+2} \mathrm{d}\Phi_m J_m^{(m)}\end{aligned}$$

where a sample diagram for each ingredient with $m = 2$ in the pure gluon channel is given in figure 4.1. As usual the individual contributions in the $(m+2)$, $(m+3)$ and $(m+4)$-parton channels are all separately divergent although their sum is finite.

In the 4-parton channel (or virtual-virtual channel), $A_4^{(2\times 0)}(gg \to gg)$ represents the interference between the tree level $2 \to 2$ matrix element with the two-loop $2 \to 2$ gluon matrix element. It was derived in [106, 107]. The remaining two-loop matrix elements, for quark-quark and quark-gluon scattering, needed for the NNLO contribution to inclusive jet production were obtained in [108–111]. This contribution contains explicit infrared divergences coming from the integration over the loop momentum. This singular behaviour is predictable with the Catani formula

for the IR pole structure for a general on-shell QCD amplitude at two loop order derived in [112]. Also the self interference of the one-loop $A_4^{(1\times1)}(gg \to gg)$ amplitude contributes in the 4-parton channel and it was calculated in [113].

In the 5-parton channel (or real-virtual channel), $A_5^{(1\times0)}(gg \to ggg)$ is the interference between the tree level $2 \to 3$ matrix element with the one-loop $2 \to 3$ matrix element. It was derived in [114]. This contribution contains explicit infrared divergences coming from integrating over the loop momenta and implicit poles in the regions of the phase space where 1 of the final state partons becomes unresolved. This corresponds to the soft and collinear limits of the one-loop amplitude that were analysed in [115, 116].

Finally, in the 6-parton channel (or real-real channel), $A_6^{(0)}(gg \to gggg)$ is the $2 \to 4$ tree level matrix element squared. It was derived in [25, 27, 28]. In this channel the singularities occur in the phase space regions corresponding to two gluons becoming simultaneously soft and/or collinear. However this "double" unresolved behaviour is universal and was discussed in section 1.8.

Understanding the origin of the singularities of the different contributions is fundamental to constructing a subtraction procedure that can achieve their analytic cancellation. In the antenna subtraction method we have the following general formula for subtraction at NNLO [67]:

$$\begin{aligned} \mathrm{d}\sigma_{NNLO} &= \int_{\mathrm{d}\Phi_{m+2}} \left(\mathrm{d}\sigma^R_{NNLO} - \mathrm{d}\sigma^S_{NNLO}\right) + \int_{\mathrm{d}\Phi_{m+2}} \mathrm{d}\sigma^S_{NNLO} \\ &+ \int_{\mathrm{d}\Phi_{m+1}} \left(\mathrm{d}\sigma^{V,1}_{NNLO} - \mathrm{d}\sigma^{VS,1}_{NNLO}\right) + \int_{\mathrm{d}\Phi_{m+1}} \mathrm{d}\sigma^{VS,1}_{NNLO} \\ &+ \int_{\mathrm{d}\Phi_m} \mathrm{d}\sigma^{V,2}_{NNLO} \end{aligned} \tag{4.1}$$

where, for $pp \to m$-jets, $\mathrm{d}\sigma^S_{NNLO}$ denotes the real radiation subtraction term coinciding with the $(m+4)$-parton tree level cross section $\mathrm{d}\sigma^R_{NNLO}$ in all singular limits. Likewise, $\mathrm{d}\sigma^{VS,1}_{NNLO}$ is the one-loop virtual subtraction term coinciding with the one-loop $(m+3)$-parton cross section $\mathrm{d}\sigma^{V,1}_{NNLO}$ in all singular limits. Finally, the two-loop correction to the $(m+2)$-parton cross section is denoted by $\mathrm{d}\sigma^{V,2}_{NNLO}$.

In chapter 6 we will give an explicit formula for $\mathrm{d}\sigma^S_{NNLO}$ for $gg \to gggg$ and show in chapter 7 that indeed the phase space singularities of the double real correction

can be written in terms of antenna functions. In the next section we will show how to derive the tree level double real radiation subtraction term $\mathrm{d}\sigma^S_{NNLO}$.

4.2 Tree level double real subtraction term $d\sigma^S_{NNLO}$

Let us consider the construction of the subtraction term for the double radiation contribution $\mathrm{d}\sigma^S_{NNLO}$, which shall correctly subtract all single and double unresolved singularities contained in the $(m+4)$-parton real radiation contribution to m-jet final states in pp collisions,

$$\begin{aligned}\mathrm{d}\sigma^R_{NNLO} = \mathcal{N} \sum_{\text{perms}} \mathrm{d}\Phi_{m+2}(k_1,\ldots,k_{m+2};p_1,p_2)\frac{1}{S_{m+2}} \\ \times \quad |\mathcal{M}_{m+4}(k_1,\ldots,k_{m+2};p_1,p_2)|^2 \; J^{(m+2)}_m(k_1,\ldots,k_{m+2}) \; . \end{aligned} \tag{4.2}$$

Single real radiation singularities correspond to one parton becoming soft or collinear, while double real radiation singularities occur if two partons become soft or collinear simultaneously. Singular terms in these limits can be identified by requiring a minimum number of invariants tending to zero in a given kinematical configuration. This number depends on the limit under consideration and follows from the phase space volume available to a given configuration. A detailed discussion of the kinematical definition of double unresolved limits was already given in section 1.8.

We must distinguish the following configurations according to the colour connection of the unresolved partons:

(a) One unresolved parton but the experimental observable selects only m jets.

(b) Two colour-connected unresolved partons (colour-connected).

(c) Two unresolved partons that are not colour connected but share a common radiator (almost colour-unconnected).

(d) Two unresolved partons that are well separated from each other in the colour chain (colour-unconnected).

For each configuration mentioned the subtraction formula has a characteristic antenna structure. Therefore in the following subsections we will discuss the individual formulae for each of the configurations (a) to (d).

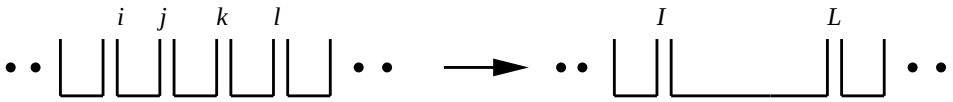

Figure 4.2: Colour connection of the partons showing the parent and daughter partons for the double unresolved antenna.

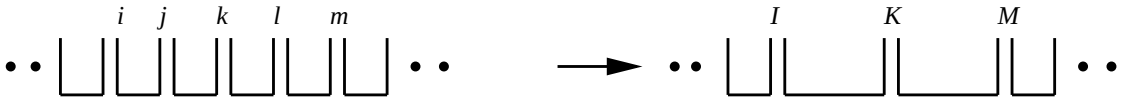

Figure 4.3: Colour connection of the partons showing the parent and daughter partons for two adjacent single unresolved antennae.

The first configuration was treated already in the context of antenna subtraction at NLO in section 3.2. In the context of the construction of $\mathrm{d}\sigma^S_{NNLO}$, the same single-particle subtraction terms can be used. These do however not yet guarantee a finite $(m+4)$-parton contribution in all single unresolved regions for two reasons: (1) while the jet function in $\mathrm{d}\sigma^S_{NLO}$ ensured that the subtraction term is non-zero only in the single unresolved limit it was constructed for, this is no longer the case for single unresolved radiation at NNLO; (2) the subtraction terms for the remaining three double unresolved configurations will in general be singular in the single unresolved regions, where they do not match the matrix element. Both problems will be addressed below.

The remaining three configurations (b)–(d) are illustrated in Figures 4.2, 4.3 and 4.4. The singular behaviour of the full $(m+4)$-parton matrix element in these configurations is the product of double unresolved factors (see section 1.8) and reduced $(m+2)$-parton matrix elements. Subtraction terms for all these configurations can be constructed using either single four-parton antenna functions or products of two three-parton antenna functions. In all cases, attention has to be paid to the matching of different double and single unresolved regions. This problem has been addressed already in publications on subtraction at NNLO [70, 82–84, 117, 118], the most concise discussion can be found in [84].

In the following, we construct the subtraction terms for all four configurations.

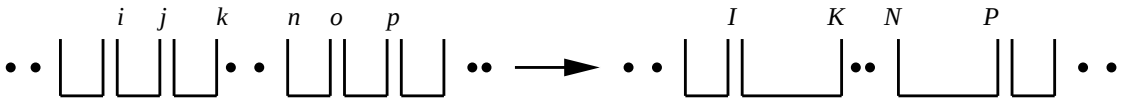

Figure 4.4: Colour connection of the partons showing the parent and daughter partons for two disconnected single unresolved antennae.

4.2.1 Subtraction terms for single unresolved partons $d\sigma^{S,a}_{NNLO}$

The starting point for the subtraction terms for single unresolved partons are the NLO single unresolved antenna subtraction terms (3.8), (3.16), (3.21):

$$\begin{aligned}\mathrm{d}\sigma^{S,a,(ff)}_{NNLO} = \mathcal{N} \sum_{\text{perms}} \mathrm{d}\Phi_{m+2}(k_1,\ldots,k_{m+2};p_1,p_2)\frac{1}{S_{m+2}} \\ \times \quad \Bigg[\sum_j X^0_{ijk}\,|\mathcal{M}_{m+3}(k_1,\ldots,\tilde{K}_{IJ},\tilde{K}_{JK},\ldots,k_{m+2};p_1,p_2)|^2 \\ J^{(m+1)}_m(k_1,\ldots,\tilde{K}_{IJ},\tilde{K}_{JK},\ldots,k_{m+2})\Bigg],\end{aligned} \tag{4.3}$$

$$\begin{aligned}\mathrm{d}\sigma^{S,a,(if)}_{NNLO} = \mathcal{N} \sum_{\text{perms}} \mathrm{d}\Phi_{m+2}(k_1,\ldots,k_{m+2};p_1,p_2)\frac{1}{S_{m+2}} \\ \times \quad \Bigg[\sum_j X^0_{2,jk}\,|\mathcal{M}_{m+3}(k_1,\ldots,\tilde{K}_{JK},\ldots,k_{m+2};p_1,xp_2)|^2 \\ J^{(m+1)}_m(k_1,\ldots,\tilde{K}_{JK},\ldots,k_{m+2})\Bigg], \quad + (1\leftrightarrow 2)\end{aligned} \tag{4.4}$$

$$\begin{aligned}\mathrm{d}\sigma^{S,a,(ii)}_{NNLO} = \mathcal{N} \sum_{\text{perms}} \mathrm{d}\Phi_{m+2}(k_1,\ldots,k_{j-1},k_j,k_{j+1},\ldots,k_{m+2};p_1,p_2)\frac{1}{S_{m+2}} \\ \times \quad \Bigg[\sum_j X^0_{12,j}|\mathcal{M}_{m+3}(\tilde{k}_1,\ldots,\tilde{k}_{j-1},\tilde{k}_{j+1},\ldots,\tilde{k}_{m+2};x_1p_1,x_2p_2)|^2 \\ J^{(m+1)}_m(\tilde{k}_1,\ldots,\tilde{k}_{j-1},\tilde{k}_{j+1},\ldots,\tilde{k}_{m+2})\Bigg]\end{aligned} \tag{4.5}$$

where the NLO jet function $J^{(m)}_m$ is now replaced by $J^{(m+1)}_m$. The sum over j is the sum over all unresolved partons in a colour ordered amplitude between radiators i and k which can be both located in the final state (4.3), i in the initial state and k

in the final state (4.4) or both in the initial state (4.5). Their position defines the type of the three-parton antenna which is used X_{ijk}, $X_{i,jk}$ or $X_{ij,k}$ respectively and the mapping used to generate the momenta in the reduced colour ordered amplitude $|\mathcal{M}_{m+3}|^2$.

When j is unresolved, $\mathrm{d}\sigma^{S,a}_{NNLO}$ coincides with the matrix element (4.2). However at NNLO the jet function $J^{(m+1)}_m$ allows one of the $(m+1)$ momenta to become unresolved while at NLO $J^{(m)}_m$ required all m momenta to be hard. In this limit $\mathrm{d}\sigma^{S,a}_{NNLO}$ does not coincide with the matrix element (4.2). We distinguish two cases: (1) when one of the new momenta, $\tilde{K}_{IJ}$ or $\tilde{K}_{JK}$, becomes unresolved and case (2) where any other momentum k_o or $\tilde{k}_o$ becomes unresolved.

Case (1) is necessarily a double unresolved limit since the new momenta $\tilde{K}_{IJ}$, $\tilde{K}_{JK}$, are linear combinations of two momenta and we discuss it below.

In case (2) $\mathrm{d}\sigma^{S,a}_{NNLO}$ becomes singular as k_o or $\tilde{k}_o$ become unresolved and it does not coincide with the limit of the full $(m+4)$-parton matrix element. However if we take this limit we find that $\mathrm{d}\sigma^{S,a}_{NNLO}$ collapses into the product of two almost colour-connected or colour-unconnected antenna functions with reduced $(m+2)$-parton matrix element which coincide with the structures (c) and (d) that we will define below. This means that this spurious limit cancels exactly against $\mathrm{d}\sigma^{S,c}_{NNLO}$ and $\mathrm{d}\sigma^{S,d}_{NNLO}$.

For the double unresolved limits we have on the one hand the limit where one of the new momenta $\tilde{K}_{IJ}$, $\tilde{K}_{JK}$, is unresolved, or the colour-neighbouring limit, where two pairs of momenta become independently collinear but one pair lies inside the antenna while the other pair consists of the remaining antenna momentum and its colour-connected neighbour. Each of these appears twice in the sum over j giving the two possibilities of attributing the inside/outside pair. These spurious limits will cancel exactly against similar terms that also appear twice in the structure (b) of $\mathrm{d}\sigma^{S,b}_{NNLO}$ that we will define below. Any other colour connected unresolved configuration vanishes.

On the other hand, double unresolved limits involving k_j and any other momenta k_o in the reduced matrix element that are almost colour connected or colour unconnected are not vanishing in $\mathrm{d}\sigma^{S,a}_{NNLO}$. In fact they yield twice these double

unresolved limits of the $(m+4)$-parton matrix element because the role of k_j and k_o can be interchanged and having $j = o$ in the sum results in two identical terms contributing to the same limit. The formulas for $\mathrm{d}\sigma^{S,c}_{NNLO}$ and $\mathrm{d}\sigma^{S,d}_{NNLO}$ will be defined to compensate this oversubtraction.

The analytic integration of this piece proceeds by using the formulas for the phase space factorisations given in section 3.2 with the results for the integrated antennae at NLO.

4.2.2 Subtraction terms for two colour-connected unresolved partons $d\sigma^{S,b}_{NNLO}$

When two unresolved partons j and k are adjacent, we construct the subtraction term starting from the four-particle tree-level antennae X_{ijkl}, $X_{i,jkl}$, $X_{il,jk}$. By construction they contain all colour connected double unresolved limits of the $(m+4)$-parton matrix element associated with partons j and k unresolved between radiators i and l. However this antenna can also become singular in *single* unresolved limits associated with j or k where it does not coincide with limits of the matrix element. To ensure a finite subtraction term in all these single unresolved limits, we therefore subtract the appropriate limits of the four-particle tree antennae, which are products of two tree-level three-particle antennae, such that the colour-connected double subtraction term reads:

$$\begin{aligned}
\mathrm{d}\sigma^{S,b,(ff)}_{NNLO} = \mathcal{N} \sum_{\text{perms}} \mathrm{d}\Phi_{m+2}(k_1,\ldots,k_{m+2};p_1,p_2)\frac{1}{S_{m+2}} \\
\times \quad \Bigg[\sum_{jk} \left(X^0_{ijkl} - X^0_{ijk}X^0_{IKl} - X^0_{jkl}X^0_{iJL}\right) \\
|\mathcal{M}_{m+2}(k_1,\ldots,\tilde{K}_{IJK},\tilde{K}_{LKJ},\ldots,k_{m+2};p_1,p_2)|^2 \\
J^{(m)}_m(k_1,\ldots,\tilde{K}_{IJK},\tilde{K}_{LKJ},\ldots,k_{m+2}) \Bigg] ,
\end{aligned} \tag{4.6}$$

$$\begin{aligned}
\mathrm{d}\sigma^{S,b,(if)}_{NNLO} &= \mathcal{N} \sum_{\text{perms}} \mathrm{d}\Phi_{m+2}(k_1,\ldots,k_{m+2};p_1,p_2)\frac{1}{S_{m+2}} \\
&\times \quad \Bigg[\sum_{jk} \left(X^0_{2,jkl} - X^0_{2,jk}X^0_{\tilde{2},Kl} - X^0_{jkl}X^0_{2,JL}\right)
\end{aligned}$$

$$
\begin{aligned}
& |\mathcal{M}_{m+2}(k_1,\ldots,K_{JKL},\ldots,k_{m+2};p_1,xp_2)|^2 \\
& J^{(m)}_m(k_1,\ldots,K_{JKL},\ldots,k_{m+2}) \quad + (1\leftrightarrow 2)\Bigg] , \qquad (4.7)
\end{aligned}
$$

$$
\begin{aligned}
\mathrm{d}\sigma^{S,b,(ii)}_{NNLO} &= \mathcal{N}\sum_{\text{perms}} \mathrm{d}\Phi_{m+2}(k_1,\ldots,k_j,k_l,\ldots,k_{m+2};p_1,p_2)\frac{1}{S_{m+2}} \\
&\times \Bigg[\sum_{jk}\left(X^0_{12,jk}-X^0_{2,jk}X^0_{1\bar{2},K}-X^0_{1,kj}X^0_{\bar{1}2,J}\right) \\
&\quad |\mathcal{M}_{m+2}(\tilde{k}_1,\ldots,\tilde{k}_{j-1},\tilde{k}_{k+1},\ldots,\tilde{k}_{m+2};x_1p_1,x_2p_2)|^2 \\
&\quad J^{(m)}_m(\tilde{k}_1,\ldots,\tilde{k}_{j-1},\tilde{k}_{k+1},\ldots,\tilde{k}_{m+2})\Bigg] \qquad (4.8)
\end{aligned}
$$

where the sum runs over all colour-adjacent pairs j,k and implies the appropriate selection of hard momenta i,l which as usual have three possible assignments of radiators. In all cases the $(m+2)$-parton matrix element is evaluated with new on-shell momenta given by a momentum mapping that we will discuss in section 4.3 when we describe the numerical implementation of this formula.

The products of three-parton antenna functions in $d\sigma^{S,b}_{NNLO}$ subtract the singular limits of the associated four parton antenna and each contribute equally in the colour-neighbouring configuration and spurious limits of $\mathrm{d}\sigma^{S,a}_{NNLO}$ discussed in the previous section. In all genuinely colour-connected limits, the four-parton antenna functions correctly match the singular structure of the $(m+4)$-parton matrix element (4.2). Singularities in the $(m+2)$-parton matrix element itself are forbidden by the jet function.

The analytic integration of this counterterm follows from the antenna factorisation of both the squared matrix elements and the $(m+2)$-particle phase space in figures 4.5, 4.6, 4.7.

The factorisation of the phase space reads for final-final, initial-final and initial-initial respectively:

$$
\begin{aligned}
\mathrm{d}\Phi_{m+2}(k_1,\ldots,k_{m+2};p_1,p_2) &= \mathrm{d}\Phi_m(k_1,\ldots,\tilde{K}_{IJK},\tilde{K}_{LKJ},\ldots,k_{m+2};p_1,p_2) \\
&\times \mathrm{d}\Phi_{X_{ijkl}}(k_i,k_j,k_k,k_l;\tilde{K}_{IJK}+\tilde{K}_{LKJ}) , \qquad (4.9)
\end{aligned}
$$

$$
\mathrm{d}\Phi_{m+2}(k_1,\ldots,k_{m+2};p_1,p_2) = \mathrm{d}\Phi_m(k_1,\ldots,K_{JKL},\ldots,k_{m+2};p_1,xp_2)
$$

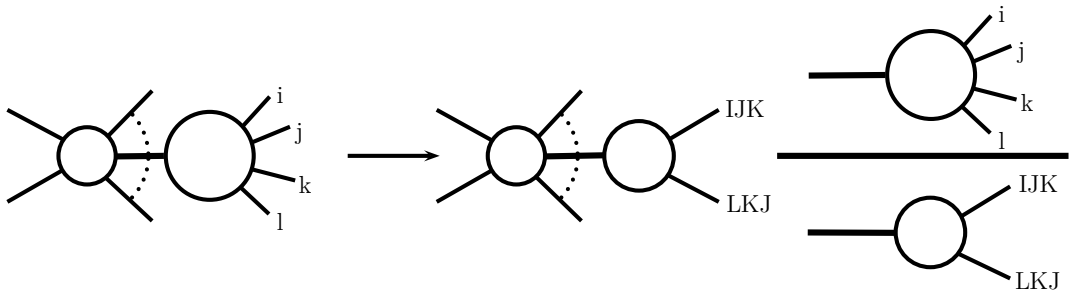

Figure 4.5: Illustration of NNLO antenna factorisation representing the factorisation of both the squared matrix elements and the $(m+2)$-particle phase space when the unresolved particles are colour connected between two final state radiators.

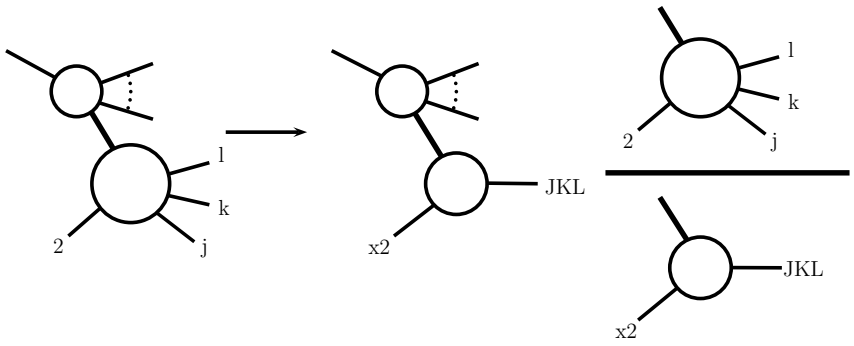

Figure 4.6: Illustration of NNLO antenna factorisation representing the factorisation of both the squared matrix elements and the $(m+2)$-particle phase space when the unresolved particles are colour connected between and initial state i and a final state l radiator.

$$\times \quad \frac{Q^2}{2\pi} \mathrm{d}\Phi_3(k_j, k_k, k_l; p_2, q) \frac{\mathrm{d}x}{x}\,, \tag{4.10}$$

$$\begin{aligned} \mathrm{d}\Phi_{m+2}(k_1, \ldots, k_{m+2}; p_1, p_2) \;&=\; \mathrm{d}\Phi_m(\tilde{k}_1, \ldots, \tilde{k}_{j-1}, \tilde{k}_{k+1}, \ldots, \tilde{k}_{m+2}; x_1 p_1, x_2 p_2) \\ &\quad \times \delta(x_1 - \hat{x}_1)\, \delta(x_2 - \hat{x}_2)\, [\mathrm{d}k_j][\mathrm{d}k_k]\, \mathrm{d}x_1\, \mathrm{d}x_2\,, \end{aligned} \tag{4.11}$$

where in (4.10) $Q^2 = -q^2$, $q = k_j + k_k + k_l - p_2$. A similar factorisation holds with $(1 \leftrightarrow 2)$ for initial state singularities with parton 1. Using (4.9), (4.10), (4.11) we can rewrite each of the genuine four-particle subtraction terms in the form,

$$|\mathcal{M}_{m+2}|^2\, J^{(m)}_m\, \mathrm{d}\Phi_m \int \mathrm{d}\Phi_{X_{ijkl}}\, X^0_{ijkl}, \tag{4.12}$$

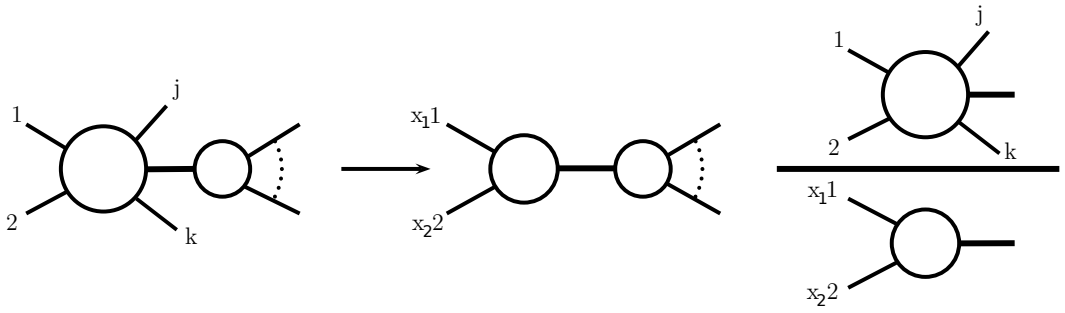

Figure 4.7: Illustration of NNLO antenna factorisation representing the factorisation of both the squared matrix elements and the $(m+2)$-particle phase space when the unresolved particles are colour connected between two initial state radiators.

$$|\mathcal{M}_{m+2}|^2 \, J_m^{(m)} \, \mathrm{d}\Phi_m \int \frac{Q^2}{2\pi} \mathrm{d}\Phi_3(k_j, k_k, k_l; p, q) \; X^0_{i,jkl} \frac{\mathrm{d}x}{x}, \tag{4.13}$$

$$|\mathcal{M}_{m+2}|^2 \, J_m^{(m)} \, \mathrm{d}\Phi_m \int [\mathrm{d}k_j][\mathrm{d}k_k] \delta(x_1 - \hat{x}_1) \, \delta(x_2 - \hat{x}_2) \; X^0_{il,jk} \mathrm{d}x_1 \, \mathrm{d}x_2 \tag{4.14}$$

The antennae integrals can be worked out separately once and for all to become universal building blocks for subtraction at NNLO. The integrated antenna is the antenna function integrated over the fully inclusive antenna phase space including a normalisation factor to account for powers of the QCD coupling constant,

$$\mathcal{X}^0_{ijkl} = \frac{1}{[C(\epsilon)]^2} \int \mathrm{d}\Phi_{X_{ijkl}} \; X^0_{ijkl} \tag{4.15}$$

$$\mathcal{X}^0_{i,jkl} = \frac{1}{[C(\epsilon)]^2} \int \mathrm{d}\Phi_3 \frac{Q^2}{2\pi} X^0_{i,jkl} \tag{4.16}$$

$$\mathcal{X}^0_{il,jk} = \frac{1}{[C(\epsilon)]^2} \int [\mathrm{d}k_j][\mathrm{d}k_k] \; x_1 \; x_2 \; \delta(x_1 - \hat{x}_1) \, \delta(x_2 - \hat{x}_2) X^0_{il,jk} \tag{4.17}$$

where $C(\epsilon)$ is given in (3.11). These integrations are performed analytically in d dimensions to make the infrared singularities explicit. Using the techniques in [104] all integrated antennae in (4.15) were obtained and are documented in [67]. Also all integrated antennae of (4.16) were computed recently in [105, 119]. The remaining integrals in (4.17) are the presently unknown NNLO initial-initial integrated antennae functions. Work on their analytic evaluation is underway [120].

4.2.3 Subtraction terms for two almost colour-unconnected unresolved partons $d\sigma^{S,c}_{NNLO}$

There are double unresolved configurations where the unresolved partons are separated by a hard radiator parton, for example, i, j, k, l, m where j and l are unresolved. In this case we take the strongly ordered approach where i, j, k form an antenna with hard partons I and K yielding an ordered amplitude involving I, K, l, m. As usual, the momenta of the hard radiator partons I and K are constructed from k_i, k_j, k_k. The cases where l is unresolved are then treated using an antenna K, l, m with hard partons K and M. The momenta of the hard radiator partons K and M are made from $\tilde{K}_{JK}, k_l, k_m$. The other case where first k, l, m form an antenna followed by i, j, K is also included.

In this configuration there is a common radiator that can be in the final or the initial state. The subtraction term for the almost colour-connected configuration reads:

$$
\begin{aligned}
\mathrm{d}\sigma^{S,c,(ff)}_{NNLO} &= -\mathcal{N} \sum_{\text{perms}} \mathrm{d}\Phi_{m+2}(k_1,\ldots,k_{m+2};p_1,p_2)\frac{1}{S_{m+2}} \\
&\times \Bigg[\sum_{j,l} X^0_{ijk}\, x^0_{mlK}\, |\mathcal{M}_{m+2}(k_1,\ldots,\tilde{K}_{IJ},\tilde{\tilde{K}}_{(JK)L},\tilde{\tilde{K}}_{(LM)},\ldots,k_{m+2})|^2 \\
&\qquad J^{(m)}_m(k_1,\ldots,\tilde{K}_{IJ},\tilde{\tilde{K}}_{(JK)L},\tilde{\tilde{K}}_{(LM)},\ldots,k_{m+2}) \\
&\quad + \sum_{j,l} X^0_{klm}\, x^0_{ijK}\, |\mathcal{M}_{m+2}(k_1,\ldots,\tilde{\tilde{K}}_{(IJ)},\tilde{\tilde{K}}_{(KL)J},\tilde{K}_{LM},\ldots,k_{m+2})|^2 \\
&\qquad J^{(m)}_m(k_1,\ldots,\tilde{\tilde{K}}_{(IJ)},\tilde{\tilde{K}}_{(KL)J},\tilde{K}_{LM},\ldots,k_{m+2}) \Bigg], \qquad (4.18)
\end{aligned}
$$

$$
\begin{aligned}
\mathrm{d}\sigma^{S,c1,(if)}_{NNLO} &= -\mathcal{N} \sum_{\text{perms}} \mathrm{d}\Phi_{m+2}(k_1,\ldots,k_{m+2};p_1,p_2)\frac{1}{S_{m+2}} \\
&\times \Bigg[\sum_{j,l} X^0_{2,jk}\, x^0_{mlK}\, |\mathcal{M}_{m+2}(k_1,\ldots,\tilde{\tilde{K}}_{(KJ)L},\tilde{K}_{LM},\ldots,k_{m+2};p_1,xp_2)|^2 \\
&\qquad J^{(m)}_m(k_1,\ldots,\tilde{\tilde{K}}_{(KJ)L},\tilde{K}_{LM},\ldots,k_{m+2}) \\
&\quad + \sum_{j,l} X^0_{klm}\, x^0_{2,jK}\, |\mathcal{M}_{m+2}(k_1,\ldots,\tilde{\tilde{K}}_{(KL)J},\tilde{K}_{LM},\ldots,k_{m+2};p_1,xp_2)|^2
\end{aligned}
$$

$$J_m^{(m)}(k_1,\ldots,\tilde{\tilde{K}}_{(KL)J},\tilde{K}_{LM},\ldots,k_{m+2})\Big] + (1\leftrightarrow 2)$$

, (4.19)

$$\begin{aligned}
\mathrm{d}\sigma^{S,c2,(if)}_{NNLO} &= -\mathcal{N}\sum_{\text{perms}}\mathrm{d}\Phi_{m+2}(k_1,\ldots,k_{m+2};p_1,p_2)\frac{1}{S_{m+2}} \\
&\times \Bigg[\sum_{j,l} X^0_{2,jk}\, x^0_{\tilde{2},lm}\,|\mathcal{M}_{m+2}(k_1,\ldots,\tilde{K}_{JK},\tilde{K}_{LM},\ldots,k_{m+2};p_1,xx^{'}p_2)|^2 \\
&\qquad J_m^{(m)}(k_1,\ldots,\tilde{K}_{JK},\tilde{K}_{LM},\ldots,k_{m+2}) \\
&\quad +\sum_{j,l} X^0_{2,lm}\, x^0_{\tilde{2},jk}\,|\mathcal{M}_{m+2}(k_1,\ldots,\tilde{K}_{LM},\tilde{K}_{JK},\ldots,k_{m+2};p_1,xx^{'}p_2)|^2 \\
&\qquad \times J_m^{(m)}(k_1,\ldots,\tilde{K}_{LM},\tilde{K}_{JK},\ldots,k_{m+2})\Bigg] + (1\leftrightarrow 2)
\end{aligned}$$

, (4.20)

$$\begin{aligned}
\mathrm{d}\sigma^{S,c,(ii)}_{NNLO} &= -\mathcal{N}\sum_{\text{perms}}\mathrm{d}\Phi_{m+2}(k_1,\ldots,k_{m+2};p_1,p_2)\frac{1}{S_{m+2}} \\
&\times \Bigg[\sum_{j,l} X^0_{2,jk}\, x^0_{\tilde{21},l}\,|\mathcal{M}_{m+2}(\tilde{k}_1,\ldots,\tilde{k}_{j-1},\tilde{k}_{l+1},\ldots,\tilde{k}_{m+2};x_1^{'}p_1,x_2^{'}x_2p_2)|^2 \\
&\qquad \times J_m^{(m)}(\tilde{k}_1,\ldots,\tilde{k}_{j-1},\tilde{k}_{l+1},\ldots,\tilde{k}_{m+2}) \\
&\quad +\sum_{j,l} X^0_{21,l}\, x^0_{\tilde{2},jk}\,|\mathcal{M}_{m+2}(\tilde{k}_1,\ldots,\tilde{k}_{j-1},\tilde{k}_{l+1},\ldots,\tilde{k}_{m+2};x_1p_1,x_2x_2^{'}p_2)|^2 \\
&\qquad \times J_m^{(m)}(\tilde{k}_1,\ldots,\tilde{k}_{j-1},\tilde{k}_{l+1},\ldots,\tilde{k}_{m+2})\Bigg] + (1\leftrightarrow 2)
\end{aligned}$$

, (4.21)

where x^0_{mlK} denotes a sub-antenna, that contains only the collinear limit of m with l, but not the collinear limit of l with K. In the soft limit of l, this sub-antenna yields half the soft eikonal factor. (4.19) applies if the common radiator is in the final state, while (4.20) applies if the common radiator is in the initial state.

In the almost colour connected configuration $\mathrm{d}\sigma^{S,c}_{NNLO}$ yields minus the double unresolved limit of the matrix element and therefore cancels the oversubtraction of $\mathrm{d}\sigma^{S,a}_{NNLO}$ in the same configuration. In the single unresolved limits when either j or l is unresolved $\mathrm{d}\sigma^{S,c}_{NNLO}$ exactly cancels the spurious single unresolved singularities

encountered in $\mathrm{d}\sigma^{S,a}_{NNLO}$ for the configuration of an unresolved momentum p_o in the $(m+3)$-parton matrix element.

To obtain the integrated form of this counterterm we exploit the factorisation of the $(m+2)$-parton phase space into a m-parton phase space and the phase space for the product of the two antennae.

4.2.4 Subtraction terms for two colour-unconnected unresolved partons $d\sigma^{S,d}_{NNLO}$

When two unresolved partons j and o are completely disconnected i,j,k,...,n,o,p the $(m+4)$-parton matrix element factorises into the product of two uncorrelated single unresolved factors with a reduced $(m+2)$-parton matrix element. The subtraction for the colour-unconnected configuration reads:

$$\begin{aligned}
\mathrm{d}\sigma^{S,d,(ff)}_{NNLO} &= -\mathcal{N}\sum_{\text{perms}}\mathrm{d}\Phi_{m+2}(k_1,\ldots,k_{m+2};p_1,p_2)\frac{1}{S_{m+2}} \\
&\times \Bigg[\sum_{j,o} X^0_{ijk}\,X^0_{nop}\,|\mathcal{M}_{m+2}(k_1,\ldots,\tilde{K}_{IJ},\tilde{K}_{JK},\ldots,\tilde{K}_{NO},\tilde{K}_{OP},\ldots,k_{m+2})|^2 \\
&\times J^{(m)}_m(k_1,\ldots,\tilde{K}_{IJ},\tilde{K}_{JK},\ldots,\tilde{K}_{NO},\tilde{K}_{OP},\ldots,k_{m+2})\Bigg]\,, \qquad (4.22)
\end{aligned}$$

$$\begin{aligned}
\mathrm{d}\sigma^{S,d,(if)}_{NNLO} &= -\mathcal{N}\sum_{\text{perms}}\mathrm{d}\Phi_{m+2}(k_1,\ldots,k_{m+2};p_1,p_2)\frac{1}{S_{m+2}}\Bigg[\sum_{j,o} X^0_{2,jk}\,X^0_{nop} \\
&\times |\mathcal{M}_{m+2}(k_1,\ldots,\tilde{K}_{JK},\ldots,\tilde{K}_{NO},\tilde{K}_{OP},\ldots,k_{m+2};p_1,xp_2)|^2 \\
&\times J^{(m)}_m(k_1,\ldots,\tilde{K}_{JK},\ldots,\tilde{K}_{NO},\tilde{K}_{OP},\ldots,k_{m+2})\Bigg] + (1\leftrightarrow 2)\,, \qquad (4.23)
\end{aligned}$$

$$\begin{aligned}
\mathrm{d}\sigma^{S,d1,(ii)}_{NNLO} &= -\mathcal{N}\sum_{\text{perms}}\mathrm{d}\Phi_{m+2}(k_1,\ldots,k_{m+2};p_1,p_2)\frac{1}{S_{m+2}}\Bigg[\sum_{j,o} X^0_{1,jk}\,X^0_{2,op} \\
&\times |\mathcal{M}_{m+2}(k_1,\ldots,\tilde{K}_{JK},\ldots,\tilde{K}_{OP},\ldots,k_{m+2};x_1p_1,x_2p_2)|^2 \\
&\times J^{(m)}_m(k_1,\ldots,\tilde{K}_{JK},\ldots,\tilde{K}_{OP},\ldots,k_{m+2})\Bigg]\,, \qquad (4.24)
\end{aligned}$$

$$\mathrm{d}\sigma^{S,d2,(ii)}_{NNLO} = -\mathcal{N}\sum_{\text{perms}}\mathrm{d}\Phi_{m+2}(k_1,\ldots,k_{m+2};p_1,p_2)\frac{1}{S_{m+2}}\Bigg[\sum_{j,o} X^0_{12,j}\,X^0_{nop}$$

$$\times \quad |\mathcal{M}_{m+2}(\tilde{k}_1,\ldots,\tilde{k}_{j-1},\tilde{k}_{j+1},\ldots,\tilde{k}_{NO},\tilde{k}_{OP},\ldots,\tilde{k}_{m+2};x_1p_1,x_2p_2)|^2$$
$$\times \quad J^{(m)}_m(k_1,\ldots,\tilde{k}_{j-1},\tilde{k}_{j+1},\ldots,\tilde{k}_{NO},\tilde{k}_{OP},\ldots,\tilde{k}_{m+2})\Bigg], \tag{4.25}$$

where the summation over o is such that it only includes two antenna configurations with no common momenta. The nature of the radiator pairs i,k and n,p defines the formula to be used.

In the colour unconnected configuration $\mathrm{d}\sigma^{S,d}_{NNLO}$ yields minus the double unresolved limit of the matrix element and therefore cancels the oversubtraction of $\mathrm{d}\sigma^{S,a}_{NNLO}$ in the same configuration. In the single unresolved limits when either j or o is unresolved $\mathrm{d}\sigma^{S,d}_{NNLO}$ exactly cancels the spurious single unresolved singularities encountered in $\mathrm{d}\sigma^{S,a}_{NNLO}$ for the configuration of an unresolved momentum in the $(m+3)$-parton matrix element.

To obtain the integrated form of this counterterm we exploit the factorisation of the $(m+2)$-parton phase space into a m-parton phase space and the phase space for the product of the two antennae.

4.2.5 Subtraction terms for large angle soft emission

It was shown in [93, 94] that the previous antenna subtraction terms result in an oversubtraction of large-angle soft gluon radiation. If we take a single soft gluon limit $j \to 0$ of the formulae of the previous sections we obtain the following contributions. final-final:

$$X_{ilk}\,|M_{m+2}(k_1,\ldots,\tilde{K}_{IL},\tilde{K}_{LK},\ldots,k_{m+2};p_1,p_2)|^2 \times$$
$$(-S_{(il)j(lk)}+S_{ijk}+S_{hj(il)}-S_{hji}+S_{(lk)jm}-S_{kjm}) \tag{4.26}$$

final-initial:

$$X_{2,lk}\,|M_{m+2}(k_1,\ldots,k_{j-1},k_{j+1},\ldots,\tilde{K}_{LK},\ldots,k_{m+2};p_1,xp_2)|^2 \times$$
$$(-S_{\bar{2}j(lk)}+S_{2jk}+S_{hj\bar{2}}-S_{hj2}+S_{(lk)jm}-S_{kjm}) \;+\; (1\leftrightarrow 2) \tag{4.27}$$

initial-initial:

$$X_{12,l}\,|M_{m+2}(\tilde{k}_1,\ldots,\tilde{k}_{j-1},\tilde{k}_{j+1},\ldots,\tilde{k}_{k-1},\tilde{k}_{k+1},\ldots,\tilde{k}_{m+2};x_1p_1,x_2p_2)|^2 \times$$

$$(-S_{\bar{1}j\bar{2}} + S_{1j2} + S_{hj\bar{1}} - S_{hj1} + S_{\bar{2}jm} - S_{2jm}) \tag{4.28}$$

where

$$S_{abc} = 2\frac{s_{ac}}{s_{ab}s_{bc}} \tag{4.29}$$

are eikonal factors related with the remnant soft behaviour of the phase space mappings. To account for this large angle soft radiation, a new subtraction term $\mathrm{d}\sigma^A_{NNLO}$ is introduced and added to the $(m+4)$-parton piece $\mathrm{d}\sigma^S_{NNLO}$:

$$\begin{aligned}
\mathrm{d}\sigma^{A,(ff)}_{NNLO} &= X_{(ij)l(jk)}|\mathcal{M}_{m+2}(k_1,\ldots,\tilde{\tilde{K}}_{(IJ)L},\tilde{\tilde{K}}_{(JK)L},\ldots\ k_{m+2};p_1,p_2)|^2 \times \\
&\quad (S_{((ij)l)j((jk)l)} - S_{(ij)j(jk)} - S_{hj((ij)l)} + S_{hj(ij)} - S_{((jk)l)jm} + S_{(jk)jm}) \qquad (4.30)\\
\mathrm{d}\sigma^{A,(if)}_{NNLO} &= X_{\bar{2},l(jk)}|\mathcal{M}_{m+2}(k_1,\ldots,k_{j-1},k_{j+1},\ldots,\tilde{\tilde{K}}_{(JK)L},\ldots\ k_{m+2};p_1,xx^{'}p_2)|^2 \times \\
&\quad (S_{\bar{\tilde{2}}j((jk)l)} - S_{\bar{\tilde{2}}j(jk)} - S_{hj\bar{\tilde{2}}} + S_{hj\bar{2}} - S_{((jk)l)jm} + S_{(jk)jm}) \ + \ (1\leftrightarrow 2) \qquad (4.31)\\
\mathrm{d}\sigma^{A,(ii)}_{NNLO} &= X_{\bar{1}\bar{2},l}|\mathcal{M}_{m+2}(\tilde{\tilde{k}}_1,\ldots,\tilde{\tilde{k}}_{j-1},\tilde{\tilde{k}}_{j+1},\ldots,\tilde{\tilde{k}}_{k-1},\tilde{\tilde{k}}_{k+1},\ldots,\tilde{\tilde{k}}_{m+2};x_1x_1^{'}p_1,x_2x_2^{'}p_2)|^2 \times \\
&\quad (S_{\bar{\tilde{1}}\tilde{j}\bar{\tilde{2}}} - S_{\bar{1}j\bar{2}} - S_{hj\bar{\tilde{1}}} + S_{hj\bar{1}} - S_{\bar{\tilde{2}}jm} + S_{\bar{2}jm}) \qquad (4.32)
\end{aligned}$$

These large-angle soft subtraction terms $\mathrm{d}\sigma^A_{NNLO}$ contains soft antenna functions of the form S_{ajc} which is simply the eikonal factor for a soft gluon j emitted between hard partons a and c, that precisely cancels the behaviour in (4.26), (4.27), (4.28). Those soft factors are associated with an antenna phase space mapping $(i,j,k)\to(IJ,JK)$ (final-final), $(p,j,k)\to(xp,JK)$ (initial-final), $(p_1,p_2,j)\to(x_1p_1,x_2p_2)$ (initial-initial). The hard momenta a, c do not need to be equal to the hard momenta i, k in the antenna phase space - they can be arbitrary on-shell momenta. In the l soft limit the eikonal factors cancel between each other in (4.30), (4.31), (4.32) such that no new spurious limits are introduced.

Once this terms is included in $\mathrm{d}\sigma^S_{NNLO}$ the subtraction term for the $(m+4)$-parton matrix element becomes finite in the single soft limit.

4.2.6 Correction terms in the m-jet region

The full double radiation subtraction term is given as sum of all subtraction terms constructed above:

$$\mathrm{d}\sigma^S_{NNLO} = \mathrm{d}\sigma^{S,a}_{NNLO} + \mathrm{d}\sigma^{S,b}_{NNLO} + \mathrm{d}\sigma^{S,c}_{NNLO} + \mathrm{d}\sigma^{S,d}_{NNLO} + \mathrm{d}\sigma^A_{NNLO}\ . \tag{4.33}$$

As outlined in the previous subsections, this subtraction term correctly approximates the $(m+4)$-parton matrix element contribution to m-jet final states as defined in (4.2) in all double and single unresolved regions. Although individual terms in (4.33) contain spurious singularities in these limits, they cancel among each other in the sum.

The integrated form of (a) corresponds to an $(m+3)$-parton configuration, while the integrated forms of (b), (c) and (d) are either $(m+3)$-parton or $(m+2)$-parton configurations (for all but the four-parton antenna terms in (b), we can actually choose which type of configuration we want to integrate). They are added with the two-loop $(m+2)$-parton and the one-loop $(m+3)$-parton contributions to m-jet final states to yield an integrand free of explicit infrared poles.

4.3 Numerical implementation of NNLO antenna functions

Having looked at the general formula for the double real radiation piece it is important to discuss its numerical implementation and to do so, we focus on a specific example. If we concentrate on the pure gluon channel contributing to the two-jet cross section we find that the four gluon antenna F_4^0 (given in the appendix B.1) is the genuinely new ingredient at NNLO. In F_4^0, derived from $H \to gggg$, the gluonic emissions are colour ordered. The colour structure is a trace over the gluon indices and F_4^0 is symmetric under cyclic interchanges of momenta. We will take this into account when we discuss the numerical implementation of F_4^0 for the final-final, initial-final and initial-initial arrangements of radiators.

4.3.1 Final-Final emitters

The decomposition of $F_4^0(1_g, 2_g, 3_g, 4_g)$ is needed since any pair of two gluons can become soft. Its unintegrated and integrated form has been written down in [67]. In the case of the final-final configuration, this antenna has all the partons in the final state and can be used to subtract double unresolved final state singularities

of colour ordered matrix elements when the unresolved gluons are colour connected between two final state gluons. We consider eight different mappings to achieve the decomposition:

$$\begin{aligned}
&\text{(a): } (1,2,3,4) \to (\widetilde{123},\widetilde{432})\,, && \text{(b): } (1,2,4,3) \to (\widetilde{124},\widetilde{342})\,,\\
&\text{(c): } (1,4,3,2) \to (\widetilde{143},\widetilde{234})\,, && \text{(d): } (1,4,2,3) \to (\widetilde{142},\widetilde{324})\,,\\
&\text{(e): } (2,3,1,4) \to (\widetilde{231},\widetilde{413})\,, && \text{(f): } (2,1,4,3) \to (\widetilde{214},\widetilde{341})\,,\\
&\text{(g): } (4,3,1,2) \to (\widetilde{431},\widetilde{213})\,, && \text{(h): } (4,1,2,3) \to (\widetilde{412},\widetilde{321})
\end{aligned} \tag{4.34}$$

In each mapping of the type $\{p_{i_1}, p_{i_2}, p_{i_3}, p_{i_4}\} \to \{\widetilde{p_{i_1 i_2 i_3}}, \widetilde{p_{i_4 i_3 i_2}}\}$ partons i_2 and i_3 become unresolved and i_1 and i_4 are the hard radiators. The new momenta are given by:

$$\begin{aligned}
\widetilde{p_{(i_1 i_2 i_3)}} &= x\,p_{i_1} + r_1\,p_{i_2} + r_2\,p_{i_3} + z\,p_{i_4}\\
\widetilde{p_{(i_4 i_3 i_2)}} &= (1-x)\,p_{i_1} + (1-r_1)\,p_{i_2} + (1-r_2)\,p_{i_3} + (1-z)\,p_{i_4}\,.
\end{aligned} \tag{4.35}$$

Defining $s_{kl} = (p_{i_k} + p_{i_l})^2$, the coefficients are given by [117]:

$$\begin{aligned}
r_1 &= \frac{s_{23}+s_{24}}{s_{12}+s_{23}+s_{24}}\\
r_2 &= \frac{s_{34}}{s_{13}+s_{23}+s_{34}}\\
x &= \frac{1}{2(s_{12}+s_{13}+s_{14})}\Big[(1+\rho)\,s_{1234}\\
&\quad -r_1\,(s_{23}+2\,s_{24}) - r_2\,(s_{23}+2\,s_{34})\\
&\quad +(r_1-r_2)\frac{s_{12}s_{34}-s_{13}s_{24}}{s_{14}}\Big]\\
z &= \frac{1}{2(s_{14}+s_{24}+s_{34})}\Big[(1-\rho)\,s_{1234}\\
&\quad -r_1\,(s_{23}+2\,s_{12}) - r_2\,(s_{23}+2\,s_{13})\\
&\quad -(r_1-r_2)\frac{s_{12}s_{34}-s_{13}s_{24}}{s_{14}}\Big]\\
\rho &= \Big[1+\frac{(r_1-r_2)^2}{s_{14}^2\,s_{1234}^2}\,\lambda(s_{12}\,s_{34}, s_{14}\,s_{23}, s_{13}\,s_{24})\\
&\quad +\frac{1}{s_{14}\,s_{1234}}\Big\{2\,\big(r_1\,(1-r_2)+r_2(1-r_1)\big)\big(s_{12}s_{34}+s_{13}s_{24}-s_{23}s_{14}\big)\\
&\qquad +4\,r_1\,(1-r_1)\,s_{12}s_{24} + 4\,r_2\,(1-r_2)\,s_{13}s_{34}\Big\}\Big]^{\frac{1}{2}}\,,\\
\lambda(u,v,w) &= u^2+v^2+w^2-2(uv+uw+vw)\,.
\end{aligned}$$

This mapping smoothly interpolates all colour connected double unresolved singularities. It satisfies the following properties:

$$\begin{aligned}
\widetilde{p_{(i_1 i_2 i_3)}} \to p_{i_1} \qquad \widetilde{p_{(i_4 i_3 i_2)}} \to p_{i_4} \qquad & \text{when } i_2, i_3 \to 0 \\
\widetilde{p_{(i_1 i_2 i_3)}} \to p_{i_1} + p_{i_2} + p_{i_3} \qquad \widetilde{p_{(i_4 i_3 i_2)}} \to p_{i_4} \qquad & \text{when } i_1 // i_2 // i_3 \\
\widetilde{p_{(i_1 i_2 i_3)}} \to p_{i_1} \qquad \widetilde{p_{(i_4 i_3 i_2)}} \to p_{i_4} + p_{i_3} + p_{i_2} \qquad & \text{when } i_2 // i_3 // i_4 \\
\widetilde{p_{(i_1 i_2 i_3)}} \to p_{i_1} \qquad \widetilde{p_{(i_4 i_3 i_2)}} \to p_{i_4} + p_{i_3} \qquad & \text{when } i_2 \to 0 + i_3 // i_4 \\
\widetilde{p_{(i_1 i_2 i_3)}} \to p_{i_1} + p_{i_2} \qquad \widetilde{p_{(i_4 i_3 i_2)}} \to p_{i_2} \qquad & \text{when } i_3 \to 0 + i_1 // i_2 \\
\widetilde{p_{(i_1 i_2 i_3)}} \to p_{i_1} + p_{i_2} \qquad \widetilde{p_{(i_4 i_3 i_2)}} \to p_{i_3} + p_{i_4} \qquad & \text{when } i_1 // i_2 + i_3 // i_4
\end{aligned} \tag{4.36}$$

Moreover in single unresolved limits it collapses into an NLO mapping allowing the subtraction of single unresolved limits of $F_4^0(1_g, 2_g, 3_g, 4_g)$ with products of three parton antenna functions as in equation (4.6).

The task left now is to disentangle the various double and single unresolved limits of the full antenna $F_4^0(1_g, 2_g, 3_g, 4_g)$ into eight sub-antennae such that each sub-antenna (a),(b),...,(h) contains only those singularities appropriate to the mapping (a),(b),...,(h).

These numerous double and single unresolved limits can be disentangled very elegantly by repeatedly exploiting the $\mathcal{N} = 1$ supersymmetry relation [31] among the different triple collinear splitting functions [31–34, 121, 122]. Using this relation, one can show that the following left-over combination is finite in all single unresolved and double unresolved limits:

$$\begin{aligned}
F_{4,l}^0(1,2,3,4) \;=\; & F_4^0(1,2,3,4) - \\
& \Big[D_4^0(1,2,3,4) + D_4^0(2,3,4,1) + D_4^0(3,4,1,2) + D_4^0(4,1,2,3) \\
& - A_4^0(1,2,3,4) - A_4^0(2,3,4,1) - A_4^0(3,4,1,2) - A_4^0(4,1,2,3) \\
& - \tilde{A}_4^0(1,2,4,3) - \tilde{A}_4^0(2,3,1,4) + H_4^0(2,1,4,3) + H_4^0(4,1,2,3) \\
& + A_3^0(4,1,2)\, J_3^0(\widetilde{(12)}, 3, \widetilde{(14)}) + A_3^0(1,2,3)\, J_3^0(\widetilde{(12)}, \widetilde{(23)}, 4) \\
& + A_3^0(2,3,4)\, J_3^0(1, \widetilde{(23)}, \widetilde{(34)}) + A_3^0(3,4,1)\, J_3^0(\widetilde{(14)}, 2, \widetilde{(34)}) \\
& + \frac{1}{2} G_3^0(4,1,2)\, K_3^0(\widetilde{(12)}, \widetilde{(14)}, 3) + \frac{1}{2} G_3^0(1,2,3)\, K_3^0(\widetilde{(23)}, \widetilde{(12)}, 4)
\end{aligned}$$

$$
\begin{aligned}
&+\frac{1}{2}G_3^0(2,3,4)\,K_3^0(\widetilde{(34)},\widetilde{(23)},1)+\frac{1}{2}G_3^0(3,4,1)\,K_3^0(\widetilde{(14)},\widetilde{(34)},2)\\
&+\frac{1}{2}G_3^0(2,1,4)\,K_3^0(\widetilde{(14)},\widetilde{(12)},3)+\frac{1}{2}G_3^0(3,1,2)\,K_3^0(\widetilde{(12)},\widetilde{(23)},4)\\
&+\frac{1}{2}G_3^0(4,3,2)\,K_3^0(\widetilde{(23)},\widetilde{(34)},1)+\frac{1}{2}G_3^0(1,4,3)\,K_3^0(\widetilde{(34)},\widetilde{(14)},2)\Big]
\end{aligned}
\tag{4.37}
$$

where J_3^0 and K_3^0 are useful combinations of the following three parton antenna functions:

$$
\begin{aligned}
J_3^0(1,2,3) &= F_3^0(1,2,3)+A_3^0(3,1,2)+A_3^0(1,2,3)+A_3^0(1,3,2)\\
&\quad -D_3^0(1,2,3)-D_3^0(2,3,1)-D_3^0(3,1,2) \qquad (4.38)\\
K_3^0(1,2,3) &= F_3^0(1,2,3)-D_3^0(2,3,1)-D_3^0(3,1,2)+A_3^0(3,1,2)\\
&\quad +G_3^0(1,2,3) \qquad (4.39)
\end{aligned}
$$

Neither J_3^0 or K_3^0 contains any soft or collinear limit, but to distribute the single unresolved limits among the momentum mappings it is convenient to introduce the following antennae:

$$
\begin{aligned}
T_3^0(1,2,3) &= f_3^0(1,2,3)+A_3^0(1,2,3)-d_3^0(1,2,3)-d_3^0(3,2,1) \qquad (4.40)\\
U_3^0(1,2,3) &= f_3^0(1,2,3)-d_3^0(1,2,3) \qquad (4.41)
\end{aligned}
$$

where T_3^0 is finite in all single unresolved limits but U_3^0 contains the $1 \parallel 2$ limit. We can now rewrite J_3^0 and K_3^0 as:

$$
\begin{aligned}
J_3^0(1,2,3) &= T_3^0(1,2,3)+T_3^0(1,3,2)+T_3^0(2,1,3) \qquad (4.42)\\
K_3^0(1,2,3) &= U_3^0(2,3,1)+U_3^0(3,2,1)+T_3^0(2,1,3)+G_3^0(1,2,3) \qquad (4.43)
\end{aligned}
$$

Starting from the terms in the expression (4.37) the following sub-antennae can be constructed:

$$
\begin{aligned}
F_{4,a}^0(1,2,3,4) &= \frac{1}{4}F_{4,l}^0(1,2,3,4)+D_{4,a}^0(1,2,3,4)+D_{4,a}^0(4,3,2,1)\\
&\quad -A_4^0(1,2,3,4)+\frac{1}{2}H_4^0(1,2,3,4)\\
&\quad +A_3^0(1,2,3)\,T_3^0(\widetilde{(12)},\widetilde{(23)},4)+A_3^0(2,3,4)\,T_3^0(1,\widetilde{(23)},\widetilde{(34)})\\
&\quad -\frac{1}{2}G_3^0(1,2,3)\,T_3^0(\widetilde{(12)},\widetilde{(23)},4)\;-\frac{1}{2}G_3^0(4,3,2)\,T_3^0(\widetilde{(34)},\widetilde{(23)},1)
\end{aligned}
$$

$$
\begin{aligned}
F^0_{4,b}(1,2,3,4) &= D_{4,c}(1,2,3,4) + D_{4,c}(3,4,1,2) - \tilde{A}^0_{4,a}(1,2,4,3) \\
&\quad + a^0_3(1,2,3)\, T^0_3((\widetilde{12}),4,(\widetilde{23})) + a^0_3(3,4,1)\, T^0_3((\widetilde{14}),2,(\widetilde{34})) \\
&\quad - \frac{1}{2} G^0_3(1,4,3)\left(U^0_3((\widetilde{14}),2,(\widetilde{34})) + U^0_3(2,(\widetilde{14}),(\widetilde{34})) + G^0_3((\widetilde{34}),(\widetilde{14}),2)\right) \\
&\quad - \frac{1}{2} G^0_3(3,2,1)\left(U^0_3((\widetilde{23}),4,(\widetilde{12})) + U^0_3(4,(\widetilde{23}),(\widetilde{12})) + G^0_3((\widetilde{12}),(\widetilde{23}),4)\right) \\
&\quad + \frac{1}{2} G^0_3(4,1,2)\left(U^0_3((\widetilde{41}),3,(\widetilde{12})) - U^0_3(3,(\widetilde{41}),(\widetilde{12}))\right) \\
&\quad - \frac{1}{2} G^0_3(1,4,3)\left(U^0_3((\widetilde{14}),2,(\widetilde{43})) - U^0_3(2,(\widetilde{14}),(\widetilde{43}))\right) \\
F^0_{4,c}(1,2,3,4) &= F^0_{4,a}(1,4,3,2) \\
F^0_{4,d}(1,2,3,4) &= F^0_{4,b}(1,4,3,2) \\
F^0_{4,e}(1,2,3,4) &= F^0_{4,b}(2,3,4,1) \\
F^0_{4,f}(1,2,3,4) &= F^0_{4,a}(2,1,4,3) \\
F^0_{4,g}(1,2,3,4) &= F^0_{4,b}(4,3,2,1) \\
F^0_{4,h}(1,2,3,4) &= F^0_{4,a}(4,1,2,3)
\end{aligned}
\tag{4.44}
$$

where the definition of $D^0_{4,a}$ and $D^0_{4,c}$ is given by decomposition:

$$D^0_4 = D^0_{4,a} + D^0_{4,b} + D^0_{4,c} + D^0_{4,d}$$

obtained in [91].

The sum of the $F^0_{4,i}$ is given by F^0_4:

$$F^0_4 = F^0_{4,a} + F^0_{4,b} + F^0_{4,c} + F^0_{4,d} + F^0_{4,e} + F^0_{4,f} + F^0_{4,g} + F^0_{4,h}$$

such that we can organise the calculation in a way that only F^0_4 must be integrated analytically over the antenna phase space. That integral has been calculated and documented in [67]. For the numerical implementation we only need to implement the sub-antennae $F_{4,a}$ and $F_{4,b}$ because we can rewrite the previous equation in the following way:

$$
\begin{aligned}
F^0_4(1,2,3,4) &= F^0_{4,a}(1^h,2,3,4^h) + F^0_{4,b}(1^h,2,3^h,4) \\
&\quad + F^0_{4,a}(1^h,4,3,2^h) + F^0_{4,b}(1^h,4,3^h,2) \\
&\quad + F^0_{4,b}(2^h,3,4^h,1) + F^0_{4,a}(2^h,1,4,3^h) \\
&\quad + F^0_{4,b}(4^h,3,2^h,1) + F^0_{4,a}(4^h,1,2,3^h)
\end{aligned}
\tag{4.45}
$$

We can then reconstruct the full $F_4^0(1_g, 2_g, 3_g, 4_g)$ by adding four $F_{4,a}$ and four $F_{4,b}$ with different orderings of the gluon indices. The label h identifies the hard momenta within each sub-antennae. This means that the sub-antenna vanishes if we take the h soft limit and therefore each sub-antenna has only the singularities appropriate to the mappings (4.34). This disentanglement of the different double and single unresolved limits is the following:

$$
\begin{aligned}
F^0_{4,h}(1,2,3,4) &\overset{1_g\to 0,2_g\to 0}{\longrightarrow} S_{4123}\ ,\\
F^0_{4,e}(1,2,3,4) + F_{4,g}(1,2,3,4) &\overset{1_g\to 0,3_g\to 0}{\longrightarrow} S_{412}S_{234}\ ,\\
F^0_{4,f}(1,2,3,4) &\overset{1_g\to 0,4_g\to 0}{\longrightarrow} S_{3412}\ ,\\
F^0_{4,a}(1,2,3,4) &\overset{2_g\to 0,3_g\to 0}{\longrightarrow} S_{1234}\ ,\\
F^0_{4,b}(1,2,3,4) + F_{4,d}(1,2,3,4) &\overset{2_g\to 0,4_g\to 0}{\longrightarrow} S_{123}S_{341}\ ,\\
F^0_{4,c}(1,2,3,4) &\overset{3_g\to 0,4_g\to 0}{\longrightarrow} S_{2341}\ ,\\
F^0_{4,a}(1,2,3,4) + F^0_{4,e}(1,2,3,4) + F^0_{4,g}(1,2,3,4) &\overset{1_g\|2_g,3_g\to 0}{\longrightarrow} S_{4;312}(z)\,\frac{1}{s_{12}}\,P_{gg\to G}(z)\ ,\\
F^0_{4,b}(1,2,3,4) + F^0_{4,d}(1,2,3,4) + F^0_{4,f}(1,2,3,4) &\overset{1_g\|2_g,4_g\to 0}{\longrightarrow} S_{3;412}(z)\,\frac{1}{s_{12}}\,P_{gg\to G}(z)\ ,\\
F^0_{4,e}(1,2,3,4) + F^0_{4,g}(1,2,3,4) + F^0_{4,h}(1,2,3,4) &\overset{2_g\|3_g,1_g\to 0}{\longrightarrow} S_{4;123}(z)\,\frac{1}{s_{23}}\,P_{gg\to G}(z)\ ,\\
F^0_{4,b}(1,2,3,4) + F^0_{4,c}(1,2,3,4) + F^0_{4,d}(1,2,3,4) &\overset{2_g\|3_g,4_g\to 0}{\longrightarrow} S_{1;432}(z)\,\frac{1}{s_{23}}\,P_{gg\to G}(z)\ ,\\
F^0_{4,e}(1,2,3,4) + F^0_{4,f}(1,2,3,4) + F^0_{4,g}(1,2,3,4) &\overset{3_g\|4_g,1_g\to 0}{\longrightarrow} S_{2;143}(z)\,\frac{1}{s_{34}}\,P_{gg\to G}(z)\ ,\\
F^0_{4,a}(1,2,3,4) + F^0_{4,b}(1,2,3,4) + F^0_{4,d}(1,2,3,4) &\overset{3_g\|4_g,2_g\to 0}{\longrightarrow} S_{1;234}(z)\,\frac{1}{s_{34}}\,P_{gg\to G}(z)\ ,\\
F^0_{4,b}(1,2,3,4) + F^0_{4,d}(1,2,3,4) + F^0_{4,h}(1,2,3,4) &\overset{4_g\|1_g,2_g\to 0}{\longrightarrow} S_{3;214}(z)\,\frac{1}{s_{14}}\,P_{gg\to G}(z)\ ,\\
F^0_{4,c}(1,2,3,4) + F^0_{4,e}(1,2,3,4) + F^0_{4,g}(1,2,3,4) &\overset{4_g\|1_g,3_g\to 0}{\longrightarrow} S_{2;341}(z)\,\frac{1}{s_{14}}\,P_{gg\to G}(z)\ ,
\end{aligned}
$$

$$
\begin{aligned}
F^0_{4,a}(1,2,3,4) + F^0_{4,e}(1,2,3,4) + F^0_{4,g}(1,2,3,4) + F^0_{4,h}(1,2,3,4) &\overset{1_g\|2_g\|3_g}{\longrightarrow} P_{123\to G}(w,x,y)\ ,\\
F^0_{4,a}(1,2,3,4) + F^0_{4,b}(1,2,3,4) + F^0_{4,c}(1,2,3,4) + F^0_{4,d}(1,2,3,4) &\overset{2_g\|3_g\|4_g}{\longrightarrow} P_{234\to G}(w,x,y)\ ,\\
F^0_{4,c}(1,2,3,4) + F^0_{4,e}(1,2,3,4) + F^0_{4,f}(1,2,3,4) + F^0_{4,g}(1,2,3,4) &\overset{3_g\|4_g\|1_g}{\longrightarrow} P_{341\to G}(w,x,y)\ ,\\
F^0_{4,b}(1,2,3,4) + F^0_{4,d}(1,2,3,4) + F^0_{4,f}(1,2,3,4) + F^0_{4,h}(1,2,3,4) &\overset{4_g\|1_g\|2_g}{\longrightarrow} P_{412\to G}(w,x,y)\ ,\\
F^0_{4,a}(1,2,3,4) + F^0_{4,b}(1,2,3,4) + F^0_{4,f}(1,2,3,4) + F^0_{4,g}(1,2,3,4) &\\
\overset{1_g\|2_g,3_g\|4_g}{\longrightarrow} \frac{1}{s_{12}s_{34}}\,P_{gg\to G}(z)\,P_{gg\to G}(y)\ ,&
\end{aligned}
$$

$$F^0_{4,c}(1,2,3,4) + F^0_{4,d}(1,2,3,4) + F^0_{4,e}(1,2,3,4) + F^0_{4,h}(1,2,3,4) \overset{2_g \| 3_g, 4_g \| 1_g}{\longrightarrow} \frac{1}{s_{23}s_{14}}\, P_{gg\to G}(z)\, P_{gg\to G}(y)\,,$$

$$\begin{aligned}
F^0_{4,f}(1,2,3,4) &\overset{1_g\to 0}{\longrightarrow} S_{412}\, f^0_3(3,4,2)\,,\\
F^0_{4,h}(1,2,3,4) &\overset{1_g\to 0}{\longrightarrow} S_{412}\, f^0_3(3,2,4)\,,\\
F^0_{4,e}(1,2,3,4) + F^0_{4,g}(1,2,3,4) &\overset{1_g\to 0}{\longrightarrow} S_{412}\, f^0_3(2,3,4)\,,\\
F^0_{4,a}(1,2,3,4) &\overset{2_g\to 0}{\longrightarrow} S_{123}\, f^0_3(1,3,4)\,,\\
F^0_{4,h}(1,2,3,4) &\overset{2_g\to 0}{\longrightarrow} S_{123}\, f^0_3(3,1,4)\,,\\
F^0_{4,b}(1,2,3,4) + F^0_{4,d}(1,2,3,4) &\overset{2_g\to 0}{\longrightarrow} S_{123}\, f^0_3(3,4,1)\,,\\
F^0_{4,a}(1,2,3,4) &\overset{3_g\to 0}{\longrightarrow} S_{234}\, f^0_3(1,2,4)\,,\\
F^0_{4,c}(1,2,3,4) &\overset{3_g\to 0}{\longrightarrow} S_{234}\, f^0_3(1,4,2)\,,\\
F^0_{4,e}(1,2,3,4) + F^0_{4,g}(1,2,3,4) &\overset{3_g\to 0}{\longrightarrow} S_{234}\, f^0_3(2,1,4)\,,\\
F^0_{4,c}(1,2,3,4) &\overset{4_g\to 0}{\longrightarrow} S_{341}\, f^0_3(1,3,2)\,,\\
F^0_{4,f}(1,2,3,4) &\overset{4_g\to 0}{\longrightarrow} S_{341}\, f^0_3(2,1,3)\,,\\
F^0_{4,b}(1,2,3,4) + F^0_{4,d}(1,2,3,4) &\overset{4_g\to 0}{\longrightarrow} S_{341}\, f^0_3(3,2,1)\,,\\
F^0_{4,a}(1,2,3,4) + F^0_{4,g}(1,2,3,4) &\overset{1_g\| 2_g}{\longrightarrow} \frac{1}{s_{12}}\, P_{gg\to G}(z)\, f^0_3(4,3,(12)) \ + \text{ang.}\,,\\
F^0_{4,b}(1,2,3,4) + F^0_{4,f}(1,2,3,4) &\overset{1_g\| 2_g}{\longrightarrow} \frac{1}{s_{12}}\, P_{gg\to G}(z)\, f^0_3((12),4,3) \ + \text{ang.}\,,\\
F^0_{4,h}(1,2,3,4) &\overset{1_g\| 2_g}{\longrightarrow} \frac{1}{s_{12}}\, P_{gg\to G}(z)\, f^0_3(3,(12),4) \ + \text{ang.}\,,\\
F^0_{4,c}(1,2,3,4) + F^0_{4,d}(1,2,3,4) &\overset{2_g\| 3_g}{\longrightarrow} \frac{1}{s_{23}}\, P_{gg\to G}(z)\, f^0_3(1,4,(23)) \ + \text{ang.}\,,\\
F^0_{4,e}(1,2,3,4) + F^0_{4,h}(1,2,3,4) &\overset{2_g\| 3_g}{\longrightarrow} \frac{1}{s_{23}}\, P_{gg\to G}(z)\, f^0_3((23),1,4) \ + \text{ang.}\,,\\
F^0_{4,a}(1,2,3,4) &\overset{2_g\| 3_g}{\longrightarrow} \frac{1}{s_{12}}\, P_{gg\to G}(z)\, f^0_3(4,(23),1) \ + \text{ang.}\,,\\
F^0_{4,a}(1,2,3,4) + F^0_{4,b}(1,2,3,4) &\overset{3_g\| 4_g}{\longrightarrow} \frac{1}{s_{34}}\, P_{gg\to G}(z)\, f^0_3(1,2,(34)) \ + \text{ang.}\,,\\
F^0_{4,f}(1,2,3,4) + F^0_{4,g}(1,2,3,4) &\overset{3_g\| 4_g}{\longrightarrow} \frac{1}{s_{34}}\, P_{gg\to G}(z)\, f^0_3((34),1,2) \ + \text{ang.}\,,\\
F^0_{4,c}(1,2,3,4) &\overset{3_g\| 4_g}{\longrightarrow} \frac{1}{s_{34}}\, P_{gg\to G}(z)\, f^0_3(2,(34),1) \ + \text{ang.}\,,\\
F^0_{4,c}(1,2,3,4) + F^0_{4,e}(1,2,3,4) &\overset{4_g\| 1_g}{\longrightarrow} \frac{1}{s_{14}}\, P_{gg\to G}(z)\, f^0_3(2,3,(14)) \ + \text{ang.}\,,\\
F^0_{4,d}(1,2,3,4) + F^0_{4,h}(1,2,3,4) &\overset{4_g\| 1_g}{\longrightarrow} \frac{1}{s_{14}}\, P_{gg\to G}(z)\, f^0_3((14),2,3) \ + \text{ang.}\,,
\end{aligned}$$

$$F^0_{4,f}(1,2,3,4) \quad \overset{4_g \| 1_g}{\longrightarrow} \quad \frac{1}{s_{14}} \, P_{gg\to G}(z) \; f^0_3(3,(14),2) \; + \text{ang.} \tag{4.46}$$

All other limits are vanishing. It can be seen that certain limits are shared among several antenna functions, which can be largely understood due to two reasons:

1. in a gluon-gluon collinear splitting, either gluon can become soft, and the gluon-gluon splitting function is always shared between two sub-antennae, as in (3.28) to disentangle the two soft limits.

2. the unresolved emission of gluon pairs 1_g and 3_g and also 2_g and 4_g is shared between the mappings (e) and (g) and (b) and (d) respectively according to the decomposition of the non-ordered antenna function $\tilde{A}^0_4$, which distributes the soft limit of both gluons between both mappings.

4.3.2 Angular terms

The angular terms in the single unresolved limits are associated with a gluon splitting into two gluons or into a quark-antiquark pair. In this collinear configuration the four-parton antenna functions factorise into the corresponding tensorial splitting functions and tensorial three parton antenna functions [33, 34, 50], e.g.,

$$\begin{aligned} F^0_4(1,2,3,4) \quad &\overset{i_g \| j_g}{\longrightarrow} \quad \frac{1}{s_{ij}} P^{\mu\nu}_{gg\to G}(z) (F^0_3)_{\mu\nu}((ij),k,l) \\ &= \quad \frac{1}{s_{ij}} P_{gg\to G}(z) F^0_3((ij),k,l) + \text{ang.} \end{aligned} \tag{4.47}$$

$P^{\mu\nu}_{ij\to(ij)}$ stands for the spin dependent gluon splitting function given by [33, 34]:

$$P^{\mu\nu}_{gg} = 2\left[-g^{\mu\nu}\left(\frac{z}{1-z}+\frac{1-z}{z}\right) - 2(1-\epsilon)z(1-z)\frac{k^\mu_\perp k^\nu_\perp}{k^2_\perp}\right] \tag{4.48}$$

while $P_{ij\to(ij)}$ stands for the spin averaged gluon splitting function (1.80). The tensorial three-parton antenna function $(F^0_3)_{\mu\nu}$ can be derived by analogy with the scalar three-parton antenna functions from physical matrix elements. Their tensorial structure is obtained by leaving the polarisation index of the gluon associated with momentum P^μ uncontracted.

Since we use scalar three parton antenna functions to remove the single unresolved limits of the four parton antenna function (this was discussed in eqs (4.6), (4.7), (4.8)) we are left with uncancelling angular terms in (4.47). However, we will show that the angular terms average to zero after integration over the antenna phase space. The angular average in single collinear limits can be made using the standard momentum parametrisation [50, 123] for the $i_g \parallel j_g$ limit:

$$p_i^\mu = zp^\mu + k_\perp^\mu - \frac{k_\perp^2}{z}\frac{n^\mu}{2p\cdot n}\,, \qquad p_j^\mu = (1-z)p^\mu - k_\perp^\mu - \frac{k_\perp^2}{1-z}\frac{n^\mu}{2p\cdot n}\,,$$
$$\text{with } 2p_i\cdot p_j = -\frac{k_\perp^2}{z(1-z)}\,, \qquad p^2 = n^2 = 0\,. \tag{4.49}$$

In this p^μ denotes the collinear momentum direction, and n^μ is an auxiliary vector. The collinear limit is approached as $k_\perp^2 \to 0$.

In the simple collinear $i \parallel j$ limit of the four-parton antenna functions $F_4^0(l_g, i_g, j_g, k_g)$, one chooses $n = p_k$ to be one of the non-collinear momenta, such that the antenna function can be expressed in terms of p, n, $k_\perp$ and p_l. Expanding in $k_\perp^\mu$ yields only non-vanishing scalar products of the form $p_l \cdot k_\perp$. Expressing the integral over the antenna phase space in the (p, n) centre-of-mass frame, the angular average can be carried out as

$$\frac{1}{2\pi}\int_0^{2\pi} \mathrm{d}\phi\,(p_l\cdot k_\perp) = 0\,, \qquad \frac{1}{2\pi}\int_0^{2\pi} \mathrm{d}\phi\,(p_l\cdot k_\perp)^2 = -k_\perp^2\,\frac{p\cdot p_l\, n\cdot p_l}{p\cdot n}\,. \tag{4.50}$$

Higher powers of $k_\perp^\mu$ are not sufficiently singular to contribute to the collinear limit. Using the above average, we could analytically verify the cancellation of angular terms within each single phase space mapping, which is independent on the choice of the reference vector n_μ. This is means that in a collinear limit which is distributed between two mappings as in (4.46) the angular terms vanish within each single phase space mapping that contributes to the limit.

However this cancellation was obtained only globally after performing the azimuthal integration analytically. This means that on a point-by-point check the numerical behaviour of the subtraction terms won't be correct in the presence of a single collinear gluon splitting. One solution to this behaviour is to add a local counterterm to every four parton antenna containing gluon-gluon collinear splittings. This local counterterm should yield the correct behaviour in this particular limit and

integrate to zero over the corresponding unresolved phase-space. We should add the following replacement for an $i_g \parallel j_g$ splitting:

$$F_4^0(1,i,j,2) \to F_4^0(1,i,j,2) - \Theta_{F_3^0}(i,j,z,k_\perp) \tag{4.51}$$

where the function $\Theta_{F_3^0}(i,j,z,k_\perp)$ isolates the angular terms and is given by:

$$\begin{aligned}\Theta_{F_3^0}(i,j,z,k_\perp) &= \left[\frac{1}{s_{ij}} P^{\mu\nu}_{ij\to(ij)}(z,k_\perp)(F_3^0)_{\mu\nu} - \frac{1}{s_{ij}} P_{ij\to(ij)}(z) F_3^0(1,(ij),2)\right] \\ &= \frac{4}{s_{ij}^2 s_{1p2}^2}\left(\frac{s_{12}^2 s_{1p2}^2 + s_{1p}^2 s_{p2}^2}{s_{12}^2 s_{1p}^2 s_{p2}^2}\right)\Bigg[s_{12}s_{1p}s_{p2}\; k_\perp\cdot k_\perp \\ &\quad -4p_1\cdot k_\perp p_2\cdot k_\perp s_{1p}s_{p2} + 2(p_1\cdot k_\perp)^2 s_{p2}^2 + 2(p_2\cdot k_\perp)^2 s_{1p}^2\Bigg]\end{aligned} \tag{4.52}$$

where p and $k_\perp$ were defined in (4.49). Using (4.50) we can indeed check that (4.52) integrates to zero.

However, due to the decomposition of F_4 in eight sub-antennae (4.45) the angular terms of the full F_4^0 antenna function given by (4.52) are distributed in the subantennae that contribute in the singular limit. To make a local subtraction we have to compute this singular limit in the subantennae and subtract it explicitly. This is allowed since we checked that the angular terms vanish within each phase space mapping. For the F_4^0 initial-final and initial-initial antennae functions we will see in the next subsections that we implemented them with a single phase space mapping. This means that in that the case we can perform a local subtraction with (4.52) with appropriate crossing of particles to the initial state.

After these replacements the resulting four-parton antenna is locally free from angular terms in the single collinear ($s_{ij} \to 0$) unresolved region. However, in the regions of the phase space where other invariants in the denominator of (4.52) vanish new singularities are introduced. For example since:

$$p^\mu = p_i^\mu + p_j^\mu + \frac{s_{ij}}{s_{in}+s_{jn}} n^\mu \tag{4.53}$$

the invariants s_{1p} and s_{2p} become singular in the $1//i//j$ and $2//i//j$ triple collinear limits respectively. This means that introducing $\Theta_{F_3^0}(i,j,z,k_\perp)$ may not be the best strategy to achieve the cancellation of the angular terms. Even so, we will discuss in

subsection 7.1.5 the numerical impact of introducing (4.52) for the single collinear limit.

4.3.3 Initial-Final emitters

The NNLO antenna with one parton in the initial state $F_4^0(\hat{1}_g, 2_g, 3_g, 4_g)$ is obtained by crossing one gluon from the final state antenna $F_4^0(1_g, 2_g, 3_g, 4_g)$ to the initial state. It is used to subtract double unresolved initial state singularities when both the unresolved gluons are colour connected between an initial and a final state gluon. The unintegrated form is then obtained by making the replacements:

$$\begin{aligned} s_{1i} &\to (p_1 - k_i)^2 \\ s_{ij} &\to (k_i + k_j)^2 \qquad i,j = 2,3,4 \end{aligned}$$

In all single (double) unresolved limits this antenna collapses into a three (two) parton antenna with a gluon in the initial state. There is no need to further split this antenna since the reduced matrix elements that accompany it have a gluon in the initial state and can be convoluted with a gluon parton distribution function. However special care has to be taken with three parton or four parton gluon initiated antennae with quarks in the final state since the splitting $g \to qg$ looks like $\bar{q} \to g$ or $g \to g$ depending on the collinear limit. These collinear limits have to be split for the antenna under consideration and the corresponding sub-antennae integrated separately because each has a different reduced matrix element accompanying it.

The mapping used in the configuration $F_4^0(\hat{1}, i, j, k)$ is the following $\{4 \to 2\}$ mapping: $\{\hat{1}, i, j, k\} \to \{\hat{\hat{1}}, \widetilde{(ijk)}\}$ [68]:

$$\begin{aligned} \bar{p}_1^{\mu} &= x\, p_1^{\mu} \\ \tilde{k}_{(ijk)}^{\mu} &= k_i^{\mu} + k_j^{\mu} + k_k^{\mu} - (1-x)\, p_1^{\mu} \end{aligned} \tag{4.54}$$

where the bar denotes a rescaling of the initial state parton and x is given by [68]:

$$x = \frac{s_{1i} + s_{1j} + s_{1k} + s_{ij} + s_{ik} + s_{jk}}{s_{1i} + s_{1j} + s_{1k}} \tag{4.55}$$

It satisfies the appropriate limits in all double singular configurations:

1. i and j soft: $x \to 1$, $\tilde{k}_{(ijk)} \to k_k$,

2. i soft and $p_j \parallel p_k$: $x \to 1$, $\tilde{k}_{(ijk)} \to k_j + k_k$,

3. $k_i = zp_1 \parallel p_1$ and j soft: $x \to 1-z$, $\tilde{k}_{(ijk)} \to k_k$,

4. $k_i = zp_1 \parallel p_1$ and $k_j \parallel k_k$: $x \to 1-z$, $\tilde{k}_{(ijk)} \to k_j + k_k$,

5. $k_i \parallel k_j \parallel k_k$: $x \to 1$, $\tilde{k}_{(ijk)} \to k_i + k_j + k_k$,

6. $k_i + k_j = zp_1 \parallel p_1$: $x \to 1-z$, $\tilde{k}_{(ijk)} \to k_k$,

where partons i and j can be interchanged in all the cases. In single unresolved limits this mapping collapses into an NLO mapping (3.34) allowing their subtraction from the four-parton antenna $F_4^0(\hat{1}_g, 2_g, 3_g, 4_g)$ with products of three parton antennae.

We can identify the initial state parton as the hard radiator and because of the symmetry under $i \leftrightarrow j$,$i \leftrightarrow k$,$j \leftrightarrow k$ of the mapping (4.54) any of final state partons i,j,k can act as a hard radiator. We could do a decomposition where the radiator in the final state is uniquely identified but we would end up with three sub-antennae where we would use the same mapping for each. Because of this we use the full $F_4^0(\hat{1}_g, 2_g, 3_g, 4_g)$ in the numerical implementation. Its integral over the antenna phase space (initial-state kinematics) was obtained recently in [105, 119].

4.3.4 Initial-Initial emitters

The NNLO antenna function with two partons in the initial state is obtained from the corresponding initial-final antenna of the previous section by crossing one final-state gluon to the initial state. We have to distinguish the cases where the two initial state partons are adjacent $F_4^0(\hat{1}_g, \hat{2}_g, 3_g, 4_g)$ or non-adjacent $F_4^0(\hat{1}_g, 3_g, \hat{2}_g, 4_g)$. In each case the unintegrated form is obtained by making the replacements:

$$\begin{aligned} s_{12} &\to (p_1 + p_2)^2 \\ s_{1i} &\to (p_1 - k_i)^2 \\ s_{2i} &\to (p_2 - k_i)^2 \\ s_{ij} &\to (k_i + k_j)^2 \qquad\qquad i, j = 3, 4 \end{aligned}$$

They are used to subtract double unresolved initial state singularities when both the unresolved gluons are colour connected between two initial-state gluons. Since

in the single (double) unresolved limits these antennae collapse into a three (two) parton antenna with gluons in the initial state no further splitting is required. The reduced matrix elements accompanying this antenna have gluons in the initial state and can be doubly convoluted with a gluon parton distribution function.

The mapping used in the numerical implementation when i and j are the unresolved partons in the final state is the following mapping: $\{\hat{1},\hat{2},i,j,...,m,l,...\} \to \{\hat{\hat{1}},\hat{\hat{2}},...\tilde{m},\tilde{l},...\}$ [68]:

$$\begin{aligned}
\bar{p}_1^\mu &= x_1\, p_1^\mu \\
\bar{p}_2^\mu &= x_2\, p_2^\mu \\
&... \\
\tilde{k}_l^\mu &= k_l^\mu - \frac{2k_l\cdot(q+\tilde{q})}{(q+\tilde{q})^2}\,(q^\mu+\tilde{q}^\mu) + \frac{2k_l\cdot q}{q^2}\,\tilde{q}^\mu \\
&... \\
q^\mu &= p_1^\mu + p_2^\mu - k_i^\mu - k_j^\mu \\
\tilde{q}^\mu &= \bar{p}_1^\mu + \bar{p}_2^\mu
\end{aligned} \tag{4.56}$$

where the bar denotes rescaling of both the initial state partons and the tilde momenta are all the momenta in the final state that are not actually part of the antenna but require boosting in order to restore momentum conservation. The x_1 and x_2 are given by [68]:

$$\begin{aligned}
x_1 &= \sqrt{\frac{s_{12}+s_{2i}+s_{2j}}{s_{12}+s_{1i}+s_{1j}}}\sqrt{\frac{s_{12}+s_{1i}+s_{1j}+s_{2i}+s_{2j}+s_{ij}}{s_{12}}} \\
x_2 &= \sqrt{\frac{s_{12}+s_{1i}+s_{1j}}{s_{12}+s_{2i}+s_{2j}}}\sqrt{\frac{s_{12}+s_{1i}+s_{1j}+s_{2i}+s_{2j}+s_{ij}}{s_{12}}}
\end{aligned} \tag{4.57}$$

These two momentum fractions satisfy the following limits in double unresolved configurations:

1. i and j soft: $x_1 \to 1$, $x_2 \to 1$,

2. i soft and $k_j = z_1 p_1 \parallel p_1$: $x_1 \to 1-z_1$, $x_2 \to 1$,

3. $k_i = z_1 p_1 \parallel p_1$ and $k_j = z_2 p_2 \parallel p_2$: $x_1 \to 1-z_1$, $x_2 \to 1-z_2$,

4. $k_i + k_j = z_1 p_1 \parallel p_1$: $x_1 \to 1 - z_1$, $x_2 \to 1$,

and all the limits obtained from the ones above by exchange of p_1 with p_2 and of k_i with k_j. Moreover in single unresolved limits this mapping turns into a NLO mapping (3.37) allowing the subtraction of these limits from the four-parton antennae functions.

The integrated form of the initial-initial four parton antenna over the antenna phase space (initial state kinematics), for the adjacent and non-adjacent crossing is underway [120].

4.4 Summary

In this chapter we examined the structure of perturbative calculations at next-to-next-to leading order. We identified the new ingredients that appear at this order in perturbation theory at the matrix element level and found out that there are infrared divergences in the different pieces in intermediate steps of the calculation. These are the real-real, virtual-real and virtual-virtual channels. Their cancellation is very intricate since it occurs between phase spaces of different multiplicity.

The antenna subtraction method is a procedure that can solve this problem by introducing subtraction terms with known building blocks that render the real-virtual and double real contributions finite. The integrated form of the building blocks makes their infrared divergences explicit such that they can be analytically canceled against the virtual contributions.

We introduced a general formula in section 4.2 to generate a subtraction for the real-real channel. We will apply it in a particular case in chapter 6.

The current status of the method at NNLO is that it is fully general for massless fermions for colourless initial states [67] or one coloured parton in the initial state [105, 119]. The extension to two coloured partons in the initial state is currently underway and expected to be concluded soon.

Chapter 5

Sector decomposition

In this chapter we discuss the sector decomposition method used to isolate divergences from parameter integrals occurring in perturbative quantum field theory. A good review of this topic can be found in [124].

As we have seen in the previous two chapters precise theory predictions become increasingly difficult at higher orders. The structure of the singularities is cumbersome as the divergences overlap in regions of the Feynman parameter space. We will illustrate this using the parametric form of both the virtual and real corrections. The sector decomposition method is a solution to perform the extraction of these singularities and we review in section 5.1 its application to the computation of multi-loop Feynman integrals and, in section 5.2, its treatment of real radiation phase space integrals at NNLO.

In both cases, working in $D = 4 - 2\epsilon$ dimensions, the method isolates the overlapping singular parts and disentangles them producing a Laurent series in ϵ, where the coefficients of the pole and finite terms are sums of regular parameter integrals which can be evaluated numerically. The very algorithmic nature of method leads to automatised programs to compute the Laurent series.

As an example, more related to the previous chapters of this thesis, we work out, in section 5.3 a direct check with sector decomposition of the analytic result for the integrated antenna F_4^0 obtained in [67] for final-final kinematics.

5.1 The algorithm for multi-loop integrals

The original idea of sector decomposition goes back to the proof of the BPHZ theorem by Hepp [125], who used a decomposition of integration parameter space into certain sectors in order to disentangle overlapping ultraviolet singularities.

The starting point application for a multi-loop diagram is the generic expression for a scalar Feynman graph in d dimensions at L loops with N propagators, where the propagators can have arbitrary powers:

$$G = (-1)^{N_\nu} \frac{\Gamma(N_\nu - Ld/2)}{\prod_{j=1}^{N} \Gamma(\nu_j)} \int_0^\infty \prod_{j=1}^{N} dx_j \; x_j^{\nu_j - 1} \, \delta(1 - \sum_{l=1}^{N} x_l) \; \frac{\mathcal{U}^{N_\nu - (L+1)d/2}}{\mathcal{F}^{N_\nu - Ld/2}} \tag{5.1}$$

In this expression $N_\nu = \sum_{j=1}^{N} \nu_j$ where ν_j is the power of the j propagator in the Feynman graph. Integration over loop momenta has been performed with the aid of the Feynman parameters x_j. The functions $\mathcal{U}$ and $\mathcal{F}$ can be constructed from the topology of the corresponding Feynman graph and contain the Feynman parameters x_j as well as Lorentz invariants. For example for the massless double box:

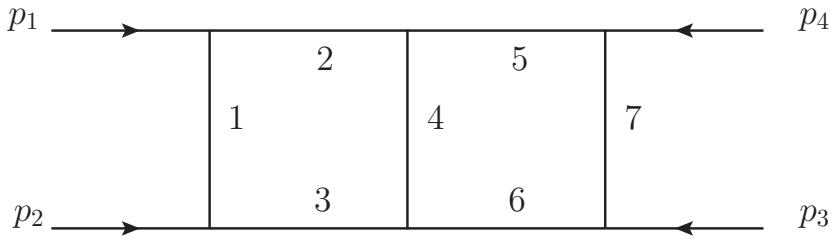

Figure 5.1: Massless double box

we have:

$$G = -\Gamma(3 + 2\epsilon) \int_0^\infty \prod_{l=1}^{7} dx_l \, \delta(1 - \sum_{l=1}^{7} x_l) \frac{\mathcal{U}^{1+3\epsilon}}{\mathcal{F}^{3+2\epsilon}} \tag{5.2}$$

$$\begin{aligned} \mathcal{U} &= (x_1 + x_2 + x_3)(x_5 + x_6 + x_7) \\ &\quad + x_4(x_1 + x_2 + x_3 + x_5 + x_6 + x_7) \end{aligned} \tag{5.3}$$

$$\begin{aligned} \mathcal{F} &= (-s)\Big\{ x_2 x_3 (x_4 + x_5 + x_6 + x_7) \\ &\quad + x_5 x_6 (x_1 + x_2 + x_3 + x_4) \end{aligned}$$

$$+x_2x_4x_6 + x_3x_4x_5\Big\}$$
$$+(-t)x_1x_4x_7 \tag{5.4}$$

where $s = (p_1 + p_2)^2$ and $t = (p_2 + p_3)^2$.

A necessary condition for the infrared divergence is:

$$\mathcal{F} = 0 \tag{5.5}$$

and, from the example above, we see that singularities are overlapping as several x_j should vanish. The sector decomposition method proposed in [126,127] is a solution to disentangle the regions of overlapping infrared divergences. The strategy adopted is the following:

1 - Generate primary sectors

Decompose the integration range into N sectors, where in each sector l, x_l is the largest:

$$\int_0^\infty d^N x = \sum_{l=1}^{N} d^N x \prod_{\substack{j=1 \\ j\neq l}}^{N} \theta(x_l \geq x_j) \tag{5.6}$$

The θ-function is defined as

$$\theta(x \geq y) = \begin{cases} 1 & \text{if } x \geq y \text{ is true} \\ 0 & \text{otherwise.} \end{cases}$$

This produces N new G_l integrals and in each we substitute:

$$x_j = \begin{cases} x_l t_j & \text{for} \quad j < l \\ x_l & \text{for} \quad j = l \\ x_l t_{j-1} & \text{for} \quad j > l \end{cases} \tag{5.7}$$

As $\mathcal{U}$ (5.3), $\mathcal{F}$ (5.4) are homogeneous of degree L , L+1, respectively, and x_l factorises completely, we have $\mathcal{U}(\vec{x}) \rightarrow \mathcal{U}_l(\vec{t})\, x_l^L$ and $\mathcal{F}(\vec{x}) \rightarrow \mathcal{F}_l(\vec{t})\, x_l^{L+1}$ and thus, we can integrate over x_l in sector l using the delta function: $\int dx_l/x_l\, \delta(1-x_l(1+\sum_{k=1}^{N-1} t_k)) = 1$. Performing the integration this way makes the θ function condition (5.6) produce integrals from 0 and 1 and the singularities are located when a set of parameters t_i goes to zero. The sector l of the original Feynman graph is of the following form:

$$G_l \;=\; \int_0^1 \prod_{j=1}^{N-1} \mathrm{d}t_j\, t_j^{\nu_j - 1}\, \frac{\mathcal{U}_l^{N_\nu - (L+1)D/2}(\vec{t})}{\mathcal{F}_l^{N_\nu - LD/2}(\vec{t})} \quad , \quad l = 1, \ldots, N\ . \tag{5.8}$$

2 - Iterated sector decomposition

For each of the G_l determine a set of parameters $\mathcal{S} = \{t_{\alpha_1}, \ldots, t_{\alpha_r}\}$, such that $\mathcal{U}_l$, respectively $\mathcal{F}_l$, vanish if the parameters of $\mathcal{S}$ are set to zero.

Once a set has been found decompose the sector l into a $r-$cube containing r subsectors with:

$$\prod_{j=1}^{r} \theta(1 \geq t_{\alpha_j} \geq 0) = \sum_{k=1}^{r} \prod_{\substack{j=1 \\ j\neq k}}^{r} \theta(t_{\alpha_k} \geq t_{\alpha_j} \geq 0) \tag{5.9}$$

Remap the variables to the unit hypercube in each new subsector by the substitution

$$t_{\alpha_j} \to \begin{cases} t_{\alpha_k} t_{\alpha_j} & \text{for} \quad j \neq k \\ t_{\alpha_k} & \text{for} \quad j = k\,. \end{cases} \tag{5.10}$$

This gives a Jacobian factor of $t_{\alpha_k}^{r-1}$. By construction t_{α_k} factorises from at least one of the functions $\mathcal{U}_l$, $\mathcal{F}_l$. The resulting subsector integrals have the general form

$$G_{lk} \;=\; \int_0^1 \left(\prod_{j=1}^{N-1} \mathrm{d}t_j \; t_j^{a_j - b_j\epsilon} \right) \frac{\mathcal{U}_{lk}^{N_\nu - (L+1)D/2}}{\mathcal{F}_{lk}^{N_\nu - LD/2}}\,, \quad k = 1, \ldots, r\,. \tag{5.11}$$

This procedure is now repeated for each subsector G_{lk} by looking at the set of parameters where now $\mathcal{U}_{lk}$, $\mathcal{F}_{lk}$ vanish. This means that for each subsector new subsectors are created and the process grows in a tree-like structure until the functions $\mathcal{U}_{lk_1k_2\ldots}$ or $\mathcal{F}_{lk_1k_2\ldots}$ contain a constant term:

$$\begin{aligned} \mathcal{U}_{lk_1k_2\ldots} &= 1 + u(\vec{t}) \\ \mathcal{F}_{lk_1k_2\ldots} &= -s_0 + \sum_\beta (-s_\beta) f_\beta(\vec{t})\,, \end{aligned} \tag{5.12}$$

where $u(\vec{t})$ and $f_\beta(\vec{t})$ are polynomials in the variables t_j (without a constant term), and s_β are kinematic invariants.

3 - Extraction of the poles

Let us consider Eq. (5.11) for a particular t_j, i.e. let us focus on

$$I_j = \int_0^1 dt_j \, t_j^{(a_j - b_j\epsilon)} \, \mathcal{I}(t_j, \{t_{i\neq j}\}, \epsilon)\,, \tag{5.13}$$

where $\mathcal{I} = \mathcal{U}_{lk}^{N_\nu-(L+1)D/2}/\mathcal{F}_{lk}^{N_\nu-LD/2}$ in a particular subsector. If $a_j > -1$, the integration does not lead to an ϵ–pole. In this case no subtraction is needed and one can go to the next variable t_{j+1}. For $a_j = -1$, which is the generic case for renormalisable theories (logarithmic divergence), this simply amounts to

$$I_j = -\frac{1}{b_j\epsilon}\,\mathcal{I}_j(0,\{t_{i\neq j}\},\epsilon) + \int_0^1 dt_j\, t_j^{-1-b_j\epsilon}\left(\mathcal{I}(t_j,\{t_{i\neq j}\},\epsilon) - \mathcal{I}_j(0,\{t_{i\neq j}\},\epsilon)\right),$$

which is equivalent to applying the "plus prescription". We can then repeat the same step for the remaining t_j variables to extract all the poles in the subsector G_{lk} and expand the resulting expression in ϵ. The original Feynman graph G (5.1) is now written as a Laurent series in ϵ with coefficients $C_{lk,m}$ for each subsector:

$$G_{lk} = \sum_{m=-r}^{2L} \frac{C_{lk,m}}{\epsilon^m} + \mathcal{O}(\epsilon^{r+1}), \quad G = (-1)^{N_\nu}\Gamma(N_\nu - LD/2)\sum_{l=1}^{N}\sum_{k=1}^{\alpha(l)} G_{lk}\,. \quad (5.14)$$

The $C_{lk,m}$ are finite integrals over parameters t_j that can be evaluated numerically for a given phase space point.

Using this technique numerical checks for the analytic formulae for massless planar [128] and non-planar [129] two-loop box diagrams were done in [126]. In the same work results for the same diagrams with one leg off-shell were given before any analytic formulae as well as some 3-loop 3-point graphs with two on-shell legs.

Subsequently, sector decomposition was used to check a considerable number of analytical results for two-loop [127,130–136], three-loop [137–139] and four-loop [127, 140] diagrams.

In references [141, 142] a combination of sector decomposition and contour deformation has been worked out to allow the evaluation of multi-loop Feynman diagrams with infrared and threshold singularities. In [143], an implementation of an algorithm based on sector decomposition extracts the $1/\epsilon$ poles as well as large logarithms of type $\ln(s/M^2)$ in the high-energy limit, contributing to the next-to-leading logarithmic electroweak corrections of multi-loop diagrams.

Further improvements of the method were given in [144] where there is a formal proof that the iterated sector decomposition procedure is guaranteed to stop and a public code, with a implementation of the method, is available.

5.2 Sector decomposition for infrared divergent real radiation integrals

Following its application in multiloop calculations references [145–147] extended its use to phase space integrals as well. To achieve this we begin by rewriting the phase space integral into a dimensionally regulated multi-parameter integral over the unit hypercube. In this case, the singularities arise in the unresolved configurations obtained when a certain number of invariants tends to zero. These invariants are located in the *denominators* of matrix elements and therefore, if they can be written in a form amenable to sector decomposition, the extraction of the infrared divergences can be done within this framework.

As an example we will work out the $1 \to 4$ ($q \to p_1 + p_2 + p_3 + p_4$) phase space treatment in sector decomposition. Setting $m = 2$ in equation (4.9) we find that the antenna phase space for the four-parton antennae in the final-final configuration is proportional to the four-particle phase space:

$$\mathrm{d}\Phi_4 = P_2 \, \mathrm{d}\Phi_{X_{ijkl}} \tag{5.15}$$

where P_2 is the volume of the two particle phase space:

$$P_2 = \int \mathrm{d}\Phi_2 = 2^{-3+2\epsilon}\pi^{-1+\epsilon}\frac{\Gamma(1-\epsilon)}{\Gamma(2-2\epsilon)}(q^2)^{-\epsilon} \tag{5.16}$$

To proceed we start from the definition of the phase space for a $1 \to 4$ decay in d dimensions:

$$\begin{aligned}\int \mathrm{d}\Phi_{1\to4} &= \frac{(2\pi)^d}{(2\pi)^{4(d-1)}}\int \frac{\mathrm{d}^{d-1}p_1}{2E_1}\frac{\mathrm{d}^{d-1}p_2}{2E_2}\frac{\mathrm{d}^{d-1}p_3}{2E_3}\frac{\mathrm{d}^{d-1}p_4}{2E_4}\delta^d(q-p_1-p_2-p_3-p_4) \\ &= \frac{(2\pi)^d}{(2\pi)^{4(d-1)}}\int \frac{\mathrm{d}^{d-1}p_1}{2E_1}\frac{\mathrm{d}^{d-1}p_2}{2E_2}\frac{\mathrm{d}^{d-1}p_3}{2E_3}\delta((q-p_1-p_2-p_3)^2)\end{aligned} \tag{5.17}$$

where we used the delta function to perform one integration:

$$\int \frac{\mathrm{d}^{d-1}p_4}{2E_4} = \int \mathrm{d}^d p_4 \delta(p_4^2) \tag{5.18}$$

Going to the rest frame of the decaying particle we parametrise the momenta in the following way:

$$q = (E, \vec{0}^{(D-1)})$$

$$\begin{aligned} p_1 &= E_1\,(1,\vec{0}^{(D-2)},1) \\ p_2 &= E_2\,(1,\vec{0}^{(D-3)},\sin\theta_1,\cos\theta_1) \\ p_3 &= E_3\,(1,\vec{0}^{(D-4)},\sin\theta_2\sin\theta_3,\sin\theta_2\cos\theta_3,\cos\theta_2) \\ p_4 &= Q-p_1-p_2-p_3\;, \end{aligned} \tag{5.19}$$

which leads to a description of the phase space in terms of energies and angles:

$$\begin{aligned} \int \mathrm{d}\Phi_{1\to 4} &= \frac{1}{8}(2\pi)^{4-3d}\int \mathrm{d}E_1\,\mathrm{d}E_2\,\mathrm{d}E_3\,\mathrm{d}\theta_1\,\mathrm{d}\theta_2\,\mathrm{d}\theta_3[E_1E_2E_3\sin\theta_1\sin\theta_2]^{d-3}\sin\theta_3^{d-4} \\ &\quad \mathrm{d}\Omega_{d-1}\,\mathrm{d}\Omega_{d-2}\,\mathrm{d}\Omega_{d-3}\Theta(E_1)\,\Theta(E_2)\,\Theta(E_3)\Theta(E-E_1-E_2-E_3) \\ &\quad \delta(E^2-2E(E_1+E_2+E_3)+2(p_1\cdot p_2+p_1\cdot p_3+p_2\cdot p_3))\;, \end{aligned} \tag{5.20}$$

since:

$$\mathrm{d}^{d-1}p_r = E_r^{d-2}\mathrm{d}E_r\mathrm{d}\Omega_{d-1} \tag{5.21}$$

and:

$$V_d = \int \mathrm{d}\Omega_d = \frac{2\pi^{\frac{d}{2}}}{\Gamma(\frac{d}{2})} \tag{5.22}$$

is the solid angle in d dimensions. Now we carry out change of variables

$$\{E_1,E_2,E_3,\theta_1,\theta_2,\theta_3\}\to\{s_{12},s_{13},s_{14},s_{23},s_{24},s_{34}\}$$

to obtain the phase space in terms of invariants. The jacobian of the transformation is given by:

$$\begin{aligned} \mathrm{d}s_{12}\mathrm{d}s_{13}\mathrm{d}s_{14}\mathrm{d}s_{23}\mathrm{d}s_{24}\mathrm{d}s_{34} &= \left|\frac{\partial(s_{..})}{\partial(E_i,\theta_f)}\right|\mathrm{d}E_1\mathrm{d}E_2\mathrm{d}E_3\mathrm{d}\theta_1\mathrm{d}\theta_2\mathrm{d}\theta_3 \\ &= 2^6E^3E_1^2E_2^2E_3^2\sin\theta_1^2\sin\theta_2^2\sin\theta_3^2\mathrm{d}E_1\mathrm{d}E_2\mathrm{d}E_3\mathrm{d}\theta_1\mathrm{d}\theta_2\mathrm{d}\theta_3 \end{aligned}$$

which can be written as the determinant Δ_4 of the Gram matrix $G_{ij}=2p_i\cdot p_j$:

$$\Delta_4(q,p_1,p_2,p_3)=\Delta_4(p_1,p_2,p_3,p_4)=\begin{vmatrix} 2p_1\cdot p_1 & 2p_1\cdot p_2 & \dots & 2p_1\cdot p_4 \\ 2p_2\cdot p_1 & \dots & \dots & 2p_2\cdot p_4 \\ \dots & \dots & \dots & \dots \\ 2p_4\cdot p_1 & \dots & \dots & 2p_4\cdot p_4 \end{vmatrix}$$

$$=\lambda(s_{12}s_{34},s_{13}s_{24},s_{14}s_{23})=-(4EE_1E_2E_3\sin\theta_1\sin\theta_2\sin\theta_3)^2 \tag{5.23}$$

where we introduced the Källen function $\lambda(x,y,z) = x^2+y^2+z^2-2xy-2yz-2xz$. With the dimensionless variables:

$$y_{12} = s_{12}/Q^2, y_{13} = s_{13}/Q^2, y_{14} = s_{14}/Q^2, y_{23} = s_{23}/Q^2, y_{24} = s_{24}/Q^2, y_{34} = s_{34}/Q^2 \tag{5.24}$$

we finally obtain the phase space written in terms of invariant variables:

$$\begin{aligned}\int \mathrm{d}\Phi_{1\to 4} &= (2\pi)^{4-3\,d}(Q^2)^{3d/2-4}\,2^{-2d+1}\,V_{d-1}\,V_{d-2}\,V_{d-3} \\ &\int \mathrm{d}y_{12}\mathrm{d}y_{13}\mathrm{d}y_{14}\mathrm{d}y_{23}\mathrm{d}y_{24}\mathrm{d}y_{34}\Theta(y_{12})\Theta(y_{13})\Theta(y_{14})\Theta(y_{23})\Theta(y_{24})\Theta(y_{34}) \\ &\Theta(-\Delta_4)\,[-\Delta_4]^{-1/2-\epsilon}\delta(1-y_{12}-y_{13}-y_{14}-y_{23}-y_{24}-y_{34})\end{aligned} \tag{5.25}$$

where we have:

$$\begin{aligned}\Delta_4 = \quad & y_{12}^2y_{34}^2 + y_{13}^2y_{24}^2 + y_{14}^2y_{23}^2 \\ & -2\,(y_{12}y_{23}y_{34}y_{14} + y_{13}y_{23}y_{24}y_{14} + y_{12}y_{24}y_{34}y_{13})\end{aligned} \tag{5.26}$$

Looking at (5.25) we see that Δ_4 has to be negative semi-definite and this will constrain the physical regions of the phase space.

In order to proceed and map the phase space integral into a parametric form amenable to sector decomposition we must choose the phase space variables that are convenient for our problem, that is, they should produce a simple formula for the invariants in the denominators of the matrix element. We can choose the set of five independent invariants to be $\{y_{134}, y_{234}, y_{34}, y_{13}, y_{23}\}$ introducing:

$$1 = \int \mathrm{d}y_{134}\delta(y_{134}-y_{13}-y_{14}-y_{34}) \int \mathrm{d}y_{234}\delta(y_{234}-y_{23}-y_{24}-y_{34}) \tag{5.27}$$

and map the phase space integral to the unit hypercube with:

$$\begin{aligned} y_{234} &= \lambda_1 \\ y_{34} &= \lambda_1\lambda_2 \\ y_{23} &= \lambda_1(1-\lambda_2)\lambda_4 \\ y_{134} &= \lambda_2 + \lambda_3(1-\lambda_1)(1-\lambda_2) \\ y_{13} &= \lambda_5(y_{13}^+ - y_{13}^-) + y_{13}^- \end{aligned} \tag{5.28}$$

where λ_i vary between 0 and 1 and the formulas for the remaining invariants can be obtained by linear dependence. The limits of integration on the variable y_{13} come from solving the constraint $(-\Delta_4) = -(ay_{13}^2 + by_{13} + c) \geq 0$ that gives:

$$y_{13}^{\pm} = (1-\lambda_1)\left[\sqrt{\lambda_3\lambda_4} \pm \sqrt{\lambda_2(1-\lambda_3)(1-\lambda_4)}\right]^2 \tag{5.29}$$

and for y_{134} we solve the constraint $(b^2 - 4ac) \geq 0$ that yields:

$$y_{134}^{-} = \lambda_2 \qquad y_{134}^{+} = \lambda_2 + (1-\lambda_1)(1-\lambda_2) \tag{5.30}$$

The jacobian for the transformation gives:

$$\begin{aligned} \mathrm{d}y_{234}\mathrm{d}y_{34}\mathrm{d}y_{23}\mathrm{d}y_{134}\mathrm{d}y_{13} &= 4\lambda_1^2(1-\lambda_1)^2(1-\lambda_2)^2\sqrt{\lambda_2(1-\lambda_3)\lambda_3(1-\lambda_4)\lambda_4} \\ &\quad \mathrm{d}\lambda_1\mathrm{d}\lambda_2\mathrm{d}\lambda_3\mathrm{d}\lambda_4\mathrm{d}\lambda_5 \end{aligned} \tag{5.31}$$

and the Gram determinant Δ_4 factorises:

$$\begin{aligned} -\Delta_4 &= a(y_{13}-y_{13}^{+})(y_{13}-y_{13}^{-}) = a(1-\lambda_1)\lambda_5(1-\lambda_5)(y_{13}^{+}-y_{13}^{-})^2 \\ &= 16\lambda_1^2(1-\lambda_1)^2\lambda_2(1-\lambda_2)^2\lambda_3(1-\lambda_3)\lambda_4(1-\lambda_4)\lambda_5(1-\lambda_5) \end{aligned} \tag{5.32}$$

leading to the following parametric form of the phase space:

$$\begin{aligned} \int \mathrm{d}\Phi_{1\to 4} &= (2\pi)^{4-3d}(Q^2)^{3d/2-4}2^{-2d+1}V_{d-1}V_{d-2}V_{d-3}\int_0^1 \mathrm{d}\lambda_1\mathrm{d}\lambda_2\mathrm{d}\lambda_3\mathrm{d}\lambda_4\mathrm{d}\lambda_5 \\ &\quad [\lambda_1(1-\lambda_1)(1-\lambda_2)]^{1-2\epsilon}\left[\lambda_2\lambda_3(1-\lambda_3)\lambda_4(1-\lambda_4)\right]^{-\epsilon}\left[\lambda_5(1-\lambda_5)\right]^{-1/2-\epsilon} \end{aligned} \tag{5.33}$$

When we substitute $1 \to 4$ matrix elements in massless QCD these contain denominators of the form $1/s_{34}s_{234}s_{134}$. Using the mapping (5.28) we obtain:

$$\frac{1}{s_{34}s_{234}s_{134}} = \frac{1}{\lambda_1^2\lambda_2[\lambda_2 + \lambda_3(1-\lambda_1)(1-\lambda_2)]} \tag{5.34}$$

The third term in this denominator contains the triple invariant s_{134} that can vanish for double unresolved real radiation configurations at NNLO. This happens when e.g. when both λ_2,$\lambda_3 \to 0$, but not when only one does. Combining this denominator with the integration measure (5.25) and expanding $\lambda_2^{-1-\epsilon} \to -\delta(\lambda_2)/\epsilon + \ldots$, $\lambda_3^{-\epsilon} \to 1 - \epsilon\ln(\lambda_3)$ produces unregulated singularities as $\lambda_3 \to 0$. This means that there are overlapping singularities in the phase space integral associated with the variables λ_2

and λ_3. These can be disentangled with the sector decomposition method [145–147]. To illustrate this we consider the integral:

$$I = \int_0^1 \mathrm{d}x\,\mathrm{d}y\, x^{-1-\epsilon} y^{-1-\epsilon} (x+y)^{-\epsilon}\,. \tag{5.35}$$

The $1/x$ and $1/y$ factors cannot be expanded in plus distributions, as the logarithms from the expansion of $x+y$ will produce singular terms. We split this integral into two parts,

$$I_1 = \int_0^1 \mathrm{d}x \int_0^x \mathrm{d}y\, x^{-1-\epsilon} y^{-1-\epsilon} (x+y)^{-\epsilon}\,, \quad I_2 = \int_0^1 \mathrm{d}y \int_0^y \mathrm{d}x\, x^{-1-\epsilon} y^{-1-\epsilon} (x+y)^{-\epsilon}\,. \tag{5.36}$$

In I_1 we set $y^{'} = y/x$, and in I_2 we set $x^{'} = x/y$. Performing these variable changes, we find

$$I_1 = \int_0^1 \mathrm{d}x\,\mathrm{d}y\, x^{-1-3\epsilon} y^{-1-\epsilon} (1+y)^{-\epsilon}\,, \quad I_2 = \int_0^1 \mathrm{d}x\,\mathrm{d}y\, y^{-1-3\epsilon} x^{-1-\epsilon} (1+x)^{-\epsilon}\,. \tag{5.37}$$

The singularities in x and y of (5.35) are now separated in each integral (or sector) of (5.37), and can be extracted using:

$$\lambda^{-1+\epsilon} = \frac{1}{\epsilon}\delta(\lambda) + \sum_{n=0}^{\infty} \frac{\epsilon^n}{n!} \left[\frac{\ln^n(\lambda)}{\lambda}\right]_+\,, \tag{5.38}$$

where a plus distribution is defined via

$$\int_0^1 d\lambda \left[\frac{\ln^n(\lambda)}{\lambda}\right]_+ f(\lambda) = \int_0^1 d\lambda \ln^n(\lambda) \left[\frac{f(\lambda)-f(0)}{\lambda}\right]. \tag{5.39}$$

However, before implementing these transformations it is necessary that all singularities in the λ_i occur at the origin $\lambda_i \to 0$. In (5.28) some invariants vanish at $\lambda_i \to 1$ and two cases can occur when we consider the denominators of matrix elements. In the first case the denominator has singularities when one of the $\lambda_i \to 1$. In this case the transformation $\lambda_i \to 1-\lambda_i$ remaps the singularity to the origin. In the second case the denominator causes singularities when $\lambda_i \to 0$ and $\lambda_i \to 1$. In this case it is convenient to separate the two singularities that can occur by splitting the integration:

$$\int_0^1 \mathrm{d}\lambda_i \to \int_0^{1/2} \mathrm{d}\lambda_i + \int_{1/2}^1 \mathrm{d}\lambda_i, \tag{5.40}$$

and substitute $\lambda_i = \lambda_i^{'}/2$ in the first integral and $\lambda_i = 1 - \lambda_i^{'}/2$ in the second integral to move all singularities to the origin. After these checks and steps are performed the remaining singularities are already factorised or are of the type of the example (5.35) and amenable by sector decomposition.

The great advantage of this method is in its algorithmic procedure that can be easily implemented in symbolic manipulation programs such as MAPLE or MATHEMATICA. To do that we carry out the following instructions:

1. read a term in the matrix element.

2. combine it with the phase space measure in equation (5.33) keeping the invariants in the numerator as functions of λ_i ($s_{ab}(\lambda_i)$) and the denominator replaced with (5.28).

3. remap all the singularities in the denominator to the origin $\lambda_i \to 0$ by making the split (5.40).

4. search for entangled singularities in the expression generated by the previous step. If it becomes singular when two variables $\lambda_i, \lambda_j \to 0$, but remains finite when either $\lambda_i \to 0$ or $\lambda_j \to 0$, then the transformation below (5.35) should be performed.

5. all singularities are factorised and can be expanded in a Laurent series in ϵ using (5.38).

6. proceed to the next term in the matrix element.

It should be mentioned now that it is possible [147] to combine the output of the sector decomposition procedure with any infrared safe measurement function to obtain differential results. In that case we arrive at an expansion with the following form:

$$\mathrm{d}\sigma^{RR}_{NNLO} = \sum_{j=0}^{4} \frac{f_j(\lambda_i)}{\epsilon^j} = \frac{f_4(\lambda_i)}{\epsilon^4} + \frac{f_3(\lambda_i)}{\epsilon^3} + \frac{f_2(\lambda_i)}{\epsilon^2} + \frac{f_1(\lambda_i)}{\epsilon^1} + \text{finite} \tag{5.41}$$

where we have used as an input the matrix element relevant to the double real correction at NNLO. The functions f_j are non-singular functions that can be inte-

grated numerically to yield the pole coefficients. These can then be combined with real-virtual and virtual-virtual contributions to verify their cancellation numerically.

To summarise, the key ideas to produce (5.41) is a parameterisation to the unit hypercube of the phase space of the double real correction where the singular invariants in the denominators of the matrix element can be brought to a factorised form using sector decomposition. For example the parameterisation (5.33) given by the mapping (5.28) is only convenient for expressions that do not contain s_{13} or s_{14} in the denominator. These invariants, in terms of λ_i, contain square root terms (5.28), that arise from solving the constraint $-\Delta_4 \geq 0$ for s_{13} (5.29). Because Δ_4 (5.26) is a quadratic equation the solutions always introduce square root terms and the extraction of the singularities in this case is not amenable with sector decomposition. In this case, $1/s_{13}$ develops a singularity when $\lambda_5 = 0$ and $y_{13}^- = 0 \Leftrightarrow \lambda_3\lambda_4 = \lambda_2(1-\lambda_3)(1-\lambda_4)$ (5.28). One solution is to remap the momenta of the final state particles in a way to eliminate the invariants s_{13} and s_{14} from appearing in the denominators. However this is not possible in general for all the $1 \to 4$ massless matrix elements to which this parameterisation applies. The other solution is to shuffle the square root terms to the numerator with the following non-linear transformation of λ_5 in (5.33) to bring the limits of the s_{13} integration from 0 to 1 [147]:

$$\hat{\lambda}_5 = \frac{y_{13} - y_{13}^-}{y_{13^+} - y_{13}^-}\frac{y_{13}^+}{y_{13}}\,, \quad y_{13}(\hat{\lambda}_5) = \frac{y_{13}^+ y_{13}^-}{(y_{13}^+ - y_{13}^-)(1-\hat{\lambda}_5) + y_{13}^-} \tag{5.42}$$

The jacobian of the transformation is given by:

$$\begin{aligned} \mathrm{d}\lambda_5 &= \frac{y_{13}^+ y_{13}^-}{\Big((y_{13}^+ - y_{13}^-)(1-\hat{\lambda}_5) + y_{13}^-\Big)^2}\,\mathrm{d}\hat{\lambda}_5 \\ &= \frac{y_{13}(\hat{\lambda}_5)}{(y_{13}^+ - y_{13}^-)(1-\hat{\lambda}_5) + y_{13}^-}\,\mathrm{d}\hat{\lambda}_5 \end{aligned} \tag{5.43}$$

and we derive the following parameterisation of the $1 \to 4$ phase space to the unit hypercube:

$$\begin{aligned} \int \mathrm{d}\Phi_{1\to 4} \quad &= (2\pi)^{4-3d}(Q^2)^{3d/2-4}2^{-2d+1}V_{d-1}V_{d-2}V_{d-3}\int_0^1 \mathrm{d}\lambda_1\mathrm{d}\lambda_2\mathrm{d}\lambda_3\mathrm{d}\lambda_4\mathrm{d}\hat{\lambda}_5 \\ &\quad [\lambda_1(1-\lambda_1)(1-\lambda_2)]^{1-2\epsilon}\,[\lambda_2\lambda_3(1-\lambda_3)\lambda_4(1-\lambda_4)]^{-\epsilon}\left[\hat{\lambda}_5(1-\hat{\lambda}_5)\right]^{-1/2-\epsilon} \\ &\quad y_{13}(\hat{\lambda}_5)\left[y_{13}^+ y_{13}^-\right]^{-1/2-\epsilon}\left\{(1-\hat{\lambda}_5)(y_{13}^+ - y_{13}^-) + y_{13}^-\right\}^{2\epsilon} \end{aligned} \tag{5.44}$$

The jacobian of the non-linear transformation is proportional to s_{13} and therefore, in this parameterisation, factors of s_{13} in denominators of matrix elements are cancelled. The transformation of $\lambda_5 \to \hat{\lambda}_5$ (5.42) does not change the other invariants in (5.28) that keep simple forms amenable to sector decomposition and there are no singularities in (5.44) associated with $\hat{\lambda}_5$.

However, using (5.29) we find:

$$\left[y_{13}^{+}y_{13}^{-}\right]^{-1/2-\epsilon} = (1-\lambda_1)^{-1-2\epsilon}|\lambda_2(1-\lambda_3)(1-\lambda_4)-\lambda_3\lambda_4|^{-1-2\epsilon} \tag{5.45}$$

This expression is singular on a manifold of points in the interior of the phase space. It is a new type of singularity and, as before, we wish to move it to the boundary of the integration region. The singularity occurs when:

$$\lambda_4 \to \lambda_4^s = \frac{\lambda_2(1-\lambda_3)}{\lambda_3+\lambda_2(1-\lambda_3)} \tag{5.46}$$

and this value is always in the integration region. To remap the singularities we split the λ_4 integration:

$$\int_0^1 \mathrm{d}\lambda_4 = \int_0^{\lambda_4^s} \mathrm{d}\lambda_4 + \int_{\lambda_4^s}^1 \mathrm{d}\lambda_4 \tag{5.47}$$

and we substitute $\lambda_4 = \lambda_4^s\hat{\lambda}_4$ in the first integral and $\lambda_4 = 1-(1-\lambda_4^s)\hat{\lambda}_4$ in the second to obtain integrals from zero to one. Doing this produces two integrals (or sectors) where the invariants in (5.28) have now a slightly different form due to the transformations in λ_4 mentioned. However their singularities can be extracted using the sector decomposition technique.

In conclusion, to extract the singularties in $1 \to 4$ massless matrix elements, relevant to the computation of NNLO real corrections to $1 \to 2$ processes, it is convenient to use as much as possible the phase space parameterisation of (5.33). This means that it is better to avoid, with rotations of the final-state momenta, terms with s_{13} or s_{14} in the denominator. This can be implemented as a new step in the start of the algorithm. If this is not possible then proceed using the parameterisation (5.44) of the phase space. The number of times this happens should be kept minimal because using (5.44) introduces two sectors (5.47) in the beginning of the algorithmic procedure. This number increases further according

to the complexity of the structure of the denominator in terms of the λ_i making the size of the functions f_j in (5.41) considerably lengthy which means harder to evaluate numerically and impossible analytically.

In general the NNLO matrix elements are lengthy to begin with, and, their expansion in a Laurent series of the type (5.41), using sector decomposition leads to unavoidable even lengthier formulas for the functions f_j. The size of the matrix element and the number of times (5.44) needs to be applied determines the number of coefficients in (5.41) that can be computed analytically. In the best cases the first three terms in the series, corresponding to the deepest poles, can be evaluated analytically and the remaining ones numerically. We will see an example in the next section.

It is important to understand these limitations when applying this method as new ideas may be needed to improve its behaviour. For example a parameterisation for the $1 \to 5$ massless phase space derived in [148] relevant to calculate $e^+e^- \to 3$ jets at NNLO using sector decomposition leads to an unacceptable number of terms to evaluate [124] with the necessary numerical precision. This is due to the large number of massless particles in the final state generating an extremely complicated infrared structure. On the other hand, if massive particles are involved, the infrared structure is in this case less complex as the mass regulates some of the infrared divergences and the number of terms produced by sector decomposition is reduced. The invariants may have a complicated formula in the unit hypercube, but, as long as they do not vanish, sector decomposition and the non-linear transformation (5.42) used in the massless case is no longer needed.

Examples of differential results at NNLO using this method are $e^+e^- \to 2$ jets [149], Higgs production [150–153], vector boson production [154]. In [155] the complete $\mathcal{O}(\alpha^2)$ QED corrections to the electron energy spectrum in muon decay were computed. $\mathcal{O}(\alpha_s^2)$ corrections to fully differential decay rates for $b \to cl\bar{\nu}_l$ were derived in [156].

For the calculation of $pp \to 2$ jets that this thesis refers to, an application of the sector decomposition method is not straightforward. As we have discussed, the most difficult part is to extract the divergences from the double real emission matrix

element, without integrating over any kinematic parameter that describes the real emission process. To achieve this we need to derive parameterisations for the $2 \to 4$ particle phase space to the unit hypercube. Although this is possible, the number of massless particles in the final state makes the infrared structure very complicated. In this case multiple invariants develop square root terms, making it impossible to find a parameterisation that can handle simultaneously all the invariants that appear in the most complicated denominators of six-parton matrix elements. In addition to this, we want to avoid squaring the matrix elements and use the compact expressions for scattering amplitudes derived in the helicity basis, but it is not clear how to use the helicity amplitudes efficiently.

5.3 Numerical integration of final-final NNLO antenna functions

In this section we are going to perform a direct check with sector decomposition of the analytic results for the integrated antenna F_4^0 obtained in [67]. As we explained in the previous chapter this antenna is the matrix element for $H \to gggg$ normalised to the squared two-parton basic matrix element. Its unintegrated form is given in appendix B.1. The terms of $\mathcal{O}(\epsilon)$ are omitted there but the integration of the antenna over the antenna phase space has to be performed in d dimensions to obtain the full singular structure. This is because at NNLO we expect poles up to $1/\epsilon^4$ that can hit the $\mathcal{O}(\epsilon)$ terms and therefore contribute to the pole structure and finite pieces. Also in the sector decomposition approach we need the $\mathcal{O}(\epsilon)$ terms in the matrix elements to expand the singular structure in a Laurent series.

By inspection of the formula for $F_4^0(1_g, 2_g, 3_g, 4_g)$ in B.1 we find that are denominators that contain the invariant s_{13} or s_{14} that cannot be avoided by rotations of the momenta of the final state particles. This means that in our implementation of the sector decomposition procedure we use both the parameterisations given by (5.33) and (5.44).

We also notice the presence of denominators of the type $1/(s_{12}^2 s_{34}^2)$. When we combine this denominator with the phase space measure we produce a parameter

integral of the form:

$$\int_0^1 \mathrm{d}x x^{a+b\epsilon} f(x) \tag{5.48}$$

with $a = -2$. This is not expected because *physical* singularities in a renormalisable theory are not worse than logarithmic and $a \geq -1$ always. In these few cases we may choose not to keep the numerator as a symbolic function $f(x)$ but introduce its explicit form at the level of the ϵ-expansion to cancel the quadratic singularity. Alternatively we can expand these higher order singularities in plus distributions using:

$$\int_0^1 \mathrm{d}x x^{-n+b\epsilon} f(x) = \int_0^1 \mathrm{d}x x^{b\epsilon} \frac{f(x) - \sum_{k=0}^{n-1} x^k \frac{f^{(k)}(0)}{k!}}{x^n} + \sum_{k=0}^{n-1} \frac{f^{(k)}(0)}{k!(k+1-n+b\epsilon)} \tag{5.49}$$

and introduce $f(x)$ only for the numerical integration.

As we mentioned in the previous section the antenna phase space is proportional to the $1 \to 4$ phase space and we worked out there its treatment within sector decomposition. With these ingredients we can do a check on the analytic results of the integrated antennae functions for final-final kinematics.

The analytic integral of the F_4^0 antenna function was obtained in [67]. In this work, the phase space integrals were related to loop integrals in the form of a cut diagram. A reduction procedure using integration-by-parts (IBP) identities showed that all antennae integrals can be expressed as a linear combination of four master integrals. These were computed in [104] analytically and numerically with sector decomposition. An analytic result for the F_4^0 antenna function was then obtained:

$$\begin{aligned} F(1_g, 2_g, 3_g, 4_g) &= 2\left[\frac{5}{2\epsilon^4} + \frac{121}{12\epsilon^3} + \frac{1}{\epsilon^2}\left(\frac{436}{9} - \frac{11\pi^2}{13}\right) + \frac{1}{\epsilon}\left(\frac{23455}{108} - \frac{1067\pi^2}{72}\right.\right. \\ &\quad \left.\left. - \frac{379}{6}\zeta(3)\right) + \left(\frac{304951}{324} - \frac{7781\pi^2}{108} - \frac{2288}{9}\zeta(3) + \frac{479\pi^4}{720}\right)\right] \\ &= \left[\frac{5}{\epsilon^4} + \frac{121}{6\epsilon^3} + \frac{24.51178992}{\epsilon^2} - \frac{10.03211182}{\epsilon} - 21.2942539\right] \end{aligned}$$

The same integral computed directly with the sector decomposition approach gives:

$$F(1_g, 2_g, 3_g, 4_g) = \left[\frac{5}{\epsilon^4} + \frac{121}{6\epsilon^3} + \frac{24.49 \pm 0.02}{\epsilon^2} - \frac{10.18 \pm 0.14}{\epsilon} - 21.9 \pm 1.1\right]$$

The output of the procedure were parameter integrals for all the coefficients. In this case the first two poles contain fewer integrations and are simple functions that could be evaluated analytically. For the remaining coefficients, the large size of the parametric function to be evaluated where complicated logarithmic functions involving multiple variables appear, makes an analytic result impossible.

We proceeded using VEGAS [157] to perform the multi-dimensional integral over the unit hypercube and quote the errors produced in the integration routine. The comparison reveals a good agreement but for the finite piece the precision is worse. This can be improved with a more sophisticated numerical integration technique. Numerical results for the remaining four-particle antennae functions were also obtained as these are of the same level of complexity as the F_4^0 antenna function and, for all, an agreement with the analytic results was observed.

5.4 Summary

In this chapter we examined the uses of the sector decomposition method for phenomenological applications. As we have seen from its description, the method can regarded as an universal method in the extraction of singularities from parameter integrals. Within field theory and using dimensional regularisation it provides factorisation and subtraction of infrared poles to (in principle) all orders in perturbation theory, not only for individual integrals, but also for entire squared matrix elements.

For multi-loop integrals it has been very successful to arrive at numerical results before analytic formulae were available but it provides also a cross-check of subsequent cutting-edge analytic calculations of two and three loop integrals. Alternative techniques include the Mellin-Barnes representation [158, 159] but this will not be discussed.

For phase space integrals the method has been useful to obtain results for full processes at NNLO where the advantages, compared to analytic subtraction, are an automated procedure starting from suitable phase space parameterisations and the production of expressions with good numerical behaviour. Also in this case there is

no need for an analytic integration of subtraction terms over the singular regions of the phase space.

Chapter 6

NNLO real corrections for gluon scattering

In this chapter we describe the calculation of the NNLO real corrections to gluon scattering. Infrared singularities due to double real radiation at tree level are subtracted from the full QCD matrix element for $gg \to gggg$ using antenna functions. All relevant formulae were written down in chapter 4 for the general case. Here we will apply them to the pure gluon channel to obtain finite contributions for the six-parton process.

In section 6.1 we write down the double real radiation contribution to the cross section split into three topologies that we define. For each, the relevant counterterms will be derived.

6.1 Six-gluon subtraction term

In this section we will consider the six-parton double real radiation contribution to the NNLO cross section. In the gluon-gluon channel we have the tree-level six parton process $gg \to gggg$. This process requires subtraction of all double unresolved and single unresolved singularities. The double real radiation is given by:

$$\begin{aligned} \mathrm{d}\sigma^{R}_{NNLO} &= N^2\, N_{born} \left(\frac{\alpha_s}{2\pi}\right)^2 \mathrm{d}\Phi_4(p_3,\ldots,p_6;p_1;p_2)\,\frac{1}{4!} \\ &\quad \sum_{\{2,\ldots,6\}'} A^0_6(\hat{1}_g,\hat{2}_g,i_g,j_g,k_g,l_g) J^{(4)}_2(p_i,\ldots,p_l) + \mathcal{O}\left(\frac{1}{N^2}\right) \end{aligned} \tag{6.1}$$

where the sum with the *prime*, $\sum_{\{2,\ldots,6\}'}$ is over all 5! *non-cyclic* permutations of $\hat{2}, 3, ..., 6$ and we have suppressed sub-leading colour terms. The squared amplitude A_6^0 summed over helicities is obtained by:

$$A_6^0(\hat{1}_g, \hat{2}_g, 3_g, 4_g, 5_g, 6_g) = \sum_h \mathcal{M}(\hat{1}_g, \hat{2}_g, 3_g, 4_g, 5_g, 6_g)\mathcal{M}^*(\hat{1}_g, \hat{2}_g, 3_g, 4_g, 5_g, 6_g) \quad (6.2)$$

where the sum includes MHV and next-to-MHV 6 gluon primitive amplitudes [25, 27, 28] that we evaluate as a complex number and square to obtain A_6^0. These are written down in the appendix A.6 and their evaluation was described in section 1.6.

We can now use the cyclic symmetry of the colour ordered squared amplitudes A_6^0 and reduce (6.1) to three independent topologies:

$$\begin{aligned} \mathrm{d}\sigma^R_{NNLO} &= N^2\, N_{born} \left(\frac{\alpha_s}{2\pi}\right)^2 \mathrm{d}\Phi_4(p_3,\ldots,p_6;p_1,p_2)\Bigg(\\ &\quad \frac{2}{4!} \sum_{P(i,j,k,l)\in(3,4,5,6)} A_6^0(\hat{1}_g, \hat{2}_g, i_g, j_g, k_g, l_g) J_2^{(4)}(p_i,\ldots,p_l) \\ &\quad + \frac{2}{4!} \sum_{P(i,j,k,l)\in(3,4,5,6)} A_6^0(\hat{1}_g, i_g, \hat{2}_g, j_g, k_g, l_g) J_2^{(4)}(p_i,\ldots,p_l) \\ &\quad + \frac{2}{4!} \sum_{P_C(i,j,k,l)\in(3,4,5,6)} A_6^0(\hat{1}_g, i_g, j_g, \hat{2}_g, k_g, l_g) J_2^{(4)}(p_i,\ldots,p_l)\Bigg) \end{aligned} \quad (6.3)$$

where the first two sums are over the 4! permutations of the gluon momenta in the final state and in the last sum only 4!/2 cyclic permutations are summed. Therefore, depending on the position of the initial state gluons we have different topologies. These are labelled IIFFFF, IFIFFF, IFFIFF respectively. In the following subsections we will write down the counterterm that regularises the infrared divergences of the double real correction for each topology separately.

6.1.1 IIFFFF topology

The real radiation contribution to the cross section for the first topology is obtained by averaging over all possible 24 orderings:

$$\begin{aligned} \mathrm{d}\sigma^R_{NNLO} &= N^2\, N_{born} \left(\frac{\alpha_s}{2\pi}\right)^2 \mathrm{d}\Phi_4(p_3,\ldots,p_6;p_1,p_2)\, \frac{2}{4!} \\ &\quad \sum_{(i,j,k,l)\in P(3,4,5,6)} A_6^0(\hat{1}_g, \hat{2}_g, i_g, j_g, k_g, l_g) J_2^{(4)}(p_i,\ldots,p_l) \end{aligned}$$

$$
\begin{aligned}
&= N^2\, N_{born} \left(\frac{\alpha_s}{2\pi}\right)^2 \mathrm{d}\Phi_4(p_3,\ldots,p_6;p_1,p_2)\,\frac{2}{4!} \\
&\quad \Big[X_6^0(\hat{1}_g,\hat{2}_g,3_g,4_g,5_g,6_g) + X_6^0(\hat{1}_g,\hat{2}_g,3_g,5_g,4_g,6_g) \\
&\quad + X_6^0(\hat{1}_g,\hat{2}_g,3_g,4_g,6_g,5_g)\Big] J_2^{(4)}(p_3,\ldots,p_6)
\end{aligned} \tag{6.4}
$$

where each X_6^0 contains 8 colour ordered squared amplitudes given by the 4 cyclic permutations of the final state gluons plus their line reversals:

$$
\begin{aligned}
X_6^0(\hat{1}_g,\hat{2}_g,3_g,4_g,5_g,6_g) \;=\;& A_6^0(\hat{1}_g,\hat{2}_g,3_g,4_g,5_g,6_g) + A_6^0(\hat{1}_g,\hat{2}_g,6_g,5_g,4_g,3_g) \\
&+A_6^0(\hat{1}_g,\hat{2}_g,4_g,5_g,6_g,3_g) + A_6^0(\hat{1}_g,\hat{2}_g,3_g,6_g,5_g,4_g) \\
&+A_6^0(\hat{1}_g,\hat{2}_g,5_g,6_g,3_g,4_g) + A_6^0(\hat{1}_g,\hat{2}_g,4_g,3_g,6_g,5_g) \\
&+A_6^0(\hat{1}_g,\hat{2}_g,6_g,3_g,4_g,5_g) + A_6^0(\hat{1}_g,\hat{2}_g,5_g,4_g,3_g,6_g)
\end{aligned} \tag{6.5}
$$

For the numerical implementation we use the X_6^0 function because this form of the real correction is more appropriate for the construction of the subtraction term. It matches onto the full $F_4^0(i_g,j_g,k_g,l_g)$ final-final antenna function which has a cyclic ambiguity in the momentum arrangements. This is because as it was mentioned in section 4.3.1 $F_4^0(i_g,j_g,k_g,l_g)$ contains four-different colour-ordered antennae. The real correction should have 4 colour-ordered squared amplitudes per each $F_4^0(i_g,j_g,k_g,l_g)$ in the subtraction term too. There is an extra factor of 2 because in the subtraction term we will use initial-final antennae of the type $F_4^0(\hat{2},i,j,k)$ which has the unresolved limits of i and j between $\hat{2}$ and k and the unresolved limits of k and j between $\hat{2}$ and i that come from two different orderings in the real radiation. This brings the total number of squared ordered amplitudes to implement in this topology to 8 (6.5).

The remaining 16 orderings in this topology corresponding to the last two X_6^0 functions are obtained by permutations of the gluon indices when calling the IIFFFF routine. These actually yield the same contribution to the cross section and need not to be evaluated. However if we sum over all orderings the topology becomes symmetric with respect to all gluon indices and this is better for the Monte Carlo integration.

The real radiation subtraction term for this topology to be used with

$X_6^0(\hat{1}_g, \hat{2}_g, 3_g, 4_g, 5_g, 6_g)$ is given by the following sum where:

$$(i,j,k,l) = (3,4,5,6),(4,5,6,3),(5,6,3,4),(6,3,4,5)$$

$$\begin{aligned}
\mathrm{d}\sigma^S_{NNLO} = N^2\, N_{born} \left(\frac{\alpha_s}{2\pi}\right)^2 \mathrm{d}\Phi_4(p_3,\ldots,p_6;p_1,p_2)\, \frac{2}{4!} \sum_{(ijkl)} \Bigg\{ \\
f_3^0(\hat{2}_g, i_g, j_g)\, A_5^0(\hat{1}_g, \hat{\hat{2}}_g, (\widetilde{ij})_g, k_g, l_g)\, J_2^{(3)}(\widetilde{p_{ij}}, p_k, p_l) \\
+ f_3^0(i_g, j_g, k_g) A_5^0(\hat{1}_g, \hat{2}_g, (\widetilde{ij})_g, (\widetilde{jk})_g, l_g) J_2^{(3)}(\widetilde{p_{ij}}, \widetilde{p_{jk}}, p_l) \\
+ f_3^0(j_g, k_g, l_g) A_5^0(\hat{1}_g, \hat{2}_g, i_g, (\widetilde{jk})_g, (\widetilde{kl})_g) J_2^{(3)}(p_i, \widetilde{p_{jk}}, \widetilde{p_{kl}}) \\
+ f_3^0(k_g, l_g, \hat{1}_g) A_5^0(\hat{\hat{1}}_g, \hat{2}_g, i_g, j_g, (\widetilde{kl})_g) J_2^{(3)}(p_i, p_j, \widetilde{p_{kl}}) \\
\\
+ f_3^0(\hat{2}_g, l_g, k_g)\, A_5^0(\hat{1}_g, \hat{\hat{2}}_g, (\widetilde{lk})_g, j_g, i_g)\, J_2^{(3)}(\widetilde{p_{lk}}, p_j, p_i) \\
+ f_3^0(l_g, k_g, j_g) A_5^0(\hat{1}_g, \hat{2}_g, (\widetilde{lk})_g, (\widetilde{kj})_g, i_g) J_2^{(3)}(\widetilde{p_{lk}}, \widetilde{p_{kj}}, p_i) \\
+ f_3^0(k_g, j_g, i_g) A_5^0(\hat{1}_g, \hat{2}_g, l_g, (\widetilde{kj})_g, (\widetilde{ji})_g) J_2^{(3)}(p_l, \widetilde{p_{kj}}, \widetilde{p_{ji}}) \\
+ f_3^0(j_g, i_g, \hat{1}_g) A_5^0(\hat{\hat{1}}_g, \hat{2}_g, l_g, k_g, (\widetilde{ji})_g) J_2^{(3)}(p_l, p_k, \widetilde{p_{ji}}) \\
\\
+ \Big(F_{4,a}^0(i_g, j_g, k_g, l_g) - f_3^0(i_g, j_g, k_g) f_3^0(\widetilde{(ij)}_g, \widetilde{(jk)}_g, l_g) \\
- f_3^0(j_g, k_g, l_g) f_3^0(i_g, \widetilde{(jk)}_g, \widetilde{(kl)}_g) \Big) A_4^0(\hat{1}_g, \hat{2}_g, \widetilde{(ijk)}_g, \widetilde{(lkj)}_g) J_2^{(2)}(\widetilde{p_{ijk}}, \widetilde{p_{lkj}}) \\
+ \Big(F_{4,b}^0(i_g, j_g, k_g, l_g) \\
- f_3^0(i_g, j_g, k_g) f_3^0(\widetilde{(ij)}_g, l_g, \widetilde{(jk)}_g) \Big) A_4^0(\hat{1}_g, \hat{2}_g, \widetilde{(ijl)}_g, \widetilde{(klj)}_g) J_2^{(2)}(\widetilde{p_{ijl}}, \widetilde{p_{klj}}) \\
+ \frac{1}{2} f_3^0(i_g, j_g, k_g) f_3^0(\widetilde{(ij)}_g, l_g, \widetilde{(jk)}_g) A_4^0(\hat{1}_g, \hat{2}_g, \widetilde{((ij)l)}_g, \widetilde{((jk)l)}_g) J_2^{(2)}(\widetilde{p_{(ij)l}}, \widetilde{p_{(jk)l}}) \\
\\
+ \Big(F_{4,a}^0(l_g, k_g, j_g, i_g) - f_3^0(l_g, k_g, j_g) f_3^0(\widetilde{(lk)}_g, \widetilde{(kj)}_g, i_g) \\
- f_3^0(k_g, j_g, i_g) f_3^0(l_g, \widetilde{(kj)}_g, \widetilde{(ji)}_g) \Big) A_4^0(\hat{1}_g, \hat{2}_g, \widetilde{(lkj)}_g, \widetilde{(ijk)}_g) J_2^{(2)}(\widetilde{p_{lkj}}, \widetilde{p_{ijk}}) \\
+ \Big(F_{4,b}^0(l_g, k_g, j_g, i_g) \\
- f_3^0(l_g, k_g, j_g) f_3^0(\widetilde{(lk)}_g, i_g, \widetilde{(kj)}_g) \Big) A_4^0(\hat{1}_g, \hat{2}_g, \widetilde{(lki)}_g, \widetilde{(jik)}_g) J_2^{(2)}(\widetilde{p_{lki}}, \widetilde{p_{jik}}) \\
+ \frac{1}{2} f_3^0(l_g, k_g, j_g) f_3^0(\widetilde{(lk)}_g, i_g, \widetilde{(kj)}_g) A_4^0(\hat{1}_g, \hat{2}_g, \widetilde{((lk)i)}_g, \widetilde{((kj)i)}_g) J_2^{(2)}(\widetilde{p_{(lk)i}}, \widetilde{p_{(kj)i}})
\end{aligned}$$

$$
\begin{aligned}
&+\Bigg(F_4^0(\hat{1}_g, l_g, k_g, j_g) \\
&\quad - f_3^0(\hat{1}_g, l_g, k_g) F_3^0(\hat{\tilde{1}}_g, \widetilde{(lk)}_g, j_g) - f_3^0(l_g, k_g, j_g) F_3^0(\hat{1}_g, \widetilde{(lk)}_g, \widetilde{(kj)}_g) \\
&\quad - f_3^0(k_g, j_g, \hat{1}_g) F_3^0(\hat{\tilde{1}}_g, l_g, \widetilde{(jk)}_g) \Bigg) A_4^0(\hat{\tilde{1}}_g, \hat{2}_g, i_g, \widetilde{(lkj)}_g) J_2^{(2)}(p_i, \widetilde{p_{lkj}}) \\
&+\Bigg(F_4^0(\hat{2}_g, i_g, j_g, k_g) \\
&\quad - f_3^0(\hat{2}_g, i_g, j_g) F_3^0(\hat{\tilde{2}}_g, \widetilde{(ij)}_g, k_g) - f_3^0(i_g, j_g, k_g) F_3^0(\hat{2}_g, \widetilde{(ij)}_g, \widetilde{(jk)}_g) \\
&\quad - f_3^0(j_g, k_g, \hat{2}_g) F_3^0(\hat{\tilde{2}}_g, i_g, \widetilde{(kj)}_g) \Bigg) A_4^0(\hat{1}_g, \hat{\tilde{2}}_g, \widetilde{(ijk)}_g, l_g) J_2^{(2)}(p_{ijk}, p_l) \\
&+\frac{1}{2} f_3^0(\hat{1}_g, l_g, k_g) f_3^0(\hat{\tilde{1}}_g, j_g, \widetilde{(lk)}_g) A_4^0(\hat{\tilde{\tilde{1}}}_g, \hat{2}_g, i_g, \widetilde{((lk)j)}_g) J_2^{(2)}(p_i, \widetilde{p_{(lk)j}}) \\
&+\frac{1}{2} f_3^0(\hat{1}_g, j_g, k_g) f_3^0(\hat{\tilde{1}}_g, l_g, \widetilde{(jk)}_g) A_4^0(\hat{\tilde{\tilde{1}}}_g, \hat{2}_g, i_g, \widetilde{((jk)l)}_g) J_2^{(2)}(p_i, \widetilde{p_{(jk)l}}) \\
&+\frac{1}{2} f_3^0(\hat{2}_g, i_g, j_g) f_3^0(\hat{\tilde{2}}_g, k_g, \widetilde{(ij)}_g) A_4^0(\hat{1}_g, \hat{\tilde{\tilde{2}}}_g, \widetilde{((ij)k)}_g, l_g) J_2^{(2)}(\widetilde{p_{(ij)k}}, p_l) \\
&+\frac{1}{2} f_3^0(\hat{2}_g, k_g, j_g) f_3^0(\hat{\tilde{2}}_g, i_g, \widetilde{(kj)}_g) A_4^0(\hat{1}_g, \hat{\tilde{\tilde{2}}}_g, \widetilde{((jk)i)}_g, l_g) J_2^{(2)}(\widetilde{p_{(jk)i}}, p_l)
\end{aligned}
$$

$$
\begin{aligned}
&-\Bigg(F_4^0(\hat{1}_g, i_g, \hat{2}_g, k_g) - F_3^0(\hat{1}_g, i_g, \hat{2}_g) F_3^0(\hat{\tilde{1}}_g, \hat{\tilde{2}}_g, \tilde{k}_g) \\
&\quad - F_3^0(\hat{1}_g, k_g, \hat{2}_g) F_3^0(\hat{\tilde{1}}_g, \hat{\tilde{2}}_g, \tilde{i}_g) \Bigg) A_4^0(\hat{\tilde{1}}_g, \hat{\tilde{2}}_g, \tilde{j}_g, \tilde{l}_g) J_2^{(2)}(\tilde{p}_j, \tilde{p}_l) \\
&-\frac{1}{2} F_3^0(\hat{1}_g, i_g, \hat{2}_g) F_3^0(\hat{\tilde{1}}_g, \hat{\tilde{2}}_g, \tilde{k}_g) A_4^0(\hat{\tilde{\tilde{1}}}_g, \hat{\tilde{\tilde{2}}}_g, \tilde{\tilde{j}}_g, \tilde{\tilde{l}}_g) J_2^{(2)}(\tilde{\tilde{p}}_j, \tilde{\tilde{p}}_l) \\
&-\frac{1}{2} F_3^0(\hat{1}_g, k_g, \hat{2}_g) F_3^0(\hat{\tilde{1}}_g, \hat{\tilde{2}}_g, \tilde{i}_g) A_4^0(\hat{\tilde{\tilde{1}}}_g, \hat{\tilde{\tilde{2}}}_g, \tilde{\tilde{j}}_g, \tilde{\tilde{l}}_g) J_2^{(2)}(\tilde{\tilde{p}}_j, \tilde{\tilde{p}}_l)
\end{aligned}
$$

$$
\begin{aligned}
&-\frac{1}{2} f_3^0(\hat{2}_g, i_g, j_g) f_3^0(l_g, k_g, \widetilde{(ij)}_g) A_4^0(\hat{1}_g, \hat{\tilde{2}}_g, \widetilde{((ij)k)}_g, \widetilde{(kl)}_g) J_2^{(2)}(\widetilde{p_{(ij)k}}, \widetilde{p_{kl}}) \\
&-\frac{1}{2} f_3^0(l_g, k_g, j_g) f_3^0(\hat{2}_g, i_g, \widetilde{(kj)}_g) A_4^0(\hat{1}_g, \hat{\tilde{2}}_g, \widetilde{((kj)i)}_g, \widetilde{(kl)}_g) J_2^{(2)}(\widetilde{p_{(kj)i}}, \widetilde{p_{kl}}) \\
&-\frac{1}{2} f_3^0(\hat{1}_g, l_g, k_g) f_3^0(i_g, j_g, \widetilde{(lk)}_g) A_4^0(\hat{\tilde{1}}_g, \hat{2}_g, \widetilde{(ij)}_g, \widetilde{((lk)j)}_g) J_2^{(2)}(\widetilde{p_{ij}}, \widetilde{p_{(lk)j}}) \\
&-\frac{1}{2} f_3^0(i_g, j_g, k_g) f_3^0(\hat{1}_g, l_g, \widetilde{(jk)}_g) A_4^0(\hat{\tilde{1}}_g, \hat{2}_g, \widetilde{(ij)}_g, \widetilde{((jk)l)}_g) J_2^{(2)}(\widetilde{p_{ij}}, \widetilde{p_{(jk)l}}) \\
&-\frac{1}{2} f_3^0(\hat{2}_g, l_g, k_g) f(i_g, j_g, \widetilde{(lk)}_g) A_4^0(\hat{1}_g, \hat{\tilde{2}}_g, \widetilde{((lk)j)}_g, \widetilde{(ij)}_g) J_2^{(2)}(\widetilde{p_{(lk)j}}, \widetilde{p_{ij}}) \\
&-\frac{1}{2} f_3^0(i_g, j_g, k_g) f_3^0(\hat{2}_g, l_g, \widetilde{(jk)}_g) A_4^0(\hat{1}_g, \hat{\tilde{2}}_g, \widetilde{((jk)l)}_g, \widetilde{(ij)}_g) J_2^{(2)}(\widetilde{p_{(jk)l}}, \widetilde{p_{ij}}) \\
&-\frac{1}{2} f_3^0(\hat{1}_g, i_g, j_g) f_3^0(l_g, k_g, \widetilde{(ij)}_g) A_4^0(\hat{\tilde{1}}_g, \hat{2}_g, \widetilde{(kl)}_g, \widetilde{((ij)l)}_g) J_2^{(2)}(\widetilde{p_{kl}}, \widetilde{p_{(ij)l}})
\end{aligned}
$$

$$
\begin{aligned}
&-\frac{1}{2}f_3^0(l_g,k_g,j_g)f_3^0(\hat{1}_g,i_g,\widetilde{(kj)}_g)A_4^0(\hat{\tilde{1}}_g,\hat{2}_g,\widetilde{(kl)}_g,\widetilde{((kj)i)}_g)J_2^{(2)}(\widetilde{p_{kl}},\widetilde{p_{(kj)i}})\\
&\\
&-f_3^0(\hat{2}_g,i_g,j_g)f_3^0(k_g,l_g,\hat{1}_g)A_4^0(\hat{\tilde{1}}_g,\hat{\tilde{2}}_g,\widetilde{(ij)}_g,\widetilde{(lk)}_g)J_2^{(2)}(\widetilde{p_{ij}},\widetilde{p_{lk}})\\
&-f_3^0(\hat{2}_g,l_g,k_g)f_3^0(j_g,i_g,\hat{1}_g)A_4^0(\hat{\tilde{1}}_g,\hat{\tilde{2}}_g,\widetilde{(lk)}_g,\widetilde{(ij)}_g)J_2^{(2)}(\widetilde{p_{lk}},\widetilde{p_{ij}})\\
&\\
&+\frac{1}{2}f_3^0(\hat{2}_g,k_g,j_g)F_3^0(\hat{1}_g,\hat{\tilde{2}}_g,i_g)A_4^0(\hat{\tilde{1}}_g,\hat{\tilde{\tilde{2}}}_g,\widetilde{(kj)}_g,\tilde{l}_g)J_2^{(2)}(\widetilde{p_{kl}},\tilde{p}_l)\\
&-\frac{1}{2}F_3^0(\hat{1}_g,\hat{2}_g,i_g)f_3^0(\hat{\tilde{2}}_g,\tilde{k}_g,\tilde{j}_g)A_4^0(\hat{\tilde{1}}_g,\hat{\tilde{\tilde{2}}}_g,\widetilde{(kj)}_g,\tilde{l}_g)J_2^{(2)}(\widetilde{p_{kj}},\tilde{p}_l)\\
&+\frac{1}{2}f_3^0(\hat{2}_g,i_g,j_g)F_3^0(\hat{1}_g,\hat{\tilde{2}}_g,k_g)A_4^0(\hat{\tilde{1}}_g,\hat{\tilde{\tilde{2}}}_g,\widetilde{(ij)}_g,\tilde{l}_g)J_2^{(2)}(\widetilde{p_{ij}},\tilde{p}_l)\\
&-\frac{1}{2}F_3^0(\hat{1}_g,\hat{2}_g,k_g)f_3^0(\hat{\tilde{2}}_g,\tilde{i}_g,\tilde{j}_g)A_4^0(\hat{\tilde{1}}_g,\hat{\tilde{\tilde{2}}}_g,\widetilde{(ij)}_g,\tilde{l}_g)J_2^{(2)}(\widetilde{p_{ij}},\tilde{p}_l)\\
&+\frac{1}{2}f_3^0(\hat{1}_g,k_g,j_g)F_3^0(\hat{\tilde{1}}_g,\hat{2}_g,i_g)A_4^0(\hat{\tilde{\tilde{1}}}_g,\hat{\tilde{2}}_g,\tilde{l}_g,\widetilde{(kj)}_g)J_2^{(2)}(\tilde{p}_l,\widetilde{p_{kj}})\\
&-\frac{1}{2}F_3^0(\hat{1}_g,\hat{2}_g,i_g)f_3^0(\hat{\tilde{1}}_g,\tilde{k}_g,\tilde{j}_g)A_4^0(\hat{\tilde{\tilde{1}}}_g,\hat{\tilde{2}}_g,\tilde{l}_g,\widetilde{(kj)}_g)J_2^{(2)}(\tilde{p}_l,\widetilde{p_{kj}})\\
&+\frac{1}{2}f_3^0(\hat{1}_g,i_g,j_g)F_3^0(\hat{\tilde{1}}_g,\hat{2}_g,l_g)A_4^0(\hat{\tilde{\tilde{1}}}_g,\hat{\tilde{2}}_g,\tilde{l}_g,\widetilde{(ij)}_g)J_2^{(2)}(\tilde{p}_l,\widetilde{p_{ij}})\\
&-\frac{1}{2}F_3^0(\hat{1}_g,\hat{\tilde{2}}_g,l_g)f_3^0(\hat{\tilde{1}}_g,\tilde{i}_g,\tilde{j}_g)A_4^0(\hat{\tilde{\tilde{1}}}_g,\hat{\tilde{2}}_g,\tilde{l}_g,\widetilde{(ij)}_g)J_2^{(2)}(\tilde{p}_l,\widetilde{p_{ij}})\Bigg\}
\end{aligned}
\tag{6.6}
$$

In the numerics we explicitly implemented the summation over (i,j,k,l). This is needed to reconstruct the full $F_4^0(i_g,j_g,k_g,l_g)$ from the $F_{4,a}$ and $F_{4,b}$ as in (4.45). This makes sure that all the double unresolved limits of the amplitudes in (6.5) are subtracted and only $F_4^0(i_g,j_g,k_g,l_g)$ must be analytically integrated over the antenna phase-space. It is important to notice that this six-gluon subtraction term introduces spurious limits from large angle soft radiation. The single soft limit of (6.6) is non-vanishing. To account for this large angle soft radiation a new subtraction term $\mathrm{d}\sigma^A_{NNLO}$, defined in section 4.2.5, is introduced. Its contribution reads:

$$
\begin{aligned}
\mathrm{d}\sigma^A_{NNLO} = N^2\, N_{born}\left(\frac{\alpha_s}{2\pi}\right)^2 \mathrm{d}\Phi_4(p_3,\ldots,p_6;p_1,p_2)\,\frac{2}{4!}\sum_{(ijkl)}\Bigg\{\\
\frac{1}{2}\Big(-S_{2l((il)j)}+S_{2l(il)}-S_{1l((kl)j)}+S_{1l(kl)}+S_{((il)j)l((kl)j)}-S_{(il)l(kl)}\Big)\\
\times f_3^0(\widetilde{(il)}_g,j_g,\widetilde{(kl)}_g)A_4^0(\hat{1}_g,\hat{2}_g,\widetilde{((il)j)}_g,\widetilde{((kl)j)}_g)J_2^{(2)}(\widetilde{p_{(il)j}},\widetilde{p_{(kl)j}})\\
+\frac{1}{2}\Big(-S_{2i((il)k)}+S_{2i(il)}-S_{1i((ij)k)}+S_{1i(ij)}+S_{((il)k)i((ij)k)}-S_{(il)i(ij)}\Big)
\end{aligned}
$$

$$
\begin{aligned}
&\times f_3^0(\widetilde{(il)}_g, k_g, \widetilde{(ij)}_g) A_4^0(\hat{1}_g, \hat{2}_g, \widetilde{((il)k)}_g, \widetilde{((ij)k)}_g) J_2^{(2)}(\widetilde{p_{(il)k}}, \widetilde{p_{(ij)k}}) \\
&+\frac{1}{2}\Big(- S_{il((kl)j)} + S_{il(kl)} + S_{\bar{\hat{1}}l((kl)j)} - S_{\bar{1}l(kl)} - S_{\bar{\hat{1}}l2} + S_{\bar{1}l2}\Big) \\
&\times f_3^0(\hat{\bar{1}}_g, j_g, \widetilde{(kl)}_g) A_4^0(\hat{\bar{1}}_g, \hat{2}_g, i_g, \widetilde{((kl)j)}_g) J_2^{(2)}(\tilde{p}_i, \widetilde{p_{(kl)j}}) \\
&+\frac{1}{2}\Big(- S_{ij((jk)l)} + S_{ij(jk)} + S_{\bar{\hat{1}}j((jk)l)} - S_{\bar{1}j(jk)} - S_{\bar{\hat{1}}j2} + S_{\bar{1}j2}\Big) \\
&\times f_3^0(\hat{\bar{1}}_g, l_g, \widetilde{(kj)}_g) A_4^0(\hat{\bar{1}}_g, \hat{2}_g, i_g, \widetilde{((kj)l)}_g) J_2^{(2)}(p_i, \widetilde{p_{(kj)l}}) \\
&+\frac{1}{2}\Big(- S_{lk((jk)i)} + S_{lk(jk)} + S_{\bar{\hat{2}}k((jk)i)} - S_{\bar{2}k(jk)} - S_{1k\bar{\hat{2}}} + S_{1k\bar{2}}\Big) \\
&\times f_3^0(\hat{\bar{2}}_g, i_g, \widetilde{(jk)}_g) A_4^0(\hat{1}_g, \hat{\bar{2}}_g, \widetilde{((jk)i)}_g, l_g) J_2^{(2)}(\widetilde{p_{(jk)i}}, p_l) \\
&+\frac{1}{2}\Big(- S_{li((ij)k)} + S_{li(ij)} + S_{\bar{\hat{2}}i((ij)k)} - S_{\bar{2}i(ij)} - S_{1i\bar{\hat{2}}} + S_{1i\bar{2}}\Big) \\
&\times f_3^0(\hat{\bar{2}}_g, k_g, \widetilde{(ij)}_g) A_4^0(\hat{1}_g, \hat{\bar{2}}_g, \widetilde{((ij)k)}_g, l_g) J_2^{(2)}(\widetilde{p_{(ij)k}}, p_l) \\
&+\frac{1}{2}\Big(- S_{\bar{\hat{1}}\tilde{i}\bar{\hat{2}}} + S_{\bar{1}i\bar{2}} - S_{\bar{2}i\tilde{j}} + S_{\bar{\hat{2}}\tilde{i}\tilde{\hat{j}}} - S_{\bar{1}i\tilde{l}} + S_{\bar{\hat{1}}i\tilde{\hat{l}}}\Big) \\
&\times F_3^0(\hat{\bar{1}}_g, \tilde{k}_g, \hat{\bar{2}}_g) A_4^0(\hat{\bar{1}}_g, \hat{\bar{2}}_g, \tilde{\hat{j}}_g, \tilde{\hat{l}}_g) J_2^{(2)}(\tilde{p}_j, \tilde{p}_l) \\
&+\frac{1}{2}\Big(- S_{\bar{\hat{1}}\tilde{k}\bar{\hat{2}}} + S_{\bar{1}k\bar{2}} - S_{\bar{2}k\tilde{j}} + S_{\bar{\hat{2}}\tilde{k}\tilde{\hat{j}}} - S_{\bar{1}k\tilde{l}} + S_{\bar{\hat{1}}k\tilde{\hat{l}}}\Big) \\
&\times F_3^0(\hat{\bar{1}}_g, \tilde{i}_g, \hat{\bar{2}}_g) A_4^0(\hat{\bar{1}}_g, \hat{\bar{2}}_g, \tilde{\hat{j}}_g, \tilde{\hat{l}}_g) J_2^{(2)}(\tilde{p}_j, \tilde{p}_l)
\end{aligned}
\tag{6.7}
$$

6.1.2 IFIFFF topology

The real radiation contribution to the cross section for the second topology is obtained by averaging over all possible twenty-four orderings:

$$
\begin{aligned}
\mathrm{d}\sigma^R_{NNLO} &= N^2\, N_{born} \left(\frac{\alpha_s}{2\pi}\right)^2 \mathrm{d}\Phi_4(p_3,\ldots,p_6;p_1,p_2)\,\frac{2}{4!} \\
&\quad \sum_{(i,j,k,l)\in P(3,4,5,6)} A_6^0(\hat{1}_g, i_g, \hat{2}_g, j_g, k_g, l_g) J_2^{(4)}(p_3,\ldots,p_6) \\
&= N^2\, N_{born} \left(\frac{\alpha_s}{2\pi}\right)^2 \mathrm{d}\Phi_4(p_3,\ldots,p_6;p_1,p_2)\,\frac{2}{4!} \\
&\quad \Big[X_6^0(\hat{1}_g, 3_g, \hat{2}_g, 4_g, 5_g, 6_g) + X_6^0(\hat{1}_g, 4_g, \hat{2}_g, 5_g, 6_g, 3_g) \\
&\quad + X_6^0(\hat{1}_g, 5_g, \hat{2}_g, 6_g, 3_g, 4_g) + X_6^0(\hat{1}_g, 6_g, \hat{2}_g, 3_g, 4_g, 5_g)\Big] \\
&\quad J_2^{(4)}(p_3,\ldots,p_6)
\end{aligned}
\tag{6.8}
$$

where each X_6^0 contains 6 colour ordered squared amplitudes where the first final state gluon index is kept fixed and we sum the 3 cyclic permutations of the remaining final state gluons:

$$
X_6^0(\hat{1},3,\hat{2},4,5,6) = A_6^0(\hat{1},3,\hat{2},4,5,6) + A_6^0(\hat{1},3,\hat{2},4,6,5) + A_6^0(\hat{1},3,\hat{2},5,4,6)
$$

$$+A_6^0(\hat{1},3,\hat{2},5,6,4)+A_6^0(\hat{1},3,\hat{2},6,4,5)+A_6^0(\hat{1},3,\hat{2},6,5,4) \tag{6.9}$$

This form (6.8) is more appropriate for the construction of the real radiation subtraction term, since it matches onto the symmetry of the full F_4^0 initial-final antenna function. $F_4^0(\hat{2},j,k,l)$ contains the unresolved limits of j and k between $\hat{2}$ and l and the unresolved limits of k and l between $\hat{2}$ and j. It is suitable to use it when subtracting the singular limits of the ordered emissions $A_6^0(\hat{1},i,\hat{2},j,k,l)+A_6^0(\hat{1},i,\hat{2},l,k,j)$. Also the initial-initial antenna function $F_4^0(\hat{1},i,\hat{2},j)$ subtracts double unresolved limits of the ordered emissions $A_6^0(\hat{1},i,\hat{2},j,k,l)+A_6^0(\hat{1},i,\hat{2},k,l,j)$. Combining these symmetries brings the total number of ordered squared amplitudes to implement in this topology to 6 and the remaining 18, corresponding to the remaining 3 X_6^0 functions, can be obtained by permutations of the gluon indices when calling the IFIFFF routine. The real radiation subtraction term to be used with $X_6^0(\hat{1},i,\hat{2},j,k,l)$ is the following:

$$\begin{aligned}
\mathrm{d}\sigma^S_{NNLO} = N^2\, N_{born} \left(\frac{\alpha_s}{2\pi}\right)^2 \mathrm{d}\Phi_4(p_3,\ldots,p_6;p_1,p_2)\,\frac{2}{4!}\sum_{P_C(j,k,l)}\Bigg\{ \\
F_3^0(\hat{1}_g,i_g,\hat{2}_g)\,A_5^0(\hat{\tilde{1}}_g,\hat{\tilde{2}}_g,\tilde{j}_g,\tilde{k}_g,\tilde{l}_g)\,J_2^{(3)}(\tilde{p}_j,\tilde{p}_k,\tilde{p}_l) \\
+f_3^0(\hat{2}_g,j_g,k_g)\,A_5^0(\hat{1}_g,i_g,\hat{\tilde{2}}_g,\widetilde{(jk)}_g,l_g)\,J_2^{(3)}(p_i,\widetilde{p_{jk}},p_l) \\
+f_3^0(j_g,k_g,l_g)\,A_5^0(\hat{1}_g,i_g,\hat{2}_g,\widetilde{(jk)}_g,\widetilde{(kl)}_g)\,J_2^{(3)}(p_i,\widetilde{p_{jk}},\widetilde{p_{kl}}) \\
+f_3^0(k_g,l_g,\hat{1}_g)\,A_5^0(\hat{\tilde{1}}_g,i_g,\hat{2}_g,j_g,\widetilde{(kl)}_g)\,J_2^{(3)}(p_i,p_j,\widetilde{p_{kl}}) \\
\\
+F_3^0(\hat{1}_g,i_g,\hat{2}_g)\,A_5^0(\hat{\tilde{1}}_g,\hat{\tilde{2}}_g,\tilde{l}_g,\tilde{k}_g,\tilde{j}_g)\,J_2^{(3)}(\tilde{p}_l,\tilde{p}_k,\tilde{p}_j) \\
+f_3^0(\hat{2}_g,l_g,k_g)\,A_5^0(\hat{1}_g,i_g,\hat{\tilde{2}}_g,\widetilde{(lk)}_g,j_g)\,J_2^{(3)}(p_i,\widetilde{p_{lk}},p_j) \\
+f_3^0(l_g,k_g,j_g)\,A_5^0(\hat{1}_g,i_g,\hat{2}_g,\widetilde{(lk)}_g,\widetilde{(kj)}_g)\,J_2^{(3)}(p_i,\widetilde{p_{lk}},\widetilde{p_{kj}}) \\
+f_3^0(k_g,j_g,\hat{1}_g)\,A_5^0(\hat{\tilde{1}}_g,i_g,\hat{2}_g,l_g,\widetilde{(jk)}_g)\,J_2^{(3)}(p_i,p_l,\widetilde{p_{jk}}) \\
\\
+\Bigg(F_4^0(\hat{2}_g,j_g,k_g,l_g) \\
-f_3^0(\hat{2}_g,j_g,k_g)\,F_3^0(\hat{\tilde{2}}_g,\widetilde{(jk)}_g,l_g)-f_3^0(j_g,k_g,l_g)\,F_3^0(\hat{2}_g,\widetilde{(jk)}_g,\widetilde{(kl)}_g)
\end{aligned}$$

$$
\begin{aligned}
&\left. -f_3^0(k_g,l_g,\hat{2}_g)\,F_3^0(\hat{\tilde{2}}_g,j_g,\widetilde{(kl)}_g)\right) A_4^0(\hat{1}_g,i_g,\hat{\tilde{2}}_g,\widetilde{(jkl)}_g)\,J_2^{(2)}(p_i,\widetilde{p_{jkl}})\\
&+\Bigg(F_4^0(\hat{1}_g,l_g,k_g,j_g)\\
&\quad -f_3^0(\hat{1}_g,l_g,k_g)\,F_3^0(\hat{\tilde{1}}_g,\widetilde{(kl)}_g,j_g)-f_3^0(l_g,k_g,j_g)\,F_3^0(\hat{1}_g,\widetilde{(lk)}_g,\widetilde{(kj)}_g)\\
&\quad \left. -f_3^0(k_g,j_g,\hat{1}_g)\,F_3^0(\hat{\tilde{1}}_g,l_g,\widetilde{(jk)}_g)\right) A_4^0(\hat{\tilde{1}}_g,i_g,\hat{2}_g,\widetilde{(lkj)}_g)\,J_2^{(2)}(p_i,\widetilde{p_{lkj}})\\
&+\frac{1}{2}f_3^0(\hat{2}_g,j_g,k_g)f_3^0(\hat{\tilde{2}}_g,l_g,\widetilde{(jk)}_g)\,A_4^0(\hat{1}_g,i_g,\hat{\tilde{\tilde{2}}}_g,\widetilde{(jk)l}_g)\,J_2^{(2)}(p_i,\widetilde{p_{(jk)l}})\\
&+\frac{1}{2}f_3^0(\hat{2}_g,l_g,k_g)f_3^0(\hat{\tilde{2}}_g,j_g,\widetilde{(lk)}_g)\,A_4^0(\hat{1}_g,i_g,\hat{\tilde{\tilde{2}}}_g,\widetilde{(lk)j}_g)\,J_2^{(2)}(p_i,\widetilde{p_{(lk)j}})\\
&+\frac{1}{2}f_3^0(\hat{1}_g,l_g,k_g)f_3^0(\hat{\tilde{1}}_g,j_g,\widetilde{(lk)}_g)\,A_4^0(\hat{\tilde{\tilde{1}}}_g,i_g,\hat{2}_g,\widetilde{(lk)j}_g)\,J_2^{(2)}(p_i,\widetilde{p_{(lk)j}})\\
&+\frac{1}{2}f_3^0(\hat{1}_g,j_g,k_g)f_3^0(\hat{\tilde{1}}_g,l_g,\widetilde{(jk)}_g)\,A_4^0(\hat{\tilde{\tilde{1}}}_g,i_g,\hat{2}_g,\widetilde{(jk)l}_g)\,J_2^{(2)}(p_i,\widetilde{p_{(jk)l}})\\
&+\Bigg(F_4^0(\hat{1}_g,i_g,\hat{2}_g,j_g)-F_3^0(\hat{1}_g,i_g,\hat{2}_g)\,F_3^0(\hat{\tilde{1}}_g,\hat{\tilde{2}}_g,\tilde{j}_g)\\
&\quad \left. -F_3^0(\hat{2}_g,j_g,\hat{1}_g)\,F_3^0(\hat{\tilde{1}}_g,\tilde{i}_g,\hat{\tilde{2}}_g)\right) A_4^0(\hat{\tilde{1}}_g,\hat{\tilde{2}}_g,\tilde{k}_g,\tilde{l}_g)\,J_2^{(2)}(\widetilde{p_k},\widetilde{p_l})\\
&+\Bigg(F_4^0(\hat{1}_g,i_g,\hat{2}_g,l_g)-F_3^0(\hat{1}_g,i_g,\hat{2}_g)\,F_3^0(\hat{\tilde{1}}_g,\hat{\tilde{2}}_g,\tilde{l}_g)\\
&\quad \left. -F_3^0(\hat{2}_g,l_g,\hat{1}_g)\,F_3^0(\hat{\tilde{1}}_g,\tilde{i}_g,\hat{\tilde{2}}_g)\right) A_4^0(\hat{\tilde{1}}_g,\hat{\tilde{2}}_g,\tilde{k}_g,\tilde{j}_g)\,J_2^{(2)}(\widetilde{p_k},\widetilde{p_j})\\
&+\frac{1}{2}F_3^0(\hat{2}_g,j_g,\hat{1}_g)F_3^0(\hat{\tilde{1}}_g,\tilde{i}_g,\hat{\tilde{2}}_g)\,A_4^0(\hat{\tilde{\tilde{1}}}_g,\hat{\tilde{\tilde{2}}}_g,\tilde{\tilde{k}}_g,\tilde{\tilde{l}}_g)\,J_2^{(2)}(\tilde{\tilde{p}}_k,\tilde{\tilde{p}}_l)\\
&+\frac{1}{2}F_3^0(\hat{1}_g,i_g,\hat{2}_g)F_3^0(\hat{\tilde{1}}_g,\tilde{j}_g,\hat{\tilde{2}}_g)\,A_4^0(\hat{\tilde{\tilde{1}}}_g,\hat{\tilde{\tilde{2}}}_g,\tilde{\tilde{k}}_g,\tilde{\tilde{l}}_g)\,J_2^{(2)}(\tilde{\tilde{p}}_k,\tilde{\tilde{p}}_l)\\
&+\frac{1}{2}F_3^0(\hat{2}_g,l_g,\hat{1}_g)F_3^0(\hat{\tilde{1}}_g,\tilde{i}_g,\hat{\tilde{2}}_g)\,A_4^0(\hat{\tilde{\tilde{1}}}_g,\hat{\tilde{\tilde{2}}}_g,\tilde{\tilde{k}}_g,\tilde{\tilde{j}}_g)\,J_2^{(2)}(\tilde{\tilde{p}}_k,\tilde{\tilde{p}}_j)\\
&+\frac{1}{2}F_3^0(\hat{1}_g,i_g,\hat{2}_g)F_3^0(\hat{\tilde{1}}_g,\tilde{l}_g,\hat{\tilde{2}}_g)\,A_4^0(\hat{\tilde{\tilde{1}}}_g,\hat{\tilde{\tilde{2}}}_g,\tilde{\tilde{k}}_g,\tilde{\tilde{j}}_g)\,J_2^{(2)}(\tilde{\tilde{p}}_k,\tilde{\tilde{p}}_j)\\
&-\Bigg(F_4^0(\hat{1}_g,l_g,\hat{2}_g,j_g)-F_3^0(\hat{1}_g,l_g,\hat{2}_g)\,F_3^0(\hat{\tilde{1}}_g,\hat{\tilde{2}}_g,\tilde{j}_g)\\
&\quad \left. -F_3^0(\hat{2}_g,j_g,\hat{1}_g)\,F_3^0(\hat{\tilde{1}}_g,\tilde{l}_g,\hat{\tilde{2}}_g)\right) A_4^0(\hat{\tilde{1}}_g,\tilde{i}_g,\hat{\tilde{2}}_g,\tilde{k}_g)\,J_2^{(2)}(\widetilde{p_i},\widetilde{p_k})
\end{aligned}
$$

$$-\frac{1}{2}F_3^0(\hat{1}_g,l_g,\hat{2}_g)F_3^0(\hat{\tilde{1}}_g,\hat{\tilde{2}}_g,\tilde{j}_g)\,A_4^0(\hat{\tilde{\tilde{1}}}_g,\tilde{\tilde{i}}_g,\hat{\tilde{\tilde{2}}}_g,\tilde{\tilde{k}}_g)\,J_2^{(2)}(\tilde{\tilde{p}}_i,\tilde{\tilde{p}}_k)$$
$$-\frac{1}{2}F_3^0(\hat{2}_g,j_g,\hat{1}_g)F_3^0(\hat{\tilde{1}}_g,\tilde{l}_g,\hat{\tilde{2}}_g)\,A_4^0(\hat{\tilde{\tilde{1}}}_g,\tilde{\tilde{i}}_g,\hat{\tilde{\tilde{2}}}_g,\tilde{\tilde{k}}_g)\,J_2^{(2)}(\tilde{\tilde{p}}_i,\tilde{\tilde{p}}_k)$$

$$-\frac{1}{2}f_3^0(\hat{2}_g,j_g,k_g)F_3^0(\hat{1}_g,i_g,\hat{\tilde{2}}_g)\,A_4^0(\hat{\tilde{1}}_g,\hat{\tilde{\tilde{2}}}_g,\widetilde{(jk)}_g,\tilde{l}_g)\,J_2^{(2)}(\widetilde{p_{jk}},\tilde{p}_l)$$
$$-\frac{1}{2}F_3^0(\hat{1}_g,i_g,\hat{2}_g)f_3^0(\hat{\tilde{2}}_g,\tilde{j}_g,\tilde{k}_g)\,A_4^0(\hat{\tilde{1}}_g,\hat{\tilde{\tilde{2}}}_g,\widetilde{(jk)}_g,\tilde{l}_g)\,J_2^{(2)}(\widetilde{p_{jk}},\tilde{p}_l)$$
$$-\frac{1}{2}f_3^0(\hat{1}_g,l_g,k_g)F_3^0(\hat{\tilde{1}}_g,i_g,\hat{2}_g)\,A_4^0(\hat{\tilde{\tilde{1}}}_g,\hat{\tilde{2}}_g,\tilde{j}_g,\widetilde{(lk)}_g)\,J_2^{(2)}(\tilde{p}_j,\widetilde{p_{lk}})$$
$$-\frac{1}{2}F_3^0(\hat{1}_g,i_g,\hat{2}_g)f_3^0(\hat{\tilde{1}}_g,\tilde{l}_g,\tilde{k}_g)\,A_4^0(\hat{\tilde{\tilde{1}}}_g,\hat{\tilde{2}}_g,\tilde{j}_g,\widetilde{(lk)}_g)\,J_2^{(2)}(\tilde{p}_j,\widetilde{p_{lk}})$$
$$-\frac{1}{2}f_3^0(\hat{2}_g,j_g,k_g)f_3^0(\hat{1}_g,l_g,\widetilde{(jk)}_g)\,A_4^0(\hat{\tilde{1}}_g,i_g,\hat{\tilde{2}}_g,\widetilde{(jk)l}_g)\,J_2^{(2)}(p_i,\widetilde{p_{(jk)l}})$$
$$-\frac{1}{2}f_3^0(\hat{1}_g,l_g,k_g)f_3^0(\hat{2}_g,j_g,\widetilde{(lk)}_g)\,A_4^0(\hat{\tilde{1}}_g,i_g,\hat{\tilde{2}}_g,\widetilde{(lk)j}_g)\,J_2^{(2)}(p_i,\widetilde{p_{(lk)j}})$$

$$-\frac{1}{2}f_3^0(\hat{2}_g,l_g,k_g)F_3^0(\hat{1}_g,i_g,\hat{\tilde{2}}_g)\,A_4^0(\hat{\tilde{1}}_g,\hat{\tilde{\tilde{2}}}_g,\widetilde{(lk)}_g,\tilde{j}_g)\,J_2^{(2)}(\widetilde{p_{lk}},\tilde{p}_j)$$
$$-\frac{1}{2}F_3^0(\hat{1}_g,i_g,\hat{2}_g)f_3^0(\hat{\tilde{2}}_g,\tilde{l}_g,\tilde{k}_g)\,A_4^0(\hat{\tilde{1}}_g,\hat{\tilde{\tilde{2}}}_g,\widetilde{(lk)}_g,\tilde{j}_g)\,J_2^{(2)}(\widetilde{p_{lk}},\tilde{p}_j)$$
$$-\frac{1}{2}f_3^0(\hat{1}_g,j_g,k_g)F_3^0(\hat{\tilde{1}}_g,i_g,\hat{2}_g)\,A_4^0(\hat{\tilde{\tilde{1}}}_g,\hat{\tilde{2}}_g,\tilde{l}_g,\widetilde{(jk)}_g)\,J_2^{(2)}(\tilde{p}_l,\widetilde{p_{jk}})$$
$$-\frac{1}{2}F_3^0(\hat{1}_g,i_g,\hat{2}_g)f_3^0(\hat{\tilde{1}}_g,\tilde{j}_g,\tilde{l}_g)\,A_4^0(\hat{\tilde{\tilde{1}}}_g,\hat{\tilde{2}}_g,\tilde{l}_g,\widetilde{(jk)}_g)\,J_2^{(2)}(\tilde{p}_l,\widetilde{p_{jk}})$$
$$-\frac{1}{2}f_3^0(\hat{2}_g,l_g,k_g)f_3^0(\hat{1}_g,j_g,\widetilde{(lk)}_g)\,A_4^0(\hat{\tilde{1}}_g,i_g,\hat{\tilde{2}}_g,\widetilde{(lk)j}_g)\,J_2^{(2)}(p_i,\widetilde{p_{(lk)j}})$$
$$-\frac{1}{2}f_3^0(\hat{1}_g,j_g,k_g)f_3^0(\hat{2}_g,l_g,\widetilde{(jk)}_g)\,A_4^0(\hat{\tilde{1}}_g,i_g,\hat{\tilde{2}}_g,\widetilde{(jk)l}_g)\,J_2^{(2)}(p_i,\widetilde{p_{(jk)l}})$$

$$-F_3^0(\hat{1}_g,i_g,\hat{2}_g)f_3^0(\tilde{j}_g,\tilde{k}_g,\tilde{l}_g)\,A_4^0(\hat{\tilde{1}}_g,\hat{\tilde{2}}_g,(\tilde{j}\tilde{k})_g,(\tilde{k}\tilde{l})_g)\,J_2^{(2)}(p_{(\tilde{j}\tilde{k})},p_{(\tilde{k}\tilde{l})})$$
$$-F_3^0(\hat{1}_g,i_g,\hat{2}_g)f_3^0(\tilde{l}_g,\tilde{k}_g,\tilde{j}_g)\,A_4^0(\hat{\tilde{1}}_g,\hat{\tilde{2}}_g,(\tilde{l}\tilde{k})_g,(\tilde{k}\tilde{j})_g)\,J_2^{(2)}(p_{(\tilde{l}\tilde{k})},p_{(\tilde{k}\tilde{j})})$$

$$+\frac{1}{2}f_3^0(\hat{2}_g,j_g,k_g)F_3^0(\hat{1}_g,\hat{\tilde{2}}_g,l_g)A_4^0(\hat{\tilde{1}}_g,\tilde{i}_g,\hat{\tilde{\tilde{2}}}_g,\widetilde{(jk)}_g)J_2^{(2)}(\tilde{p}_i,\widetilde{p_{jk}})$$
$$-\frac{1}{2}F_3^0(\hat{1}_g,\hat{2}_g,l_g)f_3^0(\hat{\tilde{2}}_g,\tilde{j}_g,\tilde{k}_g)A_4^0(\hat{\tilde{1}}_g,\tilde{i}_g,\hat{\tilde{\tilde{2}}}_g,(\tilde{j}\tilde{k})_g)J_2^{(2)}(\tilde{p}_i,p_{\tilde{j}\tilde{k}})$$
$$+\frac{1}{2}f_3^0(\hat{2}_g,j_g,l_g)F_3^0(\hat{1}_g,\hat{\tilde{2}}_g,k_g)A_4^0(\hat{\tilde{1}}_g,\tilde{i}_g,\hat{\tilde{\tilde{2}}}_g,\widetilde{(jl)}_g)J_2^{(2)}(\tilde{p}_i,\widetilde{p_{jl}})$$
$$-\frac{1}{2}F_3^0(\hat{1}_g,\hat{2}_g,k_g)f_3^0(\hat{\tilde{2}}_g,\tilde{j}_g,\tilde{l}_g)A_4^0(\hat{\tilde{1}}_g,\tilde{i}_g,\hat{\tilde{\tilde{2}}}_g,(\tilde{j}\tilde{l})_g)J_2^{(2)}(\tilde{p}_i,p_{\tilde{j}\tilde{l}})$$

$$
\begin{aligned}
&+\frac{1}{2}f_3^0(\hat{1}_g,j_g,k_g)F_3^0(\hat{1}_g,\hat{\tilde{2}}_g,l_g)A_4^0(\hat{\tilde{1}}_g,\tilde{\tilde{i}}_g,\hat{\tilde{2}}_g,\widetilde{(jk)}_g)J_2^{(2)}(\tilde{p}_i,\widetilde{p_{jk}})\\
&-\frac{1}{2}F_3^0(\hat{1}_g,\hat{2}_g,l_g)f_3^0(\hat{\tilde{1}}_g,\tilde{j}_g,\tilde{k}_g)A_4^0(\hat{\tilde{1}}_g,\tilde{\tilde{i}}_g,\hat{\tilde{2}}_g,(\tilde{j}\tilde{k})_g)J_2^{(2)}(\tilde{p}_i,p_{\tilde{j}\tilde{k}})\\
&+\frac{1}{2}f_3^0(\hat{1}_g,j_g,l_g)F_3^0(\hat{1}_g,\hat{\tilde{2}}_g,k_g)A_4^0(\hat{\tilde{1}}_g,\tilde{\tilde{i}}_g,\hat{\tilde{2}}_g,\widetilde{(jl)}_g)J_2^{(2)}(\tilde{p}_i,\widetilde{p_{jl}})\\
&-\frac{1}{2}F_3^0(\hat{1}_g,\hat{2}_g,k_g)f_3^0(\hat{\tilde{1}}_g,\tilde{j}_g,\tilde{l}_g)A_4^0(\hat{\tilde{1}}_g,\tilde{\tilde{i}}_g,\hat{\tilde{2}}_g,(\tilde{j}\tilde{l})_g)J_2^{(2)}(\tilde{p}_i,p_{\tilde{j}\tilde{l}})\\
\\
&+\frac{1}{2}f_3^0(\hat{2}_g,i_g,l_g)f_3^0(\hat{\tilde{2}}_g,j_g,k_g)A_4^0(\hat{1}_g,\hat{\tilde{\tilde{2}}}_g,\widetilde{(jk)}_g,\widetilde{(il)}_g)J_2^{(2)}(\widetilde{p_{jk}},\widetilde{p_{il}})\\
&-\frac{1}{2}f_3^0(\hat{2}_g,j_g,k_g)f_3^0(\hat{\tilde{2}}_g,i_g,l_g)A_4^0(\hat{1}_g,\hat{\tilde{\tilde{2}}}_g,\widetilde{(jk)}_g,\widetilde{(il)}_g)J_2^{(2)}(\widetilde{p_{jk}},\widetilde{p_{il}})\\
&-\frac{1}{2}f_3^0(\hat{2}_g,i_g,l_g)F_3^0(\hat{1}_g,j_g,\hat{\tilde{2}}_g)A_4^0(\hat{\tilde{1}}_g,\hat{\tilde{\tilde{2}}}_g,\tilde{k}_g,\widetilde{(il)}_g)J_2^{(2)}(\widetilde{p_k},\widetilde{p_{il}})\\
&+\frac{1}{2}F_3^0(\hat{1}_g,j_g,\hat{2}_g)f_3^0(\hat{\tilde{2}}_g,\tilde{i}_g,\tilde{l}_g)A_4^0(\hat{\tilde{1}}_g,\hat{\tilde{\tilde{2}}}_g,\tilde{k}_g,(\tilde{i}\tilde{l})_g)J_2^{(2)}(\widetilde{p_k},p_{\tilde{i}\tilde{l}})\\
&+\frac{1}{2}f_3^0(\hat{2}_g,i_g,j_g)f_3^0(\hat{\tilde{2}}_g,l_g,k_g)A_4^0(\hat{1}_g,\hat{\tilde{\tilde{2}}}_g,\widetilde{(lk)}_g,\widetilde{(ij)}_g)J_2^{(2)}(\widetilde{p_{lk}},\widetilde{p_{ij}})\\
&-\frac{1}{2}f_3^0(\hat{2}_g,l_g,k_g)f_3^0(\hat{\tilde{2}}_g,i_g,j_g)A_4^0(\hat{1}_g,\hat{\tilde{\tilde{2}}}_g,\widetilde{(lk)}_g,\widetilde{(ij)}_g)J_2^{(2)}(\widetilde{p_{lk}},\widetilde{p_{ij}})\\
&-\frac{1}{2}f_3^0(\hat{2}_g,i_g,j_g)F_3^0(\hat{1}_g,l_g,\hat{\tilde{2}}_g)A_4^0(\hat{\tilde{1}}_g,\hat{\tilde{\tilde{2}}}_g,\tilde{k}_g,\widetilde{(ij)}_g)J_2^{(2)}(\widetilde{p_k},\widetilde{p_{ij}})\\
&+\frac{1}{2}F_3^0(\hat{1}_g,l_g,\hat{2}_g)f_3^0(\hat{\tilde{2}}_g,\tilde{i}_g,\tilde{j}_g)A_4^0(\hat{\tilde{1}}_g,\hat{\tilde{\tilde{2}}}_g,\tilde{k}_g,(\tilde{i}\tilde{j})_g)J_2^{(2)}(\widetilde{p_k},p_{\tilde{i}\tilde{j}})\\
\\
&+\frac{1}{2}f_3^0(\hat{1}_g,i_g,l_g)f_3^0(\hat{\tilde{1}}_g,j_g,k_g)A_4^0(\hat{\tilde{\tilde{1}}}_g,\hat{2}_g,\widetilde{(il)}_g,\widetilde{(jk)}_g)J_2^{(2)}(\widetilde{p_{il}},\widetilde{p_{jk}})\\
&-\frac{1}{2}f_3^0(\hat{1}_g,j_g,k_g)f_3^0(\hat{\tilde{1}}_g,i_g,l_g)A_4^0(\hat{\tilde{\tilde{1}}}_g,\hat{2}_g,\widetilde{(il)}_g,\widetilde{(jk)}_g)J_2^{(2)}(\widetilde{p_{il}},\widetilde{p_{jk}})\\
&-\frac{1}{2}f_3^0(\hat{1}_g,i_g,l_g)F_3^0(\hat{\tilde{1}}_g,j_g,\hat{2}_g)A_4^0(\hat{\tilde{\tilde{1}}}_g,\hat{\tilde{2}}_g,\widetilde{(il)}_g,\tilde{k}_g)J_2^{(2)}(\widetilde{p_{il}},\widetilde{p_k})\\
&+\frac{1}{2}F_3^0(\hat{1}_g,j_g,\hat{2}_g)f_3^0(\hat{\tilde{1}}_g,\tilde{i}_g,\tilde{l}_g)A_4^0(\hat{\tilde{\tilde{1}}}_g,\hat{\tilde{2}}_g,(\tilde{i}\tilde{l})_g,\tilde{k}_g)J_2^{(2)}(p_{\tilde{i}\tilde{l}},\widetilde{p_k})\\
&+\frac{1}{2}f_3^0(\hat{1}_g,i_g,j_g)f_3^0(\hat{\tilde{1}}_g,l_g,k_g)A_4^0(\hat{\tilde{\tilde{1}}}_g,\hat{2}_g,\widetilde{(ij)}_g,\widetilde{(lk)}_g)J_2^{(2)}(\widetilde{p_{ij}},\widetilde{p_{lk}})\\
&-\frac{1}{2}f_3^0(\hat{1}_g,l_g,k_g)f_3^0(\hat{\tilde{1}}_g,i_g,j_g)A_4^0(\hat{\tilde{\tilde{1}}}_g,\hat{2}_g,\widetilde{(ij)}_g,\widetilde{(lk)}_g)J_2^{(2)}(\widetilde{p_{ij}},\widetilde{p_{lk}})\\
&-\frac{1}{2}f_3^0(\hat{1}_g,i_g,j_g)F_3^0(\hat{\tilde{1}}_g,l_g,\hat{2}_g)A_4^0(\hat{\tilde{\tilde{1}}}_g,\hat{\tilde{2}}_g,\widetilde{(ij)}_g,\tilde{k}_g)J_2^{(2)}(\widetilde{p_{ij}},\widetilde{p_k})\\
&+\frac{1}{2}F_3^0(\hat{1}_g,l_g,\hat{2}_g)f_3^0(\hat{\tilde{1}}_g,\tilde{i}_g,\tilde{j}_g)A_4^0(\hat{\tilde{\tilde{1}}}_g,\hat{\tilde{2}}_g,(\tilde{i}\tilde{j})_g,\tilde{k}_g)J_2^{(2)}(p_{\tilde{i}\tilde{j}},\widetilde{p_k})
\end{aligned}
$$

$$
\Bigg\}
$$

(6.10)

It is important to notice that this six-gluon subtraction term introduces spurious limits from large angle soft radiation. The single soft limit of (6.10) is non-vanishing. To account for this large angle soft radiation a new subtraction term $\mathrm{d}\sigma^{A}_{NNLO}$ is introduced. Its contribution reads:

$$
\begin{aligned}
\mathrm{d}\sigma^{A}_{NNLO} = N^2\, N_{born} \left(\frac{\alpha_s}{2\pi}\right)^2 \mathrm{d}\Phi_4(p_3,\ldots,p_6;p_1,p_2)\, \frac{2}{4!} \sum_{P_C(j,k,l)} \Bigg\{ \\
&\frac{1}{2}\left(-S_{\bar{\tilde{2}}\tilde{j}\tilde{k}} + S_{\bar{2}j\tilde{k}} - S_{\bar{\tilde{1}}\tilde{j}\tilde{l}} + S_{\bar{1}j\tilde{l}} - S_{\bar{2}j\bar{1}} + S_{\bar{\tilde{2}}\tilde{j}\bar{\tilde{1}}}\right) F_3^0(\hat{\tilde{1}}_g, \tilde{i}_g, \hat{\tilde{2}}_g) \\
&\times A_4^0(\hat{\bar{\tilde{1}}}_g, \hat{\bar{\tilde{2}}}_g, \tilde{\tilde{k}}_g, \tilde{\tilde{l}}_g) J_2^{(2)}(p_{\tilde{k}}, p_{\tilde{l}}) \\
+&\frac{1}{2}\left(-S_{\bar{\tilde{2}}\tilde{l}\tilde{k}} + S_{\bar{2}l\tilde{k}} - S_{\bar{\tilde{1}}l\tilde{j}} + S_{\bar{1}l\tilde{j}} - S_{\bar{2}l\bar{1}} + S_{\bar{\tilde{2}}l\bar{\tilde{1}}}\right) F_3^0(\hat{\tilde{1}}_g, \tilde{i}_g, \hat{\tilde{2}}_g) \\
&\times A_4^0(\hat{\bar{\tilde{1}}}_g, \hat{\bar{\tilde{2}}}_g, \tilde{\tilde{k}}_g, \tilde{\tilde{j}}_g) J_2^{(2)}(p_{\tilde{k}}, p_{\tilde{j}}) \\
+&\frac{1}{2}\left(S_{\bar{\tilde{2}}\tilde{j}\tilde{k}} - S_{\bar{2}j\tilde{k}} + S_{\bar{\tilde{1}}\tilde{j}\tilde{k}} - S_{\bar{1}j\tilde{k}} + S_{\bar{2}j\bar{1}} - S_{\bar{\tilde{2}}\tilde{j}\bar{\tilde{1}}}\right) F_3^0(\hat{\tilde{1}}_g, \tilde{l}_g, \hat{\tilde{2}}_g) \\
&\times A_4^0(\hat{\bar{\tilde{1}}}_g, \tilde{\tilde{i}}_g, \hat{\bar{\tilde{2}}}_g, \tilde{\tilde{k}}_g) J_2^{(2)}(p_{\tilde{i}}, p_{\tilde{k}}) \\
+&\frac{1}{2}\left(S_{\bar{\tilde{2}}l\tilde{k}} - S_{\bar{2}l\tilde{k}} + S_{\bar{\tilde{1}}l\tilde{k}} - S_{\bar{1}l\tilde{k}} + S_{\bar{2}l\bar{1}} - S_{\bar{\tilde{2}}l\bar{\tilde{1}}}\right) F_3^0(\hat{\tilde{1}}_g, \tilde{j}_g, \hat{\tilde{2}}_g) \\
&\times A_4^0(\hat{\bar{\tilde{1}}}_g, \tilde{\tilde{i}}_g, \hat{\bar{\tilde{2}}}_g, \tilde{\tilde{k}}_g) J_2^{(2)}(p_{\tilde{i}}, p_{\tilde{k}}) \\
+&\frac{1}{2}\left(-S_{2j((kj)l)} + S_{2j(kj)} - S_{\bar{1}j(kj)} + S_{\bar{1}j(l(kj))} - S_{2j\bar{1}} + S_{2j\bar{1}}\right) f_3^0(\hat{\bar{1}}_g, l_g, (kj)_g) \\
&\times A_4^0(\hat{\bar{\tilde{1}}}_g, i_g, \hat{2}_g, \widetilde{(kj)l)}_g) J_2^{(2)}(p_i, \widetilde{p_{(kj)l)}}) \\
+&\frac{1}{2}\left(-S_{2l((kl)j)} + S_{2l(kl)} - S_{\bar{1}l(kl)} + S_{\bar{1}l(j(kl))} - S_{2l\bar{1}} + S_{2l\bar{1}}\right) f_3^0(\hat{\bar{1}}_g, j_g, (kl)_g) \\
&\times A_4^0(\hat{\bar{\tilde{1}}}_g, i_g, \hat{2}_g, \widetilde{(kl)j}_g) J_2^{(2)}(p_i, \widetilde{p_{(kl)j)}}) \\
+&\frac{1}{2}\left(-S_{1j((kj)l)} + S_{1j(kj)} - S_{\bar{2}j(kj)} + S_{\bar{\tilde{2}}j(l(kj))} - S_{1j\bar{\tilde{2}}} + S_{1j\bar{2}}\right) f_3^0(\hat{\bar{\tilde{2}}}_g, l_g, (kj)_g) \\
&\times A_4^0(\hat{1}_g, i_g, \hat{\bar{\tilde{2}}}_g, \widetilde{(kj)l}_g) J_2^{(2)}(p_3, \widetilde{p_{(kj)l)}}) \\
+&\frac{1}{2}\left(-S_{1l((kl)j)} + S_{1l(kl)} - S_{\bar{2}l(kl)} + S_{\bar{\tilde{2}}l(j(kl))} - S_{1l\bar{\tilde{2}}} + S_{1l\bar{2}}\right) f_3^0(\hat{\bar{\tilde{2}}}_g, j_g, (kl)_g) \\
&\times A_4^0(\hat{1}_g, i_g, \hat{\bar{\tilde{2}}}_g, \widetilde{(kl)j}_g) J_2^{(2)}(p_i, \widetilde{p_{(kl)j)}}) \\
+&\frac{1}{2}\left(-S_{\bar{\tilde{2}}i\tilde{l}} + S_{\bar{2}i\tilde{l}} - S_{\bar{\tilde{1}}i\tilde{l}} + S_{\bar{1}i\tilde{l}} - S_{\bar{1}i\bar{2}} + S_{\bar{\tilde{1}}i\bar{\tilde{2}}}\right) F_3^0(\hat{\tilde{1}}_g, \tilde{j}_g, \hat{\tilde{2}}_g) \\
&\times A_4^0(\hat{\bar{\tilde{1}}}_g, \hat{\bar{\tilde{2}}}_g, \tilde{\tilde{k}}_g, \tilde{\tilde{l}}_g) J_2^{(2)}(p_{\tilde{k}}, p_{\tilde{l}}) \\
+&\frac{1}{2}\left(-S_{\bar{\tilde{2}}i\tilde{j}} + S_{\bar{2}i\tilde{j}} - S_{\bar{\tilde{1}}i\tilde{j}} + S_{\bar{1}i\tilde{j}} - S_{\bar{1}i\bar{2}} + S_{\bar{\tilde{1}}i\bar{\tilde{2}}}\right) F_3^0(\hat{\tilde{1}}_g, \tilde{l}_g, \hat{\tilde{2}}_g) \\
&\times A_4^0(\hat{\bar{\tilde{1}}}_g, \hat{\bar{\tilde{2}}}_g, \tilde{\tilde{k}}_g, \tilde{\tilde{j}}_g) J_2^{(2)}(p_{\tilde{k}}, p_{\tilde{j}}) \\
\Bigg\}&
\end{aligned}
\tag{6.11}
$$

6.1.3 IFFIFF topology

The real radiation contribution to the cross section for the third topology is obtained by averaging over all possible twelve orderings:

$$\begin{aligned}
\mathrm{d}\sigma^{R}_{NNLO} &= N^2\, N_{born} \left(\frac{\alpha_s}{2\pi}\right)^2 \mathrm{d}\Phi_4(p_3,\ldots,p_6;p_1,p_2)\,\frac{2}{4!} \\
&\quad \sum_{(i,j,k,l)\in P_C(3,4,5,6)} A_6^0(\hat{1},i,j,\hat{2},k,l)J_2^{(4)}(p_i,\ldots,p_l) \\
&= N^2\, N_{born} \left(\frac{\alpha_s}{2\pi}\right)^2 \mathrm{d}\Phi_4(p_3,\ldots,p_6;p_1,p_2)\,\frac{2}{4!}\Big[X_6^0(\hat{1},3,4,\hat{2},5,6) \\
&\quad +X_6^0(\hat{1},3,4,\hat{2},6,5)+X_6^0(\hat{1},3,5,\hat{2},4,6)+X_6^0(\hat{1},3,5,\hat{2},6,4) \\
&\quad +X_6^0(\hat{1},3,6,\hat{2},4,5)+X_6^0(\hat{1},3,6,\hat{2},5,4)\Big]J_2^{(4)}(p_i,\ldots,p_l) \qquad (6.12)
\end{aligned}$$

where each X_6^0 contains 2 colour ordered amplitudes given by:

$$X_6^0(\hat{1},3,4,\hat{2},5,6) = A_6^0(\hat{1},3,4,\hat{2},5,6) + A_6^0(\hat{1},4,3,\hat{2},6,5) \qquad (6.13)$$

This form (6.12) is more appropriate for the construction of the real radiation subtraction term, since it matches onto the symmetry of the full $F_4^0(\hat{1}_g,j_g,\hat{2}_g,k_g)$ initial-initial antenna function. The real radiation subtraction term to be used with $X_6^0(\hat{1}_g,i_g,j_g,\hat{2}_g,k_g,l_g)$ is:

$$\begin{aligned}
\mathrm{d}\sigma^{S}_{NNLO} = N^2\, N_{born} \left(\frac{\alpha_s}{2\pi}\right)^2 \mathrm{d}\Phi_4(p_3,\ldots,p_6;p_1,p_2)\,\frac{2}{4!}\Bigg\{ \\
f_3^0(\hat{1}_g,i_g,j_g)\,A_5^0(\hat{\tilde{1}}_g,\widetilde{(ij)}_g,\hat{2}_g,k_g,l_g)\,J_2^{(3)}(\widetilde{p_{ij}},p_k,p_l) \\
+f_3^0(i_g,j_g,\hat{2}_g)\,A_5^0(\hat{1}_g,\widetilde{(ji)}_g,\hat{\tilde{2}}_g,k_g,l_g)\,J_2^{(3)}(\widetilde{p_{ji}},p_k,p_l) \\
+f_3^0(\hat{2}_g,k_g,l_g)\,A_5^0(\hat{1}_g,i_g,j_g,\hat{\tilde{2}}_g,\widetilde{(kl)}_g)\,J_2^{(3)}(p_i,p_j,\widetilde{p_{kl}}) \\
+f_3^0(k_g,l_g,\hat{1}_g)\,A_5^0(\hat{\tilde{1}}_g,i_g,j_g,\hat{2}_g,\widetilde{(lk)}_g)\,J_2^{(3)}(p_i,p_j,\widetilde{p_{lk}}) \\
\\
+f_3^0(\hat{1}_g,j_g,i_g)\,A_5^0(\hat{\tilde{1}}_g,\widetilde{(ji)}_g,\hat{2}_g,l_g,k_g)\,J_2^{(3)}(\widetilde{p_{ji}},p_l,p_k) \\
+f_3^0(j_g,i_g,\hat{2}_g)\,A_5^0(\hat{1}_g,\widetilde{(ij)}_g,\hat{\tilde{2}}_g,l_g,k_g)\,J_2^{(3)}(\widetilde{p_{ij}},p_l,p_k) \\
+f_3^0(\hat{2}_g,l_g,k_g)\,A_5^0(\hat{1}_g,j_g,i_g,\hat{\tilde{2}}_g,\widetilde{(lk)}_g)\,J_2^{(3)}(p_j,p_i,\widetilde{p_{lk}}) \\
+f_3^0(l_g,k_g,\hat{1}_g)\,A_5^0(\hat{\tilde{1}}_g,j_g,i_g,\hat{2}_g,\widetilde{(kl)}_g)\,J_2^{(3)}(p_j,p_i,\widetilde{p_{kl}})
\end{aligned}$$

$$
\begin{aligned}
&+\Big(F_4^0(\hat{1}_g, i_g, j_g, \hat{2}_g) - f_3^0(\hat{1}_g, i_g, j_g)\, F_3^0(\hat{\tilde{1}}_g, \widetilde{(ij)}_g, \hat{2}_g) \\
&\quad - f_3^0(i_g, j_g, \hat{2}_g)\, F_3^0(\hat{1}_g, \widetilde{(ji)}_g, \hat{\tilde{2}}_g) \Big) A_4^0(\hat{\tilde{1}}_g, \hat{\tilde{2}}_g, \tilde{k}_g, \tilde{l}_g)\, J_2^{(2)}(\widetilde{p_k}, \widetilde{p_l}) \\
&+\Big(F_4^0(\hat{2}_g, k_g, l_g, \hat{1}_g) - f_3^0(\hat{2}_g, k_g, l_g)\, F_3^0(\hat{\tilde{2}}_g, \widetilde{(kl)}_g, \hat{1}_g) \\
&\quad - f_3^0(k_g, l_g, \hat{1}_g)\, F_3^0(\hat{2}_g, \widetilde{(lk)}_g, \hat{\tilde{1}}_g) \Big) A_4^0(\hat{\tilde{1}}_g, \hat{\tilde{2}}_g, \tilde{j}_g, \tilde{i}_g)\, J_2^{(2)}(\widetilde{p_j}, \widetilde{p_i}) \\
&+\Big(F_4^0(\hat{1}_g, j_g, i_g, \hat{2}_g) - f_3^0(\hat{1}_g, j_g, i_g)\, F_3^0(\hat{\tilde{1}}_g, \widetilde{(ji)}_g, \hat{2}_g) \\
&\quad - f_3^0(j_g, i_g, \hat{2}_g)\, F_3^0(\hat{1}_g, \widetilde{(ij)}_g, \hat{\tilde{2}}_g) \Big) A_4^0(\hat{\tilde{1}}_g, \hat{\tilde{2}}_g, \tilde{l}_g, \tilde{k}_g)\, J_2^{(2)}(\widetilde{p_l}, \widetilde{p_k}) \\
&+\Big(F_4^0(\hat{2}_g, l_g, k_g, \hat{1}_g) - f_3^0(\hat{2}_g, l_g, k_g)\, F_3^0(\hat{\tilde{2}}_g, \widetilde{(lk)}_g, \hat{1}_g) \\
&- f_3^0(l_g, k_g, \hat{1}_g)\, F_3^0(\hat{2}_g, \widetilde{(kl)}_g, \hat{\tilde{1}}_g) \Big) A_4^0(\hat{\tilde{1}}_g, \hat{\tilde{2}}_g, \tilde{i}_g, \tilde{j}_g)\, J_2^{(2)}(\widetilde{p_j}, \widetilde{p_i}) \\
&+\Big(F_4^0(\hat{1}_g, j_g, \hat{2}_g, k_g) - F_3^0(\hat{1}_g, j_g, \hat{2}_g)\, F_3^0(\hat{\tilde{1}}_g, \hat{\tilde{2}}_g, \tilde{k}_g) \\
&\quad - F_3^0(\hat{2}_g, k_g, \hat{1}_g)\, F_3^0(\hat{\tilde{1}}_g, \tilde{j}_g, \hat{\tilde{2}}_g) \Big) A_4^0(\hat{\tilde{1}}_g, \tilde{i}_g, \hat{\tilde{2}}_g, \tilde{l}_g)\, J_2^{(2)}(\widetilde{p_i}, \widetilde{p_l}) \\
&+\Big(F_4^0(\hat{1}_g, i_g, \hat{2}_g, l_g) - F_3^0(\hat{1}_g, i_g, \hat{2}_g)\, F_3^0(\hat{\tilde{1}}_g, \hat{\tilde{2}}_g, \tilde{l}_g) \\
&\quad - F_3^0(\hat{2}_g, l_g, \hat{1}_g)\, F_3^0(\hat{\tilde{1}}_g, \tilde{i}_g, \hat{\tilde{2}}_g) \Big) A_4^0(\hat{\tilde{1}}_g, \tilde{j}_g, \hat{\tilde{2}}_g, \tilde{k}_g)\, J_2^{(2)}(\widetilde{p_j}, \widetilde{p_k})
\end{aligned}
$$

$$
\begin{aligned}
&+\frac{1}{2} F_3^0(\hat{1}_g, j_g, \hat{2}_g) F_3^0(\hat{\tilde{1}}_g, \hat{\tilde{2}}_g, \tilde{k}_g)\, A_4^0(\hat{\tilde{\tilde{1}}}_g, \tilde{\tilde{i}}_g, \hat{\tilde{\tilde{2}}}_g, \tilde{\tilde{l}}_g)\, J_2^{(2)}(\tilde{\tilde{p}}_i, \tilde{\tilde{p}}_l) \\
&+\frac{1}{2} F_3^0(\hat{2}_g, k_g, \hat{1}_g) F_3^0(\hat{\tilde{1}}_g, \tilde{j}_g, \hat{\tilde{2}}_g)\, A_4^0(\hat{\tilde{\tilde{1}}}_g, \tilde{\tilde{i}}_g, \hat{\tilde{\tilde{2}}}_g, \tilde{\tilde{l}}_g)\, J_2^{(2)}(\tilde{\tilde{p}}_i, \tilde{\tilde{p}}_l) \\
&+\frac{1}{2} F_3^0(\hat{1}_g, i_g, \hat{2}_g) F_3^0(\hat{\tilde{1}}_g, \hat{\tilde{2}}_g, \tilde{l}_g)\, A_4^0(\hat{\tilde{\tilde{1}}}_g, \tilde{\tilde{j}}_g, \hat{\tilde{\tilde{2}}}_g, \tilde{\tilde{k}}_g)\, J_2^{(2)}(\tilde{\tilde{p}}_j, \tilde{\tilde{p}}_k) \\
&+\frac{1}{2} F_3^0(\hat{2}_g, l_g, \hat{1}_g) F_3^0(\hat{\tilde{1}}_g, \tilde{i}_g, \hat{\tilde{2}}_g)\, A_4^0(\hat{\tilde{\tilde{1}}}_g, \tilde{\tilde{j}}_g, \hat{\tilde{\tilde{2}}}_g, \tilde{\tilde{k}}_g)\, J_2^{(2)}(\tilde{\tilde{p}}_j, \tilde{\tilde{p}}_k)
\end{aligned}
$$

$$
\begin{aligned}
&-\frac{1}{2} f_3^0(i_g, j_g, \hat{2}_g) f_3^0(\hat{\tilde{2}}_g, k_g, l_g)\, A_4^0(\hat{1}_g, \widetilde{(ji)}_g, \hat{\tilde{\tilde{2}}}_g, \widetilde{(kl)}_g)\, J_2^{(2)}(\widetilde{p_{ji}}, \widetilde{p_{kl}}) \\
&-\frac{1}{2} f_3^0(l_g, k_g, \hat{2}_g) f_3^0(\hat{\tilde{2}}_g, j_g, i_g)\, A_4^0(\hat{1}_g, \widetilde{(ji)}_g, \hat{\tilde{\tilde{2}}}_g, \widetilde{(kl)}_g)\, J_2^{(2)}(\widetilde{p_{ji}}, \widetilde{p_{kl}})
\end{aligned}
$$

$$
\begin{aligned}
&-\frac{1}{2} f_3^0(j_g,i_g,\hat{1}_g) f_3^0(\hat{\tilde{1}}_g,l_g,k_g)\, A_4^0(\hat{\tilde{\tilde{1}}}_g,\widetilde{(ij)}_g,\hat{2}_g,\widetilde{(lk)}_g)\, J_2^{(2)}(\widetilde{p_{ij}},\widetilde{p_{lk}})\\
&-\frac{1}{2} f_3^0(k_g,l_g,\hat{1}_g) f_3^0(\hat{\tilde{1}}_g,i_g,j_g)\, A_4^0(\hat{\tilde{\tilde{1}}}_g,\widetilde{(ij)}_g,\hat{2}_g,\widetilde{(lk)}_g)\, J_2^{(2)}(\widetilde{p_{ij}},\widetilde{p_{lk}})\\
&-\frac{1}{2} f_3^0(j_g,i_g,\hat{2}_g) f_3^0(\hat{\tilde{2}}_g,l_g,k_g)\, A_4^0(\hat{1}_g,\widetilde{(ij)}_g,\hat{\tilde{\tilde{2}}}_g,\widetilde{(lk)}_g)\, J_2^{(2)}(\widetilde{p_{ij}},\widetilde{p_{lk}})\\
&-\frac{1}{2} f_3^0(k_g,l_g,\hat{2}_g) f_3^0(\hat{\tilde{2}}_g,i_g,j_g)\, A_4^0(\hat{1}_g,\widetilde{(ij)}_g,\hat{\tilde{\tilde{2}}}_g,\widetilde{(lk)}_g)\, J_2^{(2)}(\widetilde{p_{ij}},\widetilde{p_{lk}})\\
&-\frac{1}{2} f_3^0(i_g,j_g,\hat{1}_g) f_3^0(\hat{\tilde{1}}_g,k_g,l_g)\, A_4^0(\hat{\tilde{\tilde{1}}}_g,\widetilde{(ji)}_g,\hat{2}_g,\widetilde{(kl)}_g)\, J_2^{(2)}(\widetilde{p_{ji}},\widetilde{p_{kl}})\\
&-\frac{1}{2} f_3^0(l_g,k_g,\hat{1}_g) f_3^0(\hat{\tilde{1}}_g,j_g,i_g)\, A_4^0(\hat{\tilde{\tilde{1}}}_g,\widetilde{(ji)}_g,\hat{2}_g,\widetilde{(kl)}_g)\, J_2^{(2)}(\widetilde{p_{ji}},\widetilde{p_{kl}})
\end{aligned}
$$

$$
\begin{aligned}
&-f_3^0(\hat{1}_g,i_g,j_g) f_3^0(\hat{2}_g,k_g,l_g)\, A_4^0(\hat{\tilde{1}}_g,\widetilde{(ij)}_g,\hat{\tilde{\tilde{2}}}_g,\widetilde{(kl)}_g)\, J_2^{(2)}(\widetilde{p_{ij}},\widetilde{p_{kl}})\\
&-f_3^0(i_g,j_g,\hat{2}_g) f_3^0(k_g,l_g,\hat{1}_g)\, A_4^0(\hat{\tilde{1}}_g,\widetilde{(ji)}_g,\hat{\tilde{\tilde{2}}}_g,\widetilde{(lk)}_g)\, J_2^{(2)}(\widetilde{p_{ji}},\widetilde{p_{lk}})\\
&-f_3^0(\hat{1}_g,j_g,i_g) f_3^0(\hat{2}_g,l_g,k_g)\, A_4^0(\hat{\tilde{1}}_g,\widetilde{(ji)}_g,\hat{\tilde{\tilde{2}}}_g,\widetilde{(lk)}_g)\, J_2^{(2)}(\widetilde{p_{ji}},\widetilde{p_{lk}})\\
&-f_3^0(j_g,i_g,\hat{2}_g) f_3^0(l_g,k_g,\hat{1}_g)\, A_4^0(\hat{\tilde{1}}_g,\widetilde{(ij)}_g,\hat{\tilde{\tilde{2}}}_g,\widetilde{(kl)}_g)\, J_2^{(2)}(\widetilde{p_{ij}},\widetilde{p_{kl}})
\end{aligned}
$$

$$
\begin{aligned}
&-\frac{1}{2} f_3^0(k_g,l_g,\hat{2}_g) F_3^0(\hat{1}_g,\hat{\tilde{2}}_g,i_g) A_4^0(\hat{\tilde{1}}_g,\tilde{j}_g,\hat{\tilde{\tilde{2}}}_g,\widetilde{(lk)}_g) J_2^{(2)}(\tilde{p}_j,\widetilde{p_{lk}})\\
&+\frac{1}{2} F_3^0(\hat{1}_g,\hat{2}_g,i_g) f_3^0(\tilde{k}_g,\tilde{l}_g,\hat{\tilde{2}}_g) A_4^0(\hat{\tilde{1}}_g,\tilde{j}_g,\hat{\tilde{\tilde{2}}}_g,(\tilde{l}\tilde{k})_g) J_2^{(2)}(\tilde{p}_j,p_{\tilde{l}\tilde{k}})\\
&-\frac{1}{2} f_3^0(l_g,k_g,\hat{2}_g) F_3^0(\hat{1}_g,\hat{\tilde{2}}_g,j_g) A_4^0(\hat{\tilde{1}}_g,\tilde{i}_g,\hat{\tilde{\tilde{2}}}_g,\widetilde{(kl)}_g) J_2^{(2)}(\tilde{p}_i,\widetilde{p_{kl}})\\
&+\frac{1}{2} F_3^0(\hat{1}_g,\hat{2}_g,j_g) f_3^0(\tilde{l}_g,\tilde{k}_g,\hat{\tilde{2}}_g) A_4^0(\hat{\tilde{1}}_g,\tilde{i}_g,\hat{\tilde{\tilde{2}}}_g,(\tilde{k}\tilde{l})_g) J_2^{(2)}(\tilde{p}_i,p_{\tilde{k}\tilde{l}})\\
&-\frac{1}{2} f_3^0(i_g,j_g,\hat{2}_g) F_3^0(\hat{1}_g,\hat{\tilde{2}}_g,k_g) A_4^0(\hat{\tilde{1}}_g,\widetilde{(ji)}_g,\hat{\tilde{\tilde{2}}}_g,\tilde{l}_g) J_2^{(2)}(\widetilde{p_{ji}},\tilde{p}_l)\\
&+\frac{1}{2} F_3^0(\hat{1}_g,\hat{2}_g,k_g) f_3^0(\tilde{i}_g,\tilde{j}_g,\hat{\tilde{2}}_g) A_4^0(\hat{\tilde{1}}_g,(\tilde{j}\tilde{i})_g,\hat{\tilde{\tilde{2}}}_g,\tilde{l}_g) J_2^{(2)}(p_{\tilde{j}\tilde{i}},\tilde{p}_l)\\
&-\frac{1}{2} f_3^0(j_g,i_g,\hat{2}_g) F_3^0(\hat{1}_g,\hat{\tilde{2}}_g,l_g) A_4^0(\hat{\tilde{1}}_g,\widetilde{(ij)}_g,\hat{\tilde{\tilde{2}}}_g,\tilde{k}_g) J_2^{(2)}(\widetilde{p_{ij}},\tilde{p}_k)\\
&+\frac{1}{2} F_3^0(\hat{1}_g,\hat{2}_g,l_g) f_3^0(\tilde{j}_g,\tilde{i}_g,\hat{\tilde{2}}_g) A_4^0(\hat{\tilde{1}}_g,(\tilde{i}\tilde{j})_g,\hat{\tilde{\tilde{2}}}_g,\tilde{k}_g) J_2^{(2)}(p_{\tilde{i}\tilde{j}},\tilde{p}_k)
\end{aligned}
$$

$$
\begin{aligned}
&-\frac{1}{2} f_3^0(k_g,l_g,\hat{1}_g) F_3^0(\hat{\tilde{1}}_g,\hat{2}_g,i_g) A_4^0(\hat{\tilde{\tilde{1}}}_g,\widetilde{(lk)}_g,\hat{\tilde{2}}_g,\tilde{j}_g) J_2^{(2)}(\widetilde{p_{lk}},\tilde{p}_j)\\
&+\frac{1}{2} F_3^0(\hat{1}_g,\hat{2}_g,i_g) f_3^0(\tilde{k}_g,\tilde{l}_g,\hat{\tilde{1}}_g) A_4^0(\hat{\tilde{\tilde{1}}}_g,(\tilde{l}\tilde{k})_g,\hat{\tilde{2}}_g,\tilde{j}_g) J_2^{(2)}(p_{\tilde{l}\tilde{k}},\tilde{p}_j)\\
&-\frac{1}{2} f_3^0(l_g,k_g,\hat{1}_g) F_3^0(\hat{\tilde{1}}_g,\hat{2}_g,j_g) A_4^0(\hat{\tilde{\tilde{1}}}_g,\widetilde{(kl)}_g,\hat{\tilde{2}}_g,\tilde{i}_g) J_2^{(2)}(\widetilde{p_{kl}},\tilde{p}_i)\\
&+\frac{1}{2} F_3^0(\hat{1}_g,\hat{2}_g,j_g) f_3^0(\tilde{l}_g,\tilde{k}_g,\hat{\tilde{1}}_g) A_4^0(\hat{\tilde{\tilde{1}}}_g,(\tilde{k}\tilde{l})_g,\hat{\tilde{2}}_g,\tilde{i}_g) J_2^{(2)}(p_{\tilde{k}\tilde{l}},\tilde{p}_i)
\end{aligned}
$$

$$
\begin{aligned}
&-\frac{1}{2} f_3^0(i_g, j_g, \hat{1}_g) F_3^0(\hat{\bar{1}}_g, \hat{2}_g, k_g) A_4^0(\hat{\bar{\bar{1}}}_g, \tilde{l}_g, \hat{\bar{\bar{2}}}_g, \widetilde{(ji)}_g) J_2^{(2)}(\tilde{p}_l, \widetilde{p_{ji}}) \\
&+\frac{1}{2} F_3^0(\hat{1}_g, \hat{2}_g, k_g) f_3^0(\tilde{i}_g, \tilde{j}_g, \hat{\bar{1}}_g) A_4^0(\hat{\bar{\bar{1}}}_g, \tilde{l}_g, \hat{\bar{\bar{2}}}_g, (\tilde{j}\tilde{i})_g) J_2^{(2)}(\tilde{p}_l, p_{\tilde{j}\tilde{i}}) \\
&-\frac{1}{2} f_3^0(j_g, i_g, \hat{1}_g) F_3^0(\hat{\bar{1}}_g, \hat{2}_g, l_g) A_4^0(\hat{\bar{\bar{1}}}_g, \tilde{k}_g, \hat{\bar{2}}_g, \widetilde{(ij)}_g) J_2^{(2)}(\tilde{p}_k, \widetilde{p_{ij}}) \\
&+\frac{1}{2} F_3^0(\hat{1}_g, \hat{2}_g, l_g) f_3^0(\tilde{j}_g, \tilde{i}_g, \hat{\bar{1}}_g) A_4^0(\hat{\bar{\bar{1}}}_g, \tilde{k}_g, \hat{\bar{2}}_g, (\tilde{i}\tilde{j})_g) J_2^{(2)}(\tilde{p}_k, p_{\tilde{i}\tilde{j}}) \\
&\Bigg\}
\end{aligned}
\tag{6.14}
$$

It is important to notice that this six-gluon subtraction term introduces spurious limits from large angle soft radiation. The single soft limit of (6.14) is non-vanishing. To account for this large angle soft radiation a new subtraction term $\mathrm{d}\sigma^A_{NNLO}$ is introduced. Its contribution reads:

$$
\begin{aligned}
\mathrm{d}\sigma^S_{NNLO} = N^2\, N_{born} \left(\frac{\alpha_s}{2\pi}\right)^2 \mathrm{d}\Phi_4(p_3, \ldots, p_6; p_1, p_2)\, \frac{2}{4!} \Bigg\{ \\
&\frac{1}{2}\left(-S_{\bar{1}i\bar{2}} + S_{\tilde{\bar{1}}i\tilde{\bar{2}}} + S_{\bar{2}i\tilde{j}} - S_{\tilde{\bar{2}}i\tilde{j}} + S_{\bar{1}i\tilde{j}} - S_{\tilde{\bar{1}}i\tilde{j}}\right) F_3^0(\hat{\bar{1}}_g, \hat{\bar{2}}_g, \tilde{l}_g) \\
&\times A_4^0(\hat{\bar{\bar{1}}}_g, \tilde{\tilde{j}}_g, \hat{\bar{\bar{2}}}_g, \tilde{\tilde{k}}_g) J_2^{(2)}(p_{\tilde{j}}, p_{\tilde{k}}) \\
&+\frac{1}{2}\left(-S_{\bar{1}j\bar{2}} + S_{\tilde{\bar{1}}j\tilde{\bar{2}}} + S_{\bar{2}j\tilde{i}} - S_{\tilde{\bar{2}}j\tilde{i}} + S_{\bar{1}j\tilde{i}} - S_{\tilde{\bar{1}}j\tilde{i}}\right) F_3^0(\hat{\bar{1}}_g, \hat{\bar{2}}_g, \tilde{k}_g) \\
&\times A_4^0(\hat{\bar{\bar{1}}}_g, \tilde{\tilde{i}}_g, \hat{\bar{\bar{2}}}_g, \tilde{\tilde{l}}_g) J_2^{(2)}(p_{\tilde{i}}, p_{\tilde{l}}) \\
&+\frac{1}{2}\left(-S_{\bar{1}k\bar{2}} + S_{\tilde{\bar{1}}k\tilde{\bar{2}}} + S_{\bar{2}k\tilde{l}} - S_{\tilde{\bar{2}}k\tilde{l}} + S_{\bar{1}k\tilde{l}} - S_{\tilde{\bar{1}}k\tilde{l}}\right) F_3^0(\hat{\bar{1}}_g, \hat{\bar{2}}_g, \tilde{j}_g) \\
&\times A_4^0(\hat{\bar{\bar{1}}}_g, \tilde{\tilde{i}}_g, \hat{\bar{\bar{2}}}_g, \tilde{\tilde{l}}_g) J_2^{(2)}(p_{\tilde{i}}, p_{\tilde{l}}) \\
&+\frac{1}{2}\left(-S_{\bar{1}l\bar{2}} + S_{\tilde{\bar{1}}l\tilde{\bar{2}}} + S_{\bar{2}l\tilde{k}} - S_{\tilde{\bar{2}}l\tilde{k}} + S_{\bar{1}l\tilde{k}} - S_{\tilde{\bar{1}}l\tilde{k}}\right) F_3^0(\hat{\bar{1}}_g, \hat{\bar{2}}_g, \tilde{i}_g) \\
&\times A_4^0(\hat{\bar{\bar{1}}}_g, \tilde{\tilde{j}}_g, \hat{\bar{\bar{2}}}_g, \tilde{\tilde{k}}_g) J_2^{(2)}(p_{\tilde{j}}, p_{\tilde{k}}) \Bigg\}
\end{aligned}
\tag{6.15}
$$

6.2 Summary

In this chapter we derived the counterterms to compute the double real correction to gluon scattering relevant to the calculation of $pp \to 2$ jets at NNLO. Remembering

the formula for subtraction at NNLO,

$$\begin{aligned} \mathrm{d}\sigma_{NNLO} &= \int_{\mathrm{d}\Phi_{m+2}} \left(\mathrm{d}\sigma^{R}_{NNLO} - \mathrm{d}\sigma^{S}_{NNLO}\right) + \int_{\mathrm{d}\Phi_{m+2}} \mathrm{d}\sigma^{S}_{NNLO} \\ &+ \int_{\mathrm{d}\Phi_{m+1}} \left(\mathrm{d}\sigma^{V,1}_{NNLO} - \mathrm{d}\sigma^{VS,1}_{NNLO}\right) + \int_{\mathrm{d}\Phi_{m+1}} \mathrm{d}\sigma^{VS,1}_{NNLO} \\ &+ \int_{\mathrm{d}\Phi_{m}} \mathrm{d}\sigma^{V,2}_{NNLO} \end{aligned} \tag{6.16}$$

the results of this chapter correspond to $\left(\mathrm{d}\sigma^{R}_{NNLO} - \mathrm{d}\sigma^{S}_{NNLO}\right)$.

To derive the counterterm we analysed the singularities present in the double real correction, that we know from the universal behaviour of the colour ordered gluonic amplitudes. The factorisation of these amplitudes for one and two unresolved gluons was discussed in section 1.8. To generate the counterterm we considered all the possible colour configurations for the double unresolved pair and used the appropriate antennae subtraction formulae written down in chapter 4.

We concentrated on the pure gluon channel and for this reason we made extensive use of the F_3^0 and F_4^0 antennae functions in different kinematic configurations (initial-initial, initial-final and final-final). This is expected since calculations for hadronic collisions require subtraction of both final and initial state singularities, described by these antennae with the three possible assignments of radiators. In all cases their numerical implementation was discussed in chapters 3, 4 respectively.

The output is a numerical routine that receives as an argument a phase space point given by a set of four-momenta P and computes the matrix element and the subtraction term. This can then be incorporated in a flexible parton-level generator to compute the pure gluon contribution to infrared-safe observables related to two jet states to NNLO accuracy at the LHC. However, this still requires a numerical implementation for the second line in equation 6.16. This term represents the mixed real-virtual contribution and subtraction of singularities in this channel can also be completed using the antenna subtraction method. That treatment is beyond the scope of this thesis.

In both cases, the analytical integration of the subtraction terms still needs the integrated form of the four-parton tree level initial-initial and three-parton one loop antenna functions. This work is currently underway and is expected to be completed

soon. Combining it with the results for the integrated antennae at NLO [67, 68] and NNLO [67, 105, 119, 120] will show the infrared poles of the antennae analytically cancelling with the infrared poles of the two-loop virtual correction.

In the next chapter we show that the infrared structure of both the matrix element and the subtraction term of this chapter coincide in all double and single unresolved regions of the phase space of the real-real correction.

Chapter 7

Numerical implementation

In this chapter we will test the limits of the matrix element and subtraction term written down in the previous chapter. We will do this numerically by generating a series of phase space points using `RAMBO` [75] that approach a given double or single unresolved limit. For each generated point we compute:

$$R = \frac{|M_{RR}|^2}{S_{term}} \tag{7.1}$$

where $|M_{RR}|^2$ is the matrix element squared given in equation (6.3) and S_{term} is the subtraction term given by equations (6.6), (6.10), (6.14) summed over all orderings and including large angle soft gluon terms of equations (6.7), (6.11), (6.15). The ratio of the matrix element and the subtraction term should approach unity as we get closer to any singularity. This tests if the subtraction term has the same infrared behaviour as the matrix element so that their difference can be integrated numerically over the unconstrained phase space in four dimensions.

7.1 Numerical checks

In this section we will discuss the numerical simulations that check if the subtraction term was implemented correctly and argue that the various unresolved singularities are in fact correctly described by the subtraction term. For each unresolved configuration, we will define a variable that controls how we approach the singularity subject to the requirement that there are at least two jets in the final state with p_T >50 GeV.

7.1.1 Double soft limit

A double soft configuration can be obtained by generating a four particle final state where one of the invariant masses s_{ij} of two final state particles takes nearly the full energy of the event s as illustrated in figure 7.1 (a).

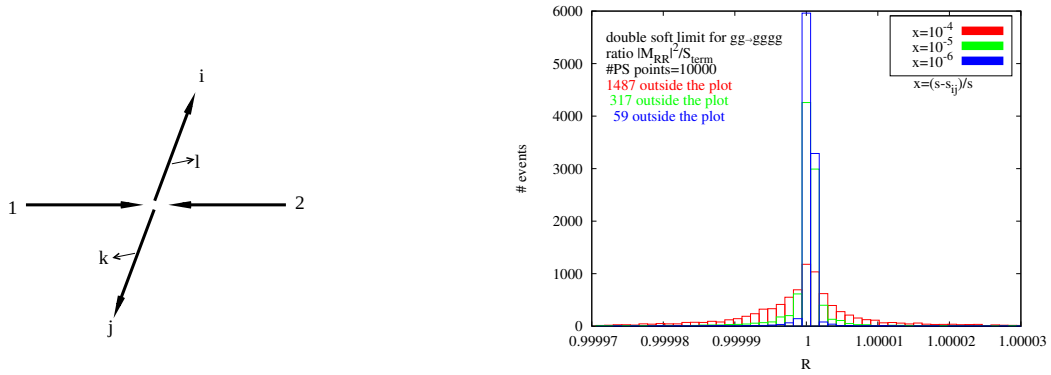

(a) (b)

Figure 7.1: (a) Example configuration of a double soft event with $s_{ij} \approx s_{12} = s$. (b) Distribution of R for 10000 double soft phase space points.

In figure 7.1(b) we generated 10000 random double soft phase space points and show the distribution of the ratio between the matrix element and the subtraction term. The three colours represent different values of $x = (s - s_{ij})/s$ [$x = 10^{-4}$ (red), $x = 10^{-5}$ (green), $x = 10^{-6}$ (blue)] and we can see that for smaller values of x we go closer to the singularity and the distribution peaks more sharply around unity. For $x = 10^{-6}$ we obtained an average of $R = 0.9999994$ and a standard deviation of $\sigma = 4.02 \times 10^{-5}$. Also in the plot we give for each distribution the number of points that lie on the outliers of the histogram. As expected this number is always decreasing as we move closer to the singular region.

In figure 7.2 we explicitly show the behaviour of the matrix element squared and the subtraction term as a function of x. It is clear that both diverge in the double soft limit $x \to 0$ but their ratio goes to 1.

7.1.2 Triple collinear limit

In this subsection we generate phase space points with three hard particles sharing a collinear direction. This probes the triple collinear region of the phase space where

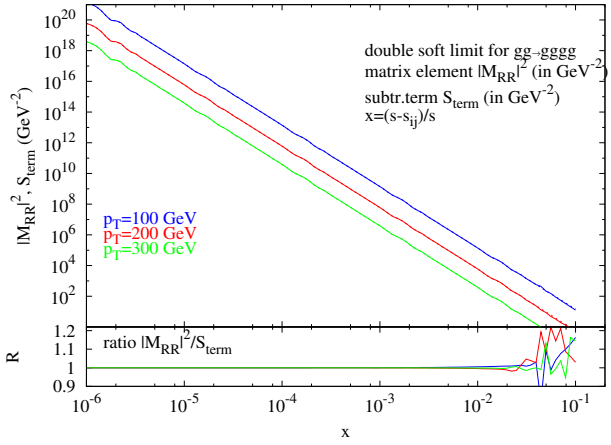

Figure 7.2: Matrix element squared (solid lines) and the subtraction term (dashed lines) as a function of $x = (s - s_{ij})/s$ for three different values of p_T for the final state. Also plotted is the ratio $|M_{RR}|^2/S_{term}$.

we demand the vanishing of the triple invariant formed by both final state (figure 7.3 (a)) and initial state particles (figure 7.4 (a)).

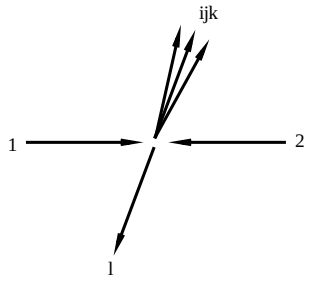

(a)

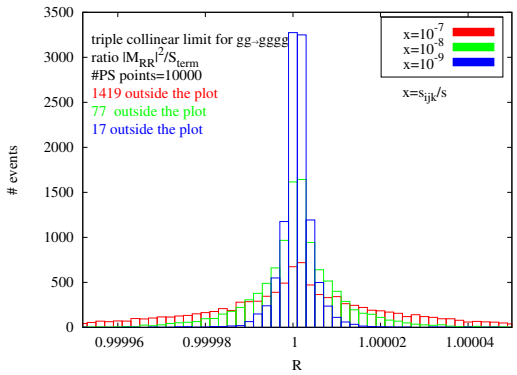

(b)

Figure 7.3: (a) Example configuration of a triple collinear event with $s_{ijk} \to 0$. (b) Distribution of R for 10000 triple collinear phase space points.

In figure 7.3 (b) we use again three colours to denote different values of $x = s_{ijk}/s$ [$x = 10^{-7}$ (red), $x = 10^{-8}$ (green), $x = 10^{-9}$ (blue)] that control how we approach the singular region and for each we plot distribution of the ratio of the matrix element squared and the subtraction term for 10000 phase space points. For $x = 10^{-9}$ we obtained an average of $R = 1.0000004$ and a standard deviation of $\sigma = 4.2 \times 10^{-5}$. This shows that, as we wanted, the subtraction term coincides with the matrix element squared in this limit. The number of points that lie on the outliers is also

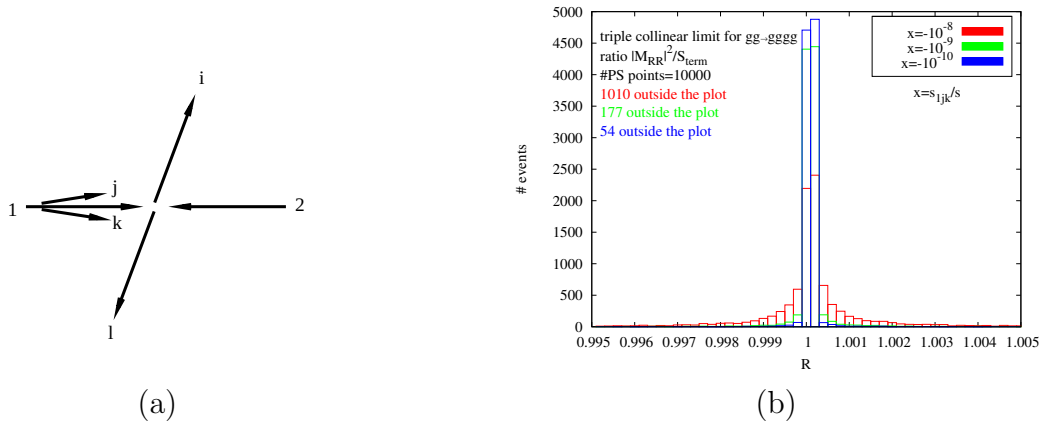

(a) (b)

Figure 7.4: (a) Example configuration of a triple collinear event with $s_{1jk} \to 0$. (b) Distribution of R for 10000 triple collinear phase space points.

shown on the plot.

In figure 7.4 (b) we do the same analysis for the initial state singularity. In this case $x = s_{1jk}/s$ [$x = -10^{-7}$ (red), $x = -10^{-8}$ (green), $x = -10^{-9}$ (blue)] and we have a configuration with two final state gluons collinear with the initial state gluon. The triple collinear configurations involving p_2 produce identical results and are not shown. For the blue distribution again with 10000 phase space points we obtained an average of $R = 0.99954$ and a standard deviation of $\sigma = 0.04$. The plot shows that this singular region is also accounted for by the subtraction term.

7.1.3 Soft and collinear limit

To probe the soft and collinear regions of the phase space, we generate an event configuration with a soft final state gluon by making a triple invariant s_{ijk} close to the full center of mass energy s. For a final state singularity we then produce a decay into two particles sharing a collinear direction making their invariant mass small (in figure 7.5 (a)), and, for an initial state singularity, we rotate the momenta to make one of the emitted gluons collinear with the initial state (in figure 7.6 (a)).

In the first case (figure 7.5 (b)) we plot three distributions in different colours where now we use two variables to approach this unresolved limit. We define $x = (s - s_{ijk})/s$ and $y = s_{ij}/s$ and make $x \to 0$ and $y \to 0$. In red we have $x = y = 10^{-4}$, green $x = y = 10^{-5}$ and in blue $x = y = 10^{-6}$. For $x = y = 10^{-6}$ again with

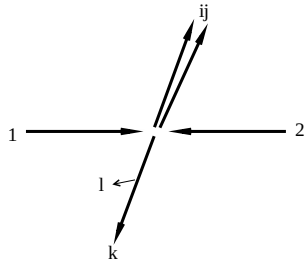

(a)

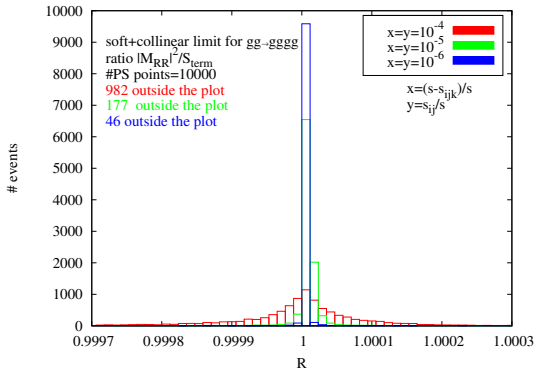

(b)

Figure 7.5: (a) Example configuration of a soft and collinear event with $s_{ijk} \approx s_{12} = s$ and $s_{ij} \to 0$. (b) Distribution of R for 10000 soft and collinear phase space points.

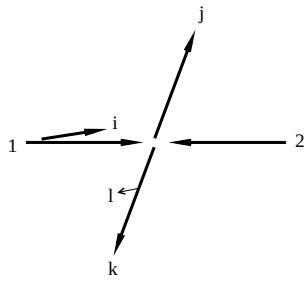

(a)

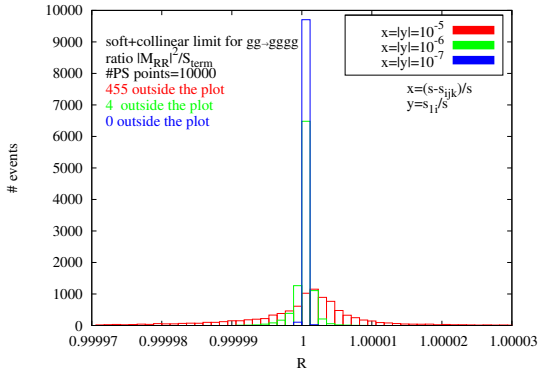

(b)

Figure 7.6: (a) Example configuration of a soft and collinear event with $s_{ijk} \approx s_{12} = s$ and $s_{1i} \to 0$. (b) Distribution of R for 10000 soft and collinear phase space points.

10000 phase space points we obtained an average of $R = 0.99999993$ and a standard deviation of $\sigma = 0.0001$.

For the initial state singularity (figure 7.6 (b)) we define $x = (s - s_{ijk})/s$ and $y = s_{1i}/s$ and make $x \to 0$ and $y \to 0$. In this case in red we have $x = |y| = 10^{-5}$, green $x = |y| = 10^{-6}$ and in blue $x = |y| = 10^{-7}$, where we obtained an average of $R = 0.99999998$ and a standard deviation of $\sigma = 1.6 \times 10^{-7}$.

The combination of the antennae implemented with the formulae of the previous chapter also converges in this limit to the matrix element.

7.1.4 Double collinear limit

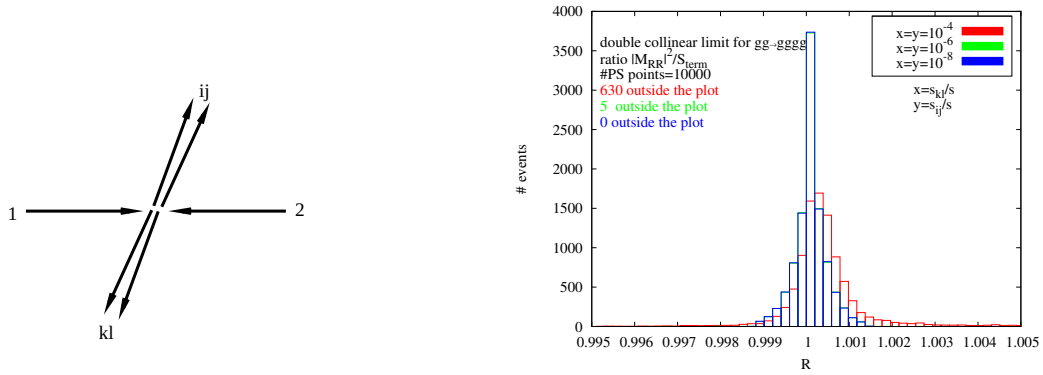

(a) (b)

Figure 7.7: (a) Example configuration of a double collinear event with $s_{ij} \to 0$ and $s_{kl} \to 0$ simultaneously. (b) Distribution of R for 10000 double collinear phase space points.

In this section we analyse the various double collinear limits. This is the last double unresolved configuration in the real correction at NNLO. In this case, we generate three different topologies where two pairs of particles can become collinear separately by demanding that two invariants vanish simultaneously. The double invariants pair can involve only final state momenta (illustrated in figure 7.7(a)), or initial and final state momenta (illustrated in figures 7.8 (a) and 7.9 (a)).

In all cases we generate 10000 phase space points that will approach the double collinear limit. For each we compute the ratio between the matrix element squared and the subtraction term and plot the distribution obtained. For the first case (in

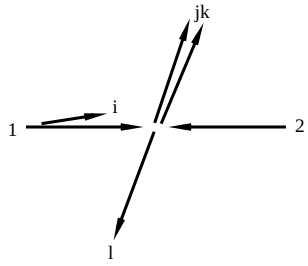

(a)

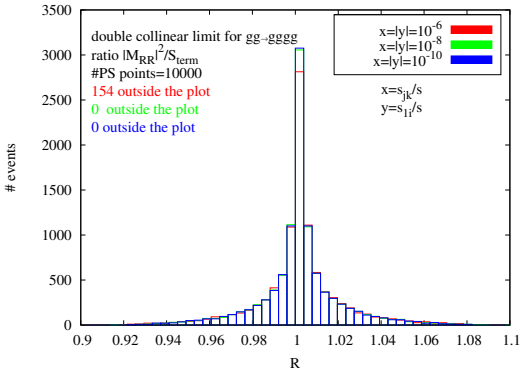

(b)

Figure 7.8: (a) Example configuration of a double collinear event with $s_{jk} \to 0$ and $s_{1i} \to 0$. (b) Distribution of R for 10000 double collinear phase space points.

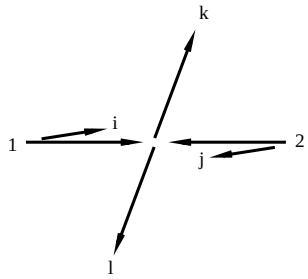

(a)

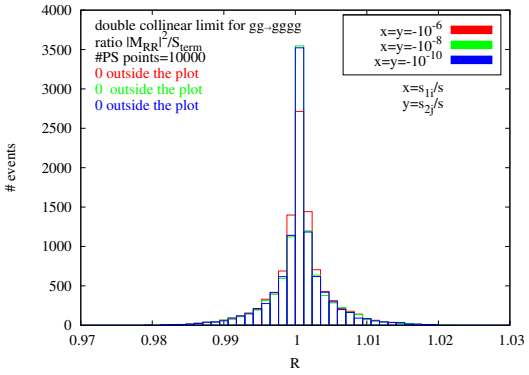

(b)

Figure 7.9: (a) Example configuration of a double collinear event with $s_{1i} \to 0$ and $s_{2j} \to 0$ simultaneously. (b) Distribution of R for 10000 double collinear phase space points.

figure 7.7 (b)) we have $x = s_{ij}/s$, $y = s_{kl}/s$ and we make $x = y = 10^{-4}$ in red, $x = y = 10^{-6}$ in green and finally $x = y = 10^{-8}$ in blue. As we approach the double collinear limit the subtraction converges to the matrix element squared. We obtained, for $x = y = 10^{-8}$ an average of $R = 0.9999995$ and a standard deviation of $\sigma = 0.00037$.

For the second configuration (in figure 7.8 (b)) we have $x = s_{jk}$, $y = s_{1i}$ and we make $x = |y| = 10^{-6}$ in red, $x = |y| = 10^{-8}$ in green and $x = |y| = 10^{-10}$ in blue. The average obtained for $x = |y| = 10^{-10}$ was $R = 1.00012$ and a standard deviation of $\sigma = 0.018$.

In the last case (in figure 7.9 (b)) we have $x = s_{1i}$, $y = s_{2j}$ and we make $x = y = -10^{-6}$ in red, $x = y = -10^{-8}$ in green and $x = y = -10^{-10}$ in blue. The average obtained for $x = y = -10^{-10}$ was $R = 1.00001$ and a standard deviation of $\sigma = 0.004$.

In all cases we found convergence of the matrix element and the counterterm as we approach these singular limits.

7.1.5 Subtraction of single unresolved final and initial state singularities

In this subsection we will check that the integrand defined in chapter 6 is integrable over the single unresolved phase space regions. Single unresolved subtraction is well understood at NLO, but, in this case it is necessary to verify that the new NNLO subtraction term does not introduce divergences when one parton becomes unresolved. In other words it has to be correct simultaneously for both double unresolved and single unresolved configurations. In the $2 \to 4$ phase space these correspond to three jet configurations and, depending on the observable, these are allowed by the jet defining function through cuts on the final state momenta.

Soft limit

In figure 7.10(a) we analyse the single soft limit. To produce these distributions we generate configurations where a triple invariant s_{ijk} is close to the full center of mass

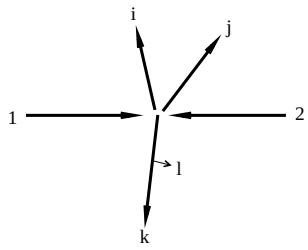

(a)

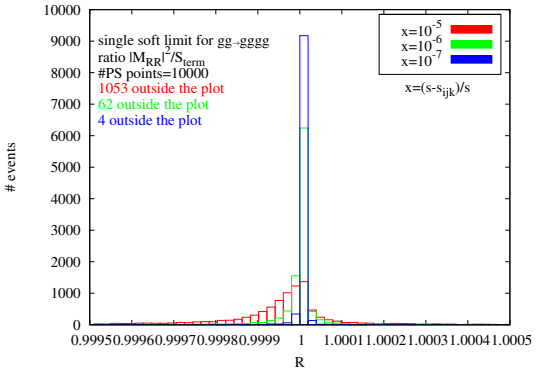

(b)

Figure 7.10: (a) Example configuration of a single soft event with $s_{ijk} \approx s_{12} = s$. (b) Distribution of R for 10000 single soft phase space points.

energy s. We defined $x = (s - s_{ijk})/s$ and plot in figure 7.10 (b) the distributions for $x = 10^{-5}$ in red, $x = 10^{-6}$ in green and $x = 10^{-7}$ in blue. The distributions show that the subtraction term converges to the matrix element as we approach this singular limit. In this case the singularities related to soft gluons cancel and, the piece of the subtraction term described in section 4.2.5 correctly subtracts point by point the oversubtraction of large-angle soft gluon radiation. When $x = 10^{-7}$ we obtained an average $R = 0.999998$ and a standard deviation of $\sigma = 1.9 \times 10^{-5}$.

Collinear limit

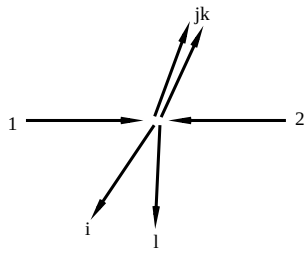

(a)

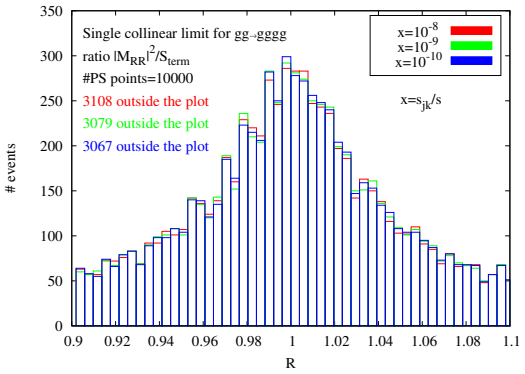

(b)

Figure 7.11: (a) Example configuration of a single collinear event with $s_{jk} \to 0$. (b) Distribution of R for 10000 single collinear phase space points.

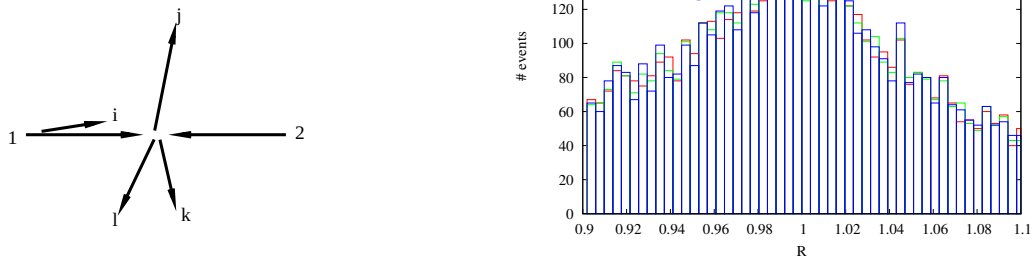

(a) (b)

Figure 7.12: (a) Example configuration of a single collinear event with $s_{1i} \to 0$. (b) Distribution of R for 10000 single collinear phase space points.

Finally we generate points corresponding to the final and initial state single collinear regions of the phase space. These are shown in figures 7.11 (a) and 7.12 (a) respectively. As we have discussed in section 4.3.2, using scalar four-parton antennae functions the factorisation in the collinear limits where a final state gluon splits into two gluons introduces angular terms. This is the reason why the distributions in figures 7.11(b) and 7.12(b) have a much broader shape than the previous examples.

For the final-final collinear singularity, we introduce the variable $x = s_{ij}/s_{12}$ and 7.11(b) shows the distribution for $x = 10^{-8}$ (red), $x = 10^{-9}$ (green) and $x = 10^{-10}$ (blue). Similarly in the initial-final collinear limit, we define $x = s_{1i}/s_{12}$ and show the distributions of R for the same x-values in 7.12(b). It is clear that as we approach the collinear limits $x \to 0$, the azimuthal terms are not suppressed and the subtraction term is not, point by point, a better representation of the matrix element.

Nevertheless, the azimuthal terms coming from the single collinear limits were shown to vanish in section 4.3.2. This happens only globally after an azimuthal integration over the unresolved phase space. Here we are performing a point-by-point analysis on the integrand defined by the matrix element squared and the subtraction term. One solution to proceed is to introduce the angular $\Theta_{F_3^0}(i, j, z, k_\perp)$ function defined in 4.3.2 to reconstruct the angular terms. Subtracting this additional term from the F_4^0 four-parton antenna functions for the final-final and, initial-final and initial-initial configurations (by crossing momenta to the initial state) produces a

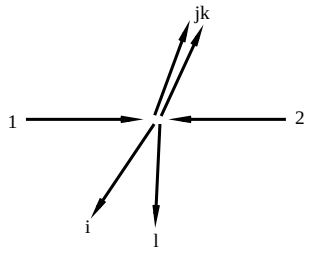

(a)

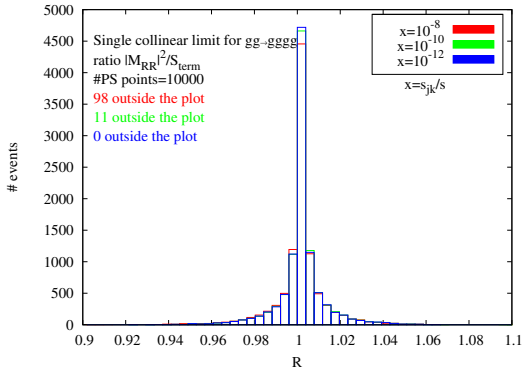

(b)

Figure 7.13: (a) Example configuration of a single collinear event with $s_{jk} \to 0$. (b) Distribution of R for 10000 single collinear phase space points.

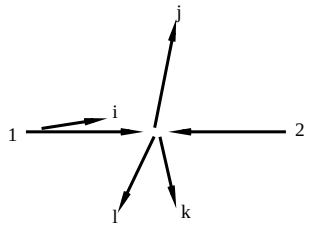

(a)

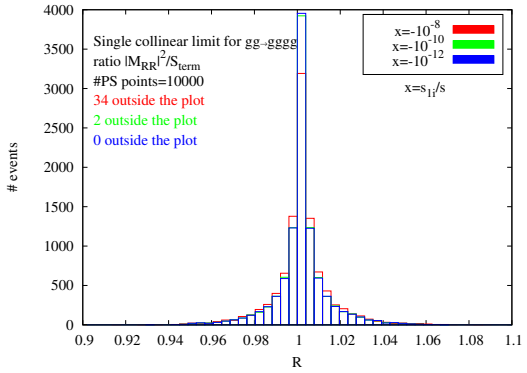

(b)

Figure 7.14: (a) Example configuration of a single collinear event with $s_{1i} \to 0$. (b) Distribution of R for 10000 single collinear phase space points.

subtraction term that is locally free of angular terms.

With this azimuthally modified subtraction term, we recompute the distributions in figures 7.13(b) and 7.14(b). In figure 7.13(b) we show the R distribution for 10000 single collinear phase space points and $x = 10^{-8}$ (red), in green $x = 10^{-10}$ (green) and in blue $x = 10^{-12}$ (blue). For $x = 10^{-12}$ we obtained an average $R = 0.99994$ and a standard deviation of $\sigma = 0.015$.

We repeat the same analysis for the initial state singularity in figure 7.14(b) for $x = -10^{-8}$ (red), in green $x = -10^{-10}$ (green) and in blue $x = -10^{-12}$ (blue). For $x = -10^{-12}$ we obtained an average of $R = 1.00007$ and a standard deviation of $\sigma = 0.012$.

For both cases, the distributions now peaks around $R = 1$ with a more pronounced peak as the limit is approached, just as in the double unresolved and single soft limits discussed earlier. This demonstrates the the convergence of the counterterm to the matrix element.

We note however that introducing $\Theta_{F_3^0}(i, j, z, k_\perp)$ may have an unfortunate side effect by generating new singularities in the previously analysed (double unresolved) phase space regions. For example, looking into equation (4.52) for $\Theta_{F_3^0}(i, j, z, k_\perp)$ we see a invariants in the denominator of that expression that are not compensated by a small quantity in the numerator when they vanish. This introduces new divergences in triple collinear regions which are not present in the matrix element. More work is needed to decide the best strategy for these single collinear limits. Alternative techniques include the cancellation of the angular terms by combining phase space points related to each other by a rotation of the system of unresolved partons in the integration routine [91].

7.2 Summary

In this chapter we demonstrated that the results of our numerical implementation of the antenna subtraction behave in the expected way. This follows from checking the same limits analytically with the known singular behaviour of both the colour ordered amplitudes in the matrix element and the three-parton F_3^0 and four-parton F_4^0 antennae functions in the subtraction term. The agreement between the analytic limits of the formula for $\mathrm{d}\sigma^S_{NNLO}$ written in chapter 6 and the numerical limits of its implementation represent the first sanity check on the NNLO subtraction method that we are developing.

All the singular regions of the phase space corresponding to a certain number of invariants tending to zero were analysed separately. With the caveat of the correct handling of the azimuthal terms associated with the single collinear limit, all of the double unresolved and single soft singularities present in the matrix elements are cancelled in a point-by point manner by the subtraction term of chapter 6.

Chapter 8

Conclusions

The aim of this thesis was to show that the antenna subtraction method can also tackle computations of NNLO processes with coloured particles in the initial state. We have particularly focused on jet production in hadron-hadron collisions.

As we have discussed, the quality of the data already collected at the Tevatron and the improved experimental accuracy which is expected with the forthcoming runs at the LHC drives an ambitious effort to perform precision studies of QCD. At the moment, the experimental error on single jet production is lower than the error of the prediction obtained with NLO QCD. This means that the measurements are sensitive to NNLO effects which are described by Feynman diagrams involving two virtual particles propagating in internal loops, diagrams with unresolved real emission of an amplitude with a virtual particle propagating and finally diagrams related with the emission of two unresolved on-shell particles.

All the matrix elements of QCD that describe these contributions are available in the literature. We list the matrix elements relating to gluon scattering in the appendix. Each of the separate building blocks is infrared divergent. The major remaining difficulty is to derive a procedure to obtain an analytic cancellation of the IR divergences between the various matrix elements to produce a physical prediction. In this thesis we made a first attempt to tackle this problem and presented an implementation based on the antenna subtraction method.

We started in chapter 1 by demonstrating that we can compute the theoretical predictions by means of a perturbative expansion in a power series of the strong cou-

pling constant. Truncation of this series leaves a residual dependence of the calculation on unphysical scales, which we saw that can only be ameliorated by computing higher order terms. We then discussed the procedure to make these higher order terms well defined. They contain ultraviolet (UV) divergences in virtual corrections arising from the high momentum limit of the loop momenta. The renormalisability of the theory guarantees that this type of divergences can be shifted to the fields and parameters of the QCD Lagrangian order by order by a multiplicative redefinition of the fields and coupling constant.

Another type of divergence, the infrared divergence (IR), is present in both the virtual and real contributions. In the virtual contribution, internal massless propagators can vanish in the low momentum limit thereby giving rise to infrared singularities. In this limit the virtual diagram is indistinguishable from the real emission diagram which also becomes singular when the emitted particle becomes unresolved. Using dimensional regularisation for both contributions at next-to-leading order, we find that the singularities appear with opposite sign and can be combined to give a finite physical prediction. Similarly, at NNLO the double virtual, real-virtual and double real contributions all have infrared singularities that ultimately cancel between the three contributions.

To conclude chapter 1 we described the techniques of helicity and colour decomposition, essential to simplify the computation of tree and loop matrix elements from which the predictions at a given order are derived. Within the colour decomposition basis we discussed the universal behaviour of the colour ordered gluonic QCD tree amplitudes when one or two particles become unresolved. As mentioned earlier, the tree amplitudes (which constitute the real corrections) become divergent in these regions of the phase space. Knowing how they factorise allows us to construct suitable counterterms, using simpler building blocks, that coincide with the matrix element of the real correction in the diverging limits. This yields a proper subtraction of infrared divergences which can be carried out at NLO or NNLO.

Chapter 2 dealt with the definition of a jet from the experimental and theoretical point of view. Jets are a *spray* of roughly collinear colourless hadrons that show up in the detectors as tracks with hadronic energy being deposited in the form of clus-

ters. Events can be classified by the number of such clusters of energy that appear in a given event. This procedure depends on the jet algorithm that is employed in both the experimental analysis and in the theoretical calculation. To make comparisons of experimental and theoretical results the same jet algorithm should be used. The details on the implementation of some jet algorithms were given and we also described the convenient variables to compute jet distributions from fixed-order perturbative QCD.

In chapter 3 we examined the antenna subtraction method at NLO. As we have discussed there, this method can be applied at this order for e^+e^-, ep and pp processes with massless fermions. We introduced the antennae functions that describe single unresolved emission between a hard pair of radiators. Details of the numerical implementation of NLO antennae for a pure gluon channel relevant to this thesis were also given there. As an example we performed the analytic subtraction of IR singularities between real and virtual corrections for dijet production using the antenna method at NLO. The aim of this thesis is to extend this calculation to NNLO accuracy and a brief motivation for work on this direction was discussed.

Chapter 4 described the antenna subtraction method at NNLO. We discussed the formulae necessary for the construction of the subtraction of infrared divergences from double real emission diagrams at this order. The singular structure is much more complicated than at NLO because both double and single unresolved limits must be subtracted to obtain a physical prediction. We gave details of the numerical implementation of the NNLO antennae functions for a pure gluon channel which is the new ingredient developed in this thesis. The gluon scattering channel is expected to be the dominant contribution at NNLO. Other channels involving quark and gluon matrix elements will make use of the same antenna building blocks and momentum mappings given in this chapter but the flavour of the antennae in the counterterm will change accordingly.

An alternative numerical method to isolate infrared divergences from parameter integrals is the sector decomposition method. We discussed in chapter 5 its applications for multi-loop Feynman integrals as well as phase space integrals. For the specific case of extraction of real radiation singularities we argued that this method

can produce differential results at NNLO. We gave an example to show how this procedure works in practice. Based on this experience, the advantages and limitations of this approach to our problem were then identified.

In chapter 6 we described the implementation of the NNLO real corrections for gluon scattering using the antenna subtraction method. The formulae given there follow from applying the general formulae discussed in chapter 4, but adapted to this particular case. By construction the counterterm subtracts double and single unresolved singularities in the final and initial state. To achieve this we used a combination of NNLO final-final, initial-final and initial-initial antennae functions. The analytic integration of the NNLO antennae functions is presently known for the final-final [67] and initial-final [105, 119] assignments of radiators. Work on the initial-initial case is expected to be concluded soon [120].

Chapter 7 constitutes the numerical check of the implementation of the double real correction derived in chapter 6. We tested the matrix element and the subtraction term in all double and single unresolved regions of the phase space. The numerical results showed that the combination of the antennae correctly describes the infrared singularity structure of the matrix element. The antenna subtraction method, which has been successfully applied to the calculation of NNLO corrections to the 3-jet cross section and related event shape distributions in electron-positron annihilation, is now being applied for an NNLO computation of a process with coloured particles in the initial state.

Future steps include the subtraction of infrared divergences in the mixed real-virtual correction. Both real-real and real-virtual subtractions are integrated analytically with the results for the NNLO integrated antennae and added to the two loop contribution. This will enable the construction of a numerical program to compute NNLO QCD estimates of jet production in hadron collisions.

Appendix A

QCD Matrix elements for gluon scattering

A.1 $gg \to gg$ tree level

For four-gluon helicity amplitudes the only non-zero sub-amplitudes will be of the form $(--++)$ up to permutations of the indices. These were initially conjectured by [160] and proven later by [161]. They are written in the following form:

$$m_{2+2-}(g_1, g_2, g_3, g_4) = ig^2 \frac{\langle IJ\rangle^4}{\langle 12\rangle\langle 23\rangle\langle 34\rangle\langle 41\rangle} \tag{A.1.1}$$

where I and J are the indices of negative helicity gluons. We can square this sub-amplitude and sum over helicities to obtain the colour-ordered amplitude squared:

$$A_4^0(g_1, g_2, g_3, g_4) = g^4 \left(\sum_{i>j} s_{ij}^4\right) \frac{1}{s_{12}s_{23}s_{34}s_{41}} \tag{A.1.2}$$

This is the colour ordered amplitude that accompanies the antenna functions in the counterterms in chapter 6.

A.2 $gg \to gg$ one-loop

We denote the squared amplitude summed over spins and colours by

$$\langle \mathcal{M}|\mathcal{M}\rangle = \sum |\mathcal{M}(g + g \to g + g)|^2 = \mathcal{D}(s, t, u) \tag{A.2.3}$$

that corresponds to the process:

$$g(p_1) + g(p_2) \to g(p_3) + g(p_4) \tag{A.2.4}$$

$\mathcal{D}(s,t,u)$ is symmetric under the exchange of s, t and u that are given by:

$$s = (p_1+p_2)^2, \qquad t = (p_1-p_3)^2, \qquad u = (p_2-p_3)^2, \qquad s+t+u = 0. \tag{A.2.5}$$

The function $\mathcal{D}$ can be expanded perturbatively to yield:

$$\mathcal{D}(s,t,u) \;=\; 16\pi^2\alpha_s^2\left[\mathcal{D}^4(s,t,u) + \left(\frac{\alpha_s}{2\pi}\right)\mathcal{D}^6(s,t,u) + \mathcal{O}\left(\alpha_s^2\right)\right],$$

where:

$$\begin{aligned}
\mathcal{D}^4(s,t,u) &= \langle \mathcal{M}^{(0)} | \mathcal{M}^{(0)} \rangle \\
&= 16\,VN^2(1-\epsilon)^2\left(3 - \frac{ut}{s^2} - \frac{us}{t^2} - \frac{st}{u^2}\right), \qquad \text{(A.2.6)} \\
\mathcal{D}^6(s,t,u) &= \left(\langle \mathcal{M}^{(0)} | \mathcal{M}^{(1)} \rangle + \langle \mathcal{M}^{(1)} | \mathcal{M}^{(0)} \rangle\right), \qquad \text{(A.2.7)}
\end{aligned}$$

and N is the number of colours and $V = N^2 - 1$. $\mathcal{D}^4(s,t,u)$ is the standard four gluon matrix element given by (A.1.2) summed over all orderings. The expression for $\mathcal{D}^6(s,t,u)$ can be obtained from [162]:

$$\begin{aligned}
\mathcal{D}^6(s,t,u) = &\left(\frac{4\pi\mu^2}{Q^2}\right)^{\epsilon}\frac{\Gamma(1+\epsilon)\Gamma^2(1-\epsilon)}{\Gamma(1-2\epsilon)} \\
&\times\Bigg[\mathcal{D}^4(s,t,u)\Bigg(-\frac{4N}{\epsilon^2} - \frac{22N}{3\epsilon} + \frac{8T_R}{3\epsilon} - \frac{67N}{9} + \frac{20T_R}{9} \\
&\qquad + N\pi^2 + \frac{11N}{3}l(-\mu^2) - \frac{4T_R}{3}l(-\mu^2)\Bigg) \\
&+ \frac{16NV^3}{\epsilon}l(s)\left(3 - \frac{2tu}{s^2} + \frac{t^4+u^4}{t^2u^2}\right) \\
&+ \frac{16NV^3}{\epsilon}l(t)\left(3 - \frac{2us}{t^2} + \frac{u^4+s^4}{u^2s^2}\right) \\
&+ \frac{16NV^3}{\epsilon}l(u)\left(3 - \frac{2st}{u^2} + \frac{s^4+t^4}{s^2t^2}\right)\Bigg] \\
&+ 4VN^2(f^d(s,t,u) + f^d(t,u,s) + f^d(u,s,t)) + \mathcal{O}(\epsilon) \qquad \text{(A.2.8)}
\end{aligned}$$

where f^d is given by

$$f^d(s,t,u) = N\left[\left(\frac{2(t^2+u^2)}{tu}\right)l^2(s) + \left(\frac{4s(t^3+u^3)}{t^2u^2} - 6\right)l(t)l(u)\right.$$

$$+\left(\frac{4}{3}\frac{tu}{s^2}-\frac{14}{3}\frac{t^2+u^2}{tu}-14-8\left(\frac{t^2}{u^2}+\frac{u^2}{t^2}\right)\right)l(s)-1-\pi^2\Bigg]$$
$$+T_R\Bigg[\left(\frac{10}{3}\frac{t^2+u^2}{tu}+\frac{16}{3}\frac{tu}{s^2}-2\right)l(s)-\frac{s^2+tu}{tu}l^2(s)$$
$$-2\frac{t^2+u^2}{tu}l(t)l(u)+2-\pi^2\Bigg] \qquad \text{(A.2.9)}$$

The poles present in eq (A.2.8) are a consequence of the singularities due to the emission of soft and collinear radiation. The notation $l(x)$ denotes the logarithm,

$$l(x)=\ln\left(-\frac{x}{Q^2}\right). \qquad \text{(A.2.10)}$$

If x is greater than zero $l(x)$ has an imaginary part since $Q^2 > 0$. In equations (A.2.8) and (A.2.9) it is understood that only the real part is kept. Explicitly:

$$\begin{aligned} l^2(x) &\to \ln^2\frac{x}{Q^2}-\pi^2, & x>0,\\ l^2(x) &\to \ln^2\left(\frac{-x}{Q^2}\right), & x<0,\\ l(x) &\to \ln\left|\frac{x}{Q^2}\right| \end{aligned} \qquad \text{(A.2.11)}$$

These assignments should be made after crossing to the appropriate region. Q^2 is an arbitrary momentum scale. It will often be most convenient to make the choice $Q^2 = s$ but the scale is left arbitrary to make the behaviour under crossing manifest. The colour structure is fixed in terms of the quantities,

$$V=N^2-1, \qquad N=3, \qquad T_R=\frac{1}{2}n_f \qquad \text{(A.2.12)}$$

and n_f is the number of quark flavours.

A.3 $gg \to gg$ two-loop

This matrix element is not implemented in our program but we reproduce it here for convenience. Subsection A.3.1 through subsection A.3.3 are taken from reference [106] and similarly, subsection A.3.4 and subsection A.3.5 are taken from [113]. The same matrix element was also computed in [107]. It corresponds to the process:

$$g(p_1)+g(p_2)+g(p_3)+g(p_4)\to 0, \qquad \text{(A.3.13)}$$

where the gluons are all incoming with light-like momenta, satisfying

$$p_1^\mu + p_2^\mu + p_3^\mu + p_4^\mu = 0, \qquad p_i^2 = 0.$$

The associated Mandelstam variables are given by

$$s = (p_1 + p_2)^2, \qquad t = (p_2 + p_3)^2, \qquad u = (p_1 + p_3)^2, \qquad s + t + u = 0. \quad \text{(A.3.14)}$$

The renormalised four point amplitude in the $\overline{\text{MS}}$ scheme can be written

$$|\mathcal{M}\rangle = 4\pi\alpha_s \left[|\mathcal{M}^{(0)}\rangle + \left(\frac{\alpha_s}{2\pi}\right) |\mathcal{M}^{(1)}\rangle + \left(\frac{\alpha_s}{2\pi}\right)^2 |\mathcal{M}^{(2)}\rangle + \mathcal{O}\left(\alpha_s^3\right) \right], \quad \text{(A.3.15)}$$

where $\alpha_s \equiv \alpha_s(\mu^2)$ is the running coupling at renormalisation scale μ and the $|\mathcal{M}^{(i)}\rangle$ represents the colour-space vector describing the renormalised i-loop amplitude. We denote the squared amplitude summed over spins and colours by

$$\langle \mathcal{M}|\mathcal{M}\rangle = \sum |\mathcal{M}(g + g \to g + g)|^2 = \mathcal{D}(s,t,u). \quad \text{(A.3.16)}$$

which is symmetric under the exchange of s, t and u. The function $\mathcal{D}$ can be expanded perturbatively to yield

$$\mathcal{D}(s,t,u) = 16\pi^2\alpha_s^2 \left[\mathcal{D}^4(s,t,u) + \left(\frac{\alpha_s}{2\pi}\right) \mathcal{D}^6(s,t,u) + \left(\frac{\alpha_s}{2\pi}\right)^2 \mathcal{D}^8(s,t,u) + \mathcal{O}\left(\alpha_s^3\right) \right], \quad \text{(A.3.17)}$$

where

$$\begin{aligned}
\mathcal{D}^4(s,t,u) &= \langle \mathcal{M}^{(0)}|\mathcal{M}^{(0)}\rangle \\
&= 16\, V N^2 (1-\epsilon)^2 \left(3 - \frac{ut}{s^2} - \frac{us}{t^2} - \frac{st}{u^2}\right), && \text{(A.3.18)} \\
\mathcal{D}^6(s,t,u) &= \left(\langle \mathcal{M}^{(0)}|\mathcal{M}^{(1)}\rangle + \langle \mathcal{M}^{(1)}|\mathcal{M}^{(0)}\rangle\right), && \text{(A.3.19)} \\
\mathcal{D}^8(s,t,u) &= \left(\langle \mathcal{M}^{(1)}|\mathcal{M}^{(1)}\rangle + \langle \mathcal{M}^{(0)}|\mathcal{M}^{(2)}\rangle + \langle \mathcal{M}^{(2)}|\mathcal{M}^{(0)}\rangle\right), && \text{(A.3.20)}
\end{aligned}$$

where N is the number of colours and $V = N^2 - 1$. Expressions for $\mathcal{D}^6$ are given in A.2 using dimensional regularisation to isolate the infrared and ultraviolet singularities.

In the next subsections the pole and finite pieces for both the two-loop contribution and one-loop self interference of (A.3.20) are given.

A.3.1 Two loop contribution - Pole piece

In the following sections, we present expressions for the infrared singular and finite two-loop contributions to $\mathcal{D}^8$

$$\mathcal{D}^{8\,(2\times0)}(s,t,u) = \langle\mathcal{M}^{(0)}|\mathcal{M}^{(2)}\rangle + \langle\mathcal{M}^{(2)}|\mathcal{M}^{(0)}\rangle. \tag{A.3.21}$$

The two-loop contribution are decomposed as a sum of two terms

$$\mathcal{D}^{8\,(2\times0)}(s,t,u) = \mathcal{P}oles(s,t,u) + \mathcal{F}inite(s,t,u). \tag{A.3.22}$$

$\mathcal{P}oles$ contains infrared singularities that will be analytically canceled by those occurring in radiative processes of the same order (ultraviolet divergences are removed by renormalisation). $\mathcal{F}inite$ is the remainder which is finite as $\epsilon \to 0$. Following the procedure outlined in Ref. [112], the infrared pole structure of the two loop contributions renormalised in the $\overline{\rm MS}$ scheme in terms of the tree and unrenormalised one-loop amplitudes, $|\mathcal{M}^{(0)}\rangle$ and $|\mathcal{M}^{(1,un)}\rangle$ respectively, can be written as

$$\begin{aligned}\mathcal{P}oles = 2\,\mathrm{Re}\Bigg[& -\frac{1}{2}\langle\mathcal{M}^{(0)}|\boldsymbol{I}^{(1)}(\epsilon)\boldsymbol{I}^{(1)}(\epsilon)|\mathcal{M}^{(0)}\rangle - \frac{2\beta_0}{\epsilon}\,\langle\mathcal{M}^{(0)}|\boldsymbol{I}^{(1)}(\epsilon)|\mathcal{M}^{(0)}\rangle \\ & + \langle\mathcal{M}^{(0)}|\boldsymbol{I}^{(1)}(\epsilon)|\mathcal{M}^{(1,un)}\rangle \\ & + e^{-\epsilon\gamma}\frac{\Gamma(1-2\epsilon)}{\Gamma(1-\epsilon)}\left(\frac{\beta_0}{\epsilon}+K\right)\langle\mathcal{M}^{(0)}|\boldsymbol{I}^{(1)}(2\epsilon)|\mathcal{M}^{(0)}\rangle \\ & + \langle\mathcal{M}^{(0)}|\boldsymbol{H}^{(2)}(\epsilon)|\mathcal{M}^{(0)}\rangle\Bigg]\end{aligned} \tag{A.3.23}$$

where the Euler constant $\gamma = 0.5772\ldots$. The first coefficient of the QCD beta function, β_0, for N_F (massless) quark flavours is

$$\beta_0 = \frac{11C_A - 4T_R N_F}{6}, \qquad C_A = N, \qquad T_R = \frac{1}{2}, \tag{A.3.24}$$

and the constant K is

$$K = \left(\frac{67}{18} - \frac{\pi^2}{6}\right)C_A - \frac{10}{9}T_R N_F. \tag{A.3.25}$$

Note that the unrenormalised one-loop amplitude $|\mathcal{M}^{(1,un)}\rangle$ is what is obtained by direct Feynman diagram evaluation of the one-loop graphs.

It is convenient to decompose $|\mathcal{M}^{(0)}\rangle$ and $|\mathcal{M}^{(1,un)}\rangle$ in terms of $SU(N)$ matrices in the fundamental representation, T^a, so that the tree amplitude may be written

as:

$$|\mathcal{M}^{(0)}\rangle = \sum_{P(2,3,4)} \mathrm{Tr}\left(T^{a_1}T^{a_2}T^{a_3}T^{a_4}\right) \mathcal{A}_4^{\mathrm{tree}}(1,2,3,4), \tag{A.3.26}$$

while the one-loop amplitude has the form:

$$\begin{aligned} |\mathcal{M}^{(1,un)}\rangle &= N \sum_{P(2,3,4)} \mathrm{Tr}\left(T^{a_1}T^{a_2}T^{a_3}T^{a_4}\right) \mathcal{A}_{4;1}^{[1]}(1,2,3,4) \\ &+ \sum_{Q(2,3,4)} \mathrm{Tr}\left(T^{a_1}T^{a_2}\right) \mathrm{Tr}\left(T^{a_3}T^{a_4}\right) \mathcal{A}_{4;3}^{[1]}(1,2,3,4) \\ &+ N_F \sum_{P(2,3,4)} \mathrm{Tr}\left(T^{a_1}T^{a_2}T^{a_3}T^{a_4}\right) \mathcal{A}_{4;1}^{[1/2]}(1,2,3,4). \end{aligned} \tag{A.3.27}$$

To evaluate Eq. (A.3.23) it is convenient to express $|\mathcal{M}^{(0)}\rangle$ and $|\mathcal{M}^{(1,un)}\rangle$ as nine-dimensional vectors in colour space

$$|\mathcal{M}^{(0)}\rangle = \left(\mathcal{T}_1,\ \mathcal{T}_2,\ \mathcal{T}_3,\ \mathcal{T}_4,\ \mathcal{T}_5,\ \mathcal{T}_6,\ 0,\ 0,\ 0\right)^T, \tag{A.3.28}$$

$$|\mathcal{M}^{(1,un)}\rangle = \left(\mathcal{L}_1,\ \mathcal{L}_2,\ \mathcal{L}_3,\ \mathcal{L}_4,\ \mathcal{L}_5,\ \mathcal{L}_6,\ \mathcal{L}_7,\ \mathcal{L}_8,\ \mathcal{L}_9\right)^T, \tag{A.3.29}$$

where $()^T$ indicates the transpose vector. Here the $\mathcal{T}_i$ and $\mathcal{L}_i$ are the components of $|\mathcal{M}^{(0)}\rangle$ and $|\mathcal{M}^{(1,un)}\rangle$ in the colour space spanned by the (non-orthogonal) basis

$$\begin{aligned} \mathcal{C}_1 &= \mathrm{Tr}\left(T^{a_1}T^{a_2}T^{a_3}T^{a_4}\right), \\ \mathcal{C}_2 &= \mathrm{Tr}\left(T^{a_1}T^{a_2}T^{a_4}T^{a_3}\right), \\ \mathcal{C}_3 &= \mathrm{Tr}\left(T^{a_1}T^{a_4}T^{a_2}T^{a_3}\right), \\ \mathcal{C}_4 &= \mathrm{Tr}\left(T^{a_1}T^{a_3}T^{a_2}T^{a_4}\right), \\ \mathcal{C}_5 &= \mathrm{Tr}\left(T^{a_1}T^{a_3}T^{a_4}T^{a_2}\right), \\ \mathcal{C}_6 &= \mathrm{Tr}\left(T^{a_1}T^{a_4}T^{a_3}T^{a_2}\right), \\ \mathcal{C}_7 &= \mathrm{Tr}\left(T^{a_1}T^{a_2}\right) \mathrm{Tr}\left(T^{a_3}T^{a_4}\right), \\ \mathcal{C}_8 &= \mathrm{Tr}\left(T^{a_1}T^{a_3}\right) \mathrm{Tr}\left(T^{a_2}T^{a_4}\right), \\ \mathcal{C}_9 &= \mathrm{Tr}\left(T^{a_1}T^{a_4}\right) \mathrm{Tr}\left(T^{a_2}T^{a_3}\right). \end{aligned} \tag{A.3.30}$$

The tree and loop amplitudes $\mathcal{T}_i$ and $\mathcal{L}_i$ are directly obtained in terms of $\mathcal{A}_4^{\mathrm{tree}}$, $\mathcal{A}_{4;1}^{[1]}$, $\mathcal{A}_{4;3}^{[1]}$ and $\mathcal{A}_{4;1}^{[1/2]}$ by reading off from Eqs. (A.3.26) and (A.3.27). However, the amplitudes themselves are not required since the computation of the interference of tree and loop amplitudes is given directly.

In the same colour basis, the infrared-singularity operator $\boldsymbol{I}^{(1)}(\epsilon)$ introduced by Catani [112] has the form

$$\boldsymbol{I}^{(1)}(\epsilon) = -\frac{e^{\epsilon\gamma}}{\Gamma(1-\epsilon)}\left(\frac{1}{\epsilon^2}+\frac{\beta_0}{N\epsilon}\right) \times \begin{pmatrix} N(\mathtt{S}+\mathtt{T}) & 0 & 0 & 0 & 0 & 0 & (\mathtt{T}-\mathtt{U}) & 0 & (\mathtt{S}-\mathtt{U}) \\ 0 & N(\mathtt{S}+\mathtt{U}) & 0 & 0 & 0 & 0 & (\mathtt{U}-\mathtt{T}) & (\mathtt{S}-\mathtt{T}) & 0 \\ 0 & 0 & N(\mathtt{T}+\mathtt{U}) & 0 & 0 & 0 & 0 & (\mathtt{T}-\mathtt{S}) & (\mathtt{U}-\mathtt{S}) \\ 0 & 0 & 0 & N(\mathtt{T}+\mathtt{U}) & 0 & 0 & 0 & (\mathtt{T}-\mathtt{S}) & (\mathtt{U}-\mathtt{S}) \\ 0 & 0 & 0 & 0 & N(\mathtt{S}+\mathtt{U}) & 0 & (\mathtt{U}-\mathtt{T}) & (\mathtt{S}-\mathtt{T}) & 0 \\ 0 & 0 & 0 & 0 & 0 & N(\mathtt{S}+\mathtt{T}) & (\mathtt{T}-\mathtt{U}) & 0 & (\mathtt{S}-\mathtt{U}) \\ (\mathtt{S}-\mathtt{U}) & (\mathtt{S}-\mathtt{T}) & 0 & 0 & (\mathtt{S}-\mathtt{T}) & (\mathtt{S}-\mathtt{U}) & 2N\mathtt{S} & 0 & 0 \\ 0 & (\mathtt{U}-\mathtt{T}) & (\mathtt{U}-\mathtt{S}) & (\mathtt{U}-\mathtt{S}) & (\mathtt{U}-\mathtt{T}) & 0 & 0 & 2N\mathtt{U} & 0 \\ (\mathtt{T}-\mathtt{U}) & 0 & (\mathtt{T}-\mathtt{S}) & (\mathtt{T}-\mathtt{S}) & 0 & (\mathtt{T}-\mathtt{U}) & 0 & 0 & 2N\mathtt{T} \end{pmatrix} \tag{A.3.31}$$

where

$$\mathtt{S} = \left(-\frac{\mu^2}{s}\right)^{\epsilon}, \qquad \mathtt{T} = \left(-\frac{\mu^2}{t}\right)^{\epsilon}, \qquad \mathtt{U} = \left(-\frac{\mu^2}{u}\right)^{\epsilon}. \tag{A.3.32}$$

The matrix $\boldsymbol{I}^{(1)}(\epsilon)$ acts directly as a rotation matrix on $|\mathcal{M}^{(0)}\rangle$ and $|\mathcal{M}^{(1,un)}\rangle$ in colour space, to give a new colour vector $|X\rangle$, equal to $\boldsymbol{I}^{(1)}(\epsilon)|\mathcal{M}^{(0)}\rangle$, $\boldsymbol{I}^{(1)}(\epsilon)\boldsymbol{I}^{(1)}(\epsilon)|\mathcal{M}^{(0)}\rangle$ or $\boldsymbol{I}^{(1)}(\epsilon)|\mathcal{M}^{(1,un)}\rangle$. The contraction of the colour vector $|X\rangle$ with the conjugate tree amplitude obeys the rule

$$\langle\mathcal{M}^{(0)}|X\rangle = \sum_{\text{spins}}\sum_{\text{colours}}\sum_{i,j=1}^{9} \mathcal{T}_i^*\, X_j\, \mathcal{C}_i^*\, \mathcal{C}_j. \tag{A.3.33}$$

In evaluating these contractions, there are terms of the type $\sum_{\text{colours}} \mathcal{C}_i^*\, \mathcal{C}_j$ which are given by the ij component of the symmetric matrix $\mathcal{CC}$

$$\mathcal{CC} = \frac{V}{16N^2}\begin{pmatrix} C_1 & C_2 & C_2 & C_2 & C_2 & C_3 & NV & -N & NV \\ C_2 & C_1 & C_2 & C_2 & C_3 & C_2 & NV & NV & -N \\ C_2 & C_2 & C_1 & C_3 & C_2 & C_2 & -N & NV & NV \\ C_2 & C_2 & C_3 & C_1 & C_2 & C_2 & -N & NV & NV \\ C_2 & C_3 & C_2 & C_2 & C_1 & C_2 & NV & NV & -N \\ C_3 & C_2 & C_2 & C_2 & C_2 & C_1 & NV & -N & NV \\ NV & NV & -N & -N & NV & NV & N^2V & N^2 & N^2 \\ -N & NV & NV & NV & NV & -N & N^2 & N^2V & N^2 \\ NV & -N & NV & NV & -N & NV & N^2 & N^2 & N^2V \end{pmatrix}, \tag{A.3.34}$$

with

$$C_1 = N^4 - 3N^2 + 3, \qquad C_2 = 3 - N^2, \qquad C_3 = 3 + N^2. \tag{A.3.35}$$

Similarly, the interference of the tree-level amplitudes $\sum_{\text{spins}} \mathcal{T}_i^* \mathcal{T}_j$ is given by $\mathcal{TT}_{ij}$, where

$$\mathcal{TT} = \frac{64(1-\epsilon)^2(t^2+ut+u^2)^2}{s^2t^2u^2}\ \mathcal{V}^T\mathcal{V}, \tag{A.3.36}$$

and the vector $\mathcal{V}$ is

$$\mathcal{V} = (u,\ t,\ s,\ s,\ t,\ u,\ 0,\ 0,\ 0)\,, \tag{A.3.37}$$

while the interference of the tree-level amplitudes with one-loop amplitudes $\sum_{\text{spins}} \mathcal{T}_i^* \mathcal{L}_j$ is given by $\mathcal{TL}_{ij}$, where

$$\mathcal{TL} = \mathcal{V}^T\mathcal{W}, \tag{A.3.38}$$

and the vector $\mathcal{W}$ is

$$\mathcal{W} = \Big(\mathcal{F}(s,t),\ \mathcal{F}(s,u),\ \mathcal{F}(u,t),\ \mathcal{F}(u,t),\ \mathcal{F}(s,u),\ \mathcal{F}(s,t),\ \mathcal{G},\ \mathcal{G},\ \mathcal{G}\Big). \tag{A.3.39}$$

Here the function $\mathcal{F}(s,t)$ is symmetric under the exchange of s and t, while $\mathcal{G}$ is symmetric under the exchange of any two Mandelstam invariants, so that

$$\mathcal{F}(s,t) = f_1(s,t,u) + f_1(t,s,u), \tag{A.3.40}$$

$$\mathcal{G} = f_2(s,t,u) + f_2(s,u,t) + f_2(t,s,u) + f_2(t,u,s) + f_2(u,s,t) + f_2(u,t,s). \tag{A.3.41}$$

Here f_1 and f_2 are given in terms of the one-loop box integral in $D = 6 - 2\epsilon$ dimensions and the one-loop bubble graph in $D = 4 - 2\epsilon$,

$$\begin{aligned}
f_1(s,t,u) &= \frac{16N(1-2\epsilon)}{s^2t^2}\left[2(1-\epsilon)^2\left(s^4+s^3t+st^3+t^4\right)+3(1-5\epsilon)s^2t^2\right]\mathrm{Box}^6(s,t)\\
&+ \frac{8N_F(1-2\epsilon)}{st}\left[(1-\epsilon)^2\left(s^2+t^2\right)+\epsilon(1+3\epsilon)st\right]\mathrm{Box}^6(s,t)\\
&- \frac{16N(1-\epsilon)}{s^2t^2u\epsilon(3-2\epsilon)}\left[\left(12-22\epsilon+12\epsilon^2+2\epsilon^3\right)s^4+\left(24-58\epsilon+50\epsilon^2-6\epsilon^3-2\epsilon^4\right)s^3t\right.\\
&\qquad +\left(36-99\epsilon+93\epsilon^2-24\epsilon^3-2\epsilon^4\right)s^2t^2+(1-\epsilon)\left(24-50\epsilon+23\epsilon^2\right)st^3\\
&\qquad \left.+4(1-\epsilon)(1-2\epsilon)(3-2\epsilon)t^4\right]\mathrm{Bub}(t)\\
&+ \frac{16N_F}{st^2u(3-2\epsilon)}\left[\left(4-12\epsilon+16\epsilon^2-4\epsilon^3\right)s^3+\left(3-10\epsilon+23\epsilon^2-8\epsilon^3\right)s^2t\right.\\
&\qquad \left.+\left(6-15\epsilon+21\epsilon^2-8\epsilon^3\right)st^2+(1-\epsilon)\left(5-6\epsilon+2\epsilon^2\right)t^3\right]\mathrm{Bub}(t),
\end{aligned} \tag{A.3.42}$$

$$
\begin{aligned}
f_2(s,t,u) &= \frac{32(1-2\epsilon)}{u^2}\left[-4(1-\epsilon)^2 st + 3(1-5\epsilon)u^2\right]\mathrm{Box}^6(u,t) \\
&\quad + \frac{32(1-\epsilon)}{\epsilon s u^2}\left[4(1-2\epsilon)(1-\epsilon)t^2 + (8-17\epsilon)(1-\epsilon)ut\right. \\
&\qquad \left. + \left(6-20\epsilon+15\epsilon^2+\epsilon^3\right)u^2\right]\mathrm{Bub}(s). \qquad \text{(A.3.43)}
\end{aligned}
$$

Series expansions around $\epsilon = 0$ for the one-loop integrals are given in section A.3.3. Finally, the last term of Eq. (A.3.23) that involves $\boldsymbol{H}^{(2)}(\epsilon)$ produces only a single pole in ϵ and is given by

$$
\langle \mathcal{M}^{(0)} | \boldsymbol{H}^{(2)}(\epsilon) | \mathcal{M}^{(0)} \rangle = \frac{e^{\epsilon\gamma}}{4\,\epsilon\,\Gamma(1-\epsilon)} H^{(2)} \langle \mathcal{M}^{(0)} | \mathcal{M}^{(0)} \rangle
$$

where the constant $H^{(2)}$ is

$$
H^{(2)} = \left(2\zeta_3 + \frac{5}{3} + \frac{11}{36}\pi^2\right) N^2 + \frac{20}{27} N_F^2 + \left(-\frac{\pi^2}{18} - \frac{89}{27}\right) N N_F - \frac{N_F}{N}, \qquad \text{(A.3.44)}
$$

and ζ_n is the Riemann Zeta function with $\zeta_2 = \pi^2/6$ and $\zeta_3 = 1.202056\ldots$ In this case $H^{(2)}$ is renormalisation-scheme dependent and Eq. (A.3.44) is valid in the $\overline{\mathrm{MS}}$ scheme.

A.3.2 Two loop contribution - Finite piece

The finite two-loop contribution to $\mathcal{D}^8(s,t,u)$ is defined as

$$
\mathcal{F}inite(s,t,u) = \mathcal{D}^{8\,(2\times 0)}(s,t,u) - \mathcal{P}oles(s,t,u), \qquad \text{(A.3.45)}
$$

where the series expansions of both $\mathcal{D}^{8\,(2\times 0)}(s,t,u)$ and $\mathcal{P}oles(s,t,u)$ are subtracted and set $\epsilon \to 0$. As usual, the polylogarithms $\mathrm{Li}_n(w)$ are defined by

$$
\begin{aligned}
\mathrm{Li}_n(w) &= \int_0^w \frac{dt}{t}\mathrm{Li}_{n-1}(t) \qquad \text{for } n = 2,3,4 \\
\mathrm{Li}_2(w) &= -\int_0^w \frac{dt}{t}\log(1-t). \qquad \text{(A.3.46)}
\end{aligned}
$$

Using the standard polylogarithm identities, polylogarithms with arguments x, $1-x$ and $(x-1)/x$ are retained, where

$$
x = -\frac{t}{s}, \qquad y = -\frac{u}{s} = 1 - x, \qquad z = -\frac{u}{t} = \frac{x-1}{x}. \qquad \text{(A.3.47)}
$$

For convenience, the following logarithms are introduced

$$
X = \log\left(\frac{-t}{s}\right), \qquad Y = \log\left(\frac{-u}{s}\right), \qquad \mathrm{Ls} = \log\left(\frac{s}{\mu^2}\right), \qquad \text{(A.3.48)}
$$

where μ is the renormalisation scale.

The results are shown by grouping terms according to the power of the number of colours N and the number of light quarks N_F, so that

$$Finite(s,t,u) = V\left(N^4 A + N^2 B + N^3 N_F C + N N_F D + N^2 N_F^2 E + N_F^2 F \right), \quad \text{(A.3.49)}$$

where

$$\begin{aligned}
A \;=\; & \left\{ \left(48\,\mathrm{Li}_4(x) - 48\,\mathrm{Li}_4(y) - 128\,\mathrm{Li}_4(z) + 40\,\mathrm{Li}_3(x)\,X - 64\,\mathrm{Li}_3(x)\,Y - \frac{98}{3}\,\mathrm{Li}_3(x) \right.\right. \\
& + 64\,\mathrm{Li}_3(y)\,X - 40\,\mathrm{Li}_3(y)\,Y + 18\,\mathrm{Li}_3(y) + \frac{98}{3}\,\mathrm{Li}_2(x)\,X - \frac{16}{3}\,\mathrm{Li}_2(x)\,\pi^2 - 18\,\mathrm{Li}_2(y)\,Y \\
& - \frac{37}{6}\,X^4 + 28\,X^3\,Y - \frac{23}{3}\,X^3 - 16\,X^2\,Y^2 + \frac{49}{3}\,X^2\,Y - \frac{35}{3}\,X^2\,\pi^2 - \frac{38}{3}\,X^2 - \frac{22}{3}\,\mathrm{Ls}\,X^2 \\
& - \frac{20}{3}\,X\,Y^3 - 9\,X\,Y^2 + 8\,X\,Y\,\pi^2 + 10\,X\,Y - \frac{31}{12}\,X\,\pi^2 - 22\,\zeta_3\,X + \frac{22}{3}\,\mathrm{Ls}\,X + \frac{37}{27}\,X \\
& + \frac{11}{6}\,Y^4 - \frac{41}{9}\,Y^3 - \frac{11}{3}\,Y^2\,\pi^2 - \frac{22}{3}\,\mathrm{Ls}\,Y^2 + \frac{266}{9}\,Y^2 - \frac{35}{12}\,Y\,\pi^2 + \frac{418}{9}\,\mathrm{Ls}\,Y + \frac{257}{9}\,Y \\
& + 18\,\zeta_3\,Y - \frac{31}{30}\,\pi^4 - \frac{11}{9}\,\mathrm{Ls}\,\pi^2 + \frac{31}{9}\,\pi^2 + \frac{242}{9}\,\mathrm{Ls}^2 + \frac{418}{9}\,\zeta_3 + \frac{2156}{27}\,\mathrm{Ls} \\
& \left. - \frac{11093}{81} - 8\,\mathrm{Ls}\,\zeta_3 \right) \frac{t^2}{s^2} \\
& + \left(-256\,\mathrm{Li}_4(x) - 96\,\mathrm{Li}_4(y) + 96\,\mathrm{Li}_4(z) + 80\,\mathrm{Li}_3(x)\,X + 48\,\mathrm{Li}_3(x)\,Y - \frac{64}{3}\,\mathrm{Li}_3(x) \right. \\
& - 48\,\mathrm{Li}_3(y)\,X + 96\,\mathrm{Li}_3(y)\,Y - \frac{304}{3}\,\mathrm{Li}_3(y) + \frac{64}{3}\,\mathrm{Li}_2(x)\,X - \frac{32}{3}\,\mathrm{Li}_2(x)\,\pi^2 + \frac{304}{3}\,\mathrm{Li}_2(y)\,Y \\
& + \frac{26}{3}\,X^4 - \frac{64}{3}\,X^3\,Y - \frac{64}{3}\,X^3 + 20\,X^2\,Y^2 + \frac{136}{3}\,X^2\,Y + 24\,X^2\,\pi^2 + 76\,X^2 - \frac{88}{3}\,\mathrm{Ls}\,X^2 \\
& + \frac{8}{3}\,X\,Y^3 + \frac{104}{3}\,X\,Y^2 - \frac{16}{3}\,X\,Y\,\pi^2 + \frac{176}{3}\,\mathrm{Ls}\,X\,Y - \frac{136}{3}\,X\,Y - \frac{50}{3}\,X\,\pi^2 - 48\,\zeta_3\,X \\
& + \frac{2350}{27}\,X + \frac{440}{3}\,\mathrm{Ls}\,X + 4\,Y^4 - \frac{176}{9}\,Y^3 + \frac{4}{3}\,Y^2\,\pi^2 - \frac{176}{3}\,\mathrm{Ls}\,Y^2 - \frac{494}{9}\,Y\,\pi^2 + \frac{5392}{27}\,Y \\
& - 64\,\zeta_3\,Y + \frac{496}{45}\,\pi^4 - \frac{308}{9}\,\mathrm{Ls}\,\pi^2 + \frac{200}{9}\,\pi^2 + \frac{968}{9}\,\mathrm{Ls}^2 + \frac{8624}{27}\,\mathrm{Ls} - \frac{44372}{81} \\
& \left. + \frac{1864}{9}\,\zeta_3 - 32\,\mathrm{Ls}\,\zeta_3 \right) \frac{t}{u} \\
& + \left(\frac{88}{3}\,\mathrm{Li}_3(x) - \frac{88}{3}\,\mathrm{Li}_2(x)\,X + 2\,X^4 - 8\,X^3\,Y - \frac{220}{9}\,X^3 + 12\,X^2\,Y^2 + \frac{88}{3}\,X^2\,Y + \frac{8}{3}\,X^2\,\pi^2 \right. \\
& - \frac{88}{3}\,\mathrm{Ls}\,X^2 + \frac{304}{9}\,X^2 - 8\,X\,Y^3 - \frac{16}{3}\,X\,Y\,\pi^2 + \frac{176}{3}\,\mathrm{Ls}\,X\,Y - \frac{77}{3}\,X\,\pi^2 + \frac{1616}{27}\,X \\
& + \frac{968}{9}\,\mathrm{Ls}\,X - 8\,\zeta_3\,X + 4\,Y^4 - \frac{176}{9}\,Y^3 - \frac{20}{3}\,Y^2\,\pi^2 - \frac{176}{3}\,\mathrm{Ls}\,Y^2 - \frac{638}{9}\,Y\,\pi^2 - 16\,\zeta_3\,Y \\
& + \frac{5392}{27}\,Y - \frac{4}{15}\,\pi^4 - \frac{308}{9}\,\mathrm{Ls}\,\pi^2 - 20\,\pi^2 - 32\,\mathrm{Ls}\,\zeta_3 + \frac{1408}{9}\,\zeta_3 + \frac{968}{9}\,\mathrm{Ls}^2 - \frac{44372}{81} \\
& \left. + \frac{8624}{27}\,\mathrm{Ls} \right) \frac{t^2}{u^2} \\
& + \left(\frac{44}{3}\,\mathrm{Li}_3(x) - \frac{44}{3}\,\mathrm{Li}_2(x)\,X - X^4 + \frac{110}{9}\,X^3 - \frac{22}{3}\,X^2\,Y + \frac{14}{3}\,X^2\,\pi^2 + \frac{44}{3}\,\mathrm{Ls}\,X^2 \right.
\end{aligned}$$

$$
\begin{aligned}
&-\frac{152}{9}\,X^2 - 10\,X\,Y + \frac{11}{2}\,X\,\pi^2 + 4\,\zeta_3\,X - \frac{484}{9}\,\mathrm{Ls}\,X - \frac{808}{27}\,X + \frac{7}{30}\,\pi^4 - \frac{31}{9}\,\pi^2 \\
&+\frac{11}{9}\,\mathrm{Ls}\,\pi^2 - \frac{418}{9}\,\zeta_3 - \frac{242}{9}\,\mathrm{Ls}^2 - \frac{2156}{27}\,\mathrm{Ls} + 8\,\mathrm{Ls}\,\zeta_3 + \frac{11093}{81}\Bigg)\frac{ut}{s^2} \\
&+\Bigg(-176\,\mathrm{Li}_4(x) + 88\,\mathrm{Li}_3(x)\,X - 168\,\mathrm{Li}_3(x)\,Y - \frac{206}{3}\,\mathrm{Li}_3(x) + \frac{206}{3}\,\mathrm{Li}_2(x)\,X \\
&+\frac{65}{6}\,X^4 - \frac{40}{3}\,X^3\,Y - \frac{295}{9}\,X^3 - 15\,X^2\,Y^2 + \frac{115}{3}\,X^2\,Y + \frac{29}{3}\,X^2\,\pi^2 - \frac{670}{9}\,X^2 \\
&-\frac{242}{3}\,\mathrm{Ls}\,X^2 + \frac{64}{3}\,X\,Y\,\pi^2 + \frac{209}{3}\,X\,Y + 44\,\mathrm{Ls}\,X\,Y - \frac{1811}{36}\,X\,\pi^2 + \frac{8983}{27}\,X \\
&+\frac{1870}{9}\,\mathrm{Ls}\,X - 18\,\zeta_3\,X + \frac{31}{20}\,\pi^4 - \frac{361}{18}\,\pi^2 - \frac{517}{18}\,\mathrm{Ls}\,\pi^2 + \frac{1331}{9}\,\mathrm{Ls}^2 + \frac{12452}{27}\,\mathrm{Ls} \\
&+\frac{1543}{9}\,\zeta_3 - \frac{129475}{162} - 44\,\mathrm{Ls}\,\zeta_3\Bigg)\Bigg\} + \Big\{u \leftrightarrow t\Big\},
\end{aligned}
\tag{A.3.50}
$$

$$
\begin{aligned}
B \;=\; &\Bigg\{\Bigg(-288\,\mathrm{Li}_4(x) + 480\,\mathrm{Li}_4(y) - 288\,\mathrm{Li}_4(z) + 240\,\mathrm{Li}_3(x)\,X - 144\,\mathrm{Li}_3(x)\,Y \\
&+224\,\mathrm{Li}_3(x) + 144\,\mathrm{Li}_3(y)\,X - 432\,\mathrm{Li}_3(y)\,Y - 224\,\mathrm{Li}_3(y) + 48\,\mathrm{Li}_2(x)\,X^2 \\
&-224\,\mathrm{Li}_2(x)\,X - 176\,\mathrm{Li}_2(x)\,\pi^2 + 48\,\mathrm{Li}_2(y)\,Y^2 + 224\,\mathrm{Li}_2(y)\,Y - 16\,X^4 + 112\,X^3\,Y \\
&-\frac{556}{3}\,X^3 - 48\,X^2\,Y^2 + 180\,X^2\,Y - 40\,X^2\,\pi^2 + 220\,X^2 - 32\,X\,Y^3 - 92\,X\,Y^2 \\
&-16\,X\,Y\,\pi^2 - \frac{376}{3}\,X\,Y - 16\,X\,\pi^2 - 80\,X + 96\,\zeta_3\,X + 8\,Y^4 + \frac{292}{3}\,Y^3 - 32\,Y^2\,\pi^2 \\
&-\frac{284}{3}\,Y^2 + 16\,Y\,\pi^2 + 80\,Y - 96\,\zeta_3\,Y + \frac{38}{5}\,\pi^4 - 18\,\pi^2\Bigg)\frac{t^2}{s^2} \\
&+\Bigg(-576\,\mathrm{Li}_4(x) + 384\,\mathrm{Li}_4(y) - 1152\,\mathrm{Li}_4(z) + 1056\,\mathrm{Li}_3(x)\,X - 768\,\mathrm{Li}_3(x)\,Y \\
&+448\,\mathrm{Li}_3(x) + 768\,\mathrm{Li}_3(y)\,X - 768\,\mathrm{Li}_3(y)\,Y + 896\,\mathrm{Li}_3(y) - 192\,\mathrm{Li}_2(x)\,X^2 \\
&-448\,\mathrm{Li}_2(x)\,X - 544\,\mathrm{Li}_2(x)\,\pi^2 - 384\,\mathrm{Li}_2(y)\,X\,Y - 896\,\mathrm{Li}_2(y)\,Y - 28\,X^4 + 144\,X^3\,Y \\
&+\frac{320}{3}\,X^3 - 336\,X^2\,Y^2 - 224\,X^2\,Y - 40\,X^2\,\pi^2 - 64\,X^2 - 32\,X\,Y^3 + 128\,X\,Y^2 \\
&-64\,X\,Y\,\pi^2 + \frac{1888}{3}\,X\,Y - 288\,X\,\pi^2 + 160\,X - 1248\,\zeta_3\,X - 240\,Y^2\,\pi^2 - 928\,Y\,\pi^2 \\
&+768\,\zeta_3\,Y + \frac{1216}{15}\,\pi^4 - \frac{1912}{3}\,\pi^2 - 448\,\zeta_3\Bigg)\frac{t}{u} \\
&+\Bigg(-384\,\mathrm{Li}_4(y) - 384\,\mathrm{Li}_4(z) + 384\,\mathrm{Li}_3(x)\,X - 384\,\mathrm{Li}_3(x)\,Y + 384\,\mathrm{Li}_3(y)\,X \\
&-192\,\mathrm{Li}_2(x)\,X^2 - 192\,\mathrm{Li}_2(x)\,\pi^2 - 384\,\mathrm{Li}_2(y)\,X\,Y - 8\,X^4 - 32\,X^3\,Y - 176\,X^3 \\
&-192\,X^2\,Y^2 + 352\,X^2\,Y - 80\,X^2\,\pi^2 + \frac{752}{3}\,X^2 - 32\,X\,Y\,\pi^2 - 176\,X\,\pi^2 - 384\,\zeta_3\,X \\
&-96\,Y^2\,\pi^2 - 352\,Y\,\pi^2 + 384\,\zeta_3\,Y + 56\,\pi^4 - \frac{968}{3}\,\pi^2\Bigg)\frac{t^2}{u^2} \\
&+\Bigg(-192\,\mathrm{Li}_4(x) + 192\,\mathrm{Li}_3(x)\,X - 96\,\mathrm{Li}_2(x)\,X^2 - 4\,X^4 - 32\,X^3\,Y + 88\,X^3 \\
&+12\,X^2\,Y^2 - 88\,X^2\,Y + 48\,X^2\,\pi^2 - \frac{376}{3}\,X^2 - 48\,X\,Y\,\pi^2 + \frac{376}{3}\,X\,Y
\end{aligned}
$$

$$
\begin{aligned}
&+\frac{64}{15}\,\pi^4 + 18\,\pi^2\Bigg)\frac{ut}{s^2}\\
&+\Bigg(48\,\mathrm{Li}_3(x)\,X + 144\,\mathrm{Li}_3(x)\,Y + 672\,\mathrm{Li}_3(x) - 48\,\mathrm{Li}_2(x)\,X^2 - 672\,\mathrm{Li}_2(x)\,X + 16\,X^4\\
&-32\,X^3\,Y - \frac{4}{3}\,X^3 + 24\,X^2\,Y^2 + 12\,X^2\,Y - 192\,X^2\,\pi^2 + \frac{1444}{3}\,X^2 + 72\,X\,Y\,\pi^2\\
&+\frac{80}{3}\,X\,Y - 624\,X\,\pi^2 + 80\,X - 288\,\zeta_3\,X + \frac{509}{15}\,\pi^4 - 707\,\pi^2 - 36 - 2800\,\zeta_3\Bigg)\Bigg\}\\
&+\Big\{u \leftrightarrow t\Big\}, \qquad\qquad (A.3.51)
\end{aligned}
$$

$$
\begin{aligned}
C \;=\; &\Bigg\{\Bigg(-24\,\mathrm{Li}_4(x) + 24\,\mathrm{Li}_4(y) + 112\,\mathrm{Li}_4(z) - 44\,\mathrm{Li}_3(x)\,X + 56\,\mathrm{Li}_3(x)\,Y + \frac{74}{3}\,\mathrm{Li}_3(x)\\
&-56\,\mathrm{Li}_3(y)\,X + 44\,\mathrm{Li}_3(y)\,Y - 22\,\mathrm{Li}_3(y) - \frac{74}{3}\,\mathrm{Li}_2(x)\,X + \frac{32}{3}\,\mathrm{Li}_2(x)\,\pi^2 + 22\,\mathrm{Li}_2(y)\,Y\\
&+\frac{25}{4}\,X^4 - 26\,X^3\,Y + 4\,X^3 + 14\,X^2\,Y^2 - \frac{37}{3}\,X^2\,Y + 7\,X^2\,\pi^2 + \frac{27}{2}\,X^2 + 5\,\mathrm{Ls}\,X^2\\
&+\frac{22}{3}\,X\,Y^3 + 11\,X\,Y^2 - 4\,X\,Y\,\pi^2 - 11\,X\,Y + \frac{31}{6}\,X\,\pi^2 + 12\,\zeta_3\,X - \frac{637}{27}\,X - \frac{26}{3}\,\mathrm{Ls}\,X\\
&-\frac{19}{12}\,Y^4 - \frac{16}{9}\,Y^3 + \frac{7}{3}\,Y^2\,\pi^2 - \frac{221}{18}\,Y^2 - \frac{7}{3}\,\mathrm{Ls}\,Y^2 - \frac{25}{6}\,Y\,\pi^2 + \frac{175}{9}\,Y - 12\,\zeta_3\,Y\\
&-\frac{98}{9}\,\mathrm{Ls}\,Y + \frac{1}{5}\,\pi^4 + \frac{2}{9}\,\mathrm{Ls}\,\pi^2 + \frac{203}{54}\,\pi^2 - \frac{4}{9}\,\zeta_3 - \frac{88}{9}\,\mathrm{Ls}^2 + \frac{4849}{162} - \frac{386}{27}\,\mathrm{Ls}\Bigg)\frac{t^2}{s^2}\\
&+\Bigg(224\,\mathrm{Li}_4(x) + 48\,\mathrm{Li}_4(y) - 48\,\mathrm{Li}_4(z) - 88\,\mathrm{Li}_3(x)\,X - 24\,\mathrm{Li}_3(x)\,Y + \frac{124}{3}\,\mathrm{Li}_3(x)\\
&+24\,\mathrm{Li}_3(y)\,X - 48\,\mathrm{Li}_3(y)\,Y + \frac{280}{3}\,\mathrm{Li}_3(y) - \frac{124}{3}\,\mathrm{Li}_2(x)\,X + \frac{64}{3}\,\mathrm{Li}_2(x)\,\pi^2\\
&-\frac{280}{3}\,\mathrm{Li}_2(y)\,Y - \frac{31}{6}\,X^4 + 6\,X^3\,Y - \frac{4}{3}\,X^3 - 3\,X^2\,Y^2 - \frac{56}{3}\,X^2\,Y - \frac{55}{3}\,X^2\,\pi^2 - 2\,\mathrm{Ls}\,X^2\\
&-\frac{70}{3}\,X^2 - 6\,X\,Y^3 - 26\,X\,Y^2 - \frac{2}{3}\,X\,Y\,\pi^2 + 4\,\mathrm{Ls}\,X\,Y + \frac{148}{3}\,X\,Y - \frac{22}{3}\,X\,\pi^2\\
&-\frac{124}{3}\,\mathrm{Ls}\,X + \frac{938}{27}\,X + 64\,\zeta_3\,X + \frac{32}{9}\,Y^3 - 3\,Y^2\,\pi^2 + \frac{32}{3}\,\mathrm{Ls}\,Y^2 - \frac{4}{9}\,Y\,\pi^2 - \frac{1096}{27}\,Y\\
&+24\,\zeta_3\,Y - \frac{829}{90}\,\pi^4 - \frac{10}{9}\,\mathrm{Ls}\,\pi^2 - \frac{356}{27}\,\pi^2 - \frac{352}{9}\,\mathrm{Ls}^2 - \frac{1544}{27}\,\mathrm{Ls} - \frac{388}{9}\,\zeta_3 + \frac{9698}{81}\Bigg)\frac{t}{u}\\
&+\Bigg(-\frac{16}{3}\,\mathrm{Li}_3(x) + \frac{16}{3}\,\mathrm{Li}_2(x)\,X + \frac{40}{9}\,X^3 - \frac{16}{3}\,X^2\,Y + \frac{22}{9}\,X^2 + \frac{16}{3}\,\mathrm{Ls}\,X^2 - \frac{32}{3}\,\mathrm{Ls}\,X\,Y\\
&+\frac{14}{3}\,X\,\pi^2 - \frac{224}{27}\,X - \frac{352}{9}\,\mathrm{Ls}\,X + \frac{32}{9}\,Y^3 + \frac{32}{3}\,\mathrm{Ls}\,Y^2 + \frac{116}{9}\,Y\,\pi^2 - \frac{1096}{27}\,Y + \frac{56}{9}\,\mathrm{Ls}\,\pi^2\\
&+\frac{340}{27}\,\pi^2 - \frac{1544}{27}\,\mathrm{Ls} + \frac{9698}{81} + \frac{32}{9}\,\zeta_3 - \frac{352}{9}\,\mathrm{Ls}^2\Bigg)\frac{t^2}{u^2}\\
&+\Bigg(-\frac{8}{3}\,\mathrm{Li}_3(x) + \frac{8}{3}\,\mathrm{Li}_2(x)\,X - \frac{20}{9}\,X^3 + \frac{4}{3}\,X^2\,Y - \frac{11}{9}\,X^2 - \frac{8}{3}\,\mathrm{Ls}\,X^2 + 11\,X\,Y - X\,\pi^2\\
&+\frac{112}{27}\,X + \frac{176}{9}\,\mathrm{Ls}\,X - \frac{2}{9}\,\mathrm{Ls}\,\pi^2 - \frac{203}{54}\,\pi^2 + \frac{88}{9}\,\mathrm{Ls}^2 - \frac{4849}{162} + \frac{386}{27}\,\mathrm{Ls} + \frac{4}{9}\,\zeta_3\Bigg)\frac{ut}{s^2}
\end{aligned}
$$

$$
\begin{aligned}
&+\left(136\,\mathrm{Li}_4(x) - 68\,\mathrm{Li}_3(x)\,X + 120\,\mathrm{Li}_3(x)\,Y + \frac{206}{3}\,\mathrm{Li}_3(x) - \frac{206}{3}\,\mathrm{Li}_2(x)\,X - \frac{71}{12}\,X^4\right.\\
&+\frac{14}{3}\,X^3\,Y - \frac{68}{9}\,X^3 + 15\,X^2\,Y^2 + \frac{5}{3}\,X^2\,Y - \frac{29}{3}\,X^2\,\pi^2 + \frac{973}{18}\,X^2 + \frac{77}{3}\,\mathrm{Ls}\,X^2\\
&-\frac{62}{3}\,X\,Y\,\pi^2 - \frac{139}{6}\,X\,Y - 8\,\mathrm{Ls}\,X\,Y - \frac{317}{18}\,X\,\pi^2 - \frac{1375}{27}\,X - \frac{626}{9}\,\mathrm{Ls}\,X + 4\,\zeta_3\,X\\
&\left.-\frac{47}{30}\,\pi^4 + \frac{3799}{108}\,\pi^2 + \frac{47}{9}\,\mathrm{Ls}\,\pi^2 - \frac{484}{9}\,\mathrm{Ls}^2 - \frac{2825}{27}\,\mathrm{Ls} + \frac{932}{9}\,\zeta_3 + \frac{70025}{324}\right)\Bigg\}\\
&+\Big\{u \leftrightarrow t\Big\},
\end{aligned}
\tag{A.3.52}
$$

$$
\begin{aligned}
D \;=\; &\Bigg\{\Bigg(24\,\mathrm{Li}_4(x) - 24\,\mathrm{Li}_4(y) + 88\,\mathrm{Li}_4(z) - 52\,\mathrm{Li}_3(x)\,X + 36\,\mathrm{Li}_3(x)\,Y - \frac{46}{3}\,\mathrm{Li}_3(x)\\
&-36\,\mathrm{Li}_3(y)\,X + 52\,\mathrm{Li}_3(y)\,Y + \frac{46}{3}\,\mathrm{Li}_3(y) - 4\,\mathrm{Li}_2(x)\,X^2 + \frac{46}{3}\,\mathrm{Li}_2(x)\,X + \frac{44}{3}\,\mathrm{Li}_2(x)\,\pi^2\\
&-16\,\mathrm{Li}_2(y)\,X\,Y + 4\,\mathrm{Li}_2(y)\,Y^2 - \frac{46}{3}\,\mathrm{Li}_2(y)\,Y + \frac{79}{12}\,X^4 - \frac{82}{3}\,X^3\,Y + \frac{817}{18}\,X^3 + 3\,X^2\,Y^2\\
&-\frac{184}{3}\,X^2\,Y + \frac{13}{3}\,X^2\,\pi^2 - \frac{545}{6}\,X^2 + \frac{38}{3}\,X\,Y^3 + \frac{136}{3}\,X\,Y^2 + \frac{4}{3}\,X\,Y\,\pi^2 + \frac{155}{3}\,X\,Y\\
&-10\,X\,\pi^2 - 32\,\zeta_3\,X + \frac{76}{3}\,X - \frac{35}{12}\,Y^4 - \frac{529}{18}\,Y^3 + 3\,Y^2\,\pi^2 + \frac{235}{6}\,Y^2 + 10\,Y\,\pi^2 - \frac{76}{3}\,Y\\
&+32\,\zeta_3\,Y - \frac{11}{30}\,\pi^4 + \frac{7}{2}\,\pi^2 + 8\,\zeta_3 + 2\,\mathrm{Ls} - \frac{55}{6}\Bigg)\frac{t^2}{s^2}\\
&+\Bigg(176\,\mathrm{Li}_4(x) - 48\,\mathrm{Li}_4(y) + 48\,\mathrm{Li}_4(z) - 104\,\mathrm{Li}_3(x)\,X + 32\,\mathrm{Li}_3(x)\,Y - \frac{92}{3}\,\mathrm{Li}_3(x)\\
&-32\,\mathrm{Li}_3(y)\,X + 64\,\mathrm{Li}_3(y)\,Y - \frac{184}{3}\,\mathrm{Li}_3(y) - 8\,\mathrm{Li}_2(x)\,X^2 + \frac{92}{3}\,\mathrm{Li}_2(x)\,X + \frac{160}{3}\,\mathrm{Li}_2(x)\,\pi^2\\
&+16\,\mathrm{Li}_2(y)\,X\,Y - 16\,\mathrm{Li}_2(y)\,Y^2 + \frac{184}{3}\,\mathrm{Li}_2(y)\,Y - \frac{23}{6}\,X^4 - 10\,X^3\,Y - \frac{385}{9}\,X^3 + 19\,X^2\,Y^2\\
&+\frac{161}{3}\,X^2\,Y - 17\,X^2\,\pi^2 + \frac{80}{3}\,X^2 - \frac{14}{3}\,X\,Y^3 - 87\,X\,Y^2 - \frac{26}{3}\,X\,Y\,\pi^2 - 260\,X\,Y\\
&+\frac{215}{3}\,X\,\pi^2 - \frac{152}{3}\,X + 168\,\zeta_3\,X + 7\,Y^2\,\pi^2 + \frac{545}{3}\,Y\,\pi^2 + 8\,Y - 32\,\zeta_3\,Y - \frac{571}{90}\,\pi^4\\
&+\frac{742}{3}\,\pi^2 + \frac{188}{3}\,\zeta_3 - \frac{110}{3} + 8\,\mathrm{Ls}\Bigg)\frac{t}{u}\\
&+\Bigg(32\,X^3 - 64\,X^2\,Y - \frac{310}{3}\,X^2 + 32\,X\,\pi^2 + 64\,Y\,\pi^2 + 8\,Y + \frac{352}{3}\,\pi^2 + 8\,\mathrm{Ls}\\
&-\frac{110}{3} + 32\,\zeta_3\Bigg)\frac{t^2}{u^2}\\
&+\Bigg(-16\,X^3 + 16\,X^2\,Y + \frac{155}{3}\,X^2 - \frac{155}{3}\,X\,Y - \frac{7}{2}\,\pi^2 - 8\,\zeta_3 - 2\,\mathrm{Ls} + \frac{55}{6}\Bigg)\frac{ut}{s^2}\\
&+\Bigg(64\,\mathrm{Li}_4(x) - 20\,\mathrm{Li}_3(x)\,X - 108\,\mathrm{Li}_3(x)\,Y - 46\,\mathrm{Li}_3(x) - 12\,\mathrm{Li}_2(x)\,X^2\\
&+46\,\mathrm{Li}_2(x)\,X + \frac{5}{12}\,X^4 - 10\,X^3\,Y - \frac{401}{18}\,X^3 - \frac{21}{2}\,X^2\,Y^2 - \frac{34}{3}\,X^2\,Y - \frac{1}{3}\,X^2\,\pi^2\\
&-\frac{1303}{6}\,X^2 - \frac{16}{3}\,X\,Y\,\pi^2 - \frac{11}{6}\,X\,Y + \frac{340}{3}\,X\,\pi^2 + 104\,\zeta_3\,X - \frac{52}{3}\,X - \frac{67}{20}\,\pi^4
\end{aligned}
$$

$$+\frac{2981}{12}\,\pi^2 + 11\,\mathrm{Ls} + \frac{1166}{3}\,\zeta_3 - \frac{461}{12}\Bigg)\Bigg\} + \Bigg\{u \leftrightarrow t\Bigg\}, \tag{A.3.53}$$

$$\begin{aligned}
E \;=\; & \Bigg\{\Bigg(-\frac{1}{3}\,X^3 - \frac{2}{3}\,\mathrm{Ls}\,X^2 + \frac{2}{3}\,X^2 - \frac{2}{3}\,X\,\pi^2 + \frac{4}{3}\,\mathrm{Ls}\,X - \frac{2}{3}\,X + \frac{1}{3}\,Y^3 + \frac{2}{9}\,Y^2 + \frac{2}{3}\,\mathrm{Ls}\,Y^2 \\
& + \frac{2}{3}\,Y\,\pi^2 + \frac{4}{9}\,\mathrm{Ls}\,Y + \frac{2}{3}\,Y + \frac{2}{27}\,\pi^2 + \frac{8}{9}\,\mathrm{Ls}^2\Bigg)\,\frac{t^2}{s^2} \\
& + \Bigg(\frac{2}{3}\,X^3 - \frac{2}{3}\,X^2\,Y + \frac{4}{3}\,X^2 + \frac{4}{3}\,\mathrm{Ls}\,X^2 - \frac{2}{3}\,X\,Y^2 - \frac{8}{3}\,\mathrm{Ls}\,X\,Y + \frac{2}{3}\,X\,\pi^2 + \frac{8}{3}\,\mathrm{Ls}\,X \\
& + \frac{4}{3}\,X - \frac{2}{3}\,Y\,\pi^2 - \frac{52}{27}\,\pi^2 + \frac{4}{3}\,\mathrm{Ls}\,\pi^2 + \frac{32}{9}\,\mathrm{Ls}^2\Bigg)\,\frac{t}{u} \\
& + \Bigg(\frac{16}{9}\,X^2 + \frac{32}{9}\,\mathrm{Ls}\,X - \frac{40}{27}\,\pi^2 + \frac{32}{9}\,\mathrm{Ls}^2\Bigg)\,\frac{t^2}{u^2} \\
& + \Bigg(-\frac{8}{9}\,X^2 - \frac{16}{9}\,\mathrm{Ls}\,X - \frac{2}{27}\,\pi^2 - \frac{8}{9}\,\mathrm{Ls}^2\Bigg)\,\frac{ut}{s^2} \\
& + \Bigg(-X^3 - 2\,\mathrm{Ls}\,X^2 + \frac{26}{9}\,X^2 - 2\,X\,\pi^2 + \frac{10}{3}\,X + \frac{52}{9}\,\mathrm{Ls}\,X - \frac{43}{27}\,\pi^2 + \frac{44}{9}\,\mathrm{Ls}^2 \\
& + \frac{1}{2} + 4\,\mathrm{Ls}\Bigg)\Bigg\} + \Bigg\{u \leftrightarrow t\Bigg\},
\end{aligned} \tag{A.3.54}$$

$$\begin{aligned}
F \;=\; & \Bigg\{\frac{2}{3}\Bigg(-X + Y\Bigg)\Bigg(3\,X^2 - 4\,X\,Y - 14\,X + 3\,Y^2 - 6\,Y + 2\,\pi^2 + 4\Bigg)\,\frac{t^2}{s^2} \\
& + \Bigg(4\,X^3 - \frac{8}{3}\,X^2\,Y - \frac{8}{3}\,X^2 + \frac{8}{3}\,X\,Y^2 + \frac{80}{3}\,X\,Y - 4\,X\,\pi^2 + \frac{16}{3}\,X - \frac{8}{3}\,Y\,\pi^2 - 24\,\pi^2\Bigg)\,\frac{t}{u} \\
& - \frac{32}{3}\Bigg(-X^2 + \pi^2\Bigg)\,\frac{t^2}{u^2} + \Bigg(-\frac{16}{3}\,X^2 + \frac{16}{3}\,X\,Y\Bigg)\,\frac{ut}{s^2} \\
& + \Bigg(\frac{2}{3}\,X^3 + 2\,X^2\,Y + 20\,X^2 + \frac{4}{3}\,X\,Y - \frac{16}{3}\,X\,\pi^2 + \frac{8}{3}\,X - \frac{64}{3}\,\pi^2\Bigg)\Bigg\} + \Bigg\{u \leftrightarrow t\Bigg\}.
\end{aligned} \tag{A.3.55}$$

A.3.3 Master integrals

In this appendix, the expansions for the one-loop box integrals in $D = 6 - 2\epsilon$ are listed. The results are given in the physical region $s > 0$, $u, t < 0$, with the coefficients written in terms of logarithms and polylogarithms that are real in this domain. More precisely, the notation of Eqs. (A.3.47) and (A.3.48) is used to define the arguments of the logarithms and polylogarithms. The polylogarithms are defined as in Eq. (A.3.46).

The box integrals have the expansion

$$\begin{aligned}\mathrm{Box}^6(u,t) &= \frac{e^{\epsilon\gamma}\Gamma\left(1+\epsilon\right)\Gamma\left(1-\epsilon\right)^2}{2s\Gamma\left(1-2\epsilon\right)\left(1-2\epsilon\right)}\left(\frac{\mu^2}{s}\right)^{\epsilon}\left\{\frac{1}{2}\left[(X-Y)^2+\pi^2\right]\right.\\ &+2\epsilon\left[\mathrm{Li}_3(x)-X\mathrm{Li}_2(x)-\frac{1}{3}X^3-\frac{\pi^2}{2}X\right]\\ &-2\epsilon^2\left[\mathrm{Li}_4(x)+Y\mathrm{Li}_3(x)-\frac{1}{2}X^2\mathrm{Li}_2(x)-\frac{1}{8}X^4-\frac{1}{6}X^3Y+\frac{1}{4}X^2Y^2\right.\\ &\left.\left.-\frac{\pi^2}{4}X^2-\frac{\pi^2}{3}XY-\frac{\pi^4}{45}\right]+(u\leftrightarrow t)\right\}+\mathcal{O}\left(\epsilon^3\right), \quad \text{(A.3.56)}\end{aligned}$$

and

$$\begin{aligned}\mathrm{Box}^6(s,t) &= \frac{e^{\epsilon\gamma}\Gamma(1+\epsilon)\Gamma(1-\epsilon)^2}{2u\Gamma(1-2\epsilon)(1-2\epsilon)}\left(-\frac{\mu^2}{u}\right)^{\epsilon}\left\{\left(X^2+2i\pi X\right)\right.\\ &+\epsilon\left[\left(-2\mathrm{Li}_3(x)+2X\mathrm{Li}_2(x)-\frac{2}{3}X^3+2YX^2-\pi^2X+2\zeta_3\right)\right.\\ &\left.+i\pi\left(2\mathrm{Li}_2(x)+4YX-X^2-\frac{\pi^2}{3}\right)\right]\\ &+\epsilon^2\left[\left(2\mathrm{Li}_4(z)+2\mathrm{Li}_4(y)-2Y\mathrm{Li}_3(x)-2X\mathrm{Li}_3(y)+(2XY-X^2-\pi^2)\mathrm{Li}_2(x)\right.\right.\\ &+\frac{1}{3}X^4-\frac{5}{3}X^3Y+\frac{3}{2}X^2Y^2+\frac{2}{3}\pi^2X^2-2\pi^2XY+2Y\zeta_3+\frac{1}{6}\pi^4\Big)\\ &+i\pi\Big(-2\mathrm{Li}_3(x)-2\mathrm{Li}_3(y)+2Y\mathrm{Li}_2(x)+\frac{1}{3}X^3-2X^2Y+3XY^2\\ &\left.\left.-\frac{\pi^2}{3}Y+2\zeta_3\Big)\right]\right\}+\mathcal{O}\left(\epsilon^3\right). \quad \text{(A.3.57)}\end{aligned}$$

$\mathrm{Box}^6(s,u)$ is obtained from Eq. (A.3.57) by exchanging u and t.

Finally, the one-loop bubble integral in $D=4-2\epsilon$ dimensions is given by

$$\mathrm{Bub}(s)=\frac{e^{\epsilon\gamma}\Gamma\left(1+\epsilon\right)\Gamma\left(1-\epsilon\right)^2}{\Gamma\left(2-2\epsilon\right)\epsilon}\left(-\frac{\mu^2}{s}\right)^{\epsilon}. \quad \text{(A.3.58)}$$

A.3.4 One-loop self-interference contribution - Pole piece

The one-loop contribution is decomposed as a sum of two terms

$$\mathcal{D}^{8\,(1\times1)}(s,t,u)=\mathcal{P}oles(s,t,u)+\mathcal{F}inite(s,t,u). \quad \text{(A.3.59)}$$

$\mathcal{P}oles$ contains infrared singularities that will be analytically canceled by those occurring in radiative processes of the same order (ultraviolet divergences are removed by renormalisation). $\mathcal{F}inite$ is the remainder which is finite as $\epsilon \to 0$.

The contraction of the colour vector $|X\rangle$ with the conjugate colour vector $\langle Y|$ obeys the rule

$$\langle Y|X\rangle = \sum_{\text{spins}} \sum_{\text{colours}} \sum_{i,j=1}^{9} Y_i^* \, X_j \, \mathcal{C}_i^* \, \mathcal{C}_j. \tag{A.3.60}$$

In evaluating these contractions, the terms are typically of the type $\sum_{\text{colours}} \mathcal{C}_i^* \, \mathcal{C}_j$ which are given by (A.3.34).

For the expansion of the pole structure coming from this contribution, eqs (A.3.31) through to (A.3.43) are valid.

A.3.5 One-loop self-interference contribution - Finite piece

The finite two-loop contribution to $\mathcal{D}^8(s,t,u)$ is defined as

$$\mathcal{F}inite(s,t,u) = \mathcal{D}^{8\,(1\times1)}(s,t,u) - \mathcal{P}oles(s,t,u), \tag{A.3.61}$$

where the series expansions of both $\mathcal{D}^{8\,(1\times1)}(s,t,u)$ and $\mathcal{P}oles(s,t,u)$ is subtracted and set $\epsilon \to 0$.

The results are shown by grouping terms according to the power of the number of colours N and the number of light quarks N_F, so that

$$Finite(s,t,u) = V\left(N^4 A + N^2 B + N^3 N_F C + N N_F D + N^2 N_F^2 E + N_F^2 F + \frac{N_F^2}{N^2} G\right), \tag{A.3.62}$$

where

$$\begin{aligned}
A \;=\; & \left\{\frac{1}{2}\left(X^2 - 2\,X\,Y + Y^2 + \pi^2\right)\left(X^2 - 2\,X\,Y - 2\,X + Y^2 + 2\,Y + \pi^2\right)\frac{t^4}{s^4}\right. \\
& + \left(3\,X^4 - 4\,X^3\,Y - \frac{56}{3}\,X^3 + 6\,X^2\,Y^2 + 20\,X^2\,Y - \frac{22}{3}\,X^2\,\mathrm{Ls} + 10\,X^2\,\pi^2 + \frac{56}{9}\,X^2\right. \\
& - 4\,X\,Y^3 - 20\,X\,Y^2 - 4\,X\,Y\,\pi^2 - 6\,X\,Y + \frac{154}{9}\,X\,\mathrm{Ls} - 16\,X\,\pi^2 + \frac{785}{27}\,X + Y^4 \\
& + 4\,Y^3 - \frac{22}{3}\,Y^2\,\mathrm{Ls} + 2\,Y^2\,\pi^2 - \frac{28}{9}\,Y^2 + \frac{110}{3}\,Y\,\mathrm{Ls} + 16\,Y\,\pi^2 + \frac{721}{9}\,Y + \frac{242}{9}\,\mathrm{Ls}^2 \\
& \left. + \frac{2948}{27}\,\mathrm{Ls} + \pi^4 + \pi^2 + \frac{9014}{81}\right)\frac{t^2}{s^2} \\
& + \left(4\,X^4 + 12\,X^3 + \frac{4}{3}\,X^2\,Y - \frac{44}{3}\,X^2\,\mathrm{Ls} + 16\,X^2\,\pi^2 - \frac{56}{9}\,X^2 + \frac{40}{3}\,X\,Y^2\right.
\end{aligned}$$

$$
\begin{aligned}
&+\frac{88}{3}\,X\,Y\,\mathrm{Ls}+\frac{880}{9}\,X\,Y+\frac{220}{3}\,X\,\mathrm{Ls}+\frac{88}{3}\,X\,\pi^2+\frac{1442}{9}\,X+4\,Y^4-\frac{88}{3}\,Y^2\,\mathrm{Ls}\\
&+16\,Y^2\,\pi^2-\frac{536}{9}\,Y^2+\frac{116}{3}\,Y\,\pi^2+\frac{484}{9}\,\mathrm{Ls}^2-\frac{44}{3}\,\mathrm{Ls}\,\pi^2+\frac{5896}{27}\,\mathrm{Ls}+\frac{58}{9}\,\pi^2+\frac{18028}{81}\Bigg)\,\frac{t}{u}\\
&+X^2\left(X^2+4\,\pi^2\right)\frac{t^4}{u^4}\\
&+2\,X\left(X^3+2\,X^2+4\,X\,\pi^2+4\,\pi^2\right)\frac{t^3}{u^3}\\
&+\Bigg(7\,X^4-8\,X^3\,Y-\frac{26}{3}\,X^3+12\,X^2\,Y^2+\frac{88}{3}\,X^2\,Y-\frac{44}{3}\,X^2\,\mathrm{Ls}+24\,X^2\,\pi^2+\frac{28}{9}\,X^2\\
&-8\,X\,Y^3-\frac{44}{3}\,X\,Y^2+\frac{88}{3}\,X\,Y\,\mathrm{Ls}-8\,X\,Y\,\pi^2+\frac{536}{9}\,X\,Y+\frac{484}{9}\,X\,\mathrm{Ls}-\frac{8}{3}\,X\,\pi^2\\
&+\frac{2948}{27}\,X+4\,Y^4-\frac{88}{3}\,Y^2\,\mathrm{Ls}+12\,Y^2\,\pi^2-\frac{536}{9}\,Y^2+\frac{88}{3}\,Y\,\pi^2+\frac{484}{9}\,\mathrm{Ls}^2-\frac{44}{3}\,\mathrm{Ls}\,\pi^2\\
&+\frac{5896}{27}\,\mathrm{Ls}+2\,\pi^4+\frac{10}{9}\,\pi^2+\frac{18028}{81}\Bigg)\frac{t^2}{u^2}\\
&+\Bigg(\frac{17}{2}\,X^4-10\,X^3\,Y-\frac{7}{3}\,X^3+\frac{15}{2}\,X^2\,Y^2+11\,X^2\,Y-\frac{110}{3}\,X^2\,\mathrm{Ls}+29\,X^2\,\pi^2\\
&-\frac{122}{3}\,X^2+22\,X\,Y\,\mathrm{Ls}-5\,X\,Y\,\pi^2+\frac{596}{9}\,X\,Y+\frac{814}{9}\,X\,\mathrm{Ls}+\frac{107}{3}\,X\,\pi^2\\
&+\frac{5309}{27}\,X+\frac{605}{9}\,\mathrm{Ls}^2-11\,\mathrm{Ls}\,\pi^2+\frac{7667}{27}\,\mathrm{Ls}+\frac{5}{4}\,\pi^4+\frac{113}{18}\,\pi^2+\frac{24533}{81}\Bigg)\Bigg\}+\Big\{u\leftrightarrow t\Big\}
\end{aligned}
\tag{A.3.63}
$$

$$
\begin{aligned}
B \;=\;&\Big\{6\left(X^2-2\,X\,Y+Y^2+\pi^2\right)\left(X^2-2\,X\,Y-2\,X+Y^2+2\,Y+\pi^2\right)\frac{t^4}{s^4}\\
&+\Bigg(72\,X^4-120\,X^3\,Y-356\,X^3+48\,X^2\,Y^2+580\,X^2\,Y+156\,X^2\,\pi^2+\frac{1280}{3}\,X^2\\
&+24\,X\,Y^3-404\,X\,Y^2-144\,X\,Y\,\pi^2-\frac{1184}{3}\,X\,Y-392\,X\,\pi^2-112\,X-24\,Y^4\\
&+180\,Y^3-12\,Y^2\,\pi^2-32\,Y^2+392\,Y\,\pi^2+112\,Y+12\,\pi^4+12\,\pi^2\Bigg)\frac{t^2}{s^2}\\
&+\Bigg(-24\,X^4+144\,X^3\,Y+408\,X^3-48\,X^2\,Y^2-272\,X^2\,Y+120\,X^2\,\pi^2-64\,X^2\\
&+96\,X\,Y^3+624\,X\,Y^2+288\,X\,Y\,\pi^2+\frac{2752}{3}\,X\,Y+792\,X\,\pi^2+224\,X\\
&+144\,Y^2\,\pi^2+528\,Y\,\pi^2+\frac{2200}{3}\,\pi^2\Bigg)\frac{t}{u}\\
&+12\,X^2\left(X^2+4\,\pi^2\right)\frac{t^4}{u^4}\\
&+24\,X\left(X^3+2\,X^2+4\,X\,\pi^2+4\,\pi^2\right)\frac{t^3}{u^3}\\
&+\Bigg(84\,X^4-96\,X^3\,Y-104\,X^3+96\,X^2\,Y^2+352\,X^2\,Y+288\,X^2\,\pi^2+\frac{1184}{3}\,X^2
\end{aligned}
$$

$$
\begin{aligned}
&-96\,X\,Y\,\pi^2 - 32\,X\,\pi^2 + 96\,Y^2\,\pi^2 + 352\,Y\,\pi^2 + 24\,\pi^4 + \frac{1112}{3}\,\pi^2\Bigg)\,\frac{t^2}{u^2}\\
&+\Bigg(42\,X^4 + 32\,X^3 + 66\,X^2\,Y^2 + 416\,X^2\,Y + 288\,X^2\,\pi^2 + \frac{1808}{3}\,X^2 + 84\,X\,Y\,\pi^2\\
&+\frac{424}{3}\,X\,Y + 716\,X\,\pi^2 + 112\,X + 15\,\pi^4 + 666\,\pi^2 + 48\Bigg)\Bigg\} + \Big\{u \leftrightarrow t\Big\} \qquad \text{(A.3.64)}
\end{aligned}
$$

$$
\begin{aligned}
C \;=\; &\Bigg\{-\Big(X^2 - 2\,X\,Y + Y^2 + \pi^2\Big)\Big(X^2 - 2\,X\,Y - 2\,X + Y^2 + 2\,Y + \pi^2\Big)\,\frac{t^4}{s^4}\\
&+\Bigg(-X^4 + 2\,X^3\,Y + \frac{73}{6}\,X^3 - 3\,X^2\,Y^2 - 22\,X^2\,Y + \frac{19}{6}\,X^2\,\mathrm{Ls} - 3\,X^2\,\pi^2\\
&-\frac{185}{18}\,X^2 + 2\,X\,Y^3 + 22\,X\,Y^2 + 2\,X\,Y\,\pi^2 + 12\,X\,Y - \frac{83}{9}\,X\,\mathrm{Ls} + \frac{32}{3}\,X\,\pi^2\\
&-\frac{250}{27}\,X - \frac{19}{2}\,Y^3 - \frac{1}{2}\,Y^2\,\mathrm{Ls} + Y^2\,\pi^2 - \frac{127}{18}\,Y^2 - \frac{31}{3}\,Y\,\mathrm{Ls} - \frac{32}{3}\,Y\,\pi^2 - \frac{242}{9}\,Y\\
&-\frac{88}{9}\,\mathrm{Ls}^2 - \frac{976}{27}\,\mathrm{Ls} - \frac{1}{2}\,\pi^4 - 2\,\pi^2 - \frac{2752}{81}\Bigg)\,\frac{t^2}{s^2}\\
&+\Bigg(-4\,X^4 - 4\,X^3\,Y - 27\,X^3 + 6\,X^2\,Y^2 + 12\,X^2\,Y - X^2\,\mathrm{Ls} - 18\,X^2\,\pi^2\\
&-\frac{127}{9}\,X^2 - 4\,X\,Y^3 - 11\,X\,Y^2 + 2\,X\,Y\,\mathrm{Ls} - 4\,X\,Y\,\pi^2 - \frac{148}{9}\,X\,Y - \frac{62}{3}\,X\,\mathrm{Ls}\\
&-\frac{149}{3}\,X\,\pi^2 - \frac{484}{9}\,X + \frac{16}{3}\,Y^2\,\mathrm{Ls} - 2\,Y^2\,\pi^2 + \frac{80}{9}\,Y^2 - 16\,Y\,\pi^2 - \frac{176}{9}\,\mathrm{Ls}^2\\
&-\mathrm{Ls}\,\pi^2 - \frac{1952}{27}\,\mathrm{Ls} + \pi^4 - \frac{247}{9}\,\pi^2 - \frac{5504}{81}\Bigg)\,\frac{t}{u}\\
&-2\,X^2\Big(X^2 + 4\,\pi^2\Big)\,\frac{t^4}{u^4}\\
&-4\,X\Big(X^3 + 2\,X^2 + 4\,X\,\pi^2 + 4\,\pi^2\Big)\,\frac{t^3}{u^3}\\
&+\Bigg(-7\,X^4 - \frac{28}{3}\,X^3 - \frac{16}{3}\,X^2\,Y + \frac{8}{3}\,X^2\,\mathrm{Ls} - 28\,X^2\,\pi^2 - \frac{52}{3}\,X^2 + \frac{8}{3}\,X\,Y^2\\
&-\frac{16}{3}\,X\,Y\,\mathrm{Ls} - \frac{80}{9}\,X\,Y - \frac{176}{9}\,X\,\mathrm{Ls} - \frac{64}{3}\,X\,\pi^2 - \frac{976}{27}\,X + \frac{16}{3}\,Y^2\,\mathrm{Ls} + \frac{80}{9}\,Y^2\\
&-\frac{16}{3}\,Y\,\pi^2 - \frac{176}{9}\,\mathrm{Ls}^2 + \frac{8}{3}\,\mathrm{Ls}\,\pi^2 - \frac{1952}{27}\,\mathrm{Ls} - \frac{40}{3}\,\pi^2 - \frac{5504}{81}\Bigg)\,\frac{t^2}{u^2}\\
&+\Bigg(-4\,X^4 + 2\,X^3\,Y - \frac{13}{2}\,X^3 - \frac{3}{2}\,X^2\,Y^2 - 2\,X^2\,Y + \frac{73}{6}\,X^2\,\mathrm{Ls} - 15\,X^2\,\pi^2\\
&-\frac{131}{18}\,X^2 - 4\,X\,Y\,\mathrm{Ls} + X\,Y\,\pi^2 - \frac{97}{9}\,X\,Y - \frac{269}{9}\,X\,\mathrm{Ls} - \frac{94}{3}\,X\,\pi^2 - \frac{1936}{27}\,X\\
&-\frac{220}{9}\,\mathrm{Ls}^2 + 2\,\mathrm{Ls}\,\pi^2 - \frac{2791}{27}\,\mathrm{Ls} - \frac{1}{4}\,\pi^4 - \frac{367}{18}\,\pi^2 - \frac{9337}{81}\Bigg)\Bigg\} + \Big\{u \leftrightarrow t\Big\} \qquad \text{(A.3.65)}
\end{aligned}
$$

$$
\begin{aligned}
D \;=\; &\Bigg\{-2\Big(X^2 - 2\,X\,Y + Y^2 + \pi^2\Big)\Big(X^2 - 2\,X\,Y - 2\,X + Y^2 + 2\,Y + \pi^2\Big)\,\frac{t^4}{s^4}
\end{aligned}
$$

$$
\begin{aligned}
&+\left(-4\,X^4+8\,X^3\,Y+75\,X^3-6\,X^2\,Y^2-\frac{389}{3}\,X^2\,Y-8\,X^2\,\pi^2-\frac{446}{3}\,X^2\right.\\
&+\frac{293}{3}\,X\,Y^2+4\,X\,Y\,\pi^2+\frac{424}{3}\,X\,Y+\frac{232}{3}\,X\,\pi^2+\frac{116}{3}\,X+2\,Y^4-43\,Y^3\\
&\left.+4\,Y^2\,\pi^2+\frac{22}{3}\,Y^2-\frac{232}{3}\,Y\,\pi^2-\frac{116}{3}\,Y-\pi^4-4\,\pi^2\right)\frac{t^2}{s^2}\\
&+\left(-4\,X^4-16\,X^3\,Y-102\,X^3+12\,X^2\,Y^2+\frac{188}{3}\,X^2\,Y-32\,X^2\,\pi^2+\frac{44}{3}\,X^2\right.\\
&-8\,X\,Y^3-\frac{380}{3}\,X\,Y^2-24\,X\,Y\,\pi^2-312\,X\,Y-\frac{578}{3}\,X\,\pi^2-\frac{232}{3}\,X-4\,Y^2\,\pi^2\\
&\left.-\frac{332}{3}\,Y\,\pi^2+2\,\pi^4-\frac{820}{3}\,\pi^2\right)\frac{t}{u}\\
&-4\,X^2\left(X^2+4\,\pi^2\right)\frac{t^4}{u^4}\\
&-8\,X\left(X^3+2\,X^2+4\,X\,\pi^2+4\,\pi^2\right)\frac{t^3}{u^3}\\
&+\left(-14\,X^4+8\,X^3-64\,X^2\,Y-56\,X^2\,\pi^2-\frac{424}{3}\,X^2-16\,X\,\pi^2-64\,Y\,\pi^2\right.\\
&\left.-\frac{400}{3}\,\pi^2\right)\frac{t^2}{u^2}\\
&+\left(-4\,X^4-4\,X^3\,Y-\frac{35}{3}\,X^3-85\,X^2\,Y-26\,X^2\,\pi^2-206\,X^2-2\,X\,Y\,\pi^2\right.\\
&\left.\left.-\frac{148}{3}\,X\,Y-\frac{484}{3}\,X\,\pi^2-\frac{116}{3}\,X-\frac{1}{2}\,\pi^4-\frac{721}{3}\,\pi^2-16\right)\right\}+\left\{u\leftrightarrow t\right\}
\end{aligned}
\tag{A.3.66}
$$

$$
\begin{aligned}
E \;=\;& \left\{\frac{1}{2}\left(X^2-2\,X\,Y+Y^2+\pi^2\right)\left(X^2-2\,X\,Y-2\,X+Y^2+2\,Y+\pi^2\right)\frac{t^4}{s^4}\right.\\
&+\left(-\frac{1}{2}\,X^4+2\,X^3\,Y-X^3-3\,X^2\,Y^2+2\,X^2\,Y-\frac{1}{3}\,X^2\,\mathrm{Ls}-X^2\,\pi^2+\frac{32}{9}\,X^2\right.\\
&+2\,X\,Y^3-2\,X\,Y^2+2\,X\,Y\,\pi^2-6\,X\,Y+\frac{10}{9}\,X\,\mathrm{Ls}-\frac{2}{3}\,X\,\pi^2-\frac{22}{27}\,X-\frac{1}{2}\,Y^4\\
&+Y^3+\frac{1}{3}\,Y^2\,\mathrm{Ls}-Y^2\,\pi^2+\frac{10}{3}\,Y^2+\frac{2}{3}\,Y\,\mathrm{Ls}+\frac{2}{3}\,Y\,\pi^2+\frac{34}{9}\,Y+\frac{8}{9}\,\mathrm{Ls}^2+\frac{80}{27}\,\mathrm{Ls}\\
&\left.-\frac{1}{2}\,\pi^4+\pi^2+\frac{236}{81}\right)\frac{t^2}{s^2}\\
&+\left(X^4+6\,X^3-\frac{4}{3}\,X^2\,Y+\frac{2}{3}\,X^2\,\mathrm{Ls}+4\,X^2\,\pi^2+\frac{20}{3}\,X^2+\frac{2}{3}\,X\,Y^2-\frac{4}{3}\,X\,Y\,\mathrm{Ls}\right.\\
&+\frac{4}{3}\,X\,\mathrm{Ls}+\frac{34}{3}\,X\,\pi^2+\frac{68}{9}\,X+\frac{4}{3}\,Y\,\pi^2+\frac{16}{9}\,\mathrm{Ls}^2+\frac{2}{3}\,\mathrm{Ls}\,\pi^2+\frac{160}{27}\,\mathrm{Ls}\\
&\left.+\frac{22}{3}\,\pi^2+\frac{472}{81}\right)\frac{t}{u}\\
&+X^2\left(X^2+4\,\pi^2\right)\frac{t^4}{u^4}
\end{aligned}
$$

$$
\begin{aligned}
&+2\,X\left(X^3+2\,X^2+4\,X\,\pi^2+4\,\pi^2\right)\\
&\frac{t^3}{u^3}+\left(2\,X^4+6\,X^3+8\,X^2\,\pi^2+\frac{62}{9}\,X^2+\frac{16}{9}\,X\,\mathrm{Ls}+12\,X\,\pi^2+\frac{80}{27}\,X+\frac{16}{9}\,\mathrm{Ls}^2\right.\\
&\left.+\frac{160}{27}\,\mathrm{Ls}+\frac{44}{9}\,\pi^2+\frac{472}{81}\right)\frac{t^2}{u^2}\\
&+\left(\frac{1}{2}\,X^4-X^3\,Y+\frac{4}{3}\,X^3+\frac{3}{4}\,X^2\,Y^2-X^2\,\mathrm{Ls}+\frac{3}{2}\,X^2\,\pi^2+\frac{28}{9}\,X^2-\frac{1}{2}\,X\,Y\,\pi^2\right.\\
&+\frac{5}{9}\,X\,Y+\frac{22}{9}\,X\,\mathrm{Ls}+\frac{14}{3}\,X\,\pi^2+\frac{218}{27}\,X+\frac{20}{9}\,\mathrm{Ls}^2+\frac{254}{27}\,\mathrm{Ls}+\frac{1}{8}\,\pi^4\\
&\left.\left.+\frac{37}{9}\,\pi^2+\frac{1049}{81}\right)\right\}+\left\{u\leftrightarrow t\right\}
\end{aligned}
\tag{A.3.67}
$$

$$
\begin{aligned}
F \;=\;&\left\{-\left(X^2-2\,X\,Y+Y^2+\pi^2\right)\left(X^2-2\,X\,Y-2\,X+Y^2+2\,Y+\pi^2\right)\frac{t^4}{s^4}\right.\\
&+\left(X^4-4\,X^3\,Y-2\,X^3+6\,X^2\,Y^2+\frac{14}{3}\,X^2\,Y+2\,X^2\,\pi^2+6\,X^2-4\,X\,Y^3\right.\\
&-\frac{14}{3}\,X\,Y^2-4\,X\,Y\,\pi^2+\frac{4}{3}\,X\,Y-\frac{4}{3}\,X\,\pi^2+\frac{4}{3}\,X+Y^4+2\,Y^3+2\,Y^2\,\pi^2-\frac{22}{3}\,Y^2\\
&\left.+\frac{4}{3}\,Y\,\pi^2-\frac{4}{3}\,Y+\pi^4-2\,\pi^2\right)\frac{t^2}{s^2}\\
&+\left(-2\,X^4-4\,X^3-\frac{8}{3}\,X^2\,Y-8\,X^2\,\pi^2-\frac{44}{3}\,X^2+\frac{8}{3}\,X\,Y^2+\frac{80}{3}\,X\,Y-\frac{28}{3}\,X\,\pi^2\right.\\
&\left.-\frac{8}{3}\,X+\frac{8}{3}\,Y\,\pi^2+16\,\pi^2\right)\frac{t}{u}\\
&-2\,X^2\left(X^2+4\,\pi^2\right)\frac{t^4}{u^4}\\
&-4\,X\left(X^3+2\,X^2+4\,X\,\pi^2+4\,\pi^2\right)\frac{t^3}{u^3}\\
&+\left(-4\,X^4-12\,X^3-16\,X^2\,\pi^2-\frac{4}{3}\,X^2-24\,X\,\pi^2+\frac{8}{3}\,\pi^2\right)\frac{t^2}{u^2}\\
&+\left(-X^4+2\,X^3\,Y-\frac{4}{3}\,X^3-\frac{3}{2}\,X^2\,Y^2+2\,X^2\,Y-3\,X^2\,\pi^2+\frac{46}{3}\,X^2\right.\\
&\left.\left.+X\,Y\,\pi^2+2\,X\,Y+\frac{4}{3}\,X\,\pi^2-\frac{4}{3}\,X-\frac{1}{4}\,\pi^4+\frac{58}{3}\,\pi^2-8\right)\right\}+\left\{u\leftrightarrow t\right\}
\end{aligned}
\tag{A.3.68}
$$

$$
\begin{aligned}
G \;=\;&\left\{3\left(X^2-2\,X\,Y+Y^2+\pi^2\right)\left(X^2-2\,X\,Y-2\,X+Y^2+2\,Y+\pi^2\right)\frac{t^4}{s^4}\right.\\
&-3\left(X^2-2\,X\,Y+2\,X+Y^2-2\,Y+\pi^2-2\right)\left(X^2-2\,X\,Y-2\,X+Y^2+2\,Y+\pi^2\right)\frac{t^2}{s^2}\\
&\left.+\left(6\,X^4+24\,X^3+24\,X^2\,\pi^2+36\,X^2+48\,X\,\pi^2+24\,X+24\,\pi^2\right)\frac{t}{u}\right.
\end{aligned}
$$

$$
\begin{aligned}
&+6\,X^2\left(X^2+4\,\pi^2\right)\frac{t^4}{u^4}\\
&+12\,X\left(X^3+2\,X^2+4\,X\,\pi^2+4\,\pi^2\right)\frac{t^3}{u^3}\\
&+\left(12\,X^4+36\,X^3+48\,X^2\,\pi^2+36\,X^2+72\,X\,\pi^2+24\,\pi^2\right)\frac{t^2}{u^2}\\
&+\left(3\,X^4-6\,X^3\,Y+6\,X^3+\frac{9}{2}\,X^2\,Y^2+9\,X^2\,\pi^2+6\,X^2-3\,X\,Y\,\pi^2+6\,X\,Y\right.\\
&\left.+12\,X\,\pi^2+12\,X+\frac{3}{4}\,\pi^4+6\,\pi^2+24\right)\Bigg\}+\Big\{u\leftrightarrow t\Big\}
\end{aligned}
\tag{A.3.69}
$$

Although it is expected that the finite piece contains polylogarithms, they are all predicted by the infrared singular structure and are obtained by expanding Eq. (A.3.23) through to $\mathcal{O}(\epsilon)$. This is because the polylogarithms appear as the $\mathcal{O}(\epsilon)$ and $\mathcal{O}(\epsilon^2)$ terms in the expansion of the box integral in $D = 6$ and must be multiplied by an infrared singular term to contribute at $\mathcal{O}(1)$. At $\mathcal{O}(1)$, the interference of one box graph with another only collects the $\mathcal{O}(1)$ terms in each and therefore yields only logarithms.

A.4 $gg \to ggg$ tree level

For five-gluon helicity amplitudes the only non-zero sub-amplitudes will be of the form $(--+++)$ up to permutations of the indices. They are written in the following form [160, 161]:

$$
m_{3+2-}(g_1,g_2,g_3,g_4,g_5) = ig^3\frac{\langle IJ\rangle^4}{\langle 12\rangle\langle 23\rangle\langle 34\rangle\langle 45\rangle\langle 51\rangle} \tag{A.4.70}
$$

where I and J are the indices of negative helicity gluons. We can square this sub-amplitude and sum over helicities to obtain the colour-ordered amplitude squared:

$$
A_5^0(g_1,g_2,g_3,g_4,g_5) = 2g^6\left(\sum_{i>j}s_{ij}^4\right)\frac{1}{s_{12}s_{23}s_{34}s_{45}s_{51}} \tag{A.4.71}
$$

This is the colour ordered amplitude that accompanies the antenna functions in the counterterms in chapter 6.

A.5 $gg \to ggg$ one-loop

This matrix element is not implemented in our program. We reproduce it here from reference [114] for convenience.

In this case one first decomposes the n-gluon amplitude, depending on the external momenta, helicities, and colour indices k_i, λ_i, and a_i, into sums over certain permutations of colour factors, times partial amplitudes, in analogy to the helicity [20–25] and colour decomposition [27–29] of tree amplitudes. At one-loop order in an $SU(N)$ theory, one must also sum over the different spins J of the internal particles; this takes the following form when all internal particles transform as colour adjoints,

$$\mathcal{A}_n\left(\{k_,\lambda_i,a_i\}\right) = \sum_J n_J \sum_{c=1}^{\lfloor n/2\rfloor+1} \sum_{\sigma\in S_n/S_{n;c}} \mathrm{Gr}_{n;c}\left(\sigma\right)\, A^{[J]}_{n;c}(\sigma) \tag{A.5.72}$$

where $\mathrm{Gr}_{n;1}(1) = N\,\mathrm{Tr}\left(T^{a_1}\cdots T^{a_n}\right)$, $\mathrm{Gr}_{n;c}(1) = \mathrm{Tr}\left(T^{a_1}\cdots T^{a_{c-1}}\right)\mathrm{Tr}\left(T^{a_c}\cdots T^{a_n}\right)$, S_n is the set of all permutations of n objects, and $S_{n;c}$ is the subset leaving the trace structure $\mathrm{Gr}_{n;c}$ invariant. The T^a are the set of hermitian traceless $N\times N$ matrices, normalised so that $\mathrm{Tr}\left(T^aT^b\right) = \delta^{ab}$. For internal particles in the fundamental $(N+\bar{N})$ representation, only the single-trace colour structure ($c=1$) is present, and it is smaller by a factor of N. In each case a spin-J particle has two states: gauge bosons, Weyl fermions, and complex scalars.

The objects one calculates are the partial amplitudes $A^{[J]}_{n;c}$, which depend only on the external momenta and helicities. For the five-point function, there is only one independent partial amplitude for each configuration of external helicities; $A_{5;2}$ and $A_{5;3}$ are related to the adjoint contributions to $A_{5;1}$ via decoupling equations [163]. Taking the fifth leg to be a photon, and setting the coefficient of $\mathrm{Tr}(T^{a_1}T^{a_2}T^{a_3}T^{a_4})$ to zero yields the first decoupling equation [163],

$$\sum_{\sigma\in Z_4} A_{5;1}(\sigma(1),\sigma(2),\sigma(3),\sigma(4),5) + A_{5;2}(5,1,2,3,4) = 0 \tag{A.5.73}$$

A new feature of the five-point amplitude is the emergence of additional constraints from other trace structures, still considering the one-photon substitution; the coefficient of $\mathrm{Tr}(T^{a_1}T^{a_2})(T^{a_3}T^{a_4})$ must vanish, which means that [163]

$$A_{5;3}(1,2,3,4,5)+A_{5;3}(1,2,4,3,5)+A_{5;3}(3,4,1,2,5)+A_{5;3}(3,4,2,1,5) = 0. \tag{A.5.74}$$

Substituting two photons for gluons, only one equation emerges [163],

$$\begin{aligned}\sum_{\sigma\in \mathrm{COP}_4^{(123)}} & A_{5;1}(\sigma(1),\sigma(2),\sigma(3),\sigma(4),5) \\ & + \sum_{\sigma\in Z_3} \left(A_{5;2}(5,\sigma(1),\sigma(2),\sigma(3),4) + A_{5;2}(4,\sigma(1),\sigma(2),\sigma(3),5)\right) \\ & + A_{5;3}(4,5,1,2,3) = 0 \end{aligned} \tag{A.5.75}$$

where COP (*cyclic ordered permutations*) denotes the subsets of S_n that leaves the ordering of the a_j unchanged up to a cyclic transformation. These equations can be solved to eliminate the partial amplitudes $A_{5;2}$ and $A_{5;3}$. Using the one-photon single trace equation (A.5.73) to substitute for $A_{5;2}$ in the two-photon equation (A.5.75) gives [163]

$$A_{5;3}(4,5,1,2,3) = \sum_{\sigma\in \mathrm{COP}_4^{123}} A_{5;1}\left(\sigma(1),\sigma(2),\sigma(3),\sigma(4),5\right). \tag{A.5.76}$$

From this equation along with the one-photon double trace equation (A.5.74) generates the constraint [163]

$$\sum_{\sigma\in S_5/Z_5} A_{5;1}\left(\sigma(1),\sigma(2),\sigma(3),\sigma(4),\sigma(5)\right) = 0 \tag{A.5.77}$$

Additional equations obtained by substituting three or more photon legs are not independent. For the finite helicity amplitudes, supersymmetric identities [164] imply that the contributions of particles of different spin circulating around the loop are related, $A^{[1]}_{n;c} = -A^{[1/2]}_{n;c} = A^{[0]}_{n;c}$. (This holds true for the partial amplitudes whether or not the theory as a whole is supersymmetric.) Indeed, in the string-based method, these identities hold for the integrands of each diagram. The amplitudes are [114]

$$A^{[1]}_{5;1}\left(1^+,2^+,3^+,4^+,5^+\right) = \frac{i}{96\pi^2}\frac{s_{12}s_{23}+s_{23}s_{34}+s_{34}s_{45}+s_{45}s_{51}+s_{51}s_{12}+\varepsilon(1,2,3,4)}{\langle 1\,2\rangle\,\langle 2\,3\rangle\,\langle 3\,4\rangle\,\langle 4\,5\rangle\,\langle 5\,1\rangle} \tag{A.5.78}$$

$$\begin{aligned} A^{[1]}_{5;1}\left(1^-,2^+,3^+,4^+,5^+\right) = \frac{i}{48\pi^2}\frac{1}{[1\,2]\,\langle 2\,3\rangle\,\langle 3\,4\rangle\,\langle 4\,5\rangle\,[5\,1]}\Bigg[& (s_{23}+s_{34}+s_{45})[2\,5]^2 \\ & - [2\,4]\,\langle 4\,3\rangle\,[3\,5]\,[2\,5] - \frac{[1\,2]\,[1\,5]}{\langle 1\,2\rangle\,\langle 1\,5\rangle}\Bigg(\langle 1\,2\rangle^2\langle 1\,3\rangle^2\frac{[2\,3]}{\langle 2\,3\rangle} \end{aligned}$$

$$+ \langle 1\,3\rangle^2 \langle 1\,4\rangle^2 \frac{[3\,4]}{\langle 3\,4\rangle} + \langle 1\,4\rangle^2 \langle 1\,5\rangle^2 \frac{[4\,5]}{\langle 4\,5\rangle}\Bigg)\Bigg] \tag{A.5.79}$$

In order to present the results for the remaining, infrared-divergent amplitudes in a compact form, it is helpful to define the following functions,

$$\mathrm{L}_0(r) = \frac{\ln(r)}{1-r}\,, \qquad \mathrm{L}_1(r) = \frac{\ln(r)+1-r}{(1-r)^2}\,, \qquad \mathrm{L}_2(r) = \frac{\ln(r)-(r-1/r)/2}{(1-r)^3}\,,$$
$$\mathrm{Ls}_1(r_1,r_2) = \frac{1}{(1-r_1-r_2)^2}\Big[\mathrm{Li}_2(1-r_1)+\mathrm{Li}_2(1-r_2)+\ln r_1\,\ln r_2 - \frac{\pi^2}{6} + (1-r_1-r_2)\left(\mathrm{L}_0(r_1)+\mathrm{L}_0(r_2)\right)\Big] \tag{A.5.80}$$

where Li_2 is the dilogarithm; a prefactor,

$$c_\Gamma = \frac{(4\pi)^\epsilon}{16\pi^2}\frac{\Gamma(1+\epsilon)\Gamma^2(1-\epsilon)}{\Gamma(1-2\epsilon)} \tag{A.5.81}$$

a universal function,

$$V^g = -\frac{1}{\epsilon^2}\sum_{j=1}^{5}\left(\frac{\mu^2}{-s_{j,j+1}}\right)^\epsilon + \sum_{j=1}^{5}\ln\left(\frac{-s_{j,j+1}}{-s_{j+1,j+2}}\right)\ln\left(\frac{-s_{j+2,j-2}}{-s_{j-2,j-1}}\right) + \frac{5}{6}\pi^2 - \frac{\delta_R}{3}\,, \tag{A.5.82}$$

the following functions for the $(1^-,2^-,3^+,4^+,5^+)$ helicity configuration [114],

$$V^f = -\frac{5}{2\epsilon} - \frac{1}{2}\left[\ln\left(\frac{\mu^2}{-s_{23}}\right)+\ln\left(\frac{\mu^2}{-s_{51}}\right)\right] - 2, \qquad V^s = -\frac{1}{3}V^f + \frac{2}{9}$$
$$F^f = -\frac{1}{2}\frac{\langle 1\,2\rangle^2\left(\langle 2\,3\rangle\,[3\,4]\,\langle 4\,1\rangle + \langle 2\,4\rangle\,[4\,5]\,\langle 5\,1\rangle\right)}{\langle 2\,3\rangle\,\langle 3\,4\rangle\,\langle 4\,5\rangle\,\langle 5\,1\rangle}\frac{\mathrm{L}_0\left(\frac{-s_{23}}{-s_{51}}\right)}{s_{51}}$$
$$F^s = -\frac{1}{3}\frac{[3\,4]\,\langle 4\,1\rangle\,\langle 2\,4\rangle\,[4\,5]\left(\langle 2\,3\rangle\,[3\,4]\,\langle 4\,1\rangle + \langle 2\,4\rangle\,[4\,5]\,\langle 5\,1\rangle\right)}{\langle 3\,4\rangle\,\langle 4\,5\rangle}\frac{\mathrm{L}_2\left(\frac{-s_{23}}{-s_{51}}\right)}{s_{51}^3} - \frac{1}{3}F^f$$
$$- \frac{1}{3}\frac{\langle 3\,5\rangle\,[3\,5]^3}{[1\,2]\,[2\,3]\,\langle 3\,4\rangle\,\langle 4\,5\rangle\,[5\,1]} + \frac{1}{3}\frac{\langle 1\,2\rangle\,[3\,5]^2}{[2\,3]\,\langle 3\,4\rangle\,\langle 4\,5\rangle\,[5\,1]} + \frac{1}{6}\frac{\langle 1\,2\rangle\,[3\,4]\,\langle 4\,1\rangle\,\langle 2\,4\rangle\,[4\,5]}{s_{23}\,\langle 3\,4\rangle\,\langle 4\,5\rangle\,s_{51}}\,, \tag{A.5.83}$$

and the corresponding ones for the $(1^-,2^+,3^-,4^+,5^+)$ helicity configuration [114],

$$V^f = -\frac{5}{2\epsilon} - \frac{1}{2}\left[\ln\left(\frac{\mu^2}{-s_{34}}\right)+\ln\left(\frac{\mu^2}{-s_{51}}\right)\right] - 2, \qquad V^s = -\frac{1}{3}V^f + \frac{2}{9}$$
$$F^f = -\frac{\langle 1\,3\rangle^2\langle 4\,1\rangle[2\,4]^2}{\langle 4\,5\rangle\langle 5\,1\rangle}\frac{\mathrm{Ls}_1\left(\frac{-s_{23}}{-s_{51}},\,\frac{-s_{34}}{-s_{51}}\right)}{s_{51}^2} + \frac{\langle 1\,3\rangle^2\langle 5\,3\rangle[2\,5]^2}{\langle 3\,4\rangle\langle 4\,5\rangle}\frac{\mathrm{Ls}_1\left(\frac{-s_{12}}{-s_{34}},\,\frac{-s_{51}}{-s_{34}}\right)}{s_{34}^2}$$

$$
\begin{aligned}
&- \frac{1}{2}\frac{\langle 1\,3\rangle^3(\langle 1\,5\rangle\,[5\,2]\,\langle 2\,3\rangle - \langle 3\,4\rangle\,[4\,2]\,\langle 2\,1\rangle)}{\langle 1\,2\rangle\,\langle 2\,3\rangle\,\langle 3\,4\rangle\,\langle 4\,5\rangle\,\langle 5\,1\rangle}\frac{\mathrm{L}_0\left(\frac{-s_{34}}{-s_{51}}\right)}{s_{51}} \\
F^s = &-\frac{\langle 1\,2\rangle\langle 2\,3\rangle\langle 3\,4\rangle\langle 4\,1\rangle^2[2\,4]^2}{\langle 4\,5\rangle\langle 5\,1\rangle\langle 2\,4\rangle^2}\frac{2\,\mathrm{Ls}_1\left(\frac{-s_{23}}{-s_{51}},\frac{-s_{34}}{-s_{51}}\right)+\mathrm{L}_1\left(\frac{-s_{23}}{-s_{51}}\right)+\mathrm{L}_1\left(\frac{-s_{34}}{-s_{51}}\right)}{s_{51}^2} \\
&+\frac{\langle 3\,2\rangle\langle 2\,1\rangle\langle 1\,5\rangle\langle 5\,3\rangle^2[2\,5]^2}{\langle 5\,4\rangle\langle 4\,3\rangle\langle 2\,5\rangle^2}\frac{2\,\mathrm{Ls}_1\left(\frac{-s_{12}}{-s_{34}},\frac{-s_{51}}{-s_{34}}\right)+\mathrm{L}_1\left(\frac{-s_{12}}{-s_{34}}\right)+\mathrm{L}_1\left(\frac{-s_{51}}{-s_{34}}\right)}{s_{34}^2} \\
&+\frac{2}{3}\frac{\langle 2\,3\rangle^2\langle 4\,1\rangle^3[2\,4]^3}{\langle 4\,5\rangle\langle 5\,1\rangle\langle 2\,4\rangle}\frac{\mathrm{L}_2\left(\frac{-s_{23}}{-s_{51}}\right)}{s_{51}^3}-\frac{2}{3}\frac{\langle 2\,1\rangle^2\langle 5\,3\rangle^3[2\,5]^3}{\langle 5\,4\rangle\langle 4\,3\rangle\langle 2\,5\rangle}\frac{\mathrm{L}_2\left(\frac{-s_{12}}{-s_{34}}\right)}{s_{34}^3} \\
&+\frac{\mathrm{L}_2\left(\frac{-s_{34}}{-s_{51}}\right)}{s_{51}^3}\left(\frac{1}{3}\frac{\langle 1\,3\rangle\,[2\,4]\,[2\,5]\,(\langle 1\,5\rangle\,[5\,2]\,\langle 2\,3\rangle - \langle 3\,4\rangle\,[4\,2]\,\langle 2\,1\rangle)}{\langle 4\,5\rangle}\right. \\
&\left.+\frac{2}{3}\frac{\langle 1\,2\rangle^2\langle 3\,4\rangle^2\,\langle 4\,1\rangle\,[2\,4]^3}{\langle 4\,5\rangle\,\langle 5\,1\rangle\,\langle 2\,4\rangle}-\frac{2}{3}\frac{\langle 3\,2\rangle^2\langle 1\,5\rangle^2\,\langle 5\,3\rangle\,[2\,5]^3}{\langle 5\,4\rangle\,\langle 4\,3\rangle\,\langle 2\,5\rangle}\right) \\
&+\frac{1}{6}\frac{\langle 1\,3\rangle^3\,(\langle 1\,5\rangle\,[5\,2]\,\langle 2\,3\rangle - \langle 3\,4\rangle\,[4\,2]\,\langle 2\,1\rangle)}{\langle 1\,2\rangle\,\langle 2\,3\rangle\,\langle 3\,4\rangle\,\langle 4\,5\rangle\,\langle 5\,1\rangle}\frac{\mathrm{L}_0\left(\frac{-s_{34}}{-s_{51}}\right)}{s_{51}}+\frac{1}{3}\frac{[2\,4]^2[2\,5]^2}{[1\,2][2\,3][3\,4]\langle 4\,5\rangle[5\,1]} \\
&-\frac{1}{3}\frac{\langle 1\,2\rangle\langle 4\,1\rangle^2[2\,4]^3}{\langle 4\,5\rangle\langle 5\,1\rangle\langle 2\,4\rangle[2\,3][3\,4]s_{51}}+\frac{1}{3}\frac{\langle 3\,2\rangle\langle 5\,3\rangle^2[2\,5]^3}{\langle 5\,4\rangle\langle 4\,3\rangle\langle 2\,5\rangle[2\,1][1\,5]s_{34}}+\frac{1}{6}\frac{\langle 1\,3\rangle^2\,[2\,4]\,[2\,5]}{s_{34}\,\langle 4\,5\rangle\,s_{51}}\,.
\end{aligned}
$$

For positive values of s_{ij}, the logarithms and dilogarithms develop imaginary parts according to the prescription $s_{ij} \to s_{ij} + i\varepsilon$. The correspoding tree amplitudes are, $A_5^{\rm tree}(1^-,2^-,3^+,4^+,5^+) = i\langle 1\,2\rangle^4/(\langle 1\,2\rangle\,\langle 2\,3\rangle\,\langle 3\,4\rangle\,\langle 4\,5\rangle\,\langle 5\,1\rangle)$ and $A_5^{\rm tree}(1^-,2^+,3^-,4^+,5^+) = i\langle 1\,3\rangle^4/(\langle 1\,2\rangle\,\langle 2\,3\rangle\,\langle 3\,4\rangle\,\langle 4\,5\rangle\,\langle 5\,1\rangle)$.

In terms of these functions, the $\overline{\rm MS}$ renormalised amplitudes are

$$
\begin{aligned}
A_{5;1}^{[0]} &= c_\Gamma\left(V^s A_5^{\rm tree} + iF^s\right)\,, \\
A_{5;1}^{[1/2]} &= -c_\Gamma\left((V^f+V^s)A_5^{\rm tree} + i(F^f+F^s)\right)\,, \\
A_{5;1}^{[1]} &= c_\Gamma\left((V^g+4V^f+V^s)A_5^{\rm tree} + i(4F^f+F^s)\right)\,.
\end{aligned}
\tag{A.5.84}
$$

The rest of the helicity amplitudes are related by cyclic permutations or complex conjugation to those given above. It is interesting to note that in supersymmetric theories, the V^s and F^s terms cancel out of the final amplitude, and that in $N = 4$ supersymmetric theories only the V^g term survives. The separation implied above into g, f, and s pieces arises naturally on a diagram-by-diagram basis within the string-based approach. In this approach the V^g term represents the only cal-

culational difference between the contributions with gluons circulating around the loop, and those with fermions; this term has a particularly simple expression at every intermediate stage of the calculation. The parameter δ_R controls the variant of dimensional regularisation scheme [76, 165]: for $\delta_R = 0$, one obtains the four-dimensional helicity scheme, while for $\delta_R = 1$ one obtains the 't Hooft–Veltman scheme.

At next-to-leading order, only the infrared-divergent helicity amplitudes enter into the construction of a program for physical quantities. In order to construct such a program for three-jet quantities, one must form the interference of the tree amplitude with the loop amplitude; this has the form [163]:

$$\begin{aligned}\sum_{\text{colours}} [\mathcal{A}_5^* \mathcal{A}_5]_{\text{NLO}} = 2g^8 N^4 \left(N^2-1\right) \Bigg[& \text{Re} \sum_{\sigma \in S_5/Z_5} A_5^{\text{tree}\,*}(\sigma) A_{5;1}(\sigma) \\ & + \frac{1}{N^2} \text{Re} \sum_{\rho \in S_5/Z_5} \left[A_5^{\text{tree}\,*}(r\cdot\rho) A_{5;1}(\rho) - A_5^{\text{tree}\,*}(\rho) A_{5;1}(r\cdot\rho) \right] \\ & + \frac{2}{N^2} \text{Re} \sum_{h \in H_5} \sum_{p \in P\binom{5}{3}} A_5^{\text{tree}\,*}(h\cdot p) A_{5;3}(p) \Bigg] \,, \end{aligned} \tag{A.5.85}$$

where r is the permutation $(2\,4\,1\,3\,5)$; $P\binom{5}{3}$ is the ten-element set of distinct partitions of five elements into lists of length two and three; and $H_5 = \{(1\,2\,3\,4\,5), (3\,4\,1\,2\,5), (3\,1\,2\,4\,5), (2\,1\,3\,4\,5), (3\,2\,1\,4\,5), (3\,4\,2\,1\,5)\}$. For QCD with n_f flavors of massless quarks, one substitutes $A_{5;1} \to A_{5;1}^{[1]} + \frac{n_f}{N} A_{5;1}^{[1/2]}$ and $A_{5;3} \to A_{5;3}^{[1]}$ into equation (A.5.85).

A.6 $gg \to gggg$ tree level

For six-parton amplitudes two sets of helicity amplitudes are needed: m_{2-4+} and m_{3+3-}. The first ones are [160, 161]:

$$m_{2-4+}(g_1, g_2, g_3, g_4, g_5, g_6) = ig^3 \frac{\langle IJ\rangle^4}{\langle 12\rangle\langle 23\rangle\langle 34\rangle\langle 45\rangle\langle 56\rangle\langle 61\rangle} \tag{A.6.86}$$

where I and J are the indices of negative helicity gluons. The second ones are described by three distinct sub-amplitudes, characterised by three inequivalent helicity

orderings: $(+++--)$, $(++-+--)$ and $(+-+-+-)$. For the pure gluonic case they can be written in the following form [25, 27, 28]:

$$m_{3+3-}(g_1, g_2, \ldots, g_6) = ig^4 \left[\frac{\alpha^2}{t_{123} s_{12} s_{23} s_{45} s_{56}} + \frac{\beta^2}{t_{234} s_{23} s_{34} s_{56} s_{61}} + \frac{\gamma^2}{t_{345} s_{34} s_{45} s_{61} s_{12}} + \frac{t_{123}\beta\gamma + t_{234}\gamma\alpha + t_{345}\alpha\beta}{s_{12} s_{23} s_{34} s_{45} s_{56} s_{61}} \right], \quad \text{(A.6.87)}$$

where $t_{ijk} \equiv (p_i + p_j + p_k)^2 = s_{ij} + s_{jk} + s_{ki}$. The coefficients for α, β, γ are given in table [25].

	$1^+2^+3^+4^-5^-6^-$ $X = p_1 + p_2 + p_3$	$1^+2^+3^-4^+5^-6^-$ $Y = p_1 + p_2 + p_4$	$1^+2^-3^+4^-5^+6^-$ $Z = p_1 + p_3 + p_5$
α	0	$-[12]\langle 56\rangle\langle 4\|Y\|3\rangle$	$[13]\langle 46\rangle\langle 5\|Z\|2\rangle$
β	$[23]\langle 56\rangle\langle 1\|X\|4\rangle$	$[24]\langle 56\rangle\langle 1\|Y\|3\rangle$	$[51]\langle 24\rangle\langle 3\|Z\|6\rangle$
γ	$[12]\langle 45\rangle\langle 3\|X\|6\rangle$	$[12]\langle 35\rangle\langle 4\|Y\|6\rangle$	$[35]\langle 62\rangle\langle 1\|Z\|4\rangle$

Table A.1: Coefficients for the $m_{3+3-}(g_1, g_2, g_3, g_4, g_5, g_6)$ sub-amplitudes. We define $\langle I|K|J\rangle \equiv \langle I + |K \cdot \gamma|J+\rangle$

The evaluation of the spinor products proceeds as described in 1.6.

Appendix B

Gluon-Gluon antenna functions

B.1 $F_4^0(g_1, g_2, g_3, g_4)$

The tree-level four-parton gluon-gluon antenna contains three final states: gluon-gluon-gluon-gluon, F_4^0, and gluon-quark-antiquark-gluon at leading and subleading colour, G_4^0 and $\tilde{G}_4^0$ and quark-antiquark-quark-antiquark, H_4^0. The antenna for the $gggg$ final state is [67]:

$$\begin{aligned} F_4^0(g_1,g_2,g_3,g_4) &= f_4^0(1,2,3,4) + f_4^0(4,3,2,1) + f_4^0(2,3,4,1) + f_4^0(1,4,3,2) \\ &\quad + f_4^0(3,4,1,2) + f_4^0(2,1,4,3) + f_4^0(4,1,2,3) + f_4^0(3,2,1,4)\,, \end{aligned} \tag{B.1.1}$$

with

$$\begin{aligned} f_4^0(1,2,3,4) &= \frac{1}{s_{1234}^2}\Bigg\{ -\frac{2s_{34}s_{13}s_{14}^2}{s_{23}^2 s_{123} s_{234}} + \frac{1}{s_{23}^2}\Big[2s_{12}s_{14} - 2s_{12}s_{24} + 2s_{12}s_{34} \\ &\quad + s_{12}^2 - 2s_{13}s_{14} - 2s_{13}s_{24} - 2s_{13}s_{34} - 2s_{14}s_{24} + 2s_{14}s_{34} + s_{14}^2 + s_{34}^2\Big] \\ &\quad + \frac{s_{13}}{s_{23}^2 s_{123}}\left[4s_{13}s_{14} + 4s_{13}s_{24} + 4s_{13}s_{34} - 8s_{14}s_{34} - 2s_{14}^2 - 4s_{24}s_{34} - 4s_{34}^2\right] \\ &\quad + \frac{s_{13}^2}{s_{23}^2 s_{123}^2}\left[4s_{14}s_{24} + 4s_{14}s_{34} + 2s_{14}^2 + 4s_{24}s_{34} + 2s_{24}^2 + 2s_{34}^2\right] \\ &\quad + \frac{1}{4s_{23}s_{12}s_{34}s_{14}}\left[2s_{13}s_{24}^3 + 3s_{13}^2 s_{24}^2 + 2s_{13}^3 s_{24} + s_{13}^4 + s_{24}^4\right] \\ &\quad + \frac{1}{s_{23}s_{12}s_{34}}\Big[6s_{13}s_{14}s_{24} + 2s_{13}s_{14}^2 + 6s_{13}s_{24}^2 + 3s_{13}^2 s_{14} + 6s_{13}^2 s_{24} + 2s_{13}^3 \\ &\quad + 3s_{14}s_{24}^2 + 2s_{14}^2 s_{24} + s_{14}^3 + 2s_{24}^3\Big] + \frac{s_{24}}{s_{23}s_{12}s_{124}}\left[s_{24}s_{34} + s_{24}^2 + 2s_{34}^2\right] \end{aligned}$$

$$
\begin{aligned}
&+\frac{1}{s_{23}s_{12}s_{234}s_{124}}\left[2s_{13}s_{34}^3+3s_{13}^2s_{34}^2+2s_{13}^3s_{34}+s_{13}^4+s_{34}^4\right]\\
&+\frac{1}{s_{23}s_{12}s_{234}}\Big[2s_{13}s_{14}s_{34}+2s_{13}s_{14}^2+2s_{13}s_{34}^2+3s_{13}^2s_{14}+3s_{13}^2s_{34}+2s_{13}^3\\
&+2s_{14}s_{34}^2-s_{14}^2s_{34}+s_{14}^3\Big]+\frac{1}{s_{23}s_{12}}\Big[20s_{13}s_{14}+14s_{13}s_{24}+9s_{13}^2+16s_{14}s_{24}\\
&+4s_{14}s_{34}+19s_{14}^2+7s_{24}^2-10s_{34}^2\Big]+\frac{s_{14}}{s_{23}s_{123}s_{234}}\Big[-s_{13}s_{14}-4s_{13}s_{34}-4s_{13}^2\\
&+s_{14}s_{34}-4s_{14}^2-4s_{34}^2\Big]+\frac{1}{s_{23}s_{123}s_{134}}\Big[6s_{14}s_{24}s_{34}+6s_{14}s_{24}^2+6s_{14}^2s_{24}+s_{14}^3\\
&+6s_{24}s_{34}^2+9s_{24}^2s_{34}+6s_{24}^3+s_{34}^3\Big]+\frac{1}{s_{23}s_{123}s_{124}}\Big[-3s_{14}s_{24}s_{34}-\frac{3}{2}s_{14}s_{24}^2\\
&-\frac{3}{2}s_{14}s_{34}^2-s_{14}^2s_{24}-s_{14}^2s_{34}+\frac{3}{4}s_{14}^3-3s_{24}s_{34}^2-3s_{24}^2s_{34}-s_{24}^3-s_{34}^3\Big]\\
&+\frac{1}{4s_{23}s_{123}}\Big[-7s_{13}s_{14}+18s_{13}s_{24}-16s_{13}s_{34}-11s_{13}^2-41s_{14}s_{24}-36s_{14}s_{34}\\
&-63s_{14}^2-16s_{24}s_{34}-21s_{24}^2-18s_{34}^2\Big]+\frac{1}{s_{23}s_{134}}\Big[7s_{12}s_{14}+2s_{12}s_{24}+8s_{12}s_{34}\\
&-4s_{12}^2+4s_{14}s_{24}-3s_{14}s_{34}-s_{14}^2+2s_{24}s_{34}+3s_{24}^2-3s_{34}^2\Big]\\
&+\frac{1}{8s_{23}}\Big[21s_{12}+69s_{13}+14s_{14}+69s_{24}+21s_{34}\Big]\\
&+\frac{1}{2s_{12}^2s_{34}^2}\left[-2s_{13}s_{14}s_{23}s_{24}+s_{13}^2s_{24}^2+s_{14}^2s_{23}^2\right]\\
&+\frac{1}{s_{12}s_{34}s_{123}s_{234}}\left[4s_{14}s_{24}^3+6s_{14}^2s_{24}^2+4s_{14}^3s_{24}+s_{14}^4+s_{24}^4\right]\\
&+\frac{1}{s_{12}s_{34}s_{123}s_{134}}\left[4s_{14}s_{24}^3+6s_{14}^2s_{24}^2+4s_{14}^3s_{24}+s_{14}^4+s_{24}^4\right]\\
&+\frac{1}{8s_{12}s_{34}s_{123}}\Big[12s_{14}s_{23}s_{24}+12s_{14}s_{23}^2-12s_{14}s_{24}^2-6s_{14}^2s_{23}-18s_{14}^2s_{24}\\
&-4s_{14}^3+27s_{23}s_{24}^2+21s_{23}^2s_{24}+3s_{23}^3+5s_{24}^3\Big]+\frac{1}{8s_{12}s_{34}s_{234}}\Big[12s_{13}s_{14}s_{24}\\
&+18s_{13}s_{14}^2+3s_{13}s_{24}^2+12s_{13}^2s_{14}+3s_{13}^2s_{24}+3s_{13}^3+12s_{14}s_{24}^2+18s_{14}^2s_{24}\\
&+12s_{14}^3+3s_{24}^3\Big]+\frac{1}{8s_{12}s_{34}}\Big[16s_{13}s_{14}+31s_{13}s_{23}+45s_{13}s_{24}+25s_{13}^2\\
&-8s_{14}s_{23}+16s_{14}s_{24}+6s_{14}^2+31s_{23}s_{24}+21s_{23}^2+25s_{24}^2\Big]\\
&+\frac{5}{8s_{12}s_{123}s_{234}}\Big[12s_{14}s_{24}s_{34}+12s_{14}s_{24}^2+4s_{14}s_{34}^2+12s_{14}^2s_{24}+6s_{14}^2s_{34}\\
&+4s_{14}^3+4s_{24}s_{34}^2+6s_{24}^2s_{34}+4s_{24}^3+s_{34}^3\Big]+\frac{5}{8s_{12}s_{123}}\Big[4s_{14}s_{23}-8s_{14}s_{24}\\
&-4s_{14}s_{34}-6s_{14}^2+2s_{23}s_{24}+s_{23}s_{34}-s_{23}^2-3s_{24}s_{34}-3s_{24}^2-s_{34}^2\Big]\\
&+\frac{3}{8s_{12}s_{234}}\Big[4s_{13}s_{14}+2s_{13}s_{24}+s_{13}s_{34}+s_{13}^2+8s_{14}s_{24}+4s_{14}s_{34}+6s_{14}^2
\end{aligned}
$$

$$
\begin{aligned}
&+3s_{24}s_{34}+3s_{24}^2+s_{34}^2\Big]+\frac{3}{8s_{12}}\left[-s_{13}-4s_{14}+s_{23}-2s_{24}-s_{34}\right]\\
&+\frac{3}{8s_{34}s_{123}s_{234}}\Big[-4s_{13}s_{14}s_{24}-6s_{13}s_{14}^2-s_{13}s_{24}^2-4s_{13}^2s_{14}-s_{13}^2s_{24}-s_{13}^3\\
&-4s_{14}s_{24}^2-6s_{14}^2s_{24}-4s_{14}^3-s_{24}^3\Big]+\frac{3}{8s_{34}s_{123}}\Big[4s_{13}s_{14}-s_{13}s_{23}+s_{13}s_{24}\\
&+s_{13}^2-4s_{14}s_{23}+4s_{14}s_{24}+6s_{14}^2-s_{23}s_{24}+s_{23}^2+s_{24}^2\Big]\\
&+\frac{1}{s_{24}s_{123}s_{134}}\left[-2s_{14}+s_{24}-2s_{34}\right]+\frac{1}{s_{123}^2}\Big[2s_{14}s_{24}+2s_{14}s_{34}+s_{14}^2\\
&+2s_{24}s_{34}+s_{24}^2+s_{34}^2\Big]+\frac{1}{8s_{123}s_{234}}\Big[-12s_{13}s_{14}-6s_{13}s_{24}-3s_{13}s_{34}\\
&-3s_{13}^2-24s_{14}s_{24}-12s_{14}s_{34}+38s_{14}^2-9s_{24}s_{34}-9s_{24}^2-3s_{34}^2\Big]\\
&+\frac{1}{8s_{123}}\left[-6s_{13}+45s_{14}-3s_{23}+58s_{24}+36s_{34}\right]+\frac{35}{8}+\mathcal{O}(\epsilon)\Bigg\}\,. \qquad \text{(B.1.2)}
\end{aligned}
$$

The above expression for f_4^0 is not related to the decomposition of section 4.3.1 which is used in the numerical implementation.

Bibliography

[1] E. W. N. Glover, *Progress in NNLO calculations for scattering processes*, *Nucl. Phys. Proc. Suppl.* **116** (2003) 3–7 [hep-ph/0211412].

[2] **Particle Data Group** Collaboration, C. Amsler *et. al.*, *Review of particle physics*, *Phys. Lett.* **B667** (2008) 1.

[3] G. Dissertori *et. al.*, *Determination of the strong coupling constant using matched NNLO+NLLA predictions for hadronic event shapes in e+e- annihilations*, *JHEP* **08** (2009) 036 [0906.3436].

[4] F. Bloch and A. Nordsieck, *Note on the radiation field of the electron*, *Phys. Rev* **52** (1937) 54–59.

[5] T. Kinoshita, *Mass singularities of Feynmann amplitudes*, *J. Math. Phys* **3** (1962) 650–677.

[6] T. D. Lee and M. Nauenberg, *Degenerate systems and mass singularities*, *Phys. Rev.* **133** (1964) B1549–B1562.

[7] G. 't Hooft and M. J. G. Veltman, *Regularization and Renormalization of Gauge Fields*, *Nucl. Phys.* **B44** (1972) 189–213.

[8] R. K. Ellis, H. Georgi, M. Machacek, H. D. Politzer and G. G. Ross, *Perturbation Theory and the Parton Model in QCD*, *Nucl. Phys.* **B152** (1979) 285.

[9] R. K. Ellis, W. J. Stirling and B. R. Webber, *QCD and collider physics*, *Camb. Monogr. Part. Phys. Nucl. Phys. Cosmol.* **8** (1996) 1–435.

[10] P. Nason, *Introduction to perturbative QCD*, . Prepared for 11th Jorge Andre Swieca Summer School on Particle and Fields, Campos do Jordao, Brazil, 14-27 Jan 2001.

[11] G. Altarelli and G. Parisi, *Asymptotic Freedom in Parton Language*, *Nucl. Phys.* **B126** (1977) 298.

[12] V. N. Gribov and L. N. Lipatov, *Deep inelastic e p scattering in perturbation theory*, *Sov. J. Nucl. Phys.* **15** (1972) 438–450.

[13] Y. L. Dokshitzer, *Calculation of the Structure Functions for Deep Inelastic Scattering and e^+e^- Annihilation by Perturbation Theory in Quantum Chromodynamics*, *Sov. Phys. JETP* **46** (1977) 641–653.

[14] E. G. Floratos, D. A. Ross and C. T. Sachrajda, *Higher Order Effects in Asymptotically Free Gauge Theories: The Anomalous Dimensions of Wilson Operators*, *Nucl. Phys.* **B129** (1977) 66–88.

[15] E. G. Floratos, D. A. Ross and C. T. Sachrajda, *Higher Order Effects in Asymptotically Free Gauge Theories. 2. Flavor Singlet Wilson Operators and Coefficient Functions*, *Nucl. Phys.* **B152** (1979) 493.

[16] G. Curci, W. Furmanski and R. Petronzio, *Evolution of Parton Densities Beyond Leading Order: The Nonsinglet Case*, *Nucl. Phys.* **B175** (1980) 27.

[17] W. Furmanski and R. Petronzio, *Singlet Parton Densities Beyond Leading Order*, *Phys. Lett.* **B97** (1980) 437.

[18] S. Moch, J. A. M. Vermaseren and A. Vogt, *The three-loop splitting functions in QCD: The non-singlet case*, *Nucl. Phys.* **B688** (2004) 101–134 [hep-ph/0403192].

[19] A. Vogt, S. Moch and J. A. M. Vermaseren, *The three-loop splitting functions in QCD: The singlet case*, *Nucl. Phys.* **B691** (2004) 129–181 [hep-ph/0404111].

[20] F. A. Berends, R. Kleiss, P. De Causmaecker, R. Gastmans and T. T. Wu, *Single Bremsstrahlung Processes in Gauge Theories*, *Phys. Lett.* **B103** (1981) 124.

[21] P. De Causmaecker, R. Gastmans, W. Troost and T. T. Wu, *Multiple Bremsstrahlung in Gauge Theories at High- Energies. 1. General Formalism for Quantum Electrodynamics*, *Nucl. Phys.* **B206** (1982) 53.

[22] R. Kleiss and W. J. Stirling, *Spinor Techniques for Calculating p anti-p → $W^{\pm}/Z^0$ + Jets*, *Nucl. Phys.* **B262** (1985) 235–262.

[23] J. F. Gunion and Z. Kunszt, *Improved Analytic Techniques for Tree Graph Calculations and the G g q anti-q Lepton anti-Lepton Subprocess*, *Phys. Lett.* **B161** (1985) 333.

[24] Z. Xu, D.-H. Zhang and L. Chang, *Helicity Amplitudes for Multiple Bremsstrahlung in Massless Nonabelian Gauge Theories*, *Nucl. Phys.* **B291** (1987) 392.

[25] M. L. Mangano and S. J. Parke, *Multi-Parton Amplitudes in Gauge Theories*, *Phys. Rept.* **200** (1991) 301–367 [hep-th/0509223].

[26] L. J. Dixon, *Calculating scattering amplitudes efficiently*, hep-ph/9601359.

[27] F. A. Berends and W. Giele, *The Six Gluon Process as an Example of Weyl-Van Der Waerden Spinor Calculus*, *Nucl. Phys.* **B294** (1987) 700.

[28] M. L. Mangano, S. J. Parke and Z. Xu, *Duality and Multi - Gluon Scattering*, *Nucl. Phys.* **B298** (1988) 653.

[29] M. L. Mangano and S. J. Parke, *Quark - Gluon Amplitudes in the Dual Expansion*, *Nucl. Phys.* **B299** (1988) 673.

[30] D. R. Yennie, S. C. Frautschi and H. Suura, *The infrared divergence phenomena and high-energy processes*, *Ann. Phys.* **13** (1961) 379–452.

[31] J. M. Campbell and E. W. N. Glover, *Double Unresolved Approximations to Multiparton Scattering Amplitudes*, *Nucl. Phys.* **B527** (1998) 264–288 [hep-ph/9710255].

[32] A. Gehrmann-De Ridder and E. W. N. Glover, *A complete $\mathcal{O}(\alpha\alpha_s)$ calculation of the Photon + 1 Jet rate in e^+e^- annihilation*, *Nucl. Phys.* **B517** (1998) 269–323 [hep-ph/9707224].

[33] S. Catani and M. Grazzini, *Infrared factorization of tree level QCD amplitudes at the next-to-next-to-leading order and beyond*, *Nucl. Phys.* **B570** (2000) 287–325 [hep-ph/9908523].

[34] S. Catani and M. Grazzini, *Collinear factorization and splitting functions for next- to-next-to-leading order QCD calculations*, *Phys. Lett.* **B446** (1999) 143–152 [hep-ph/9810389].

[35] M. Gell-Mann, *A Schematic Model of Baryons and Mesons*, *Phys. Lett.* **8** (1964) 214–215.

[36] G. Zweig, *An SU(3) model for strong interaction symmetry and its breaking*, . CERN-TH-401.

[37] G. Zweig, *An SU(3) model for strong interaction symmetry and its breaking. 2*, . CERN-TH-412.

[38] G. P. Salam, *Towards Jetography*, 0906.1833.

[39] S. Catani, Y. L. Dokshitzer, M. H. Seymour and B. R. Webber, *Longitudinally invariant K_t clustering algorithms for hadron hadron collisions*, *Nucl. Phys.* **B406** (1993) 187–224.

[40] S. D. Ellis and D. E. Soper, *Successive combination jet algorithm for hadron collisions*, *Phys. Rev.* **D48** (1993) 3160–3166 [hep-ph/9305266].

[41] Y. L. Dokshitzer, G. D. Leder, S. Moretti and B. R. Webber, *Better Jet Clustering Algorithms*, *JHEP* **08** (1997) 001 [hep-ph/9707323].

[42] M. Wobisch and T. Wengler, *Hadronization corrections to jet cross sections in deep- inelastic scattering*, hep-ph/9907280.

[43] M. Cacciari, G. P. Salam and G. Soyez, *The anti-k_t jet clustering algorithm*, *JHEP* **04** (2008) 063 [0802.1189].

[44] M. Cacciari and G. P. Salam, *Dispelling the N^3 myth for the k_t jet-finder*, *Phys. Lett.* **B641** (2006) 57–61 [hep-ph/0512210].

[45] http://www.lpthe.jussieu.fr/∼salam/fastjet/.

[46] G. P. Salam and G. Soyez, *A practical Seedless Infrared-Safe Cone jet algorithm*, *JHEP* **05** (2007) 086 [0704.0292].

[47] http://projects.hepforge.org/siscone/.

[48] M. H. Seymour and C. Tevlin, *A Comparison of two different jet algorithms for the top mass reconstruction at the LHC*, *JHEP* **11** (2006) 052 [hep-ph/0609100].

[49] B. L. Combridge, J. Kripfganz and J. Ranft, *Hadron Production at Large Transverse Momentum and QCD*, *Phys. Lett.* **B70** (1977) 234.

[50] S. Catani and M. H. Seymour, *A general algorithm for calculating jet cross sections in NLO QCD*, *Nucl. Phys.* **B485** (1997) 291–419 [hep-ph/9605323].

[51] S. Frixione, Z. Kunszt and A. Signer, *Three jet cross-sections to next-to-leading order*, *Nucl. Phys.* **B467** (1996) 399–442 [hep-ph/9512328].

[52] Z. Nagy and Z. Trocsanyi, *Calculation of QCD jet cross sections at next-to-leading order*, *Nucl. Phys.* **B486** (1997) 189–226 [hep-ph/9610498].

[53] S. Frixione, *A General approach to jet cross-sections in QCD*, *Nucl. Phys.* **B507** (1997) 295–314 [hep-ph/9706545].

[54] G. Somogyi and Z. Trocsanyi, *A new subtraction scheme for computing QCD jet cross sections at next-to-leading order accuracy*, hep-ph/0609041.

[55] T. Gleisberg and F. Krauss, *Automating dipole subtraction for QCD NLO calculations*, *Eur. Phys. J.* **C53** (2008) 501–523 [0709.2881].

[56] M. H. Seymour and C. Tevlin, *TeVJet: A general framework for the calculation of jet observables in NLO QCD*, 0803.2231.

[57] K. Hasegawa, S. Moch and P. Uwer, *Automating dipole subtraction*, *Nucl. Phys. Proc. Suppl.* **183** (2008) 268–273 [0807.3701].

[58] K. Hasegawa, S. Moch and P. Uwer, *AutoDipole – Automated generation of dipole subtraction terms –*, 0911.4371.

[59] R. Frederix, T. Gehrmann and N. Greiner, *Automation of the Dipole Subtraction Method in MadGraph/MadEvent*, *JHEP* **09** (2008) 122 [0808.2128].

[60] M. Czakon, C. G. Papadopoulos and M. Worek, *Polarizing the Dipoles*, *JHEP* **08** (2009) 085 [0905.0883].

[61] R. Frederix, S. Frixione, F. Maltoni and T. Stelzer, *Automation of next-to-leading order computations in QCD: the FKS subtraction*, *JHEP* **10** (2009) 003 [0908.4272].

[62] C. F. Berger *et. al.*, *An Automated Implementation of On-Shell Methods for One- Loop Amplitudes*, *Phys. Rev.* **D78** (2008) 036003 [0803.4180].

[63] W. T. Giele and G. Zanderighi, *On the Numerical Evaluation of One-Loop Amplitudes: The Gluonic Case*, *JHEP* **06** (2008) 038 [0805.2152].

[64] G. Ossola, C. G. Papadopoulos and R. Pittau, *CutTools: a program implementing the OPP reduction method to compute one-loop amplitudes*, *JHEP* **03** (2008) 042 [0711.3596].

[65] T. Binoth, J. P. Guillet, G. Heinrich, E. Pilon and T. Reiter, *Golem95: a numerical program to calculate one-loop tensor integrals with up to six external legs*, *Comput. Phys. Commun.* **180** (2009) 2317–2330 [0810.0992].

[66] J. M. Campbell, M. A. Cullen and E. W. N. Glover, *Four jet event shapes in electron positron annihilation*, *Eur. Phys. J.* **C9** (1999) 245–265 [hep-ph/9809429].

[67] A. Gehrmann-De Ridder, T. Gehrmann and E. W. N. Glover, *Antenna Subtraction at NNLO*, *JHEP* **09** (2005) 056 [hep-ph/0505111].

[68] A. Daleo, T. Gehrmann and D. Maitre, *Antenna subtraction with hadronic initial states*, *JHEP* **04** (2007) 016 [hep-ph/0612257].

[69] A. Gehrmann-De Ridder and M. Ritzmann, *NLO Antenna Subtraction with Massive Fermions*, *JHEP* **07** (2009) 041 [0904.3297].

[70] A. Gehrmann-De Ridder, T. Gehrmann and E. W. N. Glover, *Infrared Structure of $e^+e^- \to 2$ jets at NNLO*, *Nucl. Phys.* **B691** (2004) 195–222 [hep-ph/0403057].

[71] A. Gehrmann-De Ridder, T. Gehrmann and E. W. N. Glover, *Quark-Gluon Antenna Functions from Neutralino Decay*, *Phys. Lett.* **B612** (2005) 36–48 [hep-ph/0501291].

[72] A. Gehrmann-De Ridder, T. Gehrmann and E. W. N. Glover, *Gluon-Gluon Antenna Functions from Higgs Boson Decay*, *Phys. Lett.* **B612** (2005) 49–60 [hep-ph/0502110].

[73] D. A. Kosower, *Antenna factorization of gauge-theory amplitudes*, *Phys. Rev.* **D57** (1998) 5410–5416 [hep-ph/9710213].

[74] D. A. Kosower, *Antenna factorization in strongly-ordered limits*, *Phys. Rev.* **D71** (2005) 045016 [hep-ph/0311272].

[75] R. Kleiss, W. J. Stirling and S. D. Ellis, , *Comput. Phys. Commun.* **40** (1986) 359.

[76] Z. Bern and D. A. Kosower, *The Computation of loop amplitudes in gauge theories*, *Nucl. Phys.* **B379** (1992) 451–561.

[77] **D0** Collaboration, B. Abbott *et. al.*, *The inclusive jet cross section in $\bar{p}p$ collisions at $\sqrt{s} = 1.8$ TeV*, *Phys. Rev. Lett.* **82** (1999) 2451–2456 [hep-ex/9807018].

[78] **CDF** Collaboration, A. A. Affolder *et. al.*, *Measurement of the strong coupling constant from inclusive jet production at the Tevatron $\bar{p}p$ collider*, *Phys. Rev. Lett.* **88** (2002) 042001 [hep-ex/0108034].

[79] D. Stump *et. al.*, *Inclusive jet production, parton distributions, and the search for new physics*, *JHEP* **10** (2003) 046 [hep-ph/0303013].

[80] T. C. Collaboration, *Inclusive Jet Cross Section at 10 TeV with CMS*, *CMS Physics Analysis Summary* **08-001** (2009).

[81] C. Anastasiou, L. J. Dixon, K. Melnikov and F. Petriello, *High precision QCD at hadron colliders: Electroweak gauge boson rapidity distributions at NNLO*, *Phys. Rev.* **D69** (2004) 094008 [hep-ph/0312266].

[82] S. Weinzierl, *Subtraction terms at NNLO*, *JHEP* **03** (2003) 062 [hep-ph/0302180].

[83] S. Frixione and M. Grazzini, *Subtraction at NNLO*, *JHEP* **06** (2005) 010 [hep-ph/0411399].

[84] G. Somogyi, Z. Trocsanyi and V. Del Duca, *Matching of singly- and doubly-unresolved limits of tree- level QCD squared matrix elements*, *JHEP* **06** (2005) 024 [hep-ph/0502226].

[85] G. Somogyi, Z. Trocsanyi and V. Del Duca, *A subtraction scheme for computing QCD jet cross sections at NNLO: regularization of doubly-real emissions*, *JHEP* **01** (2007) 070 [hep-ph/0609042].

[86] G. Somogyi and Z. Trocsanyi, *A subtraction scheme for computing QCD jet cross sections at NNLO: regularization of real-virtual emission*, *JHEP* **01** (2007) 052 [hep-ph/0609043].

[87] G. Somogyi and Z. Trocsanyi, *A subtraction scheme for computing QCD jet cross sections at NNLO: integrating the subtraction terms I*, *JHEP* **08** (2008) 042 [0807.0509].

[88] U. Aglietti, V. Del Duca, C. Duhr, G. Somogyi and Z. Trocsanyi, *Analytic integration of real-virtual counterterms in NNLO jet cross sections I*, *JHEP* **09** (2008) 107 [0807.0514].

[89] G. Somogyi, *Subtraction with hadronic initial states: an NNLO- compatible scheme*, *JHEP* **05** (2009) 016 [0903.1218].

[90] P. Bolzoni, S.-O. Moch, G. Somogyi and Z. Trocsanyi, *Analytic integration of real-virtual counterterms in NNLO jet cross sections II*, *JHEP* **08** (2009) 079 [0905.4390].

[91] A. Gehrmann-De Ridder, T. Gehrmann, E. W. N. Glover and G. Heinrich, *Infrared structure of $e^+e^- \to 3$ jets at NNLO*, *JHEP* **11** (2007) 058 [0710.0346].

[92] A. Gehrmann-De Ridder, T. Gehrmann, E. W. N. Glover and G. Heinrich, *Jet rates in electron-positron annihilation at $O(\alpha_s^3)$ in QCD*, *Phys. Rev. Lett.* **100** (2008) 172001 [0802.0813].

[93] S. Weinzierl, *NNLO corrections to 3-jet observables in electron-positron annihilation*, *Phys. Rev. Lett.* **101** (2008) 162001 [0807.3241].

[94] S. Weinzierl, *The infrared structure of $e^+e^- \to 3$ jets at NNLO reloaded*, *JHEP* **07** (2009) 009 [0904.1145].

[95] A. Gehrmann-De Ridder, T. Gehrmann, E. W. N. Glover and G. Heinrich, *Second-order QCD corrections to the thrust distribution*, *Phys. Rev. Lett.* **99** (2007) 132002 [0707.1285].

[96] A. Gehrmann-De Ridder, T. Gehrmann, E. W. N. Glover and G. Heinrich, *NNLO corrections to event shapes in e^+e^- annihilation*, *JHEP* **12** (2007) 094 [0711.4711].

[97] A. Gehrmann-De Ridder, T. Gehrmann, E. W. N. Glover and G. Heinrich, *NNLO moments of event shapes in e^+e^- annihilation*, *JHEP* **05** (2009) 106 [0903.4658].

[98] S. Weinzierl, *Event shapes and jet rates in electron-positron annihilation at NNLO*, *JHEP* **06** (2009) 041 [0904.1077].

[99] S. Weinzierl, *Moments of event shapes in electron-positron annihilation at NNLO*, *Phys. Rev.* **D80** (2009) 094018 [0909.5056].

[100] G. Dissertori *et. al.*, *First determination of the strong coupling constant using NNLO predictions for hadronic event shapes in e^+e^- annihilations*, *JHEP* **02** (2008) 040 [0712.0327].

[101] G. Dissertori *et. al.*, *Precise determination of the strong coupling constant at NNLO in QCD from the three-jet rate in electron–positron annihilation at LEP*, 0910.4283.

[102] **JADE** Collaboration, S. Bethke, S. Kluth, C. Pahl and J. Schieck, *Determination of the Strong Coupling α_S from hadronic Event Shapes and NNLO QCD predictions using JADE Data*, *Eur. Phys. J.* **C64** (2009) 351–360 [0810.1389].

[103] T. Gehrmann, M. Jaquier and G. Luisoni, *Hadronization effects in event shape moments*, 0911.2422.

[104] A. Gehrmann-De Ridder, T. Gehrmann and G. Heinrich, *Four-particle phase space integrals in massless QCD*, *Nucl. Phys.* **B682** (2004) 265–288 [hep-ph/0311276].

[105] A. Daleo, A. Gehrmann-De Ridder, T. Gehrmann and G. Luisoni, *Antenna subtraction at NNLO with hadronic initial states: initial-final configurations*, *JHEP* **01** (2010) 118 [0912.0374].

[106] E. W. N. Glover, C. Oleari and M. E. Tejeda-Yeomans, *Two-loop QCD corrections to gluon-gluon scattering*, *Nucl. Phys.* **B605** (2001) 467–485 [hep-ph/0102201].

[107] Z. Bern, A. De Freitas and L. J. Dixon, *Two-loop helicity amplitudes for gluon gluon scattering in QCD and supersymmetric Yang-Mills theory*, *JHEP* **03** (2002) 018 [hep-ph/0201161].

[108] C. Anastasiou, E. W. N. Glover, C. Oleari and M. E. Tejeda-Yeomans, *Two-loop QCD corrections to massless identical quark scattering*, *Nucl. Phys.* **B601** (2001) 341–360 [hep-ph/0011094].

[109] C. Anastasiou, E. W. N. Glover, C. Oleari and M. E. Tejeda-Yeomans, *Two-loop QCD corrections to massless quark-gluon scattering*, *Nucl. Phys.* **B605** (2001) 486–516 [hep-ph/0101304].

[110] Z. Bern, A. De Freitas and L. J. Dixon, *Two-loop helicity amplitudes for quark gluon scattering in QCD and gluino gluon scattering in supersymmetric Yang- Mills theory*, *JHEP* **06** (2003) 028 [hep-ph/0304168].

[111] A. De Freitas and Z. Bern, *Two-loop helicity amplitudes for quark-quark scattering in QCD and gluino gluino scattering in supersymmetric Yang-Mills theory*, *JHEP* **09** (2004) 039 [hep-ph/0409007].

[112] S. Catani, *The singular behaviour of QCD amplitudes at two-loop order*, *Phys. Lett.* **B427** (1998) 161–171 [hep-ph/9802439].

[113] E. W. N. Glover and M. E. Tejeda-Yeomans, *One-loop QCD corrections to gluon-gluon scattering at NNLO*, *JHEP* **05** (2001) 010 [hep-ph/0104178].

[114] Z. Bern, L. J. Dixon and D. A. Kosower, *One loop corrections to five gluon amplitudes*, *Phys. Rev. Lett.* **70** (1993) 2677–2680 [hep-ph/9302280].

[115] Z. Bern, V. Del Duca and C. R. Schmidt, *The infrared behavior of one-loop gluon amplitudes at next-to-next-to-leading order*, *Phys. Lett.* **B445** (1998) 168–177 [hep-ph/9810409].

[116] Z. Bern, V. Del Duca, W. B. Kilgore and C. R. Schmidt, *The infrared behavior of one-loop QCD amplitudes at next-to-next-to-leading order*, *Phys. Rev.* **D60** (1999) 116001 [hep-ph/9903516].

[117] D. A. Kosower, *Multiple singular emission in gauge theories*, *Phys. Rev.* **D67** (2003) 116003 [hep-ph/0212097].

[118] W. B. Kilgore, *Subtraction terms for hadronic production processes at next-to-next-to-leading order*, *Phys. Rev.* **D70** (2004) 031501 [hep-ph/0403128].

[119] A. Daleo, A. Gehrmann-De Ridder, T. Gehrmann and G. Luisoni, *NNLO Antenna Subtraction with One Hadronic Initial State*, 1001.2397.

[120] R. Boughezal, A. Gehrmann-De Ridder and M. Ritzmann, *NNLO antenna subtraction with two hadronic initial states*, 1001.2396.

[121] F. A. Berends and W. T. Giele, *Multiple Soft Gluon Radiation in Parton Processes*, *Nucl. Phys.* **B313** (1989) 595.

[122] V. Del Duca, A. Frizzo and F. Maltoni, *Factorization of tree QCD amplitudes in the high-energy limit and in the collinear limit*, *Nucl. Phys.* **B568** (2000) 211–262 [hep-ph/9909464].

[123] G. Altarelli and G. Parisi, , *Nucl. Phys.* **B126** (1977) 298.

[124] G. Heinrich, *Sector Decomposition*, *Int. J. Mod. Phys.* **A23** (2008) 1457–1486 [0803.4177].

[125] K. Hepp, *Proof of the Bogolyubov-Parasiuk theorem on renormalization*, *Commun. Math. Phys.* **2** (1966) 301–326.

[126] T. Binoth and G. Heinrich, *An automatized algorithm to compute infrared divergent multi-loop integrals*, *Nucl. Phys.* **B585** (2000) 741–759 [hep-ph/0004013].

[127] T. Binoth and G. Heinrich, *Numerical evaluation of multi-loop integrals by sector decomposition*, *Nucl. Phys.* **B680** (2004) 375–388 [hep-ph/0305234].

[128] V. A. Smirnov, *Analytical result for dimensionally regularized massless on-shell double box*, *Phys. Lett.* **B460** (1999) 397–404 [hep-ph/9905323].

[129] J. B. Tausk, *Non-planar massless two-loop Feynman diagrams with four on-shell legs*, *Phys. Lett.* **B469** (1999) 225–234 [hep-ph/9909506].

[130] V. A. Smirnov, *Analytical result for dimensionally regularized massless master non-planar double box with one leg off shell*, *Phys. Lett.* **B500** (2001) 330–337 [hep-ph/0011056].

[131] V. A. Smirnov, *Analytical result for dimensionally regularized massive on-shell planar double box*, *Phys. Lett.* **B524** (2002) 129–136 [hep-ph/0111160].

[132] A. I. Davydychev and V. A. Smirnov, *Analytical evaluation of certain on-shell two-loop three- point diagrams*, *Nucl. Instrum. Meth.* **A502** (2003) 621–623 [hep-ph/0210171].

[133] G. Heinrich and V. A. Smirnov, *Analytical evaluation of dimensionally regularized massive on-shell double boxes*, *Phys. Lett.* **B598** (2004) 55–66 [hep-ph/0406053].

[134] M. Czakon, J. Gluza and T. Riemann, *Master integrals for massive two-loop Bhabha scattering in QED*, *Phys. Rev.* **D71** (2005) 073009 [hep-ph/0412164].

[135] M. Awramik, M. Czakon and A. Freitas, *Bosonic corrections to the effective weak mixing angle at $\mathcal{O}(\alpha^2)$*, *Phys. Lett.* **B642** (2006) 563–566 [hep-ph/0605339].

[136] M. Awramik, M. Czakon and A. Freitas, *Electroweak two-loop corrections to the effective weak mixing angle*, *JHEP* **11** (2006) 048 [hep-ph/0608099].

[137] V. A. Smirnov, *Analytical result for dimensionally regularized massless on-shell planar triple box*, *Phys. Lett.* **B567** (2003) 193–199 [hep-ph/0305142].

[138] T. Gehrmann, G. Heinrich, T. Huber and C. Studerus, *Master integrals for massless three-loop form factors: One-loop and two-loop insertions*, *Phys. Lett.* **B640** (2006) 252–259 [hep-ph/0607185].

[139] G. Heinrich, T. Huber and D. Maitre, *Master Integrals for Fermionic Contributions to Massless Three-Loop Form Factors*, *Phys. Lett.* **B662** (2008) 344–352 [0711.3590].

[140] R. Boughezal and M. Czakon, *Single scale tadpoles and $\mathcal{O}(G_F m_t^2 \alpha_s^3)$ corrections to the ρ parameter*, *Nucl. Phys.* **B755** (2006) 221–238 [hep-ph/0606232].

[141] C. Anastasiou, S. Beerli and A. Daleo, *Evaluating multi-loop Feynman diagrams with infrared and threshold singularities numerically*, *JHEP* **05** (2007) 071 [hep-ph/0703282].

[142] C. Anastasiou, S. Beerli and A. Daleo, *The two-loop QCD amplitude gg -¿ h,H in the Minimal Supersymmetric Standard Model*, *Phys. Rev. Lett.* **100** (2008) 241806 [0803.3065].

[143] A. Denner and S. Pozzorini, *An algorithm for the high-energy expansion of multi-loop diagrams to next-to-leading logarithmic accuracy*, *Nucl. Phys.* **B717** (2005) 48–85 [hep-ph/0408068].

[144] C. Bogner and S. Weinzierl, *Resolution of singularities for multi-loop integrals*, *Comput. Phys. Commun.* **178** (2008) 596–610 [0709.4092].

[145] G. Heinrich, *A numerical method for NNLO calculations*, *Nucl. Phys. Proc. Suppl.* **116** (2003) 368–372 [hep-ph/0211144].

[146] T. Binoth and G. Heinrich, *Numerical evaluation of phase space integrals by sector decomposition*, *Nucl. Phys.* **B693** (2004) 134–148 [hep-ph/0402265].

[147] C. Anastasiou, K. Melnikov and F. Petriello, *A new method for real radiation at NNLO*, *Phys. Rev.* **D69** (2004) 076010 [hep-ph/0311311].

[148] G. Heinrich, *Towards $e^+e^- \to 3$ jets at NNLO by sector decomposition*, *Eur. Phys. J.* **C48** (2006) 25–33 [hep-ph/0601062].

[149] C. Anastasiou, K. Melnikov and F. Petriello, *Real radiation at NNLO: $e^+e^- \to 2$ jets through $O(\alpha_s^2)$*, *Phys. Rev. Lett.* **93** (2004) 032002 [hep-ph/0402280].

[150] C. Anastasiou, K. Melnikov and F. Petriello, *Higgs boson production at hadron colliders: Differential cross sections through next-to-next-to-leading order*, *Phys. Rev. Lett.* **93** (2004) 262002 [hep-ph/0409088].

[151] C. Anastasiou, K. Melnikov and F. Petriello, *Fully differential Higgs boson production and the di- photon signal through next-to-next-to-leading order*, *Nucl. Phys.* **B724** (2005) 197–246 [hep-ph/0501130].

[152] C. Anastasiou, G. Dissertori and F. Stockli, *NNLO QCD predictions for the $H \to WW \to ll\nu\nu$ signal at the LHC*, *JHEP* **09** (2007) 018 [0707.2373].

[153] C. Anastasiou, G. Dissertori, F. Stockli and B. R. Webber, *QCD radiation effects on the $H \to WW \to l\nu l\nu$ signal at the LHC*, *JHEP* **03** (2008) 017 [0801.2682].

[154] K. Melnikov and F. Petriello, *Electroweak gauge boson production at hadron colliders through $O(\alpha_s^2)$*, *Phys. Rev.* **D74** (2006) 114017 [hep-ph/0609070].

[155] C. Anastasiou, K. Melnikov and F. Petriello, *The electron energy spectrum in muon decay through $O(\alpha^2)$*, *JHEP* **09** (2007) 014 [hep-ph/0505069].

[156] K. Melnikov, *$O(\alpha_s^2)$ corrections to semileptonic decay $b \to c l \bar{\nu}_l$*, *Phys. Lett.* **B666** (2008) 336 [0803.0951].

[157] G. P. Lepage, *VEGAS: an adaptice multidimensional integration program*, . CLNS-80/447.

[158] V. A. Smirnov, *Evaluating Feynman integrals*, *Springer Tracts Mod. Phys.* **211** (2004) 1–244.

[159] V. A. Smirnov, *Evaluating multiloop Feynman integrals by Mellin-Barnes representation*, *Nucl. Phys. Proc. Suppl.* **135** (2004) 252–256 [hep-ph/0406052].

[160] S. J. Parke and T. R. Taylor, *An Amplitude for n Gluon Scattering*, *Phys. Rev. Lett.* **56** (1986) 2459.

[161] F. A. Berends and W. T. Giele, *Recursive Calculations for Processes with n Gluons*, *Nucl. Phys.* **B306** (1988) 759.

[162] R. K. Ellis and J. C. Sexton, *QCD Radiative Corrections to Parton Parton Scattering*, *Nucl. Phys.* **B269** (1986) 445.

[163] Z. Bern and D. A. Kosower, *Color decomposition of one loop amplitudes in gauge theories*, *Nucl. Phys.* **B362** (1991) 389–448.

[164] M. T. Grisaru and H. N. Pendleton, *Some Properties of Scattering Amplitudes in Supersymmetric Theories*, *Nucl. Phys.* **B124** (1977) 81.

[165] Z. Bern and D. A. Kosower, *Efficient calculation of one loop QCD amplitudes*, *Phys. Rev. Lett.* **66** (1991) 1669–1672.